MOLECULAR HYBRIDIZATION APPROACH FOR THE SYNTHESIS AND EVALUATION OF NEW HETEROCYCLIC COMPOUNDS AS POTENTIAL ANTICANCER AGENTS

Thesis submitted in the fulfillment of the

requirement of the degree of

Doctor of Philosophy

by

Iqubal Singh

(Regn. No. 901609003**)**

THAPAR INSTITUTE
OF ENGINEERING & TECHNOLOGY
(Deemed to be University)

Under the Supervision of

Dr. Kamaldeep Paul

(Associate Professor)

SCHOOL OF CHEMISTRY AND BIOCHEMISTRY

THAPAR INSTITUTE OF ENGINEERING AND TECHNOLOGY

PATIALA-147004

PUNJAB, INDIA

September, 2020

Certificate

It is certified that the work contained in the thesis entitled "**Molecular Hybridization Approach for the Synthesis and Evaluation of new Heterocyclic Compounds as Potential Anticancer Agents**" by Iqubal Singh in fulfilment of the degree of Doctor of Philosophy, is an authentic record of candidate's own independent and original research work carried out under my supervision in the School of Chemistry and Biochemistry, Thapar Institute of Engineering and Technology, Patiala, Punjab-India. The material embodied in this thesis has not been submitted in part or full to any other University or Institute for the award of any degree.

Kamaldeep Paul 16/9/20

Dr. Kamaldeep Paul

(Supervisor)

Associate Professor

School of Chemistry and Biochemistry,

Thapar Institute of Engineering and Technology,

Patiala – 147004, Punjab (India)

Prof. Amjad Ali

(Head of SCBC)

School of Chemistry and Biochemistry,

Thapar Institute of Engineering and Technology,

Patiala – 147004, Punjab (India)

Candidate's Declaration

I, hereby declared that the presented work in the thesis entitled "**Molecular Hybridization Approach for the Synthesis and Evaluation of new Heterocyclic Compounds as Potential Anticancer Agents**" in fulfilment of degree of Doctor of Philosophy is outcome of research work carried out by me under the supervision of Dr. Kamaldeep Paul, Associate Professor, School of Chemistry and Biochemistry, Thapar Institute of Engineering & Technology, Patiala, Punjab (India). In keeping with general practice of reporting scientific observations, due acknowledgements have been made whenever work described here has been based on findings of other investigator. This work has not been submitted in part or full to any other University or Institute for the award of any degree.

Iqubal Singh

Reg. No. 901609003

School of Chemistry and Biochemistry,

Thapar Institute of Engineering and Technology,

Patiala – 147004, Punjab (India)

Dr. Kamaldeep Paul 16/9/20

(Supervisor)

Associate Professor

School of Chemistry and Biochemistry,

Thapar Institute of Engineering and Technology,

Patiala – 147004, Punjab (India)

Acknowledgement

I may halt for a while to place on record my gratefulness to all those who have made a contribution towards the successful completion of this thesis. Above all, I express my gratitude to my respected supervisor Dr. Kamaldeep Paul, Associate professor, School of Chemistry and Biochemistry (SCBC), Thapar Institute of Engineering & Technology, Patiala (Punjab, India) for the opportunity to work in his group. His inspiring guidance, intellectual support encouragement and motivation for working on new research problems is what made this work possible. He also established successful collaborations, which gave me the opportunity to gain knowledge in a wide range of research problems. I thank him for help in writing of this dissertation, other research articles and improving me at scientific communication and style.

I express my gratitude to Director, Thapar Institute of Engineering & Technology, Patiala, Dr. Rafat Siddique, Dean of Research and Sponsored Projects (RSP), Prof. O. P. Pandey former Dean RSP, Dr. Amjad Ali (Head of SCBC), Prof. Bonamali Pal (Former Head of SCBC) for all facilities which have been immensely helpful in completing my work.

I am also thankful to all my respected teachers of the School of Chemistry and Biochemistry (SCBC) and my doctoral committee members Dr. Satnam Singh, Dr. Manmohan Chhibber and Dr. Siddharth Sharma for their valuable suggestion and motivation at each and every step during my whole thesis work.

During my Ph.D studies, I had the opportunity to work in close collaborations with other research groups. I would like to express my sincere thank to Dr. Vijay Luxami for initial days of collaboration and inspiring me learn to spectroscopy studies. I thank her group members, especially Gulshan Kumar and Dr. Richa Rani, for their support and discussion.

Time flew by in the company of good friends and therefore, a special thanks to Sukhveer Singh, Sudesh Rani, Richa Bansal, Ruhi Mehta, Aastha Palta, Dinesh Singla, Rekha Thakur, Saurabh Gupta, Rohini Gupta, Swati Rana, Geetika Rani, Nandan Sarkar, Rohini Verma and Bhuvnesh Malik. I would also like to extend the expression of thanks to other colleagues Bhavya Khurana, Nitya Chawla, Jasleen Kaur and Akanksha Chhikara for creating a great work atmosphere and help at different stages during my course study. I extend my gratitude to other research scholars Vanshita Goel, Pawandeep Kaur, Ashok Kumar, Jyoti Sharma, Santosh Kumar Rath, Aadil Bathla, Amanpreet Kaur, Shagun Kainth, Anju Gahalawat, Shivali Gupta, Vagish Dwibedi, Harleen Kaur Walia, Devendra Sillu and others who are not mentioned by name for their support and

encouragement. I express my warm thanks to my colleagues and friends with whom I spent and enjoyed scientific and social activities. I now have a forever collection of stories and a lot of everlasting memories to tell.

I would also like to thank Dr. Yuvraj Garg, Dr. Rayees Ahmad Rather, Dr. Amit Mishra, Dr. Richa Goel, Dr. Suraksha Gahalawat and Dr. Raman deep Kaur for scientific and non-scientific help during the Ph.D studies.

Another round of thanks for friends away from here; Dharmendra Choudhary, Vijay Yadav, Narendra Jangid, Gaurav Tulsyan, Shikha Rathore, Manish Kumar Swami, Jagdeep Singh, Ramandeep Chatha, Ram Krishan Singh, Dr. Vijay Walia and Dr. Kamlesh Verma for a laugh whenever possible.

I am also thankful to Dr. Diptiman Choudhury, Assistant Professor, School of Chemistry and Biochemistry, Thapar Institute of Enginnering and Technology, Patiala-Punjab (India) for introducing new dimension of research challenges and scientific discussion about cytotoxicity.

I acknowledge the help of Mr Mayank Sharma, office staff and Chander Singh Thakur, Chandar Shekhar, Hemant Sharma and Vishwanath Dass, technical staff of School of Chemistry and Biochemistry for their support in various aspects.

I extend my thankful acknowledgment to SAI Labs, Thapar Institute of Engineering & Technology, Patiala; SAIF Lab, Panjab University, Chandigarh; CIL, IIT Ropar; IISER, Mohali, IMTech, Mohali for providing experimental instrumentation. I extend my gratitude to Mr. Mukesh Aggarwal, SAI Labs, Thapar Institute of Engineering & Technology, Patiala for their cooperation during NMR/CHN data collection.

I thankfully acknowledge CSIR, New Delhi for providing me SRF (09/677(0033)/2018-EMR-I) during my course. I am also thankful to DST-SERB, New Delhi (EMR/2014/000669) for financial assistant.

Finally, none of this would have been possible without the constant love, support, guidance and patience of all my family members. I owe my gratitude to my respected Father-Mother whose blessings, belief and encouragement have shown me the path to pursue goals in my life. I thank my sisters and brothers for everything they have done for me. They all have been amazing and always been there for me. I cannot thank them enough. Thank you for your everlasting love and support. **This is for you!**

DEDICATED TO

MY BELOVED

FAMILY

ABBREVIATONS

μM	Micro molar
5-FU	5-Fluorouracil
AR	Analytical reagents
ArH	Aromatic hydrogen
$B(OH)_2$	Boronic acid
BSA	Bovine serum albumin
$CDCl_3$	Deuterated chloroform
CDK	Cyclin dependent kinase
CH_3COOH	Acetic acid
$CHCl_3$	Chloroform
Ct	Calf thymus
DHFR	Dihydrofolate reductase
DMF	Dimethylformamide
DMSO	Dimethylsulfoxide
DMSO-d_6	Hexadeuterodimethyl sulfoxide
DNA	Deoxyribonucleic acid
EB	Ethidium bromide
EGFR	Epidermal growth factor receptor
FRET	Förster resonance energy transfer
GI%	Percentage growth inhibition
GI_{50}	Median growth inhibition concentration
H_2SO_4	Sulphuric acid
H-bonding	Hydrogen bonding
HNO_3	Nitric acid
HSA	Human serum albumin
Hsp90	Heat shock protein 90

IC_{50}	Median inhibition concentration
IPA	Isopropanol
K_2CO_3	Potassium carbonate
KI	Potassium iodide
LC_{50}	Median lethal concentration
mg	Milligram
MG-MID	Mean graph mid-point
min	Minutes
MTT	3-(4,5-Dimethylthiazol-2-yl)-2,5-diphenyl tetrazolium bromide
NaOH	Sodium hydroxide
NCI	National cancer institute
NH_2NH_2	Hydrazine
NMR	Nuclear magnetic resonance
NT	Not treated
$Pd(PPh_3)_2Cl_2$	Bis(triphenylphosphine)palladium(II)chloride
$Pd(PPh_3)_4$	Tetrakis(triphenylphosphine)palladium(0)
PDB	Protein data bank
Phe	Phenylalanine
$POCl_3$	Phosphorusoxychloride
SAR	Structure activity relationship
TFA	Trifluoroacetic acid
TGI	Total growth inhibition concentration
TPSA	Total polar surface area
Trp	Tryptophan
Tyr	Tyrosine
USA	United States America
UV	Ultraviolet

Contents

INTRODUCTION

Cancer is the most challenging disease globally and can be described as uncontrolled production of abnormal cells. Nearby 17 million patients were diagnosed with cancer and about 9.6 million deaths from cancer were reported in 2018 worldwide. According to the cancer research reports, about 27.5 million new cancer cases will be occurred every year by 2040 (**Figure 1**). Breast, lung, prostate and colorectal cancers are the most common type of cancers diagonised globally. There are many cancer inducing factors like age, obesity, overweight, genetics, smoking, alcohol, diet, physical inactivity etc. Due to increasing worldwide load, prevention and treatment of cancer is one of the major challenging health issues of 21st century.[1]

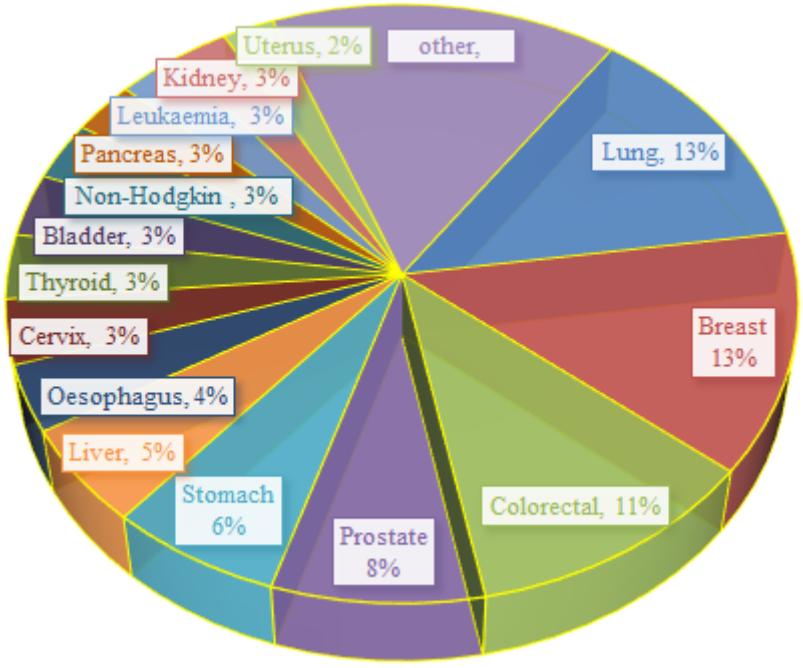

Figure 1. Worldwide % of new cancer cases diagnosed in 2018[2]

At present, cancer therapy includes medication that mainly target some biological pathway.[3] With the progress in the area of cancer therapy, there are still many problems persist with the existing anticancer medicines. Most of the available anticancer drugs are unable to overcome the resistance mechanism of cancer cells and are also incapable to distinguish cancer cells and normal cells of the body.[4] Research has been committed for the discovery and development of an efficient anticancer candidate. Immense research has been focused for the identification of tumor specific therapies, which can enhance the sensitivity of cancer cells towards

anticancer drugs.[5] Drugs, which are used in cancer chemotherapy, usually target the cell division or prompt cell death using various signaling pathways. Recently the interest is focused on the discovery of the cytotoxic agent that simultaneously affect multiple targets for cancer therapy.[6,7] Currently, hybrids of heterocycle moities are used to stimulate the multiple targets with a single drug for better therapeutic potential as well as to beat the side effects accompanying with a single drug. This approach for developing a hybrid drug inducing multiple targets is known as molecular hybridization (MH). Molecular hybridization is an efficient approach for the development of a more potent compound, which can simultaneously target two or more pathogenic pathways.[8] This approach can be used to increase the efficacy and selectivity as well as to decrease the adverse effects of the drug.[9,10] Molecular hybridization considered to be similar to the combination therapy besides, two or more drugs are present in a single entity attached with covalent linkage.[11] Various well-known heterocyclic moieties are reported with their potential anticancer and antibacterial activity.[12] On account of these heterocyclic moieties, a potent antitumor candidate could be designed by molecular hybridization.

Naphthalimide is a highly versatile functionalized moiety, that is receiving an increasing attention for the binding capacity towards DNA[13] and established pronounced therapeutic importance in pharmaceutical and medicinal chemistry.[14,15] Particularly for anticancer activities, some of the naphthalimides such as amonafide **1**, mitonafide **2** and elinafide **3** show effective cytotoxicity towards the growth of various murine and human cancer cell lines (**Figure 2**). These naphthalimides exert their anticancer action by interacting with DNA and inhibit directly the function of DNA replication and transcription, and/or topoisomerase (TOPO-II) to stabilize the supramolecular TOPO-II and DNA complex and to avoid the alteration of molecular structure of DNA.[16]

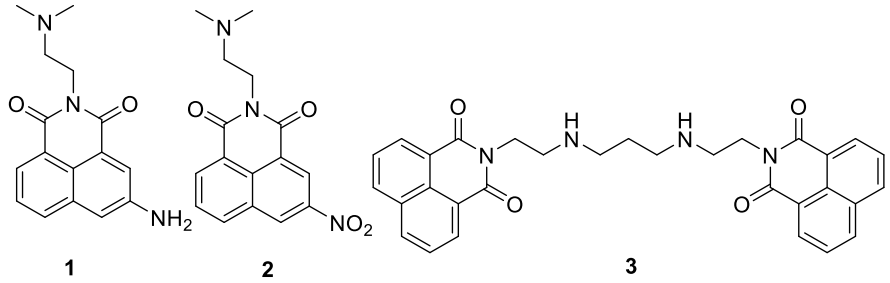

Figure 2. Naphthalimide based anticancer derivatives

A large number of derivatives based on benzimidazole/benzothiazole moieties have also been designed and evaluated for antitumor activity. Amongst these compounds, nocodazole **4**,[17] a 2-thienyl carbonyl benzimidazole; carbendazim **5**,[18] a benzimidazole carbamate and Veliparib **6**,[19] a pyrrolidine-2-yl benzimidazole are used in the clinic while mebendazole **7** is currently undergoing clinical trials.[20] The anticancer activity of these benzimidazoles appear to derive from their ability to form strong complexes with nucleic acids and thus induce DNA damage, and exert related effects such as topoisomerase poisoning, telomerase inhibition and inhibition of gene transcription (**Figure 3**). [21-23]

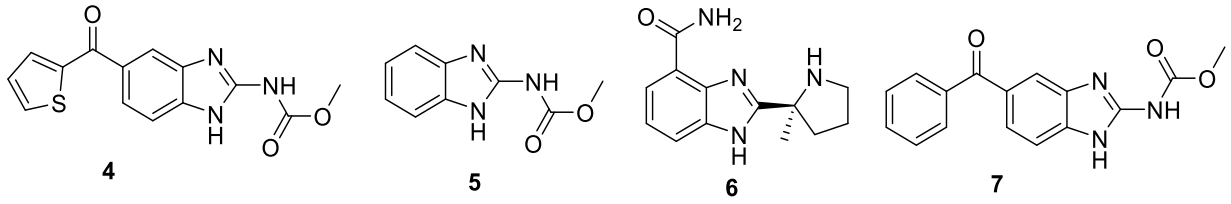

Figure 3. Benzimidazole/benzothiazole based anticancer derivatives

Imidazo[1,2-*a*]pyrazine is also an important heterocyclic entity and display cytotoxicity assisted by numerous changes at various positions of the scaffold.[24] Imidazo[1,2-*a*]pyrazines (**8-10**) exhibit significant cytotoxicity along with a broad range of inhibitory effect towards cyclin dependent kinase phosphoinositide-3-kinase, topoisomerase-II (Topo II) breast tumor kinase, Aurora kinase, spleen tyrosine kinase and check point kinase (**Figure 4**).[25-30]

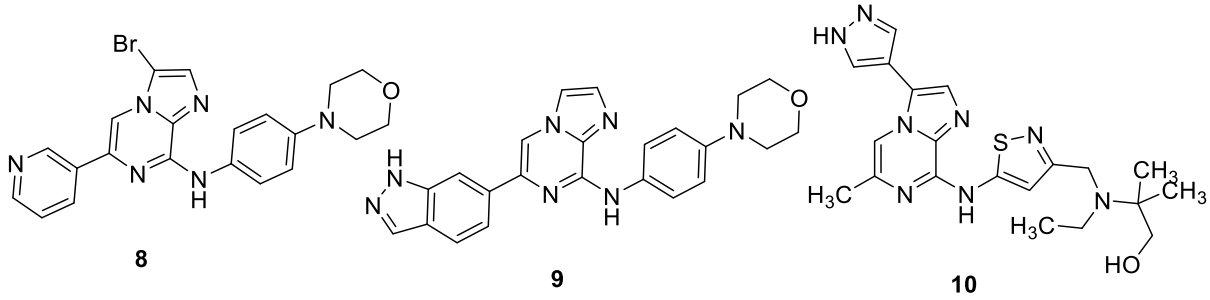

Figure 4. Imidazo[1,2-*a*]pyrazine based anticancer compounds

Phenanthrene-imidazole also shows favourable properties such as stability, ease of synthesis, high extinction coefficient and tuneable absorption and emission properties,[31] which is commonly utilized in optical sensors and probes. Only few literature reports are available for anticancer activity of phenanthrene-imidazole moieties (**11-13**) (**Figure 5**).[31,33]

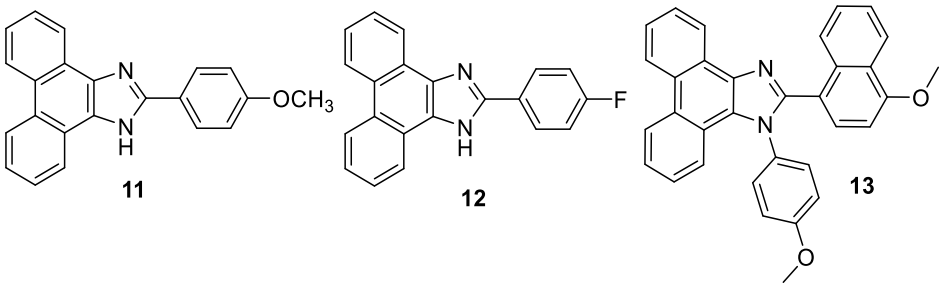

Figure 5. Phenanthro[9,10-*d*]imidazole based anticancer derivatives

We have designed and synthesized various hybrids of well-known heterocyclic moieties and evaluated for antitumor activity against human cancer cell lines. Cytotoxicity of compounds were also investigated with normal cell lines. Additionally, the mode of action for anticancer activity was also evaluated through interaction with ct-DNA using various spectroscopic techniques. The transportation behaviour of most active derivatives with human serum albumin (HSA) and bovine serum albumin (BSA) has also been performed using UV-visible and fluorescence spectroscopy. Interactions between DNA and compounds were also explored by molecular modelling. In this dissertation the total accomplished work has been divided into following parts:

Chapter 1: Review of Literature

Chapter 2: Hybrids of Imidazo[1,2-*a*]pyrazine and Benzimidazole

Chapter 3: Hybrids of Benzimidazole and Naphthalimide

Chapter 4: Hybrids of Naphthalimide and Phenanthro[9,10-*d*]imidazole

Chapter 5: Hybrids of Phenanthro[9,10-*d*]imidazole and other heterocyclic moieties

Chapter 6: Hybrids of Naphthalimide, Benzothiazole and Indole

CHAPTER 1
REVIEW OF LITERATURE

Most of the available marketed heterocyclic drug molecules with incredible versatility and optimal physicochemical properties are the real pillars of medicinal chemistry. Amongst the numerous clinical uses, heterocyclic molecules containing naphthalimide,[34] benzimidazole/benzothiazole,[35] indole,[36] imidazopyrazine,[37] phenanthroimidazole[38] etc. play a significant role in cytotoxic drugs. Therefore, the synthesis and biological evaluation of new heterocyclic derivatives with potent biological activity are essential aspects in the field of medicinal chemistry.[39]

1.1 Biological activity of naphthalimide based molecules

Quintana-Espinoza and co-workers optimized a series of 5-ethynylarylnaphthalimides and examined their *in vitro* anticancer activity towards SK-Br-3, HEL and HL60 human cancer cells along with topoisomerase II inhibitory activity. Results showed that compounds **1a**, **1h** and **1i** found most cytotoxic with IC_{50} values of 4.6 ± 0.1 μM, 4.6 ± 0.2 μM, 1.4 ± 0.06 μM for **1a**, 9.6 ± 0.4 μM, 3.5 ± 0.1 μM, 5.6 ± 0.3 μM for **1h** and >10 μM, 5.4 ± 0.3 μM, 5.0 ± 0.08 μM for **1i**, against SK-Br-3, HL60 and HEL cancer cell lines, respectively, along with strong inhibitory activity for topoisomerase II.[34]

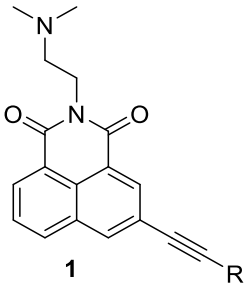

1

1a R = Ph
1b R = 3-OCH_3Ph
1c R = 3-OHPh
1d R = 4-OCH_3Ph
1e R = 4-OHPh
1f R = 3-NO_2Ph
1g R = 3-CF_3Ph
1h R = 3-furyl
1i R = 3-thienyl

Tan and co-workers prepared three series of fused naphthalimide compounds and examined their cytotoxicity towards A549 and P388 cancer cell lines as well as LO2 normal cell lines. Sulfur-containing derivatives (**2a-c**, **3a-c** and **4a-c**) showed excellent anticancer activity. Compounds **3a** and **4a** displayed cytotoxicity with IC_{50} values of 0.14 and 0.007 μM, respectively for A549 cancer cells, whereas, derivatives **3c** and **4c** showed excellent anticancer activity towards A549 and P388 cancer cells. Compounds **3d**, **4a** and **4d** showed potent topoisomerase II inhibitory activity as amonafide, while, all other synthesized derivatives showed a more potent activity than etoposide,

a well-known inhibitor of topoisomerase II. All derivatives also exhibited potent inhibitory activity against topoisomerase I.[40]

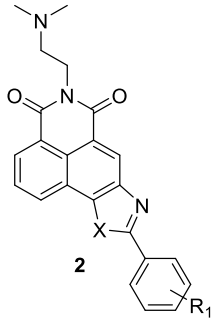

2

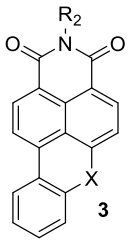

3

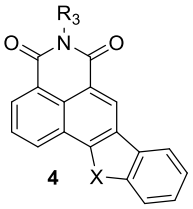

4

2a R_1 = H	X = S	**3a** R_2 = $CH_2CH_2NCH_3$	X = S	**4a** R_3 = $CH_2CH_2NCH_3$	X = S
2b R_1 = *p*-Me	X = S	**3b** R_2 = $CH_2CH_2CH_2NCH_3$	X = S	**4b** R_3 = $CH_2CH_2CH_2NCH_3$	X = S
2c R_1 = *p*-OMe	X = S	**3c** R_2 = $CH_2CH_2CH_2CH_3$	X = S	**4c** R_3 = $CH_2CH_2CH_2CH_3$	X = S
2d R_1 = H	X = O	**3d** R_2 = $CH_2CH_2NCH_3$	X = O	**4d** R_3 = $CH_2CH_2NCH_3$	X = O
2e R_1 = *p*-Me	X = O	**3e** R_2 = $CH_2CH_2CH_2NCH_3$	X = O	**4e** R_3 = $CH_2CH_2CH_2NCH_3$	X = O
2f R_1 = *p*-OMe	X = O	**3f** R_2 = $CH_2CH_2CH_2CH_3$	X = O	**4f** R_3 = $CH_2CH_2CH_2CH_3$	X = O

Wang and co-workers synthesized N^1-(2-aminoethyl)-N^2,N^2-dimethylethane-1,2-diamine substituted naphthalimide compounds and tested *in vitro* anticancer activity towards A549, MDA-MB-231 and HL-60 cancer cell lines along with LO2 and GES-1 normal cell lines. Derivative **5d-f** revealed potent anticancer activity with IC_{50} values in micromolar range, which were comparable with amonafide, a standard anticancer agent. These compounds were also evaluated for inhibition of topoisomerase II as well as receptor tyrosine kinases (RTKs). Derivatives **5a**, **5d-g** showed significant Topo II inhibition comparable with amonafide. Furthermore, derivatives **5e** and **5f** showed moderate inhibitory activity against FGFR1, VEGFR2 and PDGFRα angiogenesis-related receptor tyrosine kinases.[41]

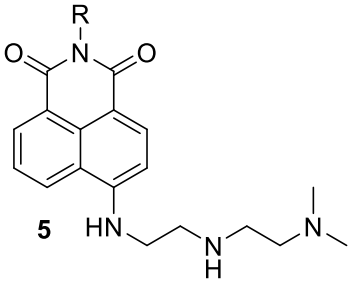

5

5a R = CH_3
5b R = C_2H_5
5c R = *n*-C_4H_9
5d R = *n*-C_6H_{13}
5e R = *n*-C_8H_{17}
5f R = *n*-$C_{12}H_{25}$
5g R = *n*-$C_{16}H_{33}$

Wang and co-workers synthesized 2-(2-(dimethylamino)ethyl)-1*H*-benzo[*de*]isoquinoline-1,3(2*H*)-dione compounds having piperazine and piperidine moieties. These derivatives were evaluated for antiproliferative activity and DNA binding affinity. It was found that compound **6c-e** containing piperidine moiety at 4-position showed significant cytotoxicity with IC_{50} values in the range of 0.73 μM-6.80 μM towards Hela, SGC-7901 and A549 tumor cell lines, whereas

compounds **6a** and **6b** containing piperazine moiety at 4-position showed strong DNA binding efficiency. Fluorescence images of derivative **6d** using A549 cancer cells revealed that fluorescence mainly seemed to occur in the cytoplasm. These results suggested the compound **6c-e** as potential anticancer candidates along with cell imaging agents.[42]

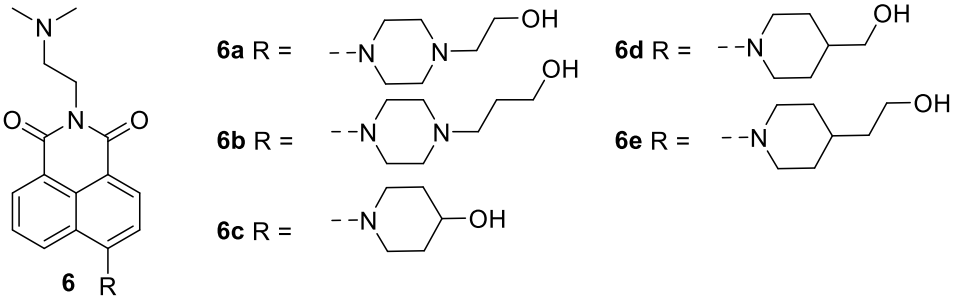

Rong and co-workers synthesized N^1-(3-aminopropyl)-N^1-methylpropane-1,3-diamine linked bis-naphthalimide compounds and tested against MCF-7, SGC-7901, A549, and Hela cancer cells for anticancer activity. All synthesized derivatives showed lower cytotoxicity towards MCF-7 human cancer cell line except derivative **7a**. Compound **7a** with substituted *N*-(2-hydroxyethyl)piperazine revealed excellent cytotoxicity with IC_{50} values of 0.88 μM, 1.21 μM, 2.31 μM, and 2.94 μM, towards Hela, SGC-7901, A549 and MCF-7 cancer cells, respectively, and have been found better than amonafide. The DNA binding study of most potent compound **7a** gave the higher binding constant 1.2×10^5 M^{-1} as a result of intercalation. Compound **7a** gave significant enhancement in the florescence intensity after binding with DNA (Hela cells), suggested that it can be a potential agent in cell imaging.[43]

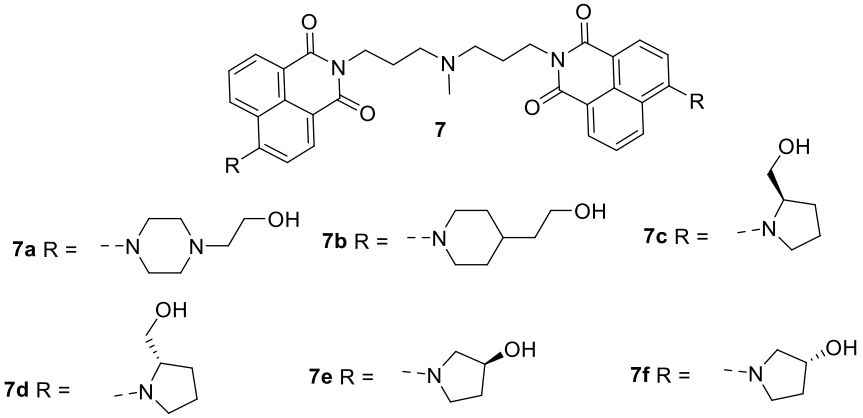

Huang and co-workers synthesized compounds of diamine linked bis-naphthalimide. The DNA binding study with ct-DNA revealed that compound **8a** with an ethylenediamine linker showed highest binding constant 3.40×10^4 M^{-1}, which was decreased with increasing linker length

and rigidity. Derivative **8a-e** were also examined for their cytotoxicity towards EC109 and BGC823 cancer cell lines with MTT assay. Anticancer results revealed that compound **8d** with *p*-xylylenediamine linker showed highest activity with IC_{50} values of 142.45 μM and 77.99 μM against EC109 and BGC823 cancer cells, respectively.[44]

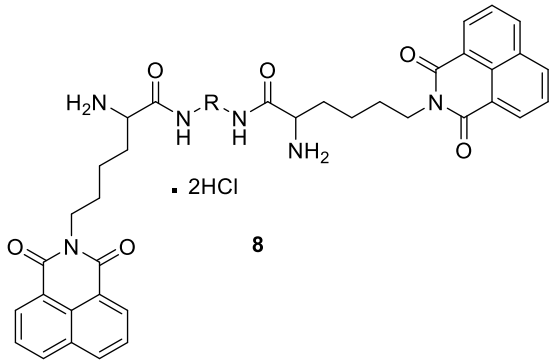

8

8a R = CH_2CH_2

8b R = $CH_2CH_2CH_2CH_2$

8c R = $CH_2CH_2CH_2CH_2CH_2CH_2$

8d R = 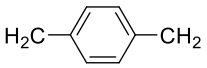

8e R = 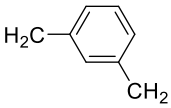

1.2 Biological activity of benzimidazole and benzothiazole based molecules

Yurttas and co-workers synthesized compounds of 2-(2-(morpholine-4-carbonothioyl)-1*H*-benzo[*d*]imidazol-1-yl)-1-phenylethan-1-one and examined for their cytotoxicity towards A549, MCF-7 and C6 cancer cells. These derivatives showed selectivity towards MCF-7 and C6 cancer cells. Compound **9d** was found to be more potent than that of cisplatin and doxorubicin towards A549 cells with IC_{50} value of 15.66 μM. Furthermore, derivative **9d** showed potency higher than cisplatin and equal to doxorubicin towards C6 cells with IC_{50} value of 9.33 μM. Results of inhibition of DNA synthesis studies suggested that, derivatives have shown concentration and time-dependent inhibitory activity. Compounds **9b** and **9c** inhibited synthesis of DNA in MCF-7 and C6 cells, whereas derivative **9d** inhibited synthesis of DNA in all tested A549, MCF-7 and C6 cancer cells. Apoptosis induction study determined that derivatives **9b**, **9c**, and **9e** induced apoptotic pathway, whereas derivative **9d** induced necrotic pathway for cytotoxicity in C6 cancer cells. Moreover, derivatives **9b** and **9d** induced cytotoxicity in MCF-7 cancer cells by apoptosis.[45]

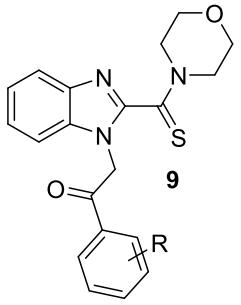

9

9a R = H
9b R = 4-Me
9c R = 4-OMe
9d R = 4-Cl
9e R = 3,4-diOMe
9f R = 2,4-diCl
9g R = 3,4-diF

Shao and co-workers synthesized 2-(((4-phenylpyrimidin-2-yl)thio)methyl)-1*H*-benzo[*d*]imidazole compounds and tested for antitumor activity towards MCF-7, SMMC-7721, EC-9706 and MGC-803 human cancer cells. Anticancer results revealed that derivatives showed highest sensitivity towards MGC-803 and MCF-7 cancer cells. Compounds **10c**, **10d**, **10e** and **10f** found as potent member of the series and shown more cytotoxicity than that of 5-florouracil against MCF-7, EC-9706 and MGC-803 cancer cells. Derivatives **10c** and **10d** have shown cytotoxicity with IC_{50} values of 1.33 μM and 2.03 μM, respectively towards MGC-803 cancer cells followed by MCF-7 cells with IC_{50} values of 1.43 μM and 2.90 μM, respectively. Compounds **10e** and **10f** exhibited cytotoxicity against MGC-803 cancer cells with IC_{50} values of 1.07 μM and 1.06 μM, respectively, whereas these compounds showed cytotoxicity against MCF-7 cancer cells with IC_{50} values of 1.40 μM and 1.95 μM, respectively. Flow cytometry analysis revealed that derivative **10e** arrested the cell cycle in G2/M phase in MGC-803 cancer cells.[46]

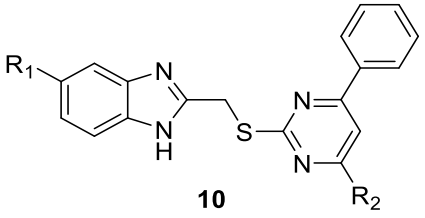

10

10a R_1 = H, R_2 = OH
10b R_1 = Cl, R_2 = OH
10c R_1 = H, R_2 = NH-C_6H_4-4CH_3
10d R_1 = H, R_2 = NH-C_6H_4-4OCH_3
10e R_1 = Cl, R_2 = NH-C_6H_4-4CH_3
10f R_1 = Cl, R_2 = NH-C_6H_4-4OCH_3.

Rahim and co-workers synthesized compounds of ethyl 2-phenyl-1*H*-benzo[*d*]imidazole-5-carboxylate and examined for anticancer activity towards MDA-MB-231 and MCF-7 cancer cell lines. The results showed that all derivatives displayed selective cytotoxicity against MDA-MB-231 cancer cells in micromolar range. Derivative **11a** has been found as the most active candidature of the series with IC_{50} value of 29.7 μM towards MDA-MB-231 cancer cells. Derivative **11c** was also exhibited good anticancer activity towards MDA-MB-231 cancer cells with IC_{50} value of 36.8 μM followed by compound **11f** with IC_{50} value of 47.6 μM. Derivatives **11b** and **11e** also showed promising anticancer activity.[47]

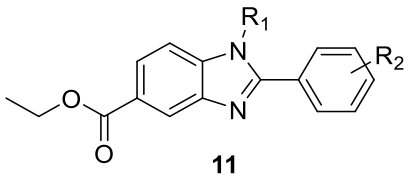

11

11a R_1 = *sec*-butyl, R_2 = H
11b R_1 = *sec*-butyl, R_2 = 4-Br
11c R_1 = *sec*-butyl, R_2 = 2-NO_2
11d R_1 = *tert*-butyl, R_2 = 4-CH_3
11e R_1 = *tert*-butyl, R_2 = 4-OCH_3
11f R_1 = *tert*-butyl, R_2 = 2,4-diCl

Mortimer and co-workers optimized synthesis and *in vitro* cytotoxicity of substituted 2-phenyl benzimidazoles towards MCF-7, MDA 468, KM 12 and HCC 2998 cancer cells.

Anticancer results shown that all compounds displayed potent cytotoxicity towards tested cancer cells and gave GI_{50} values in the range of nanomolar to micromolar. Derivative **12d** was found as a most active candidate of the series with GI_{50} value of < 0.1 nM for MCF-7 and MDA 468 cancer cells. Derivative **12d** also showed potent cytotoxicity against HCC 2998 and KM 12 cancer cells with GI_{50} values of 0.25 nM and 0.29 μM, respectively. Structure-activity relationships recognized that derivative **12d** showed cytotoxicity with highest potency, and further any structural changes showed deactivating cytotoxic effect. Furthermore, derivative **12e** also showed cytotoxicity in nanomolar range against MCF-7 cells with GI_{50} value of 0.7 nM. Derivative **12d** was also capable for the induction to expression of CYP1A1 protein in a dose-dependent manner in MCF-7 and MDA 468 cells with inducible CYP1A1.[48]

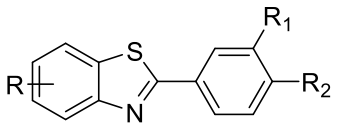

12

12a R = H, R_1 = OH, R_2 = OH
12b R = H, R_1 = OMe, R_2 = OMe
12c R = 5-F, R_1 = H, R_2 = OMe
12d R = 5-F, R_1 = OMe, R_2 = OMe
12e R = 5-F, R_1 = OEt, R_2 = OEt
12f R = 5-Cl, R_1 = OMe, R_2 = OMe

Osmaniye and co-workers synthesized derivatives of (*E*)-2-(benzo[*d*]thiazol-2-ylthio)-*N*′-(4-cyclohexylbenzylidene)acetohydrazide and examined their cytotoxicity towards MCF-7, A549, HT-29 and C6 cancer cells along with NIH3T3 normal cells. Results of anticancer studies revealed that derivatives **13d**, **13e** and **13f** exhibited potent cytotoxicity towards C6 cancer cell line. Additionally, these derivatives did not show cytotoxicity towards NIH3T3 normal cells. Derivative **13d** triggered a selective cytotoxicity towards C6 cells, equivalent to cisplatin. Derivative **13e** gave the highest anticancer activity towards A549 cells with IC_{50} value of 0.03 mM which was two-fold fewer than that of cisplatin. Derivatives **13d**, **13e**, and **13f** revealed inhibition of DNA synthesis in a dose-dependent manner in C6 cells. Additionally, derivatives **13d**, **13e** and **13f** exhibited dose-dependently induced apoptotic cell death.[49]

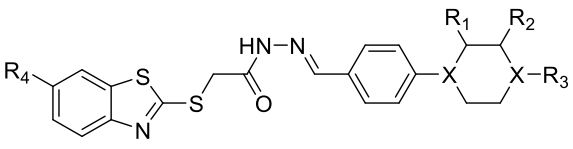

13

13a R_1 = H, R_2 = H, R_3 = H, R_4 = Cl, X = CH
13b R_1 = Me, R_2 = H, R_3 = H, R_4 = Cl, X = CH
13c R_1 = H, R_2 = Me, R_3 = H, R_4 = Cl, X = CH
13d R_1 = H, R_2 = H, R_3 = Me, R_4 = Cl, X = CH
13e R_1 = H, R_2 = H, R_3 = 4-OMePh, R_4 = Cl, X = N
13f R_1 = H, R_2 = Me, R_3= H, R_4 = OMe, X = CH

1.3 Biological activity of imidazo[1,2-*a*]pyrazine based compounds

Myadaraboina and co-workers designed and synthesized 2,3,6-tri-substituted imidazo[1,2-*a*]pyrazine derivatives and studied *in vitro* for antiproliferative activity against MCF-7, SK-N-SH,

HepG-2 and MDA-MB-231 cancer cell lines. Derivative **14a** displayed significant anti-proliferative activity towards cancer cells with IC_{50} value of 12.9 μM and 13.8 μM towards MCF-7 and SK-N-SH cancer cells, respectively. Substitution of *p*-fluoro at C3-phenyl ring (**14c**) enhanced ten-folds activity towards SK-N-SH, HepG-2 and MDAMB-231 cancer cells, whereas, in MCF-7 cancer cells only two-folds enhancement were observed. Derivative **14c** displayed the best anti-proliferative activity for all tested cancer cells with IC_{50} values of 1.0 μM, 6.2 μM, 15.2 μM and 61.1 μM against SK-N-SH, MCF-7, MD-AMB-231 and HepG-2 cancer cells, respectively. Rest of the derivatives showed much lower anticancer activities.[50]

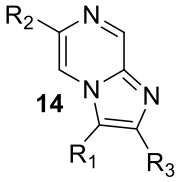

14

14a R_1 = Br, R_2 = CH_3, R_3 = 4-C_6H_4F
14b R_1 = Br, R_2 = CH_3, R_3 = 4-$C_6H_4CH_3$
14c R_1 = Br, R_2 = CH_3, R_3 = Ph
14d R_1 = Br, R_2 = H, R_3 = Ph
14e R_1 = CN, R_2 = CH_3, R_3 = Ph
14f R_1 = CN, R_2 = CH_3, R_3 = 4-C_6H_4F
14g R_1 = CN, R_2 = H, R_3 = 4-C_6H_4Cl
14h R_1 = CN, R_2 = H, R_3 = 4-C_6H_4F

Xu and co-workers studied on 8-morpholinoimidazo[1,2-*a*]pyrazine based compounds (**15-17**) and tested towards MCF-7, A549 and PC-3 cancer cells for their anticancer activity. All synthesized derivatives showed moderate to good anticancer activity towards tested cancer cells with IC_{50} values in range of 6.39 μM - 74.92 μM. Compound **17b** showed cytotoxicity with IC_{50} value of 3.69 μM against MCF-7 cancer cells, whereas compound **17c** found to be most active with IC_{50} value of 6.39 μM towards A549 cancer cells. Most potent derivatives **17b** and **17c** were further investigated for inhibitory activity towards PI3Kα kinase and found that compound **17c** showed inhibition with IC_{50} value of 1.25 μM.[51]

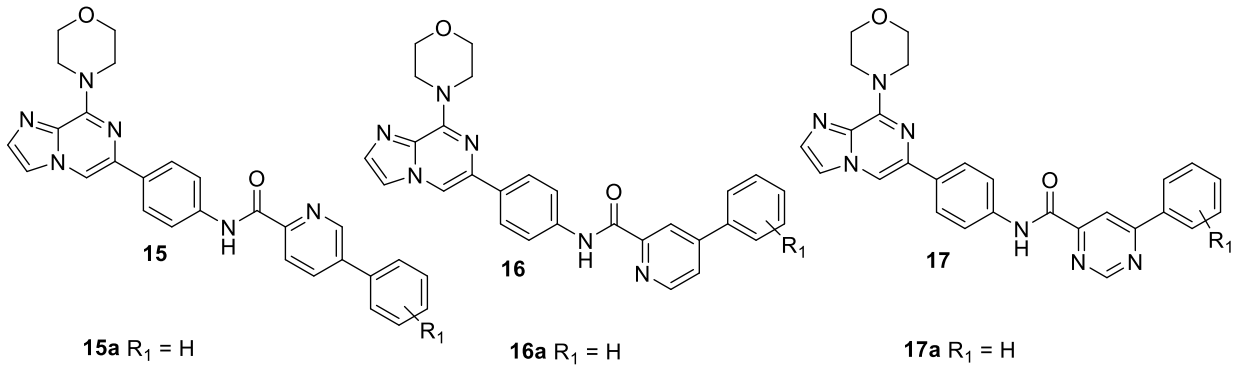

15

15a R_1 = H
15b R_1 = 3-fluoro
15c R_1 = 2,4-difluoro

16

16a R_1 = H
16b R_1= 3-fluoro
16c R_1 = 2,4-difluoro

17

17a R_1 = H
17b R_1 = 4-methyl
17c R_1 = 4-methoxy

Demirayak and co-workers synthesized compounds of 6,8-diphenylimidazo[1,2-*a*]pyrazine and examined for their anticancer activity at NCI against 60 cancer cell lines. Anticancer results showed that derivative **18b-f** gave $\log_{10}$ GI_{50} values < –4, therefore, all

derivatives exhibited significant cytotoxicity against tested cancer cells. The value of meangraph midpoint for derivative **18d** (-6.29) was found to be more than that of cisplatin (-6.20) and for derivative **18b-d** (-5.10 to -6.29), the values are more than that of melphalan (-5.09). These results demonstrated that derivative **18b-d** provided high levels of cytotoxicity. Detailed examination of anticancer results shown that all derivatives provided effective cytotoxicity in low doses towards leukemia. Derivative **18d** was found as a most potent candidate, which provided even more cytotoxicity than that of melphalan towards leukemia.[52]

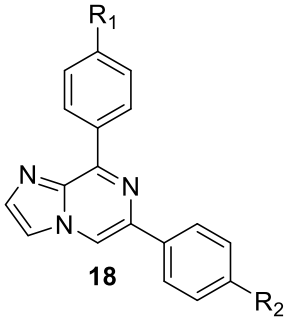

18

18a R_1 = H, R_2 = H
18b R_1 = OMe, R_2 = Me
18c R_1 = Cl, R_2 = H
18d R_1 = Cl, R_2 = Me
18e R_1 = Cl, R_2 = OMe
18f R_1 = Cl, R_2 = Cl

1.4 Biological activity of phenanthroimidazole (imidazo-phenanthroline) based molecules

Patel and co-workers synthesized compounds of 2-phenyl-1*H*-phenanthro[9,10-*d*]imidazole as well as 2-phenyl-1*H*-imidazo[4,5-*f*][1,10]phenanthroline and were examined for their antitumor activity towards HCT116, WM266.4 and MCF-7 cancer cell lines. Results of anticancer studies towards HCT116 cancer cells showed that all phenanthro[9,10-*d*]-imidazole derivatives gave potency comparable to apoptozole (GI_{50} = 7.0 μM), with GI_{50} values in the range from 3.5 μM to 11.2 μM with derivative **19c** having GI_{50} value of 3.0 μM, being two-folds more potent than apoptozole. Imidazo[4,5-*f*][1,10]phenanthroline **19g** revealed 80-folds more potent activity than

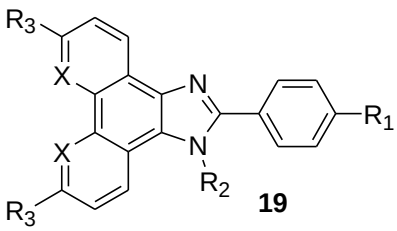

19

19a X = CH, R_1 = H, R_2 = H, R_3 = H
19b X = CH, R_1 = F, R_2 = H, R_3 = H
19c X = CH, R_1 = OMe, R_2 = H, R_3 = H
19d X = CH, R_1 = H, R_2 = H, R_3 = OMe
19e X = CH, R_1 = H, R_2 = CH_3, R_3 = H
19f X = CH, R_1 = H, R_2 = benzyl, R_3 = H
19g X = N, R_1 = H, R_2 = H, R_3 = H
19h X = N, R_1 = H, R_2 = CH_3, R_3 = H
19i X = N, R_1 = H, R_2 = benzyl, R_3 = H

apoptozole, with GI_{50} value of 0.09 μM against HCT116 cancer cells. Derivative **19g** also exhibited desired action on depletion of client protein. All derivatives exhibited cellular biomarker inhibition of Hsc70 as well as depletion of Hsp90 client proteins.[53]

Wang and co-workers have synthesized derivatives of 2-phenyl-1*H*-phenanthro[9,10-*d*]imidazole with variation in length of polyglycol side chain and were examined for their cytotoxicity as well as DNA binding. Derivative **20a** displayed higher anticancer activity than cisplatin with IC_{50} values of 4.65 μM, 6.36 μM and 7.03 μM towards Bel-7402, BGC-823 and KB cancer cells, respectively. Compounds **21b** and **21c** have been found more potent than their corresponding derivatives **20b** and **20c** towards KB, BGC-823 and Bel-7402 tumor cell lines. Results suggested that anticancer activities of **20a-c** were reduced with increasing length of polyglycol side chain, whereas the anticancer activities of **21a-c** were improved with increasing side chain length. Derivatives **21a-c** interacted with DNA through intercalation and compound **21a** gave the highest binding constant of 1.68×10^6 M^{-1}.[54]

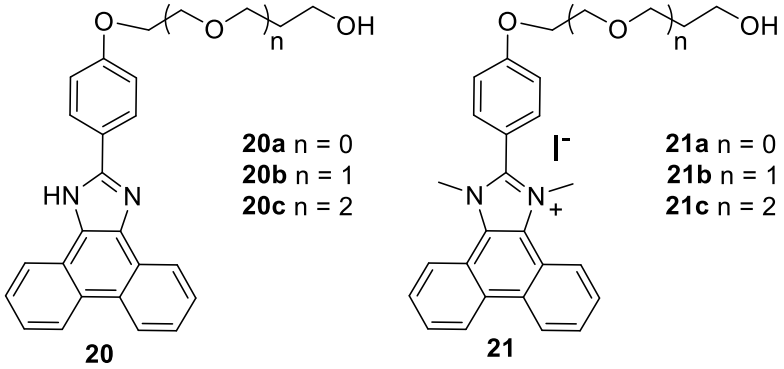

Liao and co-workers synthesized 2-(2,4-disubstitutedphenyl)-1*H*-imidazo[4,5-*f*][1,10]phenanthroline derivatives and evaluated their antitumor activity. These compounds showed potent anticancer activity towards MDA-MB-231, Hela and MCF-7 cancer cells. Derivative **22e** exhibited ten-folds more cytotoxicity than that of cisplatin towards MDA-MB-231 cancer cell line with IC_{50} value of 3.6 μM, whereas derivative **22d** found equally potent with cisplatin having IC_{50} value of 36.0 μM. Derivatives **22a**, **22d** and **22e** have been found more potent than cisplatin against Hela cells with IC_{50} values of 5.1 μM, 7.9 μM and 8.5 μM, respectively. Further studies revealed that derivative **22e** can effectively bound and stabilize *c-myc* G4 DNA structure.[55]

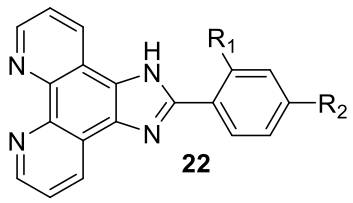

22a R_1 = H, R_2 = H
22b R_1 = SO_3H, R_2 = H
22c R_1 = H, R_2 = SO_3H
22d R_1 = Br, R_2 = H
22e R_1 = H, R_2 = Br

1.5 Biological activity of thiazolidine-2,4-dione based molecules

Liu and co-workers synthesized thiazolidine-2,4-dione derivatives and **23d** has been found as a representative member of the series with improved cytotoxicity against U937 human leukemia cancer cells with IC_{50} value of 3.4 μM. Derivatives **23a**, **23b** and **23c** also showed good cytotoxicity against U937 cancer cells with IC_{50} values of 9.4 μM, 9.6 μM and 10.0 μM, respectively. The level of p-MEK, p-ERK and p-Akt expression was significantly suppressed by derivative **23d** at 3 μM concentration in U937 cells. The results demonstrated that blockage of signals of Raf/MEK/ERK and PI3K/Akt cascades could be the reason of cytotoxicity of U937 cells. Further studies showed that derivative **23d** induced anticancer activity towards U937, DU145 and M12 cancer cell lines through apoptosis. Cell cycle analysis indicated that derivative **23d** arrested the cell cycle in S phase in U937 cancer cells.[56]

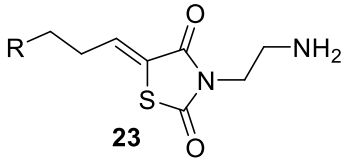

23

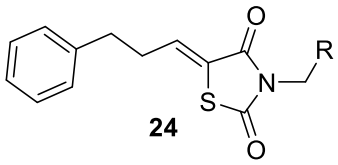

24

23a R = 4-OMePh
23b R = 4-NO_2Ph
23c R = 3-pyridine
23d R = cyclohexyl

24a R = CH_2OH
24b R = COOH
24c R = methylmorpholine

Patil and co-workers synthesized 5-benzylidene-2,4-thiazolidinedione derivatives and examined for their cytotoxicity towards a panel of seven cancer cell lines consisting of K562, HOP62, GURAV, MCF7, HEPG2, PC3 and KB cancer cell lines. Results of anticancer study suggested that derivative **25d** found as the most promising candidate with $\log_{10}GI_{50}$ values in the range of -6.73 μM to -5.60 μM towards MCF 7, PC3, KB, GURAV and K562 cancer cells. In addition, derivatives **25a**, **25b** and **25e** were also showed potent cytotoxicity against HOP62 cancer cells with $\log_{10}GI_{50}$ values of -6.72 μM, -6.73 μM and -6.77 μM, respectively. Derivatives **25c** and **25d** presented cytotoxicity comparable to that of doxorubicin towards GURAV cancer cells with$\log_{10}GI_{50}$ values of -6.71 μM and -6.73 μM, respectively. Whereas derivatives **25f** and **25g** displayed favorable anticancer activity towards GURAV cancer cells with $\log_{10}GI_{50}$ values of -4.50 μM and -4.41 μM, respectively. None of the derivatives exhibited anticancer activity towards HEPG2 liver cancer cells.[57]

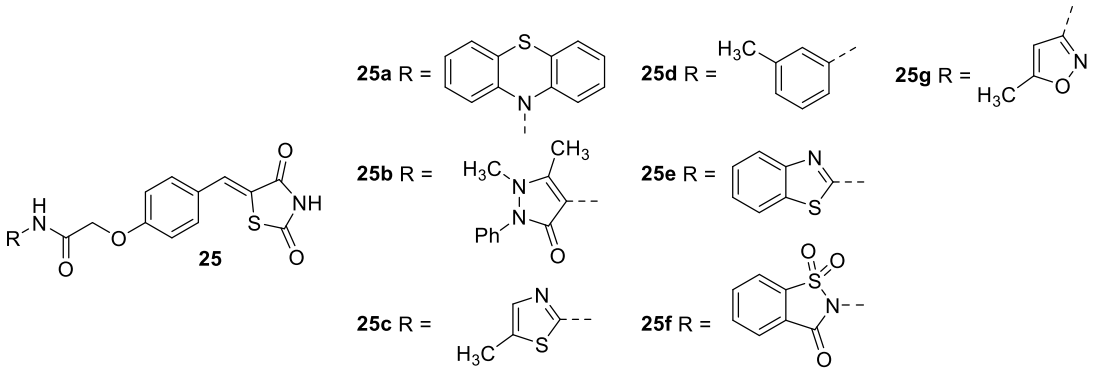

1.6 Biological activity of indole based molecules

Regina and co-workers synthesized compounds of 5, 6 or 7-substituted indole bearing 3,4,5-trimethoxyphenyl connected by sulfur or ketone linkage. It has been observed that substitution of furan or thiophene moiety at 6 or 7 position of indole, exhibited significant inhibition towards tubulin polymerization, colchicine binding and MCF-7 cancer cell line. Derivatives **26a** and **26b** showed significant inhibition towards U87MG, HCT116, T98G, PC3, U343G, MV4-11, HT29, THP-1, A-549, HepG2 and multidrug resistant NCI/ADR-RES cell lines at nanomolar concentrations. Further, in the G2/M phase, derivatives **26a** (20 nM) and **26b** (100 nM) arrested 77% and 71% cell cycle, respectively. Derivative **26a** at concentration of 50 nM, significantly inhibited tubulin polymerization, which was comparable to the reference drug vinblastine, whereas, derivative **26b** at the concentration of 100 nM affected only structural arrangement of mitotic spindle and was not able to fully inhibition of tubulin polymerization. Compounds **26a** and **26b** inhibited HepG2 cancer cells with IC_{50} values of 20 nM and 80 nM, respectively. Derivative **26a** also showed potent intibition against U87MG glioblastoma human cells at nanomolar range.[58]

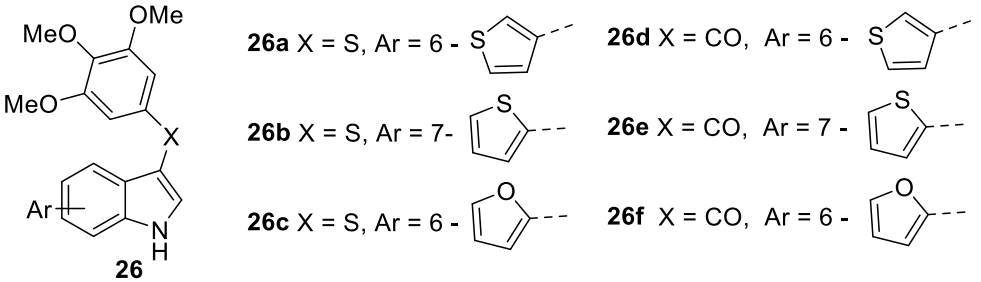

Regina and co-workers synthesized derivatives of 2-phenylindole containing 3,4,5-trimethoxyphenyl attached by sulfur, ketone or methylene linker. Inhibition of the tubulin polymerization was presented by most of the synthesized compounds with IC_{50} values of 1.0-2.0 μM. Half of the synthesized derivatives presented cytotoxicity towards MCF-7 cancer cell line

with $IC_{50} \leq 50$ nM. Derivatives **27a** and **27b** uniformly inhibited the panel of cancer cell lines at nanomolar concentration and were found superior than vinblastine and paclitaxel. Derivatives **27a** and **27b** showed excellent growth inhibition of multi-drug-resistant (MDR) cell lines namely NCI/ADR-RES as well as Messa/Dx5 at 10 nM. Further derivatives **27a** and **27b** exhibited the cytotoxicity against natural killer (NK) cells even at very low concentration i.e. 10 nM and showed more than 80% cell cycle arrest in G2/M phase of the HeLa cells at 20 - 50 nM concentration.[59]

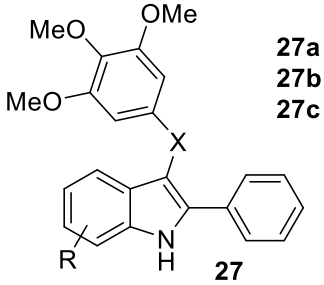

27

27a X = S, R = 6-OMe **27d** X = CO, R = 6-OMe **27g** X = CH_2, R = 5-OMe
27b X = S, R = 6,7-diCl **27e** X = CO, R = 6,7-diCl **27h** X = CH_2, R = 6-Cl
27c X = S, R = 4-Br **27f** X = CO, R = 4-Br **27i** X = CH_2, R = 5-Br

Gaikwad *et al.* synthsiszed series of 2-phenylindole derivatives and examined *in vitro* for their cytotoxicity towards B16F10, A549 and MDA-MB-231 cancer cells. Derivatives revealed significant cytotoxicity against all tested cancer cells. Derivative **28a-k** showed effective anticancer activity towards B16F10 cancer cells with IC_{50} values in range of 23.81 μM - 60.11 μM. Compound **28b** gave potent cytotoxicity towards A549 cancer cells with IC_{50} value of 29.12 μM. Moreover, derivatives **28j** and **28k** have shown good antitumor activity with IC_{50} values of 16.18 μM and 25.59 μM, respectively towards MDA-MB-231 human cancer cells. Molecular docking study revealed effective binding of these compounds with NEDD4-1 and EGFR receptor proteins.[60]

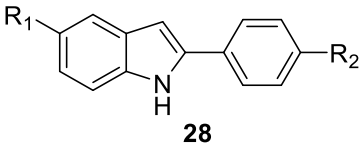

28

28a R_1 = H, R_2 = H **28g** R_1 = H, R_2 = OMe
28b R_1 = H, R_2 = Me **28h** R_1 = Me, R_2 = H
28c R_1 = Me, R_2 = Me **28i** R_1 = Me, R_2 = F
28d R_1 = H, R_2 = Cl **28j** R_1 = H, R_2 = NO_2
28e R_1 = Me, R_2 = Cl **28k** R_1 = Me, R_2 = NO_2
28f R_1 = H, R_2 = F

1.7 Molecular hybridization approch

Mixture of drugs, one of the strategies employed by clinicians to treat unresponsive patients, has further encouraged the researchers toward the design of ligands comprising two or more pharmacophores in a single biological molecule, modulating multiple targets. Hybrid drugs, designed by molecular hybridization approach, are the molecules having two or more potent pharmacophores connected by covalent bonding, which leads to a therapeutical potency superior

than individual scaffold. Hybrid drugs are basically designed to interact with multiple targets or to amplify its effect through action on another bio target as one single molecule or to counterbalance the known side effects associated with the other hybrid part.[11,12]

Chen and co-workers synthesized three series of hybrids of chalcone and indole (**29-31**), and were examined for antitumor activity towards A549, HeLa, Bel-7402, PC-3 and K562 cell lines. These derivtives revealed moderately to very good antitumor activities. Derivative **29a**, exhibited potent antitumor activity against tested five tumor cell lines with GI_{50} values in range of 0.026 μM - 0.035 μM. Further studies exhibited that derivative **29a** inhibited tubulin polymerization with IC_{50} value of 1.99 μM, which was comparable with reference combretastatin A-4. Moreover, derivative **29a** showed disruption of microtubule in HeLa cells and arrested the cell cycle in G2/M phase and led to cell apoptosis.[61]

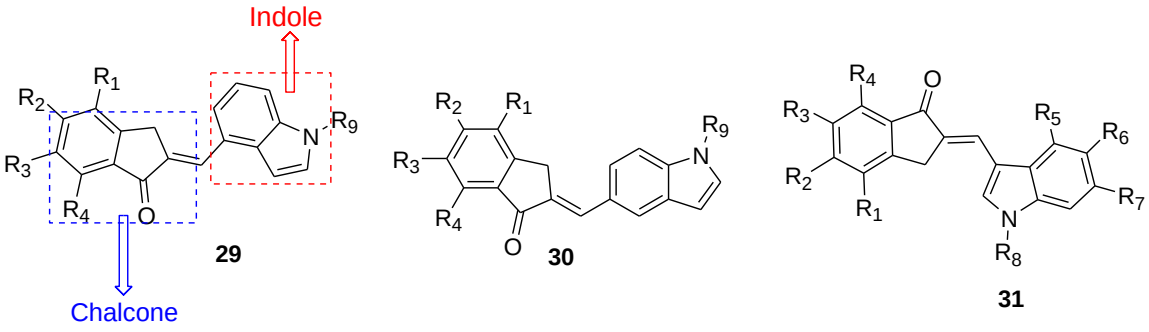

29a/30a $R_1 = R_2 = R_3 = OCH_3$, $R_4 = R_9 = H$
29b/30b $R_1 = R_2 = R_3 = OCH_3$, $R_4 = H$, $R_9 = CH_3$
29c/30c $R_2 = R_3 = R_4 = OCH_3$, $R_1 = R_9 = H$
31a $R_1 = R_2 = R_3 = R_5 = OCH_3$, $R_4 = R_6 = R_7 = R_8 = H$
31b $R_1 = R_2 = R_3 = R_5 = OCH_3$, $R_4 = R_6 = R_7 = H$, $R_8 = CH_3$
31c $R_1 = R_2 = R_3 = R_6 = OCH_3$, $R_4 = R_5 = R_7 = R_8 = H$

Wang and co-workers synthesized hybrids of chrysin-benzimidazole moieties and were examined for their cytotoxicity towards MGC-803, MCF-7, HepG2 and MFC cancer cell lines. Derivative **32a** displayed potent antitumor activity towards MFC cancer cells with IC_{50} value of 25.72 μM. Compound **32a** induced apoptosis in a dose dependent manner in MFC cancer cells and caused cell cycle arrest in the G0/G1 phase. Derivative **32a** was also evaluated *in vivo* in mice and showed significant inhibition in tumor growth.[60]

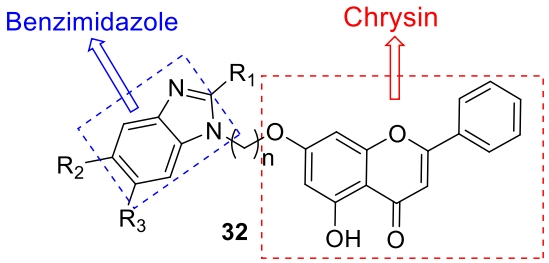

32a n = 4, $R_1 = CH_3$, $R_2 = H$, $R_3 = H$
32b n = 4, $R_1 = Cl$, $R_2 = H$, $R_3 = H$
32c n = 3, $R_1 = H$, $R_2 = H$, $R_3 = H$
32d n = 3, $R_1 = H$, $R_2 = H$, $R_3 = NO_2$
32e n = 2, $R_1 = H$, $R_2 = OCH_3$, $R_3 = OCH_3$

Li and co-workers synthesized derivatives of pyrazole-naphthalimide conjugates and evaluated i*n vitro* anticancer activity towards MCF-7, Hela and A549 cancer cells. Derivatives **33a-d** displayed better antitumor activity than amonafide towards MCF-7 cancer cells with IC_{50} values of 0.51 μM, 0.79 μM, 1.56 μM and 1.58 μM, respectively. Derivative **33a** showed potent anticancer activity towards Hela and A549 cancer cells with IC_{50} values of 3.09 μM and 5.14 μM, respectively, which were 2.2-folds and 2.5-folds lesser than that of amonafide. DNA binding experiments of derivative **33a** with ct-DNA revealed intercalation binding mode with binding constant (K_b) of 1.01×10^4 M^{-1}.[63]

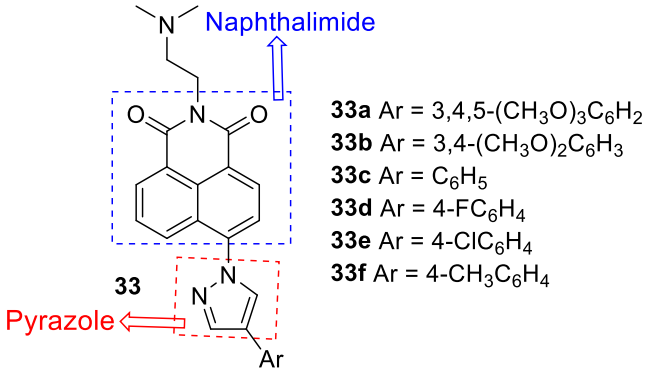

33a Ar = 3,4,5-$(CH_3O)_3C_6H_2$
33b Ar = 3,4-$(CH_3O)_2C_6H_3$
33c Ar = C_6H_5
33d Ar = 4-FC_6H_4
33e Ar = 4-ClC_6H_4
33f Ar = 4-$CH_3C_6H_4$

Singla and co-workers synthesized isomeric series of triazine-benzimidazole conjugates. Synthesized derivatives were examined towards a panel of 60 malignant cell lines and mammalian

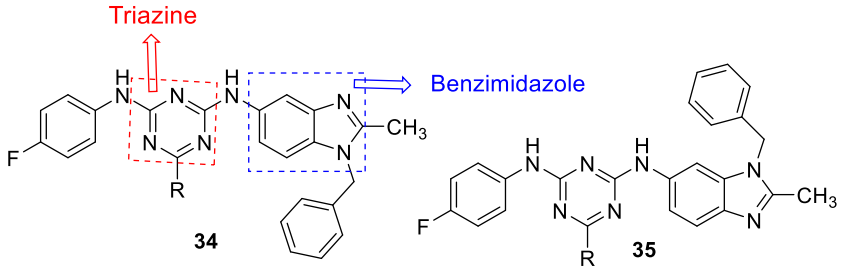

34a R = 4-methylpiperazin-1-yl
34b R = pyrrolidin-1-yl
34c R = 4-aminothiophenol
34d R = 4-fluorophenyl
34e R = 4-methoxyphenyl

35a R = pyrrolidin-1-yl
35b R = 2-aminoethylmorpholine
35c R = 4-methypiperazin-1-yl
35d R = ethylenediamine
35e R = ethanolamine

dihydrofolate reductase. Derivatives **34a** and **34b** have been found as potent anticancer compounds with mean GI_{50} values of 1.77 μM and 1.94 μM, respectively, against nine panel of cancer cell lines. Derivative **34a** was established as most active towards leukemia with GI_{50} value of 1.43 μM, while derivative **35b** significantly inhibited dihydrofolate reductase in nanomolar concentration with IC_{50} value of 2.0 nM having ligand efficiency 0.3 M. The results of DNA binding experiments were shown strong interaction of ct-DNA with triazine - benzimidazole conjugates.[64]

CHAPTER 2
HYBRIDS OF IMIDAZO[1,2-*a*]PYRAZINE AND BENZIMIDAZOLE

2.1 Introduction

DNA is one of the key targets for anti-proliferative activity. Generally, antitumor candidates damage DNA or block DNA synthesis indirectly through inhibition of nucleic acid precursor biosynthesis, or disrupt hormonal stimulation of cell growth.[65] So, more efficient, less toxic, and target-specific non-covalently DNA binding anticancer drug needs to be developed. Extensive efforts have been currently centered on the development of new anticancer drugs based on combination of two active pharmacophores, particularly, planar moieties, that are effective for binding and cleavage of DNA under physiological conditions.[66] The planar structures of benzimidazole and imidazo[1,2-*a*]pyrazine facilitate the compounds that bind strongly with DNA through intercalation and hence, affect the critical metabolic routes. A large number of derivatives based on these moieties has been designed and evaluated for antitumor activity.[17-20] The anticancer activities of benzimidazoles appear to derive from their ability to form strong complexes with nucleic acids and thus induce DNA damage, and exert related effects such as topoisomerase poisoning, telomerase inhibition and inhibition of gene transcription.[21-23] To regulate the interaction properties of drugs, different substituents as well as new rings (quinazoline, triazine, purine, naphthalimide etc) were introduced in the benzimidazole moiety. With these derivatives, maximum toxicity was obtained with compounds substituted at position -5 or -6 of benzimidazole, and in particularly with 2-chlorophenyl, 2-methoxyphenyl and pyrrolidine analogues.[32,64,67,68] Additionally, it has turned out that some of these compounds were also evaluated for cell lines which displayed positive activity on tumor cells. We anticipated that the proposed molecules with 5- or 6-substituted benzimidazole would also intercalate in DNA, and favor the interaction with nucleophilic sites of nucleic acid bases.

To check these binding interactions and antitumor activity, this chapter discuss the chemical reactivity of two series of imidazo[1,2–*a*]pyrazines, with different orientations of benzimidazole possessing cyclohexyl ring. To elucidate the impact of variation of substitution at 6- and 8- positions of imidazo[1,2-*a*]pyrazine, we have also prepared symmetrical and unsymmetrical benzimidazole substituted-imidazo[1,2-*a*]pyrazines whereby compounds showed

pronounced antitumor activity. It has been observed that the most promising compounds inhibited tumor growth, which were also related to their high DNA and BSA binding capacity.[29,69]

2.2 Chemistry

All compounds (**9-23**, **31-49** and **53-57**) were prepared according to the **Schemes 1-3** starting from 1,3- and 1,4-dibromobenzene. 1,4-Dibromobenzene **1** was first nitrated with 1:4 ratio of nitric acid and sulphuric acid to yield 1,4-dibromo-2-nitrobenzene **2** in 93% yield. Compound **2** was subjected to regioselective nucleophilic substitution reaction with cyclohexylamine in the presence K_2CO_3 in DMF to afford 4-bromo-*N*-cyclohexyl-2-nitroaniline **3** in 75% yield. Formation of intermediate **3** was supported by NMR spectral analysis, the characteristic multiplet at δ 3.52-3.43 ppm for one proton and signals ranging from 2.14 to 1.25 for ten protons correspond to cyclohexyl ring. Boronation of **3** was then carried out using bis(pinacolato)diboron in the presence of $Pd(PPh_3)_2Cl_2$ and KOAc, afforded *N*-cyclohexyl-2-nitro-4-(4,4,5,5-tetramethyl-1,3,2-dioxaborolan-2-yl)aniline **4** in 82% yield. Compound **4** was characterized by NMR with the help of characteristic signals of four methyl groups of boronate having singlet of 12 protons at δ 1.32 ppm. Suzuki-Miyaura cross coupling reaction of **4** with dibromo imidazo[1,2-*a*]pyrazine **5** (prepared in two steps from commercial available 2-aminopyrazine according to the literature method)[26,70] has been proceeded using $Pd(PPh_3)_4$ and K_2CO_3 to yield 4-(6-bromoimidazo[1,2-*a*]pyrazin-8-yl)-*N*-cyclohexyl-2-nitroaniline **6** in 73% yield with traces of disubstituted product. Reduction of **6** was carried out using sodium dithionite to afford 4-(6-bromoimidazo[1,2-*a*]pyrazin-8-yl)-N^1-cyclohexylbenzene-1,2-diamine **7** which was subsequently cyclized with triethylorthoformate in acetic acid to afford the requisite 6-bromo-8-(1-cyclohexyl-1*H*-benzo[*d*]imidazol-5-yl)imidazo[1,2-*a*]pyrazine **8** in 75% yield (**Scheme 1**). Compound **8** was confirmed by ^{1}H NMR with shifting of multiplet to downfield at δ 4.26-4.18 ppm for one proton corresponding to CH of cyclohexane and absence of NH signal at δ 8.40 ppm. Initially, the Suzuki coupling of **8** and phenyl boronic acid was selected as a model reaction for optimization of reaction parameters, and the results have been displayed in **Table 1**. Optimization for reaction condition of Suzuki coupling was done by changes in catalyst, base and solvents. The best results were obtained with (entry 6). Compound **8** was further used for Suzuki reaction with substituted phenyl, thienyl and naphthyl boronates to give derivatives **9-23** in 75-86% yields.

Table 1. Optimization of palladium catalysed Suzuki-Miyaura cross-coupling reactions

Entry	Time (h)	Catalyst	Base	Solvent	Yield (%)
1	15	$Pd(PPh_3)_2Cl$	Cs_2CO_3	CH_3CN-H_2O (9:1)	72
2	18	$Pd_2(dba)_3$	Cs_2CO_3	CH_3CN-H_2O (9:1)	70
3	12	$Pd(PPh_3)_4$	Cs_2CO_3	CH_3CN-H_2O (9:1)	80
4	15	$Pd(PPh_3)_4$	K_2CO_3	Toluene	82
5	14	$Pd(PPh_3)_4$	K_2CO_3	Toluene-H_2O (9:1)	78
6	**12**	**$Pd(PPh_3)_4$**	**K_2CO_3**	**CH_3CN-H_2O** (9:1)	**85**
7	16	$Pd(PPh_3)_4$	DIPEA	CH_3CN-H_2O (9:1)	65
8	22	$Pd(PPh_3)_4$	K_2PO_3	CH_3CN-H_2O (9:1)	45
9	13	$Pd(PPh_3)_4$	K_2CO_3	IPA	69
10	18	$Pd(PPh_3)_4$	K_2CO_3	Acetone	73
11	18	$Pd(PPh_3)_4$	K_2CO_3	DMF	72
12	16	$Pd(PPh_3)_4$	K_2CO_3	THF	78

Scheme 1. Synthesis of 6-substituted-8-(1-cyclohexyl-1*H*-benzo[*d*]imidazol-5-yl)imidazo[1,2-*a*]pyrazine[a]

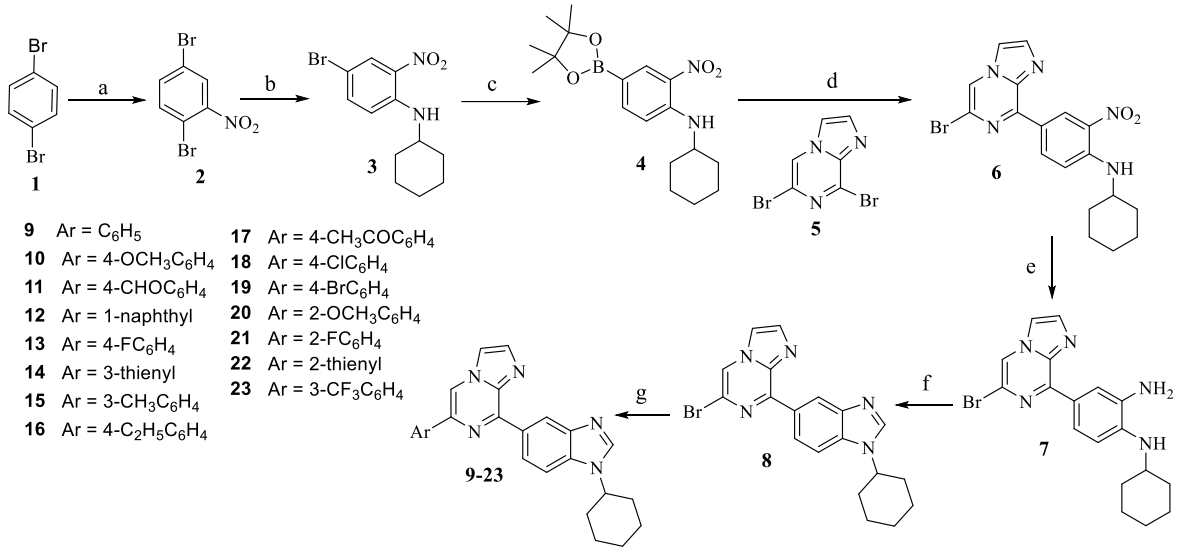

[a]Reagents and conditions: (a) H_2SO_4, HNO_3, DCM, 0 °C, 30 min., 93%; (b) Cyclohexyl amine, K_2CO_3, DMF, 100 °C, 18 h, 75%; (c) Bis(pinacolato)diboron, $Pd(PPh_3)_2Cl_2$, KOAc, 1,4-dioxane, reflux, 10 h, 82%; (d) $Pd(PPh_3)_4$, K_2CO_3, CH_3CN : water (9:1), N_2, reflux, 12 h, 73%; (e) $Na_2S_2O_4$, aq. NH_3, THF : water, rt, 1 h; (f) Triethylorthoformate, AcOH, rt, 10 min., 75%; (g) $ArB(OH)_2$, $Pd(PPh_3)_4$, K_2CO_3, CH_3CN : water (9:1), N_2, reflux, 12-15 h, 75-86%

The synthesis of intermediate **30a-b** of imidazo[1,2-*a*]pyrazine and benzimidazole conjugates followed the similar procedure with 1,3-dibromobenzene as starting material (**Scheme 2**). The commercial available 1,3-dibromobenzene **24** was nitrated to yield **25** in 95% yield which was regioselectively substituted with cyclohexylamine and benzylamine in DMF, afforded **26a** and **26b**, respectively. Formation of **26a** was confirmed with NMR spectral analysis having multiplet of eleven protons corresponding to cyclohexyl ring in the range of δ 3.46-1.22 ppm. Boronation of **26a** and **26b** using bis(pinacolato)diboron in the presence of $Pd(PPh_3)_2Cl_2$and KOAc provided **27a** and **27b**, respectively. Characteristic signal of twelve protons of four methyl groups of boronate at δ 1.35 ppm, confirmed the formation of **27a**. Suzuki reaction of **27a-b** with dibromo-imidazo[1,2-*a*]pyrazine **5** and $Pd(PPh_3)_4$, afforded compound **28a-b** alongwith traces of disubstituted products. Disappearance of singlet of methyl groups of boronate and appearance of aromatic protons of imidazopyrazine in the range of δ 8.69-7.77 ppm in proton NMR spectrum confirmed the formation of **28a**. Reduction of derivatives with sodium dithionite in ammonia provided amines **29a-b** followed by cyclization with triethylorthoformate in acetic acid to obtain intermediates **30a** and **30b** in 90% and 80% yields, respectively. Derivatives **26b-29b** have not been separated from column chromatography and used further without purification. Suzuki reactions of intermediates with unsubstituted and substituted phenyl, thienyl and naphthyl boronates were carried out in CH_3CN:H_2O using $Pd(PPh_3)_4$ and K_2CO_3 afforded **31-49** in 75-85% yields.

Interestingly, the scope of another benzimidazole at C-6 position of imidazo[1,2-*a*]pyrazine for Suzuki reaction was also explored with different synthetic route (**Scheme 3**). Reductions of **3** and **26a** were carried out with sodium dithionite in the presence of ammonia to afford **50a** and **50b**, respectively, followed by cyclization with triethylorthoformate in acetic acid, produced respective benzimidazoles **51a** and **51b**. Boronation of these derivatives using bis(pinacolato)diboron in the presence of $Pd(PPh_3)_2Cl_2$ and KOAc afforded **52a** and **52b**. Suzuki reactions of benzimidazole boronates **52a-b** with **8** and **30a-b** have been performed using $Pd(PPh_3)_4$ and K_2CO_3 to afford compounds **53-57** in 75-81% yields.

Scheme 2. Synthesis of 6-substituted-8-(1-cyclohexyl-1*H*-benzo[*d*]imidazol-6-yl)imidazo[1,2-*a*]pyrazine[b]

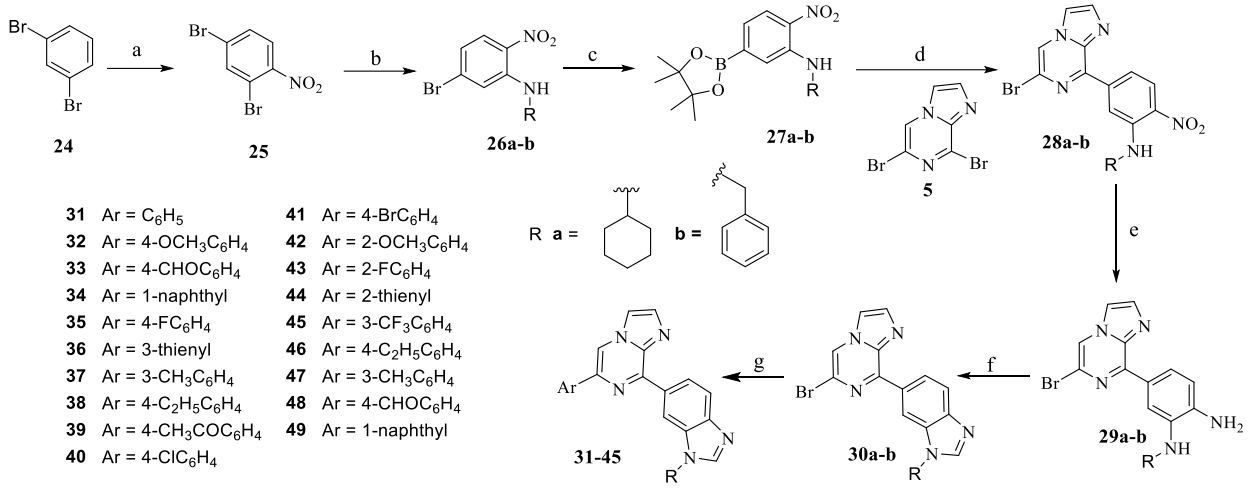

[b]Reagents and conditions: (a) H_2SO_4, HNO_3, DCM, 0 °C, 30 min., 95%; (b) Cyclohexyl amine/benzyl amine, K_2CO_3, DMF, 100 °C, 18 h, **26a**:74%; (c) Bis(pinacolato)diboron, $Pd(PPh_3)_2Cl_2$, KOAc, 1,4-dioxane, reflux, 10 h, **27a**:78%; (d) $Pd(PPh_3)_4$, K_2CO_3, CH_3CN : water (9:1), N_2, reflux, 10-12 h, **28a**:70%; (e) $Na_2S_2O_4$, aq. NH_3, THF : water, rt, 1 h; (f) Triethylorthoformate, AcOH, rt, 10 min., 80-90%; (g) $ArB(OH)_2$, $Pd(PPh_3)_4$, K_2CO_3, CH_3CN : water (9:1), N_2, reflux, 12-15 h, 75-85%

Scheme 3. Synthesis of 6,8-bis(1-cyclohexyl-1*H*-benzo[*d*]imidazol-5/6-yl)imidazo[1,2-*a*]pyrazine[c]

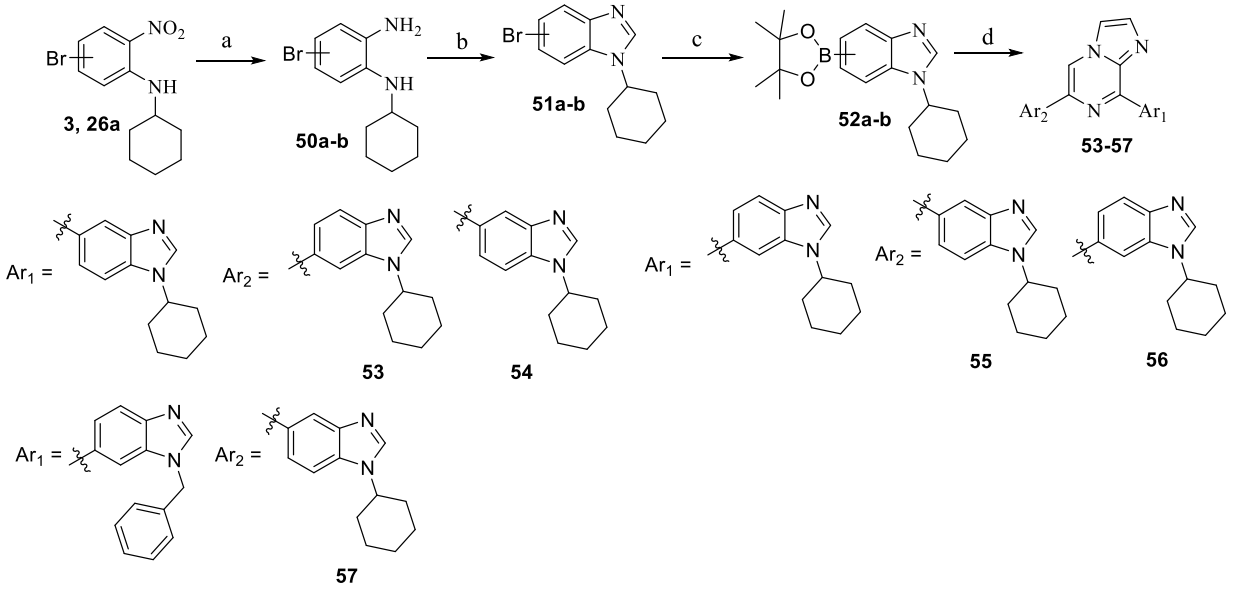

[c]Reagents and conditions: (a) $Na_2S_2O_4$, aq. NH_3, THF : water (3:2), rt, 1 h; (b) Triethylorthoformate, AcOH, rt, 10 min.,; (c) Bis(pinacolato)diboron, $Pd(PPh_3)_2Cl_2$, KOAc, 1,4-dioxane, reflux, 12 h; (d) **8, 30a-b**, $Pd(PPh_3)_4$, K_2CO_3, CH_3CN : water (9:1), N_2, reflux, 10-12 h, 75-81%

X-ray crystal structure. The molecular structure and the assignment of **31** were unambiguously confirmed by single-crystal X-ray diffraction study (**Figure 1**).

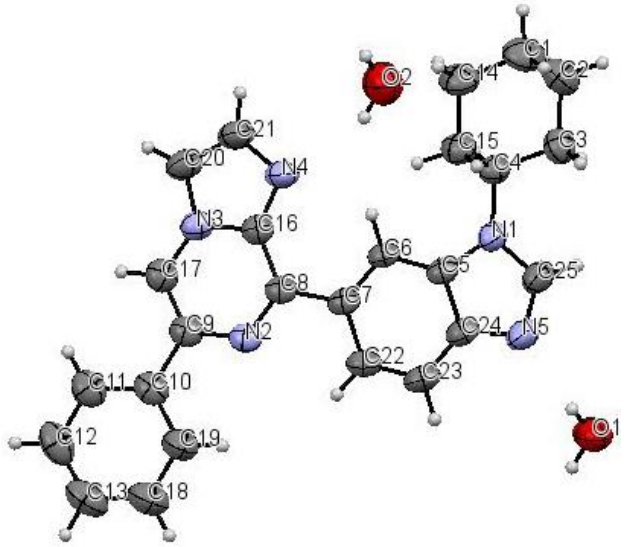

Figure 1. X-ray crystal structure of compound **31** (CCDC No. 1828636)

Compound **31** consists of two planar fragments, benzimidazole and imidazo[1,2-*a*]pyrazine which are in conjugation with phenyl ring present at C6-position of imidazo[1,2-*a*]pyrazine. Compound **31** crystallizes with Z = 4 in the space group P2/n (**Table 2**). Torsion angles along C-N and C-C of imidazo[1,2-*a*]pyrazine are 174.66 (13) Å and 5.0 (2) Å, respectively, while torsion angle along C-C bond of benzimidazole is 6.3 (2) Å. Moreover, the C-C bond length between imidazo[1,2-*a*]pyrazine and benzimidazole is shifted to double bond (1.48 Å). The six membered cyclohexyl ring present at benzimidazole ring is deviated from planarity that exist in chair conformation. Atom systems C2-C1-C14 and C3-C4-C15 having some angle strain, slightly deviated by 1.8º and 1.5º, respectively from the ideal tetrahedral value. The bond length of N5-C25 (1.31 Å) of benzimidazole ring is shorter having double bond character than longer bond length of N1-C25 (1.36 Å), indicating the presence of cyclohexyl group at N1 position and imidazo[1,2-*a*]pyrazine attached at the 6-position of benzimidazole (C7). Similarly, phenyl ring present at 6-position of imidazo[1,2-*a*]pyrazine having the bond length of 1.48 Å, indicating conjugation of these two moieties. Indeed, C-C bond length of imidazo[1,2-*a*]pyrazine with benzimidazole and phenyl ring agrees well with the standard double bond length of sp^2 hybridized carbon atoms in the rings. There is thus strong conjugation between these different planar moieties constitute the skeleton of molecule.

Table 2. Crystal data and structure refinement of compound **31**

Crystal Parameters	**Crystal Data**
Empirical formula	$C_{25}H_{23}N_5.2H_2O$
Formula weight	429.52
Temperature/K	298.15
Crystal system	Monoclinic
Space group	P2/n
a/Å	12.4417(9)
b/Å	9.8341(7)
c/Å	17.2501(10)
α/°	90
β/°	90.390(2)
γ/°	90
Volume/Å^3	2110.6(2)
Z	4
ρ_{calc}g/cm^3	1.295
μ/mm^{-1}	0.082
F(000)	872.0
Crystal size/mm^3	0.28 × 0.24 × 0.22
Radiation	MoKα (λ = 0.71073)
2Θ range for data collection/°	4.722 to 54.418
Index ranges	-15 ≤ h ≤ 15, -12 ≤ k ≤ 12, -21 ≤ l ≤ 22
Reflections collected	57943
Independent reflections	4699 [R_{int} = 0.0443, R_{sigma} = 0.0188]
Data/restraints/parameters	4699/0/287
Goodness-of-fit on F^2	1.070
Final R indexes [I>=2σ (I)]	R_1 = 0.0503, wR_2 = 0.1226
Final R indexes [all data]	R_1 = 0.0748, wR_2 = 0.1357
Largest diff. peak/hole / e Å^{-3}	0.14/-0.28

2.3 Biology

2.3.1 Cytotoxicity

2.3.1.1 Cytotoxicity against human cancer cell lines

In a preliminary test, compounds were assayed at single dose concentration (10^{-5} M) in the full panel of NCI 60 cancer cell lines.[71] The tested compounds showed diverse but strong cytotoxic effect on the evaluated panel of cell lines and most of the compounds exhibited more than 50%

inhibition of tumor growth at micromolar concentration. As revealed from results of 29 tested compounds, seven compounds with wide range of growth percentage displayed strong growth inhibitory activity (-98.48 to 99.61) at 10 μM concentration (**Table 3**). The bisbenzimidazole derivatives **53** and **57** demonstrated superior activity than mono benzimidazoles with cytotoxic effects towards 51 and 43 cell lines, respectively and among the monobenzimidazoles, 4-methoxyphenyl at C6 position of imidazo[1,2-*a*]pyrazine **32** indicated better cytostatic activity than phenyl **31**, 4-ethylphenyl **46** and 4-formylphenyl **48** derivatives in the same isomeric series of compounds. Such findings reveal that bisbenzimidazole moiety is more favorable for cytotoxic and mono benzimidazole for cytostatic activity. This superiority in the activity of bisbenzimidazole might be attributed to the corresponding increase in binding interactions through π bonding and therefore, permeability and penetration into cancer cells. On referring to the total number of sensitive cell lines for tested compounds, it has been found that most of the target compounds

Table 3. Overview of the preliminary cytotoxic assay at single dose concentration of 10 μM

Compd	Mean growth percent	[a]Range of growth inhibition	The most sensitive cell lines	[b]Positive cytostatic effect	[c]Positive cytotoxic effect	No. of sensitive cell lines/Total cell lines
31	59.72	-11.09 to 81.25	T-47D	17/57	1/57	18/57
32	20.32	-43.35 to 98.64	SF-539	42/57	9/57	51/57
46	65.98	50.00 to 94.82	T-47D	14/59	0/59	14/59
48	71.82	51.16 to 98.01	T-47D	9/59	0/59	9/59
53	-44.92	-98.48 to 98.86	SK-MEL-5	8/59	51/59	59/59
56	54.67	50.00 to 89.11	RPMI-8226	24/59	0/59	24/59
57	-26.50	-88.03 to 99.61	HCC-2998	16/59	43/59	59/59

[a]Negative (-) indicates the cell killed; [b]The ratio between number of cell lines with percent growth from 0 to 50 and total number of cell lines; [c]The ratio between number of cell lines with percent growth of <0 and total number of cell lines

exhibited broad spectrum cytotoxicity covering different cancer subpanels. Amongst these sensitive cell lines to tumor, melanoma cell lines, SK-MEL-5 and colon cancer cell lines, HCC-2998 were found to be highly sensitive with negative growth percentage value (lethal effect) for derivatives **53** and **57**, respectively. Central nervous system (SF-539) and leukemia (RPMI-8226) cancer cell lines were noticed to be the most susceptible cell lines for derivatives **32** and **56**, respectively. Moreover, T-47D (breast cancer) was also proved to be the most responsible cells to

compounds **31**, **46** and **48**. Compounds **32**, **53** and **57** attributed pronounced cytotoxicity over the majority of tested cancer cell lines with mean GP values of 20.32, -44.92 and -26.50, respectively. The detailed anti-tumor activities on growth inhibition of NCI-60 human cancer cell lines at the single dose of 10 μM, are shown in **Tables 4-7**.

Table 4. Percent growth inhibition of compounds **8-10**, **12-13**, **22** and **30-31** at 10 μM concentration

Cell Panel	Cell Line	8	9	10	12	13	22	30	31
Leukemia	CCRF-CEM	--	11.65	1.19	27.20	--	--	7.68	81.25
	HL-60(TB)	10.51	19.35	23.32	49.91	5.28	0.87	18.00	67.08
	K-562	17.36	31.12	29.17	37.95	13.25	--	18.01	70.64
	MOLT-4	17.45	39.68	34.21	51.01	11.45	12.36	26.33	67.72
	RPMI-8226	--	18.32	14.67	38.23	6.16	--	14.88	85.67
	SR	20.65	44.60	29.66	10.86	20.78	14.96	26.77	59.76
Non-Small Cell Lung Cancer	A549/ATCC	4.80	9.00	7.33	36.17	8.95	1.63	9.36	33.28
	EXVX	10.34	2.51	7.85	29.58	--	3.54	12.01	24.19
	HOP-62	12.98	12.94	3.33	13.19	13.25	0.44	21.74	NT
	HOP-92	21.90	10.87	17.39	NT	7.05	--	30.67	53.67
	NCI-H226	3.73	--	--	17.85	7.09	--	22.47	33.93
	NCI-H23	8.76	--	--	9.02	4.49	5.56	10.24	45.28
	NCI-H322M	10.94	2.91	--	8.38	--	0.45	18.08	5.25
	NCI-H460	3.26	--	2.90	7.35	--	--	--	37.76
	NCI-522	15.24	16.06	18.50	33.03	22.62	14.55	16.18	58.06
Colon Cancer	COLO 205	--	0.28	--	--	--	--	--	20.73
	HCC-2998	3.13	--	--	--	--	--	--	--
	HCT-116	6.06	3.81	18.60	23.68	6.58	--	--	59.49
	HCT-15	4.25	19.09	11.86	15.26	4.85	6.48	13.13	51.58
	HT29	4.48	9.21	--	16.53	8.33	--	5.21	48.30
	KM12	--	5.70	2.27	8.69	7.30	6.84	67.74	48.98
	SW-620	--	--	--	1.43	--	--	--	9.15
CNS Cancer	SF-268	5.80	1.33	3.96	11.82	5.13	2.5	17.11	21.67
	SF-295	7.58	--	12.47	7.88	--	--	--	39.77
	SF-539	6.65	2.17	9.71	7.72	--	--	10.04	27.79
	SNB-19	10.53	1.72	4.26	16.69	--	--	8.09	22.89
	SNB-75	16.41	5.65	15.94	9.15	--	--	21.25	44.38
	U251	--	4.44	3.40	27.93	3.57	--	1.50	37.27
Melanoma	LOX IMVI	9.14	4.86	7.86	11.39	0.76	1.01	15.19	39.56
	MALME-3M	--	--	--	--	--	--	--	NT
	M14	--	1.61	9.96	0.39	0.73	--	--	38.21
	MDA-MB-435	--	0.53	6.92	4.07	--	--	--	28.68

	SK-MEL-2	0.53	--	9.88	20.60	6.30	13.14	10.17	16.52
	SK-MEL-28	--	--	4.86	--	--	--	--	17.96
	SK-MEL-5	8.35	5.71	5.95	2.13	2.90	1.16	13.44	36.46
	UACC-257	--	--	--	35.53	--	--	--	5.22
	UACC-62	16..41	2.01	1.25	20.96	2.44	0.23	19.82	65.65
Ovarian	IGROV1	8.45	--	5.82	3.68	6.40	--	6.60	11.95
Cancer	OVCAR-3	--	--	--	4.29	--	0.91	15.80	41.81
	OVCAR-4	9.25	--	7.51	15.02	--	--	9.15	34.54
	OVCAR-5	--	--	1.45	--	--	--	6.64	7.87
	OVCAR-8	3.55	--	7.75	23.99	3.09	--	4.92	63.92
	NCI/ADR-RES	5.47	--	1.93	11.83	2.36	6.79	8.82	50.49
	SK-OV-3	6.59	--	5.37	--	--	--	--	7.52
Renal	786-0	1.30	8.24	12.65	13.33	3.12	0.59	10.03	36.82
Cancer	A498	3.51	--	--	--	NT	NT	--	26.12
	ACHN	--	--	10.91	8.22	--	--	11.53	35.90
	CAKI-1	NT	NT	NT	20.67	--	--	NT	NT
	RXF 393	--	23.31	--	0.15	35.96	--	5.58	44.97
	SN12C	--	4.83	--	13.57	--	--	6.47	28.82
	TK-10	--	--	--	5.82	--	--	5.55	2.26
	UO-31	40.12	20.86	33.47	37.85	22.83	16.37	37.59	55.15
Prostate	PC-3	10.26	13.53	22.63	13.28	10.23	7.16	17.22	92.04
Cancer	DU-145	--	2.64	--	6.09	--	3.63	6.20	29.28
Breast	MCF7	37.62	15.85	19.68	35.71	9.59	34.03	47.56	38.02
Cancer	MDA-MB-231/ATCC	3.12	6.64	--	18.16	--	7.47	24.23	41.47
	HS 578T	2.68	--	5.69	4.25	--	--	16.09	23.79
	BT-549	6.38	0.43	8.55	1.57	--	--	5.16	57.09
	T-47D	25.30	25.52	46.21	22.02	10.08	37.28	49.73	-11.09
	MDA-MB-468	6.27	--	--	5.23	--	28.31	44.40	54.44

-- indicates GI < 10%; NT, not tested; 30-40% growth inhibition; 40-50% growth inhibition; 50-70% growth inhibition; 70-90% growth inhibition; 90-100% growth inhibition; lethal to cancer cells

Table 5. Percent growth inhibition of compounds **32-36** and **39-41** at 10 μM concentration

Cell Panel	Cell Line	32	33	34	35	36	39	40	41
Leukemia	CCRF-CEM	93.27	77.93	17.47	33.42	29.22	1.10	11.41	NT
	HL-60(TB)	98.64	16.47	38.94	2.03	18.45	2.65	15.58	23.22
	K-562	92.04	NT	30.90	24.72	21.99	9.60	44.51	58.96
	MOLT-4	82.84	58.70	44.72	25.23	29.98	14.33	8.87	20.43
	RPMI-8226	95.63	82.52	22.94	50.14	37.86	20.80	18.96	32.05
	SR	91.73	47.52	6.92	20.43	14.27	23.63	18.51	60.65
Non-Small	A549/ATCC	68.62	--	NT	12.76	3.97	--	11.56	15.26
Cell Lung	EXVX	56.65	20.88	13.25	10.54	--	--	13.10	16.21

Cancer	HOP-62	NT	23.82	19.57	NT	--	7.41	NT	NT
	HOP-92	52.28	42.97	NT	35.24	27.83	24.98	30.53	34.08
	NCI-H226	35.85	0.53	9.45	23.27	6.34	--	19.37	23.32
	NCI-H23	62.15	54.54	4.32	2.36	10.03	8.60	4.11	8.38
	NCI-H322M	31.50	11.21	4.74	0.01	--	1.19	--	4.21
	NCI-H460	91.09	37.81	3.61	6.12	--	7.12	4.14	13.18
	NCI-H522	-20.93	25.25	19.28	15.51	10.25	10.40	19.78	35.46
Colon	COLO 205	-8.01	--	--	--	--	--	--	--
Cancer	HCC-2998	62.60	--	2.23	--	2.18	--	--	--
	HCT-116	91.28	92.56	17.88	18.02	13.35	15.85	7.34	31.24
	HCT-15	78.75	49.12	4.46	7.59	1.37	18.81	15.53	35.78
	HT29	92.51	17.54	4.11	--	5.68	9.20	16.42	20.87
	KM12	83.19	3.69	11.05	3.49	15.40	11.72	10.58	23.29
	SW-620	77.84	4.21	5.34	8.38	--	--	13.97	21.90
CNS	SF-268	49.94	27.12	7.84	10.67	--	5.01	4.83	15.53
Cancer	SF-295	92.51	23.08	6.34	7.93	--	--	14.51	41.27
	SF-539	-43.35	31.54	--	17.29	6.29	2.82	6.30	24.39
	SNB-19	68.39	14.40	9.08	14.21	0.39	3.96	15.76	18.31
	SNB-75	-26.28	21.40	16.54	20.96	--	--	31.15	34.55
	U251	80.94	32.00	NT	7.94	6.09	3.019	11.27	23.72
Melanoma	LOX IMVI	69.59	46.94	7.43	3.50	4.90	14.54	14.81	30.68
	MALME-3M	NT	--	--	NT	--	3.01	NT	NT
	M14	89.16	23.02	--	2.98	--	3.43	10.01	26.88
	MDA-MB-435	-18.64	13.03	--	1.78	--	6.00	36.69	58.35
	SK-MEL-2	94.26	27.77	2.30	9.82	3.68	0.58	10.91	24.10
	SK-MEL-28	47.67	7.54	--	2.67	--	--	12.09	28.33
	SK-MEL-5	92.30	56.51	4.06	7.36	24.97	24.80	12.43	23.55
	UACC-257	26.34	--	NT	--	--	--	5.44	7.30
	UACC-62	65.20	37.07	16.72	31.01	18.40	18.51	30.53	46.86
Ovarian	IGROV1	53.36	21.29	--	--	1.51	19.06	7.84	9.40
Cancer	OVCAR-3	-26.52	23.69	2.38	7.88	--	--	10.85	26.34
	OVCAR-4	46.40	16.87	19.73	5.73	--	--	4.57	10.48
	OVCAR-5	58.81	--	--	10.32	--	--	0.84	8.95
	OVCAR-8	71.19	43.99	NT	9.54	12.10	6.38	3.78	13.24
	NCI/ADR-RES	87.21	37.35	4.43	0.69	--	4.17	11.13	30.48
	SK-OV-3	74.30	5.11	--	--	--	--	6.14	6.44
Renal	786-0	83.19	46.68	6.33	11.15	6.35	--	12.13	18.00
Cancer	A498	-12.27	11.18	13.97	--	20.05	--	--	20.69
	ACHN	60.97	11.64	6.49	9.02	5.76	4.32	5.45	21.43
	CAKI-1	NT	36.55	25.15	NT	--	--	NT	NT
	RXF 393	-8.48	25.01	--	24.40	8.63	--	6.73	34.03
	SN12C	63.63	20.74	11.69	3.97	--	6.33	13.53	18.44

	TK-10	18.49	0.75	--	--	3.37	--	--	--
	UO-31	61.54	82.20	23.00	37.81	23.05	23.08	36.12	42.91
Prostate Cancer	PC-3	95.22	19.03	36.52	53.60	19.85	17.92	24.55	42.43
	DU-145	81.76	24.32	5.10	1.17	1.36	--	--	5.66
Breast Cancer	MCF7	80.23	47.80	13.01	9.17	--	11.97	21.76	46.43
	MDA-MB-231/ATCC	71.12	51.16	20.82	15.8	1.35	7.65	15.30	22.78
	HS 578T	79.97	45.54	3.62	17.61	5.56	6.34	6.35	24.50
	BT-549	68.92	33.79	--	20.30	--	4.68	23.77	35.06
	T-47D	-8.60	98.01	41.27	33.28	63.71	54.44	27.55	55.01
	MDA-MB-468	97.41	--	10.38	19.46	21.83	0.73	10.62	33.72

-- indicates GI < 10%; NT, not tested; 30-40% growth inhibition; 40-50% growth inhibition; 50-70% growth inhibition; 70-90% growth inhibition; 90-100% growth inhibition; lethal to cancer cells

Table 6. Percent growth inhibition of compounds **42-49** at 10 μM concentration

Cell Panel	Cell Line	42	43	44	45	46	47	48	49
Leukemia	CCRF-CEM	17.35	22.48	46.42	27.32	49.74	21.1	77.93	6.22
	HL-60(TB)	14.60	9.30	26.58	1.06	39.61	18.23	16.47	--
	K-562	22.59	22.79	26.95	21.53	NT	NT	NT	NT
	MOLT-4	22.40	22.48	30.76	32.92	54.23	36.93	58.70	22.34
	RPMI-8226	35.93	42.42	52.26	32.14	55.39	37.50	82.52	26.93
	SR	26.31	16.34	27.21	15.63	49.88	11.02	47.52	12.42
Non-Small Cell Lung Cancer	A549/ATCC	13.88	9.10	5.33	5.15	45.39	14.91	--	7.31
	EXVX	13.35	16.00	--	4.79	39.66	22.28	20.88	24.55
	HOP-62	NT	NT	NT	NT	17.90	9.68	23.82	13.96
	HOP-92	47.83	37.04	32.46	8.38	36.11	28.70	42.97	42.47
	NCI-H226	25.73	28.65	17.09	1.55	1.48	1.18	0.53	--
	NCI-H23	2.79	4.16	5.95	--	22.98	9.09	54.54	10.43
	NCI-H322M	--	--	--	5.83	0.89	--	11.21	1.34
	NCI-H460	9.62	8.10	1.30	4.38	42.01	10.12	37.81	3.80
	NCI-522	22.18	17.79	13.17	10.67	45.92	28.36	25.25	29.27
Colon Cancer	COLO 205	--	--	--	--	34.23	11.35	--	--
	HCC-2998	--	--	--	--	25.23	--	--	--
	HCT-116	28.28	25.76	21.08	17.63	61.22	36.66	92.56	32.93
	HCT-15	33.62	6.18	2.33	0.36	74.71	35.22	49.12	8.20
	HT29	11.06	7.26	0.09	6.41	68.82	41.96	17.54	18.60
	KM12	3.58	2.45	4.89	1.25	45.67	22.05	3.69	10.98
	SW-620	3.40	9.53	--	--	18.83	--	4.21	--
CNS Cancer	SF-268	8.04	6.04	--	3.30	30.50	7.22	27.12	10.26
	SF-295	9.76	10.38	--	--	51.20	14.30	23.08	8.22
	SF-539	8.07	4.51	--	--	21.23	7.28	31.54	4.22
	SNB-19	11.11	7.56	--	2.24	20.94	2.58	14.40	5.12
	SNB-75	34.95	29.74	8.13	4.58	29.32	21.71	21.40	16.17

	U251	20.99	11.44	3.92	5.93	46.08	19.38	32.00	5.53
Melanoma	LOX IMVI	5.13	5.77	1.07	3.45	50.15	14.76	46.94	16.46
	MALME-3M	NT	NT	NT	NT	--	--	--	--
	M14	1.12	2.92	--	--	36.41	--	23.02	4.41
	MDA-MB-435	--	--	--	--	50.93	0.94	13.03	--
	SK-MEL-2	12.13	10.54	--	--	14.80	6.34	27.77	16.95
	SK-MEL-28	--	--	--	--	19.12	--	7.54	--
	SK-MEL-5	8.94	6.50	8.05	4.32	47.91	10.11	56.51	9.69
	UACC-257	--	--	--	--	--	--	--	--
	UACC-62	25.06	38.16	24.84	4.33	24.93	2.46	37.07	12.92
Ovarian	IGROV1	--	--	--	--	24.99	9.51	21.29	11.28
Cancer	OVCAR-3	6.57	0.17	--	--	31.17	13.95	23.69	1.44
	OVCAR-4	13.15	4.51	--	--	35.11	19.34	16.87	7.88
	OVCAR-5	6.61	6.64	--	--	14.91	6.64	--	1.83
	OVCAR-8	8.78	14.05	9.34	10.13	30.81	11.52	43.99	6.22
	NCI/ADR-RES	0.06	4.51	--	--	41.17	12.13	37.35	5.83
	SK-OV-3	10.57	--	--	--	0.55	--	5.11	--
Renal	786-0	12.28	2.94	4.10	--	38.11	21.45	46.68	12.42
Cancer	A498	13.87	--	24.96	--	--	22.14	11.18	6.74
	ACHN	4.48	13.23	--	0.30	44.71	12.38	11.64	12.35
	CAKI-1	NT	NT	NT	NT	47.90	24.82	36.55	27.06
	RXF 393	0.95	12.27	--	--	30.68	2.01	25.01	--
	SN12C	7.73	10.12	2.84	8.30	22.52	4.72	20.74	5.62
	TK-10	--	--	--	--	15.54	--	0.75	--
	UO-31	24.04	22.94	10.93	22.48	57.85	41.68	82.20	31.26
Prostate	PC-3	43.14	32.57	49.07	36.45	50.42	24.81	19.03	31.40
Cancer	DU-145	--	0.96	5.07	--	19.08	14.22	24.32	--
Breast	MCF7	8.40	11.20	--	19.86	57.98	22.19	47.80	29.19
Cancer	MDA-MB-231/ATCC	15.92	21.34	10.76	21.83	43.20	28.44	51.16	28.74
	HS 578T	15.78	5.26	--	--	21.80	8.47	45.54	5.98
	BT-549	--	4.08	12.21	--	15.88	--	33.79	--
	T-47D+	36.60	77.20	70.32	52.15	94.82	86.05	98.01	73.84
	MDA-MB-468	14.64	27.62	15.13	--	17.23	16.61	--	--

-- indicates GI < 10%; NT, not tested; 30-40% growth inhibition; 40-50% growth inhibition; 50-70% growth inhibition; 70-90% growth inhibition; 90-100% growth inhibition

Table 7. Percent growth inhibition of compounds **53-57** at 10 μM concentration

Cell Panel	Cell Line	53	54	55	56	57
Leukemia	CCRF-CEM	35.14	95.72	46.13	78.45	94.40
	HL-60(TB)	32.94	-42.22	29.98	51.00	-20.83
	K-562	47.19	-4.74	38.48	69.81	NT
	MOLT-4	43.65	-30.50	56.91	79.08	95.61
	RPMI-8226	52.18	-37.92	70.77	89.11	-41.18

	SR	17.05	97.53	50.03	71.85	94.55
Non-Small	A549/ATCC	4.93	-44.85	25.30	57.56	-5.05
Cell Lung	EXVX	9.56	-13.11	60.18	30.78	-12.25
Cancer	HOP-62	20.82	-55.40	16.77	42.60	-9.39
	HOP-92	NT	NT	NT	NT	-83.63
	NCI-H226	13.10	-56.37	18.76	46.73	-63.07
	NCI-H23	4.61	-41.51	20.50	28.23	-22.78
	NCI-H322M	--	98.77	--	39.08	84.03
	NCI-H460	1.35	-48.51	11.89	53.01	-20.28
	NCI-522	17.66	-52.60	28.51	49.43	-35.21
Colon	COLO 205	--	-64.36	6.71	22.38	-29.86
Cancer	HCC-2998	--	-93.43	15.52	17.73	-88.03
	HCT-116	15.88	-61.35	29.07	80.25	-75.75
	HCT-15	26.01	-11.46	35.59	57.08	-9.03
	HT29	28.13	-26.16	58.23	71.86	-48.74
	KM12	56.20	-61.09	30.59	63.49	-39.42
	SW-620	--	-3.82	--	35.56	97.83
CNS	SF-268	4.85	-67.02	18.44	41.70	-0.11
Cancer	SF-295	10.42	-86.52	50.60	44.03	-81.35
	SF-539	25.38	-82.05	35.73	16.67	-77.58
	SNB-19	5.02	93.37	10.63	41.17	80.43
	SNB-75	6.25	-89.61	24.84	25.38	-67.41
	U251	29.66	-83.28	38.66	69.00	-22.83
Melanoma	LOX IMVI	11.71	-87.39	25.89	66.95	-87.01
	MALME-3M	8.16	-14.31	5.14	7.04	-15.43
	M14	--	-50.79	6.98	40.56	-4.44
	MDA-MB-435	--	-72.96	7.38	60.20	-6.16
	SK-MEL-2	NT	-65.61	13.70	31.74	-36.69
	SK-MEL-28	--	-19.48	--	24.42	99.56
	SK-MEL-5	20.50	-98.42	36.80	55.74	-83.96
	UACC-257	5.79	-71.51	14.93	35.50	-32.69
	UACC-62	12.43	-47.66	29.26	51.86	-31.16
Ovarian	IGROV1	--	-41.94	8.51	60.78	94.19
Cancer	OVCAR-3	--	-85.15	3.05	40.35	-35.68
	OVCAR-4	--	97.16	--	22.80	83.16
	OVCAR-5	--	-24.00	1.44	7.18	-28.99
	OVCAR-8	11.57	-24.11	42.57	59.52	97.55
	NCI/ADR-RES	4.12	98.89	27.02	48.81	99.47
	SK-OV-3	11.77	-71.86	--	14.79	-22.20
Renal	786-0	13.93	-47.08	25.84	34.27	-19.44
Cancer	A498	--	-88.07	16.30	26.23	-71.75
	ACHN	4.08	-58.83	5.48	45.07	80.06
	CAKI-1	9.21	82.80	15.90	54.57	56.69
	RXF 393	4.30	-89.06	37.41	16.76	-76.86

	SN12C	13.88	-54.59	20.48	42.72	-35.43
	TK-10	--	-59.30	--	14.39	94.80
	UO-31	26.76	-85.42	25.64	68.80	-51.36
Prostate Cancer	PC-3	27.87	-64.10	44.96	64.19	-39.52
	DU-145	6.22	-59.08	8.72	46.29	-28.20
Breast Cancer	MCF7	23.85	-3.78	19.13	44.96	97.97
	MDA-MB-231/ATCC	16.80	-68.66	28.91	49.17	-70.08
	HS 578T	18.91	96.60	23.57	43.33	99.61
	BT-549	5.90	-48.93	27.67	38.31	-44.73
	T-47D	34.66	-17.65	44.66	54.88	-2.12
	MDA-MB-468	3.28	-20.24	14.94	31.38	-35.74

-- indicates GI < 10%; NT, not tested; 30-40% growth inhibition; 40-50% growth inhibition; 50-70% growth inhibition; 70-90% growth inhibition; 90-100% growth inhibition; lethal to cancer cells

Compounds **32**, **53** and **57** have shown interesting growth inhibitory activity in the preliminary single dose screen and were evaluated for the advance 5-dose (10^{-4}-10^{-8} M) testing mode against the full panel. In five dose assay, the mono- and bis-benzimidazole derivatives seemed to

Table 8. Median growth inhibitory (GI_{50}, μM), total growth inhibitory (TGI, μM) and median lethal concentrations (LC_{50}, μM) of *in vitro* evaluation of compounds **32**, **53** and **57** against subpanel of human tumor cancer cell lines.

Compd	**Activity (μM)**	**I**	**II**	**III**	**IV**	**V**	**VI**	**VII**	**VIII**	**IX**	**MIG-MID[a]**
32	GI_{50}	1.60	1.65	1.24	1.18	6.95	3.04	1.30	0.84	1.11	2.10
	TGI	5.05	6.15	9.23	2.49	3.20	7.64	[b]	[b]	19.23	7.57
	LC_{50}	[b]	[b]	[b]	[b]	[b]	[b]	[b]	[b]	[b]	[b]
53	GI_{50}	3.11	2.88	2.00	1.72	1.79	2.23	1.71	1.73	1.94	2.12
	TGI	4.96	3.74	4.05	3.52	3.41	11.4	3.34	3.60	4.54	4.73
	LC_{50}	[b]	7.06	7.01	6.37	6.38	6.81	5.76	NT	7.07	6.63
57	GI_{50}	1.91	2.18	1.97	2.11	2.00	2.46	3.01	2.50	1.95	2.23
	TGI	5.57	4.56	3.74	2.82	4.04	5.92	3.62	4.82	3.6	4.30
	LC_{50}	[b]	3.41	6.12	[b]	[b]	[b]	[b]	[b]	[b]	4.76

I, leukemia; II, non-small cell lung cancer; III, colon cancer; IV, CNS cancer; V, melanoma; VI, ovarian cancer; VII, renal cancer; VIII, prostate cancer; IX, breast cancer. [a]Full panel mean-graph midpoint (MIG-MID) (μM). [b]Compounds showed values > 100 μM. NT = Not tested

contribute equally toward the tumor growth inhibitory activities which is evident from the similar average GI_{50} of compounds **32** (2.10 μM), **53** (2.12 μM) and **57** (2.23 μM) (**Table 8**) as these values disguise significant cell selectivity. The mean GI_{50} graph of 4-methoxyphenyl (**32**) showed potent (compared to **53** and **57**) activity in the leukemia, non-small cell lung, colon, CNS, ovarian, prostate and breast cancer subpanels. Compound **32** showed GI_{50} of 399 nM for HCT-116 and 383 nM for HT29 cells of colon cancer, 361 nM for SF-295 of CNS cancer and 312 nM for MDA-MB-435 cell lines of melanoma. Compound **53** exhibited GI_{50} of 806 nM for RPMI-8226 of leukemia while compound **57** showed GI_{50} of 799 nM for 786-0 cancer cell lines corresponding to renal. Higher LC_{50} values of compounds (usually > 100 μM) to most of the cell panels indicated their low toxicity profile.

2.3.1.2 Cytotoxicity against human normal cell line

To evaluate the safety, cytotoxicity effects of the two most potent compounds (**32** and **53)** were determined by means of colorimetric assay (MTT assay) against human kidney normal cell line (Hek293) at 10^{-4}, 10^{-5}, 10^{-6}, 10^{-7} and 10^{-8} M concentrations. It has been observed that derivative **32** showed only 19.05%, 16.51%, 15.07%, 14.79% and 13.96% cytotoxicity to Hek293 cells whereas compound **53** exhibited 18.05%, 14.53%, 14.11%, 13.60% and 12.08% cytotoxicity to Hek293 cells at above said concentrations (**Figure 2**). Cytotoxicity data showed that compounds **32** and **53** had low cytotoxicity against mammalian cells, indicating compounds were able to selectively kill cancer cells.

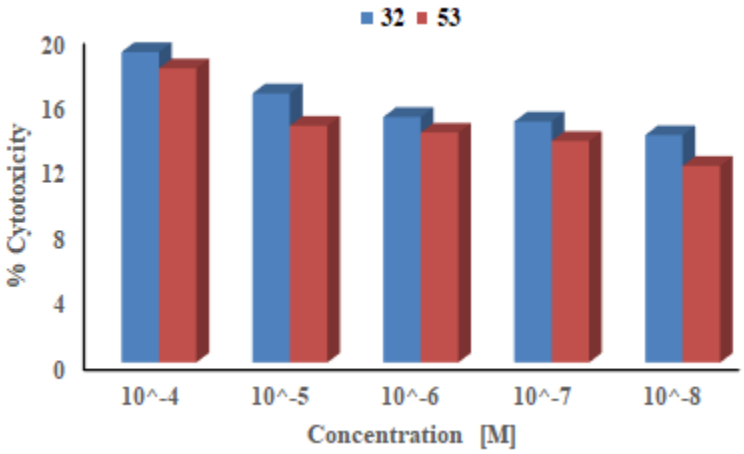

Figure 2. Effect of cytotoxicity of compounds **32** and **53** on human normal cell line Hek293

2.3.2 DNA interaction studies

The mode of anticancer activity of imidazo[1,2-*a*]pyrazine-benzimidazole conjugates might be grounded on DNA damage. Three most potent compounds **32**, **53** and **57** were studied with ct-DNA to investigate the effect on anticancer activity. X-ray crystal structure analysis of these derivatives showed the planarity of compounds and previous studies with planar heterocyclic derivatives had demonstrated the occurrence of an intercalative binding process upon complexation with DNA. Here, we have studied the capacity of binding of imidazo[1,2-*a*]pyrazine-benzimidazole derivatives to DNA macromolecule with different spectroscopic methods *viz.* UV-visible, fluorescence and circular dichroism.

2.3.2.1 UV-visible spectroscopy

The absorption spectra of compounds **32**, **53** and **57** (20 μM) showed intense band at 290 nm, 295 nm and 295 nm, respectively. On addition of ct-DNA (0-15 μM), hypochromic shifts were observed in phosphate buffer at *p*H 7.4. The absorbance of compounds **32**, **53** and **57** was decreased by 20.83%, 11.48% and 15.27%, respectively (**Figure 3a-c**). During the titration with DNA, an isosbestic point (**32**: 280 nm; **53**: 290 nm; **57**: 290 nm) was observed which suggested a single mode of binding. Hypochromic effect in absorption spectra of compounds in the presence of ct-DNA is characteristic of an intercalative binding.[72] On the basis of interaction of compounds with DNA, the binding constants (K_b) for compound-DNA complexes have been determined from the Benesi-Hildebrand equation[73] which were found to be 3.34×10^4 M^{-1} for **32**, 1.25×10^4 M^{-1} for **53** and 3.18×10^4 M^{-1} for **57 (Figure 3d**). These binding constants conclude that compound **32** has more affinity to bind with ct-DNA followed by compound **57**, and **53**.

2.3.2.2 Thermal denaturation studies

Thermal denaturation experiments were performed for further confirmation of intercalation of compounds with DNA. The ability of the drug to protect ct-DNA against thermal denaturation was used as an indication of their capacity to bind DNA and to stabilize the double strand.[74] ΔT_m values for **32**, **53** and **57** have been found to be 22 ºC, 7 ºC and 12 ºC, respectively on complexation with ct-DNA. The trend of ΔT_m of these three compounds suggested the order of **32** > **57** > **53** and found to be same as in stability constant. The ΔT_m values indicated that compound **32** has a strong affinity to bind with DNA due to less steric hindrance and thus stabilized DNA against heat denaturation.

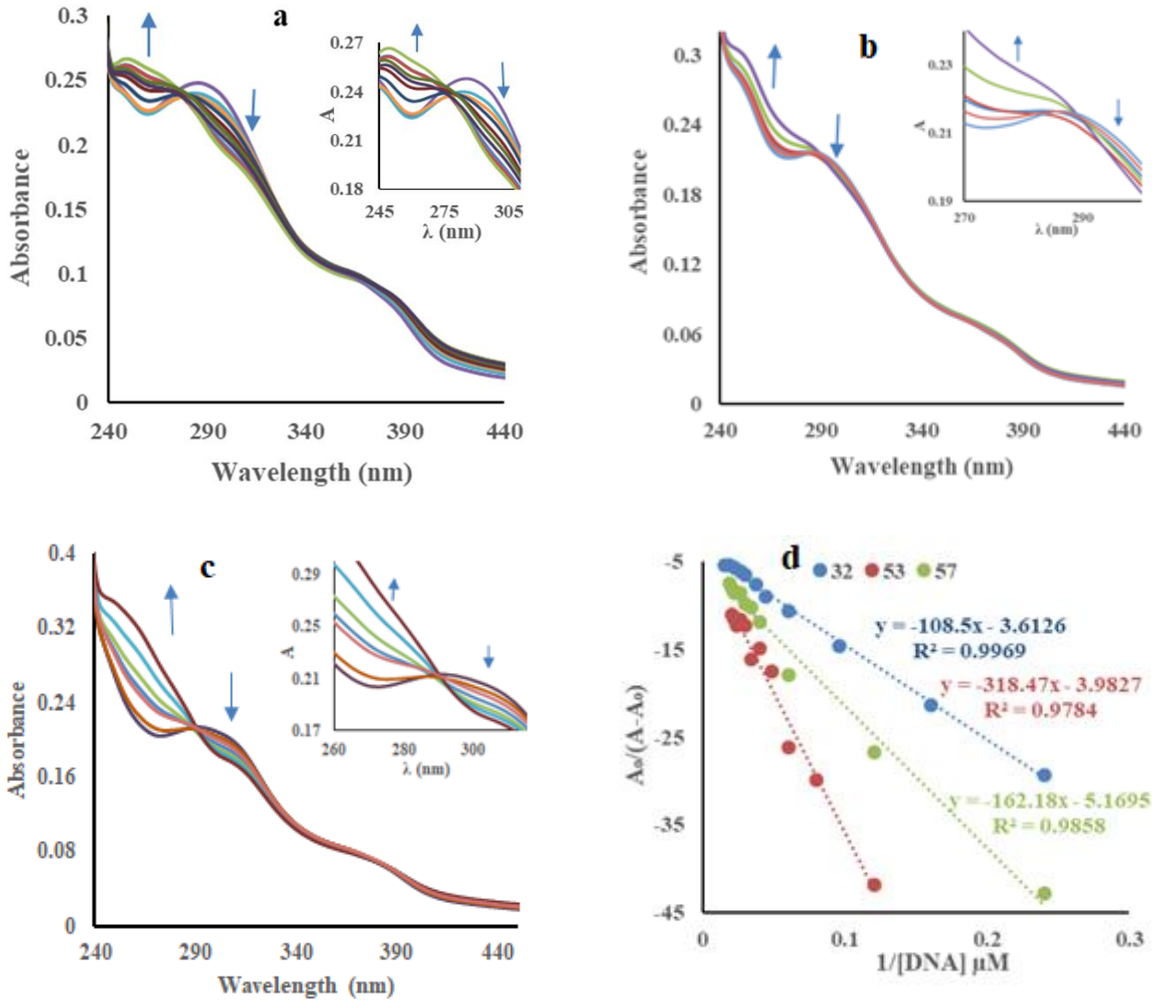

Figure 3. Effect of incremental addition of ct-DNA on absorption spectra of compounds (a) **32**, (b) **53**, (c) **57** in phosphate buffer (*p*H 7.4) at 298 K, (d) Benesi-Hildebrand plots for compounds **32**, **53** and **57**

2.3.2.3 Fluorescence spectroscopy

Emission studies provide additional information regarding the interaction mode of compounds with DNA. The binding of compounds with DNA was studied by maintaining the concentration of compounds **32**, **53** and **57** at 5 μM while varying the concentration of ct-DNA (**32**: 0-110 μM.; **53**: 0-50 μM; **57**: 0-40 μM) in phosphate buffer (*p*H 7.4) at 298 K. On excitation of compounds **32** at 280 nm, **53** at 290 nm and **57** at 290 nm, intense emission bands at respective 470, 445 and 450 nm have been shown. On increasing the concentration of ct-DNA to compounds, gradual quenching of fluorescence intensities by 75%, 25% and 35%, for compounds **32**, **53** and **57**, respectively, were observed without any significant change in emission maxima (**Figure 4a-c**).

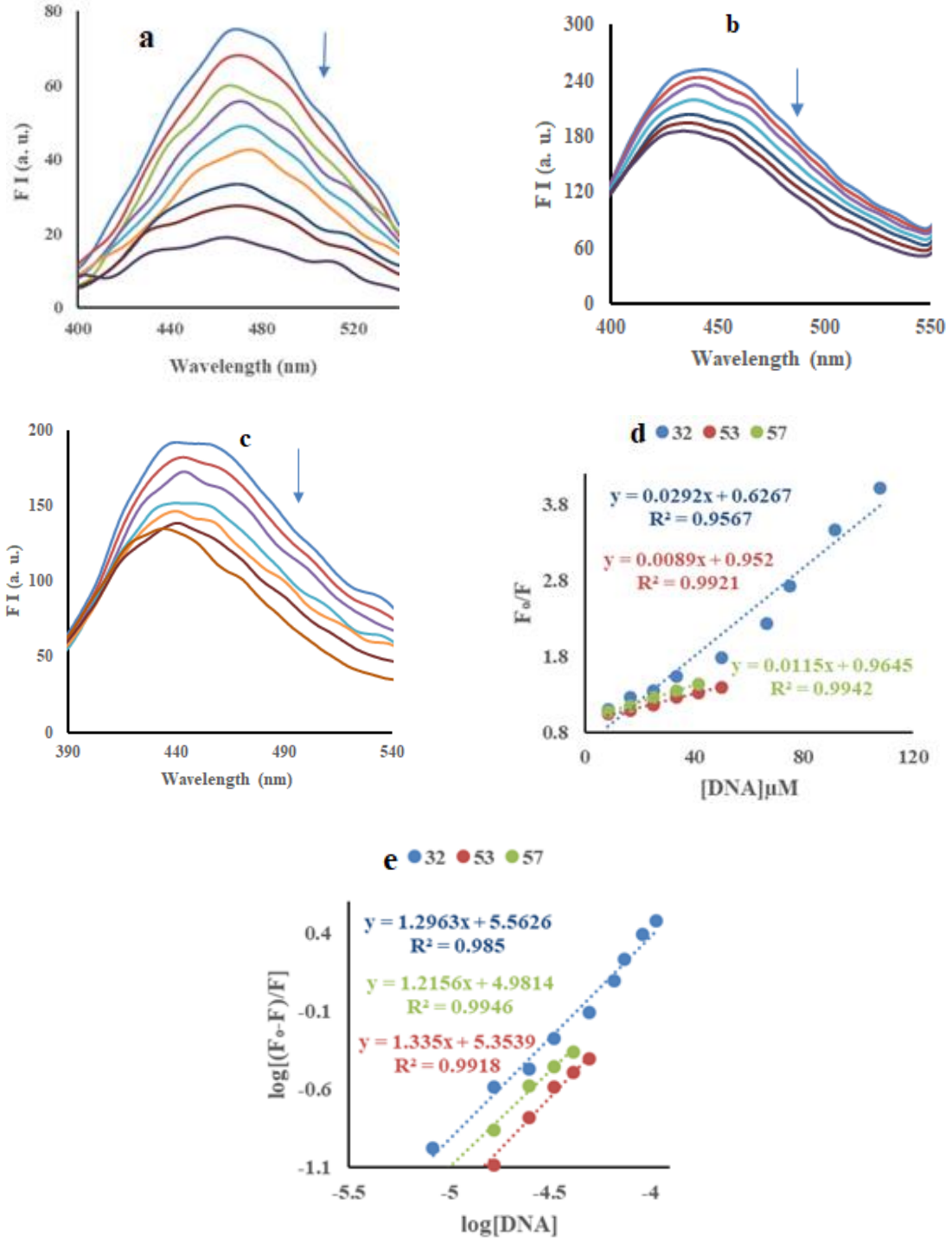

Figure 4. Effect of incremental addition of ct-DNA on emission spectra of compounds (a) **32**, (b) **53**, (c) **57** in phosphate buffer (*p*H 7.4) at 298 K**,** (d) Stern-Volmer plots and (e) Modified Stern-Volmer plots for interaction of compounds **32**, **53** and **57** with ct-DNA at 298K

Stern-Volmer equation[75] was performed to know more about the quenching process and to differentiate the probable quenching mechanism. The Stern-Volmer quenching constants (K_{SV}) was calculated from ratio of slope to intercept of Stern-Volmer plot (**Figure 4d**) and found to be in the range of 0.93-4.65 $\times 10^4$ M^{-1} at 298 K (**Table 9**). Compound **32** had the highest K_{SV} value, suggesting that compound **32** bound more strongly to ct-DNA followed by **57**, and **53**.

A linear Stern-Volmer plot was obtained with compounds **32**, **53** and **57,** suggesting the possibility of single sort of binding process, either static or dynamic interaction, which can be distinguished by bimolecular binding/quenching constant (K_q). The value of K_q was calculated using K_{SV}, where the average fluorescence lifetime (τ_o)[76] is 10^{-8} s in the absence of DNA (analyte). The values of K_q were observed in the range of 0.93-4.65 $\times$ 10^{12} M^{-1} s^{-1} for compounds **32**, **53** and **57** (**Table 9**), much greater than typically observed for dynamic enhancement (~1 $\times$ 10^{10} M^{-1} s^{-1}).[77] The values of K_q indicated that interaction probably involved the static quenching with formation of complex at ground state.

Table 9. Quenching and binding parameters of compounds upon interaction with ct-DNA

Compd	T (K)	K_{SV} ($\times 10^4$) (M^{-1})	K_q ($\times 10^{12}$) ($M^{-1}s^{-1}$)	R^2	K_b ($\times 10^4$ M^{-1})	n	R^2
32	298	4.65	4.65	0.9567	36.52	1.29	0.9850
	308	1.68	1.68	0.9445	4.57	1.08	0.9614
	318	0.73	0.73	0.9669	0.02	0.58	0.9645
53	298	0.93	0.93	0.9942	9.58	1.21	0.9630
57	298	1.19	1.19	0.9921	22.58	1.33	0.9637

R^2 is the correlation coefficients

Modified Stern-Volmer equation[78] is generally used to calculate the binding constant (K_b) and the number of binding sites (n) and in the present study, were found to be in the range of 9.58-36.52 $\times$ 10^4 M^{-1} and 1.21-1.33, respectively at 298 K (**Table 9**, **Figure 4e**). Compound **32** showed 4 and 1.5 times more binding interaction than **53** and **57**, respectively, suggested that **32** bound strongly to ct-DNA. To determine the effect of temperature on DNA binding with compounds, emission spectra of compound **32** (the most potent derivative) was recorded at 308 K and 318 K. On increasing the concentration of ct-DNA (308 K: 0-115 μM.; 318 K: 0-95 μM) to compound **32**, there is gradual quenching of the fluorescence intensities by 65% and 60% at 308 K and 318 K, respectively, without any significant change of wavelength in emission maxima (**Figure 5a-b**). The values of Stern-Volmer quenching constants (K_{SV}; 1.68 $\times$ 10^4 M^{-1} and 0.73 $\times$ 10^4 M^{-1}),

bimolecular quenching constants (K_q; 1.68 $\times 10^{12}$ M^{-1} s^{-1} and 0.73 $\times 10^{12}$ M^{-1} s^{-1}), the binding constants (K_b; 4.57 $\times$ 10^4 M^{-1} and 0.02 $\times$ 10^4 M^{-1}) and the average number of binding sites (n; 1.08 and 0.58) were calculated at 308 K and 318 K (**Table 9**, **Figure 5c-d**). A decrease in binding constant is observed with increasing temperature, indicating a reduction in the stability of DNA-compound adduct at higher temperature with exothermic nature of the binding process.

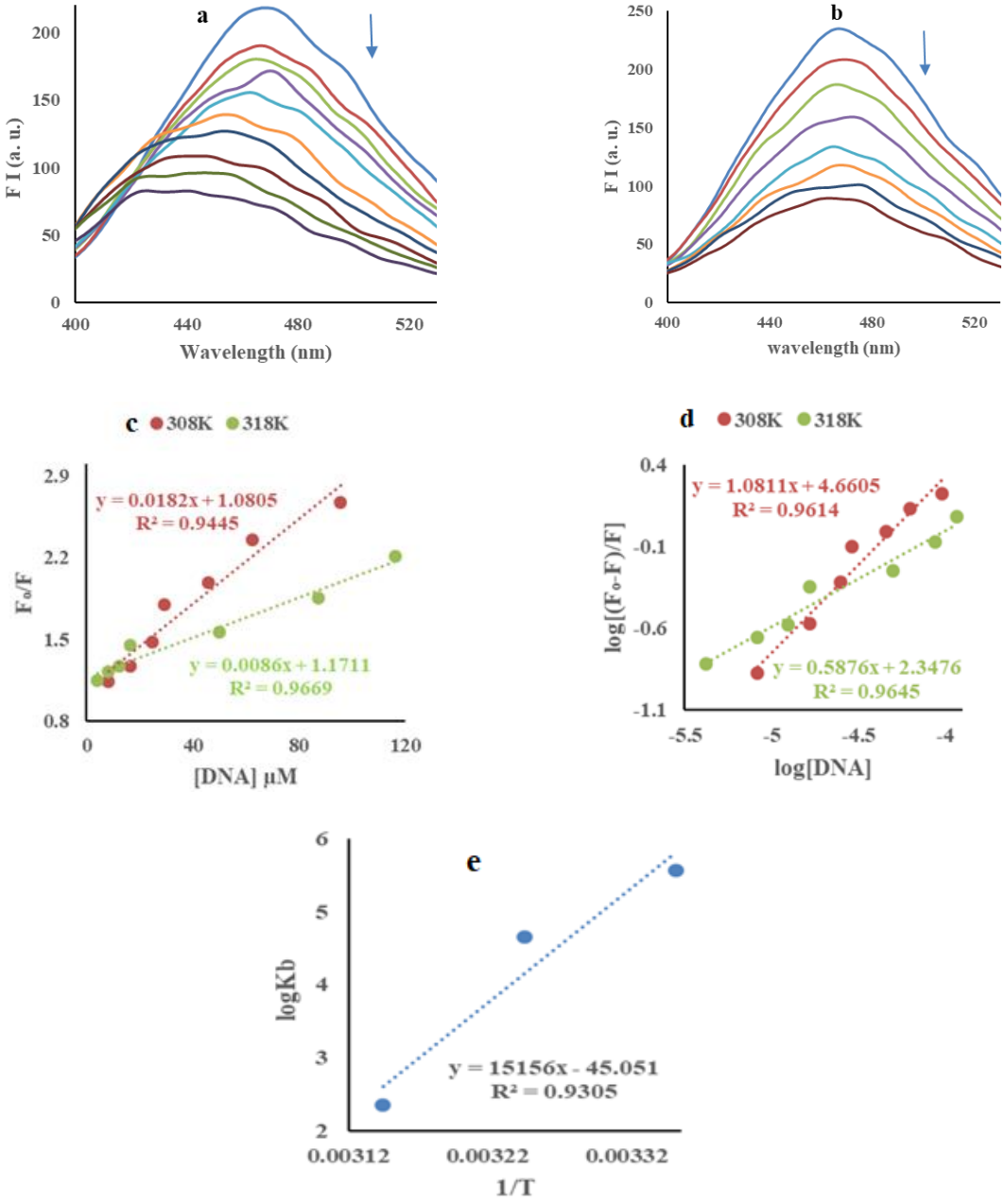

Figure 5. Effect of incremental addition of ct-DNA on emission spectra of compound **32** (20 μM) at (a) 308 K, (b) 318 K, (c) Stern-Volmer, (d) Modified Stern-Volmer and (e) Van't Hoff plots

Thermodynamic parameters were calculated for compound **32** according to the van't Hoff equation, where enthalpy change (ΔH) and entropy change (ΔS) have been found to be -69.28 kcal M^{-1} and -205.95 cal M^{-1} K^{-1}, respectively (**Table 10, Figure 5e**). The negative value of ΔH showed that binding process is exothermic. Accordingly, the negative values of ΔH and ΔS indicated that the hydrogen bonding and van der Waals contact played key roles in the binding of compound to DNA.[79] Moreover, the negative values of ΔG obtained at different temperatures revealed the favorable spontaneous nature of the binding process. It is noteworthy that increase in ΔG value with temperature, indicating the influence of temperature for interaction of compound with DNA.

Table 10. Thermodynamic parameters for the interaction of DNA with compound **32** at three different temperatures

T (K)	ΔH (Kcal M^{-1})	ΔS (cal M^{-1} K^{-1})	ΔG (Kcal M^{-1})	R^2
298	-69.28	-205.94	-7.91	0.9305
308			-5.85	
318			-3.79	

R^2 is the correlation coefficient

2.3.2.4 Ethidium bromide (EB) displacement

To evaluate the intercalation properties of compounds **32**, **53** and **57** with DNA, ethidium bromide (EB) displacement assay was performed. EB, a fluorescent probe, has a planar structure that simply binds with DNA by an intercalative binding mode.[80] The emission spectra of ethidium bromide-ct DNA complex (3 μM : 30 μM) with varying concentration of compounds (0-85 μM) at excitation of 520 nm, showed an intense band at 606 nm. The fluorescence intensity of EB-DNA complex at 606 nm decreased with increasing the concentration of compounds, indicated that some of the EB molecules, which were intercalated into DNA base pairs, have been replaced by compounds and released into the aqueous medium (**Figure 6a-c**).

2.3.2.5 Circular dichroism (CD)

In order to get insight into the conformation of ct-DNA on interaction with compounds, circular dichroism technique was used. These molecules can eventually acquire induced CD spectrum (ICD) upon binding to ct-DNA, from which mutual orientation of the molecule could be derived, consequently giving useful information about modes of interaction. It was obvious that DNA has characteristic CD signal in the UV-region, one negative band at 246 nm because of the right handed

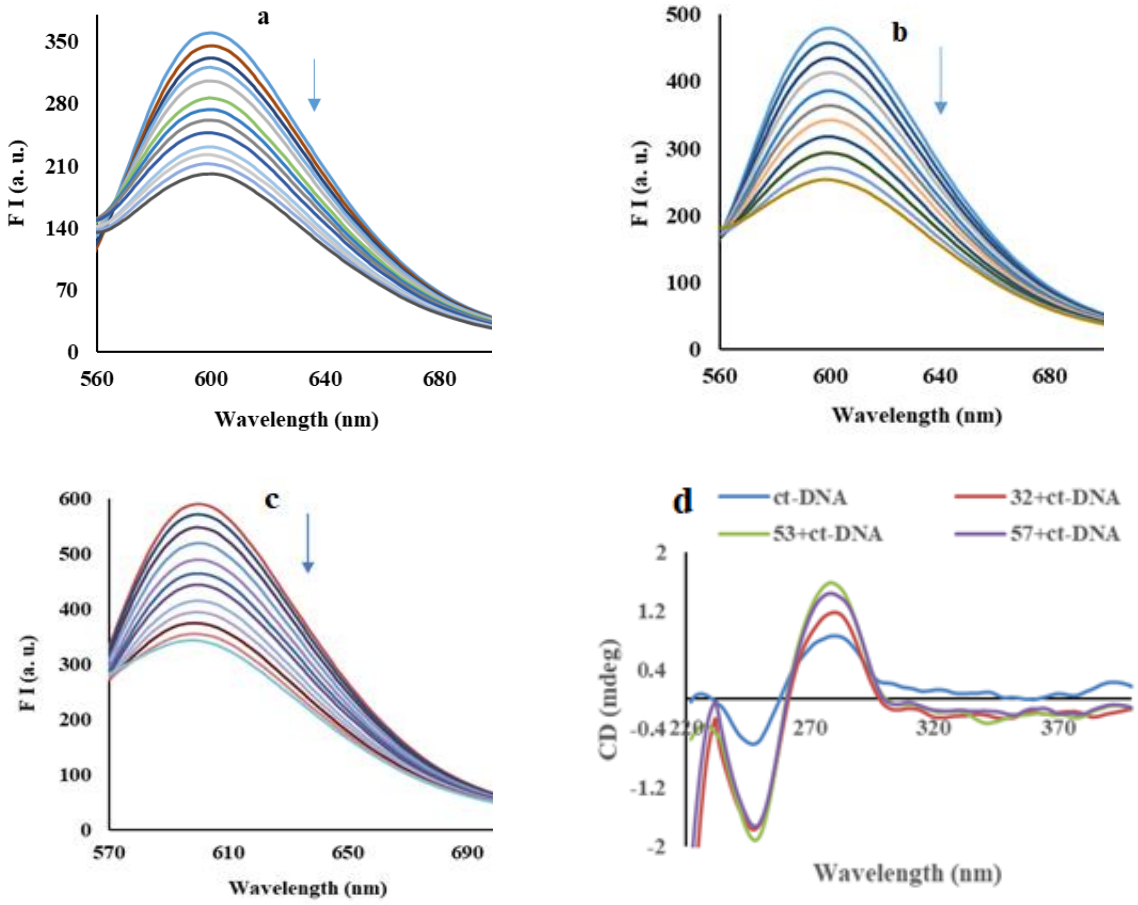

Figure 6. (a) Effect of incremental addition of compounds (a) **32**, (b) **53**, (c) **57** on emission spectra of complex of EB (3 μM) with ct-DNA (30 μM); (d) CD spectra of free ct-DNA (40 μM) (blue line), **32**/ct-DNA complex (red line), **53**/ct-DNA complex (green line) and **57**/ct-DNA complex (purple line) at ratio $r_{[compound/ct\text{-}DNA]} = 0.025$

B-form helicity, and one positive band at 278 nm because of the base stacking.[81] Addition of compounds **32**, **53** and **57** resulted in decrease in intensity of the CD band at (λ) 246 nm and increase of CD band at (λ) 278 nm (**Figure 6d**). These compounds yielded weak negative induced CD (ICD) band between (λ) 350 and 400 nm, thus excluding binding into the minor groove of ct-DNA as a dominant interaction. The results obtained for compounds **32**, **53** and **57** together with weak negative ICD band points toward intercalative mode of interaction with ct-DNA.[82,83]

2.3.3 Bovine serum albumin (BSA) interactions

Serum albumin (SA) is the most abundant protein in plasma which involves in the transport of drugs within body. Binding to these proteins may lead to loss or enhancement of biological properties of the original drug. The possible binding interactions of compounds **32**, **53** and **57** with

BSA, structural homology of human serum albumin (HSA), have been investigated by absorption and emission experiments.

2.3.3.1 UV-Visible spectroscopy

Absorption spectrum is a simple and appropriate technique to discover the structural changes of protein and to investigate the protein-ligand complex formation. Absorption spectra of BSA (10 μM) in phosphate buffer (*p*H 7.4) have been explored with incremental addition of compounds (**32**, **53** and **57**) at 0-8 μM. The absorption band at 280 nm has been observed due to aromatic amino acids of BSA (Trp, Tyr, and Phe) which can be influenced by species that interact with this protein.[84] The intensity of absorption peak of BSA has been increased with increasing concentration of the compounds (**Figure 7a-c**). These variations originated from changes in the conformation and polarity of the microenvironment around the aromatic residues of BSA. These, in turn, resulted from penetration of compounds into the structure of BSA.

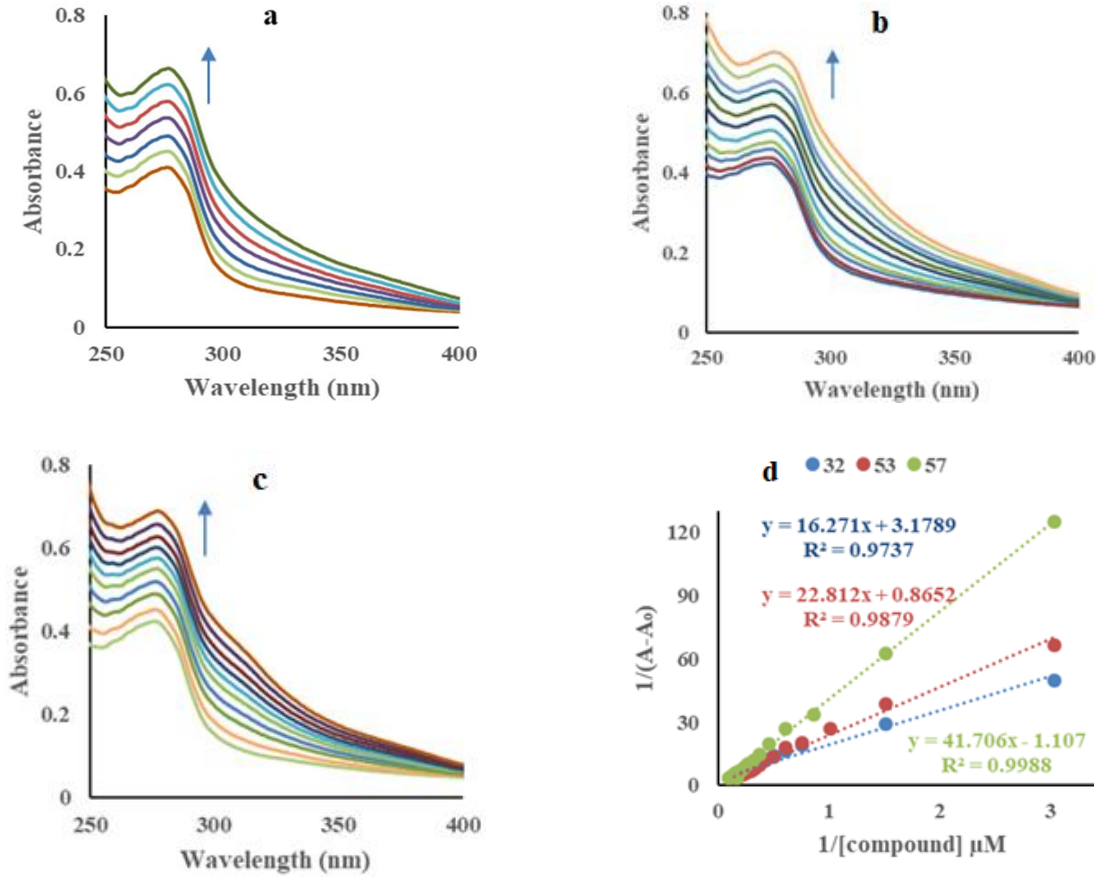

Figure 7. Effect of incremental addition of compounds (a) **32**, (b) **53**, (c) **57** on absorption spectra of BSA (10 μM), (d) Benesi-Hildebrand plots for interaction of BSA with compounds **32**, **53** and **57**

The values of binding constant (K_b) for the interaction of compounds with BSA were used to compare the affinity of each derivative towards serum albumin. The binding constants (K_b) were calculated using Benesi-Hildebrand equation,[73] to be 1.95 $\times 10^5$ M^{-1} for **32**, 3.79 $\times 10^4$ M^{-1} for **53** and 2.65 $\times 10^4$ M^{-1} for **57**. Since the value of K_b is directly related to the extent of BSA binding and provide relative affinities, in the present study, the BSA binding affinities follow the order of **32** > **53** > **57**, indicating that monobenzimidazole derivatives have more ability to penetrate into the cell than bisbenzimidazole moieties.

2.3.3.2 Fluorescence spectroscopy

The effect of **32**, **53** and **57** on the emission of BSA has also been evaluated to gain more information on the interaction between compounds and protein. Upon excitation at 280 nm, BSA exhibited an intense fluorescent emission band at around 350 nm mainly due to the presence of tryptophan residues. On increasing the concentration of compounds **32** (0-10 μM), **53** (0-16 μM) and **57** (0-10 μM) to BSA (10 μM), quenching of emission bands (70% for **53** and 75% for **57**) at 350 nm were observed, however, **32** showed ratiometric response towards BSA (**Figures 8a-c**). The emission intensity ratio at 470/350 nm has been found to be changed from 0.08 to 1.08, clearly depicted the ~12-fold ratiometric response, indicating strong interaction of compound **32** with BSA.

A comparison has also been made for the binding affinity with the help of Stern-Volmer equation[75] that showed the relation between the quenching extent for each compound and the strength of their interactions with BSA. The values of Stern-Volmer constant (K_{SV}) and the apparent bimolecular quenching constant (K_q) were calculated to evaluate the efficiency of quenching and accessibility of fluorophores to quenchers (compounds) (**Figure 8d**). A linear Stern-Volmer plot was obtained with derivatives suggesting that single sort of binding process occurs either static or dynamic that can be distinguished by calculating bimolecular quenching constant (K_q) using the lifetime of the fluorophore (τ_o)[76] 10^{-8} s in the absence of the quencher (compound).

The values of K_{SV} for **32**, **53** and **57** are in the range of 1.04-1.16 $\times 10^5$ M^{-1}. Compound **32** showed slightly higher value of K_{SV} than **53** and **57**, indicating compound **32** has strong affinity to bind with BSA. As shown in **Table 11**, the values of K_q for **32**, **53** and **57** have been found to be in the range of 1.04-1.16 $\times 10^{13}$ $M^{-1}s^{-1}$, which are significantly larger than the diffusion-

controlled limit (~1 ×10^{10} M^{-1} s^{-1}),[77] indicating binding of the compounds to BSA probably involves static quenching with formation of complex at ground state.

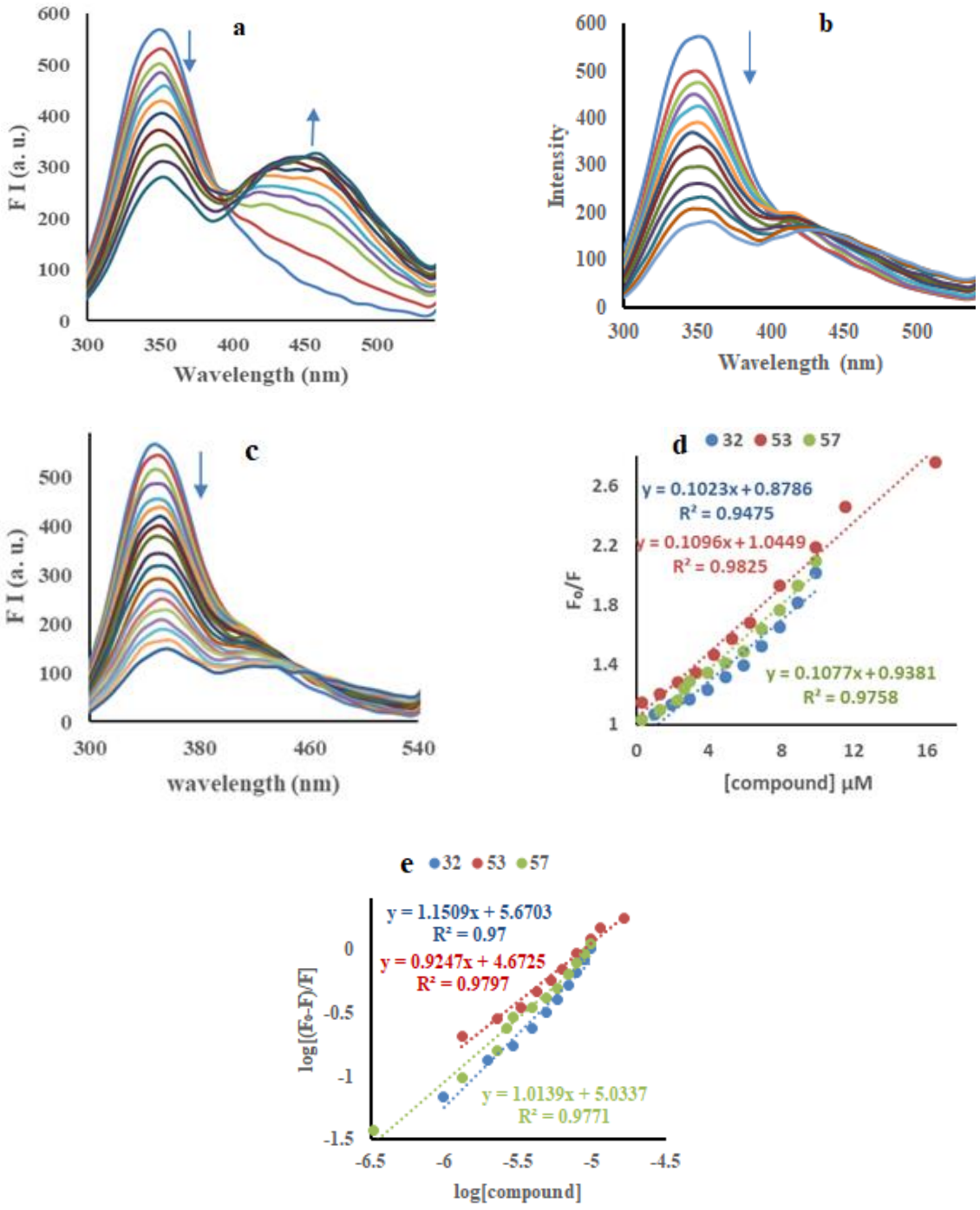

Figure 8. Effect of incremental addition of compounds (a) **32**, (b) **53**, (c) **57** on emission spectra of BSA (10 μM), (d) Stern-Volmer plots, (e) Modified Stern-Volmer plots for interaction of BSA with compounds (**32**, **53** and **57**)

The binding constants (K_b) and the average number of binding sites (n) of imidazo[1,2-*a*]pyrazine-benzimidazole conjugates have been calculated using modified Stern-Volmer equation from plot of log $(F_o-F)/F$ versus log [compound] (**Figure 8e**) and were found to be in the range of 0.47-4.68 × 10^5 M^{-1} and 0.92-1.50 values, respectively (**Table 11**). These binding parameters for the interaction, suggested that serum albumin might acts as carrier protein for these compounds and their metabolites in delivering them to target tissues.

Table 11. Quenching and binding parameters for interaction of BSA with compounds

Compd	K_{SV} (×10^5)(M^{-1})	K_q (×10^{13}) ($M^{-1}s^{-1}$)	R^2	K_b (×10^5 M^{-1})	n	R^2
32	1.16	1.16	0.9475	4.68	1.50	0.9700
53	1.04	1.04	0.9825	0.47	0.92	0.9797
57	1.14	1.14	0.9578	1.08	1.01	0.9771

R^2 is the correlation coefficients

2.4 Molecular properties and drug-likeness

Good bioavailability can be achieved with appropriate balance between solubility and partitioning properties. We have subjected a series of imidazol[1,2-*a*]pyrazine-benzimidazole derivatives (**9-23**, **31-49** and **53-57**) for the prediction of lipophilicity, solubility and Lipinski's "Rule of Five".[85] The results from the calculations (from molinspiration) revealed that all the derivatives fulfilled the Lipinski's rule of five except compounds **53-57**, in which violation was due to high molecular mass (**Table 12**). Experimental log P was determined by the octanol/water partition coefficient using UV-visible spectroscopy. All of the compounds showed log P values less than 5 indicating good lipophilicity to penetrate into the cell. Moreover, compounds possessed less number of rotatable bonds (3-5) and therefore, exhibited less conformational flexibility. These compounds showed topological polar surface area (TPSA) value of < 70 $Å^2$ which is also supported the drug absorption in digestive tract as well as blood-brain barrier penetration.[86,87] Calculation of percentage oral absorption (%ABS = 109 - 0.345 TPSA) concluded that all derivatives were likely to be absorbed well, having calculated oral absorption in the range of 86-92%.

Table 12. Pharmacokinetic properties of compounds **9-23, 31-49** and **53-57**

Compd	LogP	TPSA(Å)	natom	MW	nON	nOHNH	nviolat.	nrot	volume	%Abs
9	1.59	48.02	30	393	5	0	0	3	363.10	92.43
10	1.44	57.26	32	423	6	0	0	4	388.65	89.24

11	0.23	65.10	32	421	6	0	0	4	382.09	86.54
12	1.77	48.02	34	443	5	0	0	3	407.10	92.43
13	1.26	48.02	31	411	5	0	0	3	368.04	92.43
14	1.63	48.02	29	399	5	0	0	3	353.82	92.43
15	1.54	48.02	31	407	5	0	0	3	379.67	92.43
16	1.74	48.02	32	421	5	0	0	4	396.47	92.43
17	1.41	65.10	33	435	6	0	0	4	398.65	86.54
18	1.34	48.02	31	427	5	0	0	3	376.64	92.43
19	2.05	48.02	31	472	5	0	0	3	380.99	92.43
20	1.88	57.26	32	423	6	0	0	4	388.65	89.24
21	1.77	48.02	31	411	5	0	0	3	368.04	92.43
22	1.37	48.02	29	399	5	0	0	3	353.82	92.43
23	1.67	48.02	34	461	5	0	0	4	394.40	92.43
31	1.74	48.02	30	393	5	0	0	3	363.10	92.43
32	1.41	57.26	32	423	6	0	0	4	388.65	89.24
33	1.50	65.10	32	421	6	0	0	4	382.09	86.54
34	1.44	48.02	34	443	5	0	0	3	407.10	92.43
35	2.01	48.02	31	411	5	0	0	3	368.04	92.43
36	1.81	48.02	29	399	5	0	0	3	353.82	92.43
37	1.87	48.02	31	407	5	0	0	3	379.67	92.43
38	1.66	48.02	32	421	5	0	0	4	396.47	92.43
39	2.06	65.10	33	435	6	0	0	4	398.65	86.54
40	1.51	48.02	31	427	5	0	0	3	376.64	92.43
41	1.73	48.02	31	472	5	0	0	3	380.99	92.43
42	1.72	57.26	32	423	6	0	0	4	388.65	89.24
43	1.95	48.02	31	411	5	0	0	3	368.04	92.43
44	1.38	48.02	29	399	5	0	0	3	353.82	92.43
45	1.72	48.02	34	461	5	0	0	4	394.40	92.43

46	1.96	48.02	33	429	5	0	0	5	394.68	92.43
47	2.16	48.02	32	415	5	0	0	4	377.88	92.43
48	1.88	65.10	33	429	6	0	0	5	380.30	86.54
49	2.00	48.02	35	451	5	0	0	4	405.31	92.43
53	1.77	65.85	39	515	7	0	1	4	478.30	86.28
54	2.16	65.85	39	515	7	0	1	4	478.30	86.28
55	1.90	65.85	39	515	7	0	1	4	478.30	86.28
56	1.19	65.85	39	515	7	0	1	4	478.30	86.28
57	1.61	65.85	40	523	7	0	1	5	476.52	86.28

2.5 Molecular docking

Molecular docking is an important tool for researchers to speculate the interaction between potential drug (ligand) and biomolecules. Docking study has been carried out using AutoDock suite (vina)[88] to confirm the mode of binding between compounds **32**, **53** and **57** with DNA (pdb 1BNA).[89] The optimized cluster was ranked by energy levels in the best conformation of the ligand-DNA modeled structures, and the minimum binding energies of the DNA with compounds **32**, **53** and **57** have been found to be -9.3, -11.1 and -10.7 kcal/mol, respectively. It is evident from **Figure 9** that compounds have been incorporated between two GC base pairs of DNA and aromatic moiety of compounds are aligned parallel to the base pairs of DNA due to planar structure of compounds. Such a parallel arrangement between ligand and DNA base pairs results in π -π stacking, thus responsible for interaction in DNA double helix. Methoxy group, in case of **32** and NH of benzimidazole, in case of **53** and **57** are also involved in the H-bonding with purine moiety of the guanidine group. Hydrogen bond has been formed between oxygen linked methoxy of **32** and H-22 hydrogen atom association with N-2 of guanine (DG16 of the B chain). Similarly, compounds **53** and **57** formed two hydrogen bonds, NH of benzimidazole with H-3 hydrogen atom associated with N-3 of guanine (DG16 of B chain) and H-21 hydrogen atom associated with N-2 of guanine (DG11 of A chain) (**Table 13**). Hence, because of the strong π -π stacking interaction and the hydrogen bonding between compounds and the nucleic acid base, the torsional motion of compounds reduced substantially in DNA solution, leading to change in its emission yield. Thus,

the molecular docking studies further supported the intercalative mode of binding between compounds and DNA.

Table 13. H-bonding of compounds **32**, **53** and **57** with DNA base pairs

Compd	H-bonding within		Bond Length (Å)
	Ligand	DNA	
32	O of Methoxy	DG-16	2.4
53	NH of benzimidazole (hexyl)	DG-16	2.6
		DG-11	2.6
57	NH of benzimidazole (benzyl)	DG-16	2.6
		DG-11	2.5

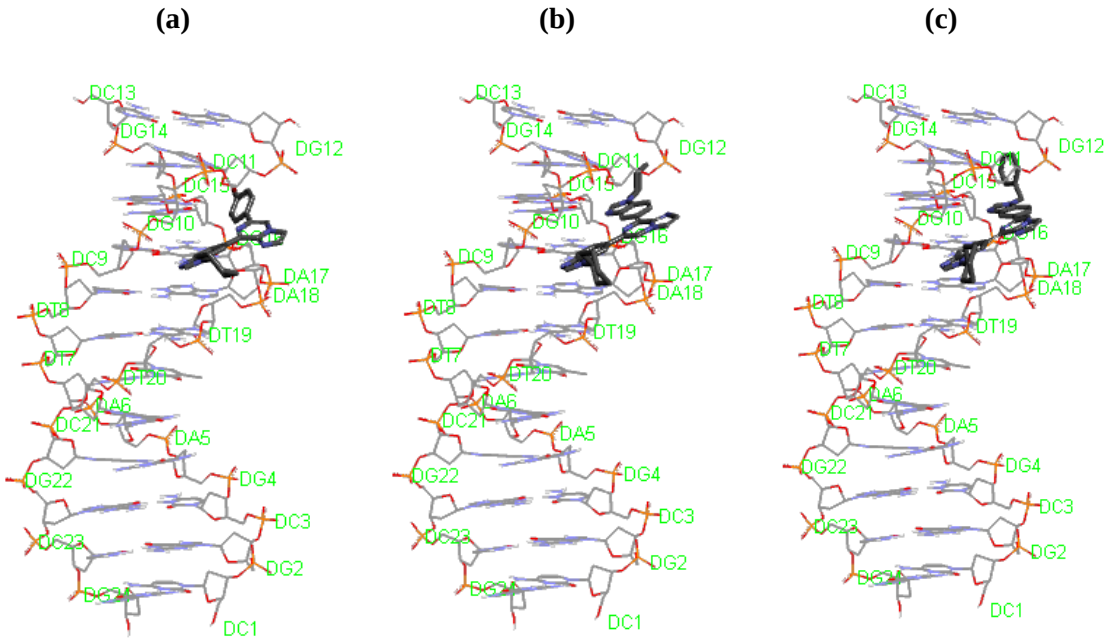

Figure 9. Molecular docking of DNA (1BNA) with compounds (a) **32**, (b) **53** and (c) **57**, obtained from Discovery Studio

2.6 Conclusion

Derivatives of new conjugated ring systems, 6-substituted-8-(1-cyclohexyl-1*H*-benzo[*d*]imidazol-5/6-yl) and 6,8-bis(1-cyclohexyl-1*H*-benzo[*d*]imidazol-5/6-yl) with imidazo[1,2-*a*]pyrazine, obtained in moderate yields from the key intermediate 6,8-dibromo-imidazo[1,2-*a*]pyrazine, exhibiting good cytotoxic activity against about 60 human tumor cell lines with GI_{50} values reaching nanomolar concentrations. A particular efficacy was observed with monobenzimidazole derivative **32** against leukemia, colon, CNS and melanoma subpanels (GI_{50} = 0.31-0.39 μM). The results with DNA interactions suggested that the fluorescence of compounds **32**, **53** and **57** was

quenched significantly and the probable quenching mechanism was static process. The binding mode of these compounds to DNA was an intercalation binding in the order of **32** > **57** > **53**, which was supported by the results from ethidium bromide assay, circular dichroism and DNA-melting measurements. Interestingly, a satisfactory correlation was observed between the extent of DNA interaction and the antiproliferative activity. Moreover, the interactions of compounds **32**, **53** and **57** with bovine serum albumin were studied through fluorescence emission spectroscopy that revealed the binding to BSA with relatively high stability constants (K_b = 0.47-4.68 × 10^5 M^{-1}) which rely between optimum range to suggest binding, transfer and release upon arrival at their targets. Thus, novel imidazo[1,2-*a*]pyrazine-benzimidazole conjugates with superior bioactivity profile and their mode of interactions with DNA and BSA have been described, and the objective is thusfully reached.

2.7 Experimental section

All commercially available compounds (Aldrich, Merck, Spectrochem etc.) were used without further purification. All the recorded melting points were uncorrected and measured in open capillaries. All ^{1}H and ^{13}C NMR characterization were performed on Jeol ECS 400 NMR spectrometer, which was operated at 400 MHz for ^{1}H nuclei and 100 MHz for ^{13}C nuclei, taking $CDCl_3$ as solvent. Chemical shifts are reported in parts per million (ppm) and TMS was used as an internal reference. Coupling constants (*J*) were reported in hertz (Hz). Mass spectra were performed with Water Micromass-Q-T of Micro. Elemental analyses have been done with Thermo Scientific (Flash 2000) analyzer. Purification of synthesized compounds through column chromatography was done with the help of silica gel having mesh size of 60-120/100-200 using hexane/ethyl acetate and chloroform/methanol in various polarity systems. UV-Vis studies were carried out on a Shimadzu UV-2600 machine using slit width of 1.0 nm and matched quartz cells. Emission spectra were determined on a Varian Cary Eclipse fluorescence spectrometer. CD spectra were carried out on Applied Photophysics CD spectrophotometer. Absorption and fluorescence scans were saved as ACS II files and further processed in Excel™ to produce all graphs shown.

1,4-Dibromo-2-nitrobenzene (2):[90] 1,4-Dibromobenzene (**1**) (5 gm, 21.18 mmol) in dichloromethane (15 ml) and sulphuric acid (10 ml) was treated with dropwise addition of cooled mixture of HNO_3 and H_2SO_4 (4:1) at 0˚C and stirred for 30 min. Then, reaction was allowed to stir at room temperature. The reaction mixture was quenched by pouring into ice. The precipitated

product was filtered and thoroughly washed with water. Air dried the crude to obtained the desired product (**2**) 5.53 gm, 93% yield; R_f 0.3 (hexane); mp 68-71 ^oC.

4-Bromo-*N*-cyclohexyl-2-nitroaniline (3): 1,4-Dibromo-2-nitrobenzene (**2**) (3 gm, 10.71 mmol), cyclohexyl amine (1.27 gm, 12.85 mmol) and potassium carbonate (1.47 gm, 10.71 mmol) were taken in dry dimethylformamide (20 ml) in 100 ml dried round bottom flask and stirred the reaction mixture for 18 h at 100 ˚C. On completion of the reaction, 100 mL water was added to the reaction mixture at room temperature and extracted with ethyl acetate (3 × 50 mL). Extract was dried over anhydrous Na_2SO_4, filtered and evaporation of solvent to get crude product. Purification of the crude was done by column chromatography using hexane/ethyl acetate (20:1) as solvent system, to yield the desired product.

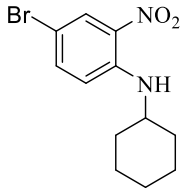

Yellow solid; 2.40 gm, 75% yield; R_f 0.3 (hexane); mp 93-96 ^oC; ^1H NMR ($CDCl_3$, 400 MHz): δ (ppm) 8.27 (d, J = 2.32 Hz, 1H, ArH), 8.12 (d, J = 7.36 Hz, 1H, NH), 7.44 (dd, ^2J = 9.16 Hz, ^3J = 2.28 Hz, 1H, ArH), 6.79 (d, J = 9.16 Hz, 1H, ArH), 3.52-3.43 (m, 1H, cyclohex-CH), 2.04-2.02 (m, 2H, cyclohex-CH_2), 1.82-1.78 (m, 2H, cyclohex-CH_2), 1.69-1.62 (m, 1H, cyclohex-CH_2), 1.47-1.25 (m, 5H, cyclohex-CH_2); ^{13}CNMR ($CDCl_3$, 100 MHz): δ (ppm) 143.5, 138.6, 131.6, 128.8, 115.8, 105.6 (ArC), 51.0 (CH), 32.4 (CH_2), 25.3 (CH_2), 24.3 (CH_2).

***N*-Cyclohexyl-2-nitro-4-(4,4,5,5-tetramethyl-1,3,2-dioxaborolan-2-yl)aniline (4):** 4-Bromo-*N*-cyclohexyl-2-nitroaniline (**3**) (2 gm, 6.68 mmol), bis(pinacolato)diboron (2.03 gm, 8.01 mmol), potassium acetate (0.98 gm, 10.02 mmol), palladium(II)bis(triphenylphosphine)dichloride (1.0 mol%) and 1,4-dioxane (20 mL) were charged in an oven dried RBF. The reaction mixture was stirred at reflux condition for 10 h until the aryl halide was completely consumed as determined by thin layer chromatography. Solvent was evaporated under reduced pressure followed by addition of 100 ml of water into it. The crude product was extracted using chloroform (3 × 50 mL). Extract was completely dried using anhydrous Na_2SO_4 and filtered to obtain the crude product. The product was purified *via* column chromatography using ethyl acetate and hexane as eluents to obtain desired product (**4**).

Reddish yellow solid; 1.89 gm, 82% yield; R_f 0.4 (10% ethyl acetate in hexane); mp 125-127 ^oC; ^1H NMR ($CDCl_3$, 400 MHz): δ (ppm) 8.63 (d, J = 1.36 Hz, 1H, ArH), 8.29 (d, J = 6.88 Hz, 1H, NH), 7.75 (dd, ^2J = 8.68 Hz, ^3J = 0.92 Hz, 1H, ArH), 6.83 (d, J = 8.72 Hz, 1H, ArH), 3.58-3.51

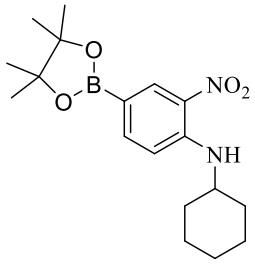

(m, 1H, cyclohex-CH), 2.06-2.03 (m, 2H, cyclohex-CH_2), 1.82-1.76 (m, 2H, cyclohex-CH_2), 1.67-1.63 (m, 1H, cyclohex-CH_2), 1.48-1.23 (m, 17H, cyclohex-CH_2 & boronate-CH_3); ^{13}C NMR ($CDCl_3$, 100 MHz): δ (ppm) 146.1, 141.3, 134.5, 131.4, 113.2 (ArC), 83.7 (C), 50.8 (CH), 32.5 (CH_2), 25.4 (CH_2), 24.7 (CH_3), 24.4 (CH_2). MS (ESI): m/z 347.2 (M^++1); Anal Calcd for $C_{18}H_{27}BN_2O_4$: C, 62.44; H, 7.86; N, 8.09; found C, 62.40; H, 7.65; N, 8.23.

4-(6-Bromoimidazo[1,2-*a*]pyrazin-8-yl)-*N*-cyclohexyl-2-nitroaniline (6): 3,6-Dibromoimidazo[1,2-*a*]pyrazine (**5**) (2 g, 7.22 mmol) in acetonitrile:water (9:1), *N*-cyclohexyl-2-nitro-4-(4,4,5,5-tetramethyl-1,3,2-dioxaborolan-2-yl)aniline (**4**) (2.49 g, 7.22 mmol) and K_2CO_3 (1.0 g, 7.22 mmol) were added under inert atmosphere. Then, $Pd(PPh_3)_4$ (5 mol%) was added with continued nitrogen purging and refluxed the reaction for 12 h. The solvent was evaporated under reduced pressure followed by 50 ml water was added and extracted with chloroform. Chloroform layer was dried over sodium sulphate. Purification of the crude product was obtained by column chromatography by adopting hexane:ethyl acetate (9:1) as eluents (**6**).

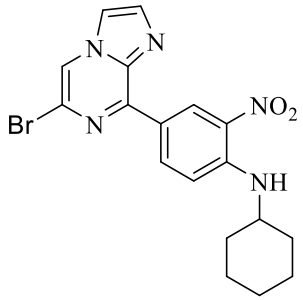

Reddish solid; 2.18 gm, 73% yield; R_f 0.2 (10% ethyl acetate in hexane); mp 158-160 ^oC; ^{1}H NMR ($CDCl_3$, 400 MHz): δ (ppm) 9.87 (d, *J* = 2.28 Hz, 1H, ArH), 8.80 (dd, ^2J = 9.16 Hz, ^3J = 1.80 Hz, 1H, ArH), 8.43 (d, *J* = 7.32 Hz, 1H, NH), 8.14 (s, 1H, ArH), 7.80 (d, *J* = 0.72 Hz, 1H, ArH), 7.68 (d, *J* = 0.92 Hz, 1H, ArH), 6.97 (d, *J* = 9.64 Hz, 1H, ArH), 3.65-3.57 (m, 1H, cyclohex-CH), 2.11-2.06 (m, 2H, cyclohex-CH_2), 1.85-1.79 (m, 2H, cyclohex-CH_2), 1.70-1.65 (m, 1H, cyclohex-CH_2), 1.51-1.24 (m, 5H, cyclohex-CH_2); ^{13}C NMR ($CDCl_3$, 100 MHz): δ (ppm) 146.4, 145.7, 137.8, 136.2, 135.6, 131.3, 129.6, 122.3, 121.5, 117.1, 113.9, 113.8 (ArC), 51.1 (CH), 32.5 (CH_2), 25.4 (CH_2), 24.3 (CH_2).

4-(6-Bromoimidazo[1,2-*a*]pyrazin-8-yl)-*N*^{1}-cyclohexylbenzene-1,2-diamine (7): Round bottom flask was charged with 4-(6-bromoimidazo[1,2-*a*]pyrazin-8-yl)-*N*-cyclohexyl-2-nitroaniline **(6)** (2 gm, 4.80 mmol) and sodium dithionite (4.18 gm, 24.03 mmol) in THF:H_2O (3:2) mixture. Ammonia solution (5 ml) was added to stirred reaction and further stirred at room temperature for 1h. The reaction mixture was extracted with ethyl acetate. Ethyl acetate layer was

dried over sodium sulphate. Crude brown product obtained was directly used for further reaction without purification.

6-Bromo-8-(1-cyclohexyl-1*H*-benzo[*d*]imidazol-5-yl)imidazo[1,2-*a*]pyrazine (8): 4-(6-Bromoimidazo[1,2-*a*]pyrazin-8-yl)-N^1-cyclohexylbenzene-1,2-diamine (**7**) (1 gm, 2.59 mmol) was stirred with triethylorthoformate (0.385 gm, 2.59 mmol) in acetic acid at room temperature for 10 min. Reaction was quenched in water and treated with $NaHCO_3$ to basify the reaction and extracted using chloroform. Sodium sulphate was used to dry the chloroform layer. Purification of crude product was done through column chromatography using ethyl acetate and hexane (3:7) as eluents.

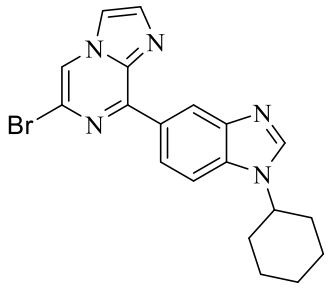

Light brown solid; 0.76 gm, 75% yield; R_f 0.4 (40% ethyl acetate in hexane); mp 175-179 ^oC; ^1H NMR ($CDCl_3$, 400 MHz): δ (ppm) 9.28 (s, 1H, ArH), 8.67 (dd, ^2J = 8.68 Hz, ^3J = 1.36 Hz, 1H, ArH), 8.18 (s, 1H, ArH), 8.09 (s, 1H, ArH), 7.82 (d, J = 0.92 Hz, 1H, ArH), 7.69 (s, 1H, ArH), 7.53 (d, J = 8.72 Hz, 1H, ArH), 4.25-4.18 (m, 1H, cyclohex-CH), 2.24-2.21 (m, 2H, cyclohex-CH_2), 1.99-1.95 (m, 2H, cyclohex-CH_2), 1.85-1.75 (m, 1H, cyclohex-CH_2), 1.57-1.25 (m, 5H, cyclohex-CH); $^{13}C\{^1H\}$ NMR ($CDCl_3$, 100 MHz): δ (ppm) 149.6, 143.5, 141.5, 138.5, 135.7, 135.2, 129.0, 124.4, 122.9, 122.4, 117.3, 113.8, 109.8 (ArC), 55.4 (CH), 33.1 (CH_2), 25.5 (CH_2), 25.2 (CH_2); MS (ESI): m/z 396.3 (M^++1); Anal Calcd for $C_{19}H_{18}BrN_5$: C, 57.59; H, 4.58; N, 17.67; found C, 57.49; H, 4.56; N, 17.53.

6-Aryl-8-(1-cyclohexyl-1*H*-benzo[*d*]imidazol-6-yl)imidazo[1,2-*a*]pyrazine (9-23): 6-Bromo-8-(1-cyclohexyl-1*H*-benzo[*d*]imidazol-5-yl)imidazo[1,2-*a*]pyrazine **(8)** (150 mg, 0.378 mmol), arylboronic acid (0.378 mmol), K_2CO_3 (52.27 mg, 0.378 mmol) and $Pd(PPh_3)_4$ (5 mol%) were taken in a mixture of acetonitrile : water (9:1). Reaction mixture was refluxed for 12-15 h under nitrogen until the completion of the reaction (checked by TLC). Solvents were evaporated under reduced pressure. Water (50 ml) was added to the mixture and extracted with chloroform. Chloroform layer was dried over sodium sulphate to get the crude product. Crude was further purified by column chromatography using hexane:ethyl acetate as eluents.

8-(1-Cyclohexyl-1*H*-benzo[*d*]imidazol-5-yl)-6-phenylimidazo[1,2-*a*]pyrazine (9): Light green solid; 126.53 mg, 85% yield; R_f 0.4 (40% ethyl acetate in hexane); mp 195-198 ^oC; ^1H NMR

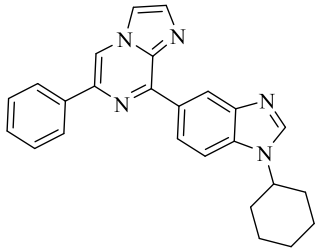

($CDCl_3$, 400 MHz): δ (ppm) 9.33 (d, *J* = 1.40 Hz, 1H, ArH), 8.92 (dd, ^2J = 8.72 Hz, ^3J = 1.36 Hz, 1H, ArH), 8.43 (s, 1H, ArH), 8.10 (d, *J* = 5.52 Hz, 3H, ArH), 7.85 (d, *J* = 0.96 Hz, 1H, ArH), 7.76 (d, *J* = 0.92 Hz, 1H, ArH), 7.58 (d, *J* = 8.28 Hz, 1H, ArH), 7.51 (t, *J* = 7.32 Hz, 2H, ArH), 7.41 (t, *J* = 7.32 Hz, 1H, ArH), 4.29-4.21 (m, 1H, cyclohex-CH), 2.28 (d, *J* = 13.28 Hz, 2H, cyclohex-CH_2), 2.01 (d, *J* = 13.72 Hz, 2H, cyclohex-CH_2), 1.88-1.78 (m, 2H, cyclohex-CH_2), 1.60-1.49 (m, 2H, cyclohex-CH_2), 1.39-1.21 (m, 2H, cyclohex-CH_2); ^{13}C NMR ($CDCl_3$, 100 MHz): δ (ppm) 149.3, 141.3, 138.9, 138.8, 136.5, 135.1, 130.7, 128.8, 128.4, 126.2, 124.7, 122.1, 114.2, 113.4, 109.7 (ArC), 55.6 (CH), 33.2 (CH_2), 25.6 (CH_2), 25.3 (CH_2); MS (ESI): m/z 394.3 (M^++1); Anal. Calcd for $C_{25}H_{23}N_5$: C, 76.31; H, 5.89; N, 17.80; found C, 76.21; H, 5.78; N, 17.83.

8-(1-Cyclohexyl-1*H*-benzo[*d*]imidazol-5-yl)-6-(4-methoxyphenyl)imidazo[1,2-*a*]pyrazine (10): Light green solid; 121.76 mg, 76% yield; R_f 0.5 (40% ethyl acetate in hexane); mp 196-199 °C; ^{1}H NMR ($CDCl_3$, 400 MHz): δ (ppm) 9.30 (s, 1H, ArH), 8.91 (d, *J* = 8.72 Hz, 1H, ArH), 8.34 (s, 1H, ArH), 8.15 (s, 1H, ArH), 8.03 (d, *J* = 8.24 Hz, 2H, ArH), 7.82 (s, 1H, ArH), 7.73 (s, 1H, ArH), 7.58 (d, *J* = 8.72 Hz, 1H, ArH), 7.02 (d, *J* = 8.72 Hz, 2H, ArH), 4.29-4.21 (m, 1H, cyclohex-CH), 3.87 (s, 3H, CH_3), 2.27 (d, *J* = 11.44 Hz, 2H, cyclohex-CH_2), 2.01 (d, *J* = 12.84 Hz, 2H, cyclohex-CH_2), 1.88-1.77 (m, 2H, cyclohex-CH_2), 1.59-1.49 (m, 2H, cyclohex-CH_2), 1.42-1.25 (m, 2H, cyclohex-CH_2); ^{13}C NMR ($CDCl_3$, 100 MHz): δ (ppm) 160.0, 148.8, 143.2, 141.2, 138.7, 138.5, 134.9, 134.7, 130.9, 129.2, 127.4, 124.7, 122.0, 114.1, 114.0, 112.4, 109.7 (ArC), 55.6 (OCH_3), 55.3 (CH), 33.2 (CH_2), 25.6 (CH_2), 25.3 (CH_2); MS (ESI): m/z 424.3 (M^++1); Anal Calcd for $C_{26}H_{25}N_5O$: C, 73.74; H, 5.95; N, 16.54; found C, 73.86; H, 5.65; N, 16.23.

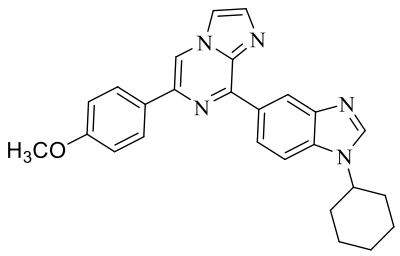

4-(8-(1-Cyclohexyl-1*H*-benzo[*d*]imidazol-5-yl)imidazo[1,2-*a*]pyrazin-6-yl)benzaldehyde (11): Light green solid; 125.97 mg, 79% yield; R_f 0.3 (40% ethyl acetate in hexane); mp 201-203 °C; ^{1}H NMR ($CDCl_3$, 400 MHz): δ (ppm) 10.06 (s, 1H, CHO), 9.31 (d, *J* = 0.92 Hz, 1H, ArH), 8.91 (dd, ^2J = 8.72 Hz, ^3J = 1.40 Hz, 1H, ArH), 8.51 (s, 1H, ArH), 8.26 (d, *J* = 8.24 Hz, 2H, ArH), 8.08 (s, 1H, ArH), 7.98 (d, *J* = 8.24 Hz, 2H, ArH), 7.86 (s, 1H, ArH), 7.77 (s, 1H, ArH), 7.58 (d, *J* = 8.72 Hz, 1H, ArH), 4.29-

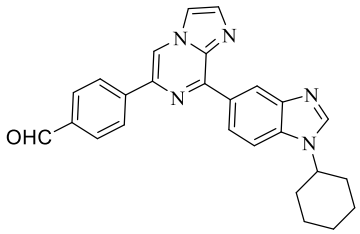

4.21 (m, 1H, cyclohex-CH), 2.28 (d, *J* = 11.0 Hz, 2H, cyclohex-CH_2), 2.02 (d, *J* = 13.76 Hz, 2H, cyclohex-CH_2), 1.88-1.78 (m, 2H, cyclohex-CH_2), 1.60-1.48 (m, 2H, cyclohex-CH_2), 1.40-1.24 (m, 2H, cyclohex-CH_2); ^{13}C NMR ($CDCl_3$, 100 MHz): δ (ppm) 191.8 (CO), 149.3, 143.8, 142.4, 141.5, 138.7, 136.9, 135.9, 135.3, 135.1, 130.2, 130.1, 126.4, 124.5, 122.4, 114.6, 114.5, 109.7 (ArC), 55.5 (CH), 33.2 (CH_2), 25.5 (CH_2), 25.3 (CH_2); MS (ESI): m/z 422.5 (M^++1); Anal Calcd for $C_{26}H_{23}N_5$: C, 74.09; H, 5.50; N, 16.62; found C, 74.32; H, 5.62; N, 16.42.

8-(1-Cyclohexyl-1*H*-benzo[*d*]imidazol-5-yl)-6-(naphthalen-1-yl)imidazo[1,2-*a*]pyrazine (12):

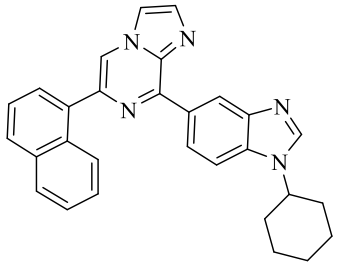

Light green solid; 134.24 mg, 80% yield; R_f 0.3 (40% ethyl acetate in hexane); mp 199-202 ^{o}C; ^{1}H NMR ($CDCl_3$, 400 MHz): δ (ppm) 9.32 (d, *J* = 0.92 Hz, 1H, ArH), 8.79 (dd, ^2J = 8.24 Hz, ^3J = 0.92 Hz, 1H, ArH), 8.29-8.27 (m, 1H, ArH), 8.22 (s, 1H, ArH), 8.03 (s, 1H, ArH), 7.93 (d, *J* = 6.88 Hz, 2H, ArH), 7.88 (s, 1H, ArH), 7.75 (s, 1H, ArH), 7.65 (t, *J* = 7.80 Hz, 1H, ArH), 7.56-7.48 (m, 4H, ArH), 4.22-4.16 (m, 1H, cyclohex-CH), 2.22 (d, *J* = 11.44 Hz, 2H, cyclohex-CH_2), 1.97 (d, *J* = 13.28 Hz, 2H, cyclohex-CH_2), 1.83-1.73 (m, 2H, cyclohex-CH_2), 1.55-1.43 (m, 2H, cyclohex-CH_2), 1.39-1.25 (m, 2H, cyclohex-CH_2); ^{13}C NMR ($CDCl_3$, 100 MHz): δ (ppm) 149.1, 143.7, 141.2, 140.0, 138.5, 135.1, 135.0, 134.9, 133.9, 131.6, 130.4, 129.0, 128.2, 127.5, 126.4, 125.9, 125.7, 125.1, 124.4, 122.6, 117.0, 114.0, 109.6 (ArC), 55.4 (CH), 33.1 (CH_2), 25.5 (CH_2), 25.2 (CH_2); MS (ESI): m/z 444.5 (M^++1); Anal Calcd for $C_{29}H_{25}N_5$: C, 78.53; H, 5.68; N, 15.79; found C, 78.51; H, 5.75; N, 15.68.

8-(1-Cyclohexyl-1*H*-benzo[*d*]imidazol-5-yl)-6-(4-fluorophenyl)imidazo[1,2-*a*]pyrazine (13):

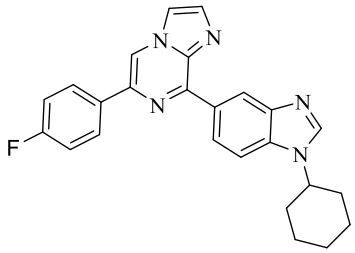

Light green solid; 126.09 mg, 81% yield; R_f 0.4 (40% ethyl acetate in hexane); mp 187-189 ^{o}C; ^{1}H NMR ($CDCl_3$, 400 MHz): δ (ppm) 9.30 (s, 1H, ArH), 8.90 (d, *J* = 8.68 Hz, 1H, ArH), 8.39 (s, 1H, ArH), 8.13 (s, 1H, ArH), 8.10-8.02 (m, 2H, ArH), 7.85 (s, 1H, ArH), 7.76 (s, 1H, ArH), 7.58 (d, *J* = 8.72 Hz, 1H, ArH), 7.18 (t, *J* = 8.68 Hz, 2H, ArH), 4.29-4.22 (m, 1H, cyclohex-CH), 2.28 (d, *J* = 12.84 Hz, 2H, cyclohex-CH_2), 2.02 (d, *J* = 13.76 Hz, 2H, cyclohex-CH_2), 1.88-1.78 (m, 2H, cyclohex-CH_2), 1.60-1.49 (m, 2H, cyclohex-CH_2), 1.42-1.25 (m, 2H, cyclohex-CH_2); ^{13}C NMR ($CDCl_3$, 100 MHz): δ (ppm) 149.1, 141.4, 138.7, 137.8, 135.2, 134.9, 132.7, 130.6, 127.9, 127.7, 124.7, 122.2, 115.8, 115.4, 114.2, 113.1, 109.7 (ArC), 55.6 (CH), 33.2 (CH_2), 25.6 (CH_2), 25.3 (CH_2);

MS (ESI): m/z 412.3 (M^++1); Anal Calcd for $C_{25}H_{22}FN_5$: C, 72.97; H, 5.39; N, 17.02; found C, 72.85; H, 5.20; N, 17.01.

8-(1-Cyclohexyl-1*H*-benzo[*d*]imidazol-5-yl)-6-(thien-3-yl)imidazo[1,2-*a*]pyrazine (14):

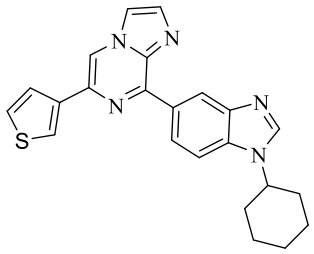

Light green solid; 126.94 mg, 84% yield; R_f 0.3 (40% ethyl acetate in hexane); mp 185-188 °C; ^{1}H NMR ($CDCl_3$, 400 MHz): δ (ppm) 9.28 (s, 1H, ArH), 8.90 (d, *J* = 8.72 Hz, 1H, ArH), 8.34 (s, 1H, ArH), 8.23 (s, 1H, ArH), 8.04 (d, *J* = 1.84 Hz, 1H, ArH), 7.83 (s, 1H, ArH), 7.74 (s, 1H, ArH), 7.62 (d, *J* = 4.12 Hz, 2H, ArH), 7.45 (dd, ^2J = 4.56 Hz, ^3J = 2.72 Hz, 1H, ArH), 4.32-4.26 (m, 1H, cyclohex-CH), 2.29 (d, *J* = 11.88 Hz, 2H, cyclohex-CH_2), 2.03 (d, *J* = 13.76 Hz, 2H, cyclohex-CH_2), 1.89-1.79 (m, 2H, cyclohex-CH_2), 1.60-1.50 (m, 2H, cyclohex-CH_2), 1.42-1.25 (m, 2H, cyclohex-CH_2); ^{13}C NMR ($CDCl_3$, 100 MHz): δ (ppm) 149.1, 138.9, 138.7, 135.4, 135.0, 130.9, 126.6, 124.9, 122.8, 122.0, 114.2, 112.9, 109.8 (ArC), 55.8 (CH), 33.2 (CH_2), 25.6 (CH_2), 25.3 (CH_2); MS (ESI): m/z 400.2 (M^++1); Anal Calcd for $C_{23}H_{21}N_5S$: C, 69.15; H, 5.30; N, 17.53; S, 8.02; found C, 69.26; H, 5.34; N, 17.51; S, 8.13.

8-(1-Cyclohexyl-1*H*-benzo[*d*]imidazol-5-yl)-6-(*m*-tolyl)imidazo[1,2-*a*]pyrazine (15): Light

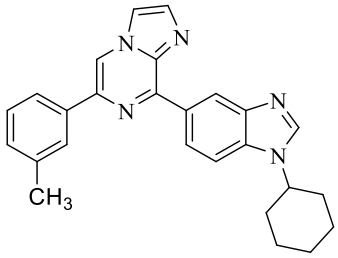

green solid; 117.16 mg, 76% yield; R_f 0.5 (40% ethyl acetate in hexane); mp 183-186 °C; ^{1}H NMR ($CDCl_3$, 400 MHz): δ (ppm) 9.32 (d, *J* = 0.88 Hz, 1H, ArH), 8.93 (dd, ^2J = 8.68 Hz, ^3J = 1.36 Hz, 1H, ArH), 8.38 (s, 1H, ArH), 8.06 (s, 1H, ArH), 7.93 (s, 1H, ArH), 7.84 (d, *J* = 7.32 Hz, 2H, ArH), 7.73 (d, *J* = 0.92 Hz, 1H, ArH), 7.57 (d, *J* = 8.68 Hz, 1H, ArH), 7.36 (t, *J* = 7.32 Hz, 1H, ArH), 7.22 (d, *J* = 7.36 Hz, 1H, ArH), 4.27-4.19 (m, 1H, cyclohex-CH), 2.45 (s, 3H, CH_3), 2.26 (d, *J* = 11.41 Hz, 2H, cyclohex-CH_2), 1.99 (d, *J* = 13.72 Hz, 2H, cyclohex-CH_2), 1.86-1.76 (m, 2H, cyclohex-CH_2), 1.57-1.46 (m, 2H, cyclohex-CH_2), 1.38-1.25 (m, 2H, cyclohex-CH_2); ^{13}C NMR ($CDCl_3$, 100 MHz): δ (ppm) 149.0, 143.8, 141.3, 138.8, 138.6, 138.4, 136.5, 134.9, 130.5, 129.2, 128.5, 126.8, 124.5, 123.0, 122.2, 114.1, 113.3, 109.5 (ArC), 55.4 (CH), 33.1 (CH_2), 25.5 (CH_2), 25.2 (CH_2), 21.5 (CH_3); MS (ESI): m/z 408.6 (M^++1); Anal Calcd for $C_{26}H_{25}N_5$: C, 76.63; H, 6.18; N, 17.19; found C, 76.51; H, 6.10; N, 17.37.

8-(1-Cyclohexyl-1*H*-benzo[*d*]imidazol-5-yl)-6-(4-ethylphenyl)imidazo[1,2-*a*]pyrazine (16): Light green solid; 132.35 mg, 83% yield; R_f 0.5 (40% ethyl acetate in hexane); mp 182-185 °C;

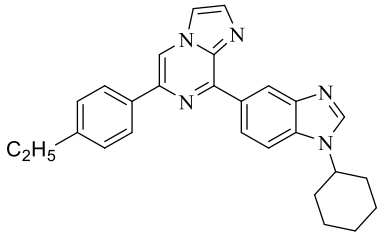

^{1}H NMR ($CDCl_3$, 400 MHz): δ (ppm) 9.33 (s, 1H, ArH), 8.93 (dd, ^2J = 8.68 Hz, ^3J = 1.36 Hz, 1H, ArH), 8.37 (s, 1H, ArH), 8.07 (s, 1H, ArH), 8.01 (d, J = 8.24 Hz, 2H, ArH), 7.82 (s, 1H, ArH), 7.73 (s, 1H, ArH), 7.57 (d, J = 8.68 Hz, 1H, ArH), 7.33 (d, J = 8.24 Hz, 2H, ArH), 4.27-4.19 (m, 1H, cyclohex-CH), 2.74 (q, J = 7.80 Hz, 2H, CH_2), 2.26 (d, J = 11.48 Hz, 2H, cyclohex-CH_2), 2.00 (d, J = 13.76 Hz, 2H, cyclohex-CH_2), 1.86-1.76 (m, 2H, cyclohex-CH_2), 1.58-1.47 (m, 2H, cyclohex-CH_2), 1.38-1.25 (m, 5H, cyclohex-CH_2, CH_3); ^{13}C NMR ($CDCl_3$, 100 MHz): δ (ppm) 148.9, 144.7, 143.9, 141.3, 138.8, 138.6, 134.9, 134.0, 130.6, 128.2, 126.1, 124.5, 122.3, 114.1, 112.9, 109.5 (ArC), 55.4 (CH), 33.1 (CH_2), 28.5 (CH_2), 25.5 (CH_2), 25.3 (CH_2), 15.5 (CH_3); MS (ESI): m/z 422.5 (M^++1); Anal Calcd for $C_{27}H_{27}N_5$: C, 76.93; H, 6.46; N, 16.61; found C, 76.72; H, 6.59; N, 16.50.

1-(4-(8-(1-Cyclohexyl-1*H*-benzo[*d*]imidazol-5-yl)imidazo[1,2-*a*]pyrazin-6-yl)phenyl)ethan-1-one (17): Light green solid; 128.52 mg, 78% yield; R_f 0.6 (40% ethyl acetate in hexane); mp 200-203 ^{o}C; ^{1}H NMR ($CDCl_3$, 400 MHz): δ (ppm) 9.33 (s, 1H, ArH), 8.92 (dd, ^2J = 8.72 Hz, ^3J = 1.40 Hz, 1H, ArH), 8.52 (s, 1H, ArH), 8.20 (d, J = 8.28 Hz, 2H, ArH), 8.13 (s, 1H, ArH), 8.08 (d, J = 8.24 Hz, 2H, ArH), 7.87 (s, 1H, ArH), 7.79 (s, 1H, ArH), 7.59 (d, J = 8.72 Hz, 1H, ArH), 4.30-4.22 (m, 1H, cyclohex-CH), 2.66 (s, 3H, CH_3), 2.29 (d, J = 11.92 Hz, 2H, cyclohex-CH_2), 2.02 (d, J = 13.72 Hz, 2H, cyclohex-CH_2), 1.89-1.79 (m, 2H, cyclohex-CH_2), 1.60-1.49 (m, 2H, cyclohex-CH_2), 1.40-1.25 (m, 2H, cyclohex-CH_2); ^{13}C NMR ($CDCl_3$, 100 MHz): δ (ppm) 197.7 (C=O), 149.3, 143.5, 141.4, 141.1, 138.8, 137.2, 136.7, 135.3, 135.0, 130.4, 128.8, 126.1, 124.7, 122.3, 114.5, 114.4, 109.7 (ArC), 55.6 (CH), 33.2 (CH_2), 26.7 (CH_3), 25.6 (CH_2), 25.3 (CH_2); MS (ESI): m/z 436.4 (M^++1); Anal Calcd for $C_{27}H_{25}N_5O$: C, 74.46; H, 5.79; N, 16.08; found C, 74.77; H, 5.72; N, 16.01.

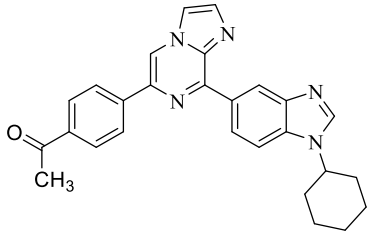

6-(4-Chlorophenyl)-8-(1-cyclohexyl-1*H*-benzo[*d*]imidazol-5-yl)imidazo[1,2-*a*]pyrazine (18): Light green solid; 121.30 mg, 75% yield; R_f 0.5 (40% ethyl acetate in hexane); mp 193-196 ^{o}C; ^{1}H NMR ($CDCl_3$, 400 MHz): δ (ppm) 9.30 (s, 1H, ArH), 8.90 (d, J = 8.28 Hz, 1H, ArH), 8.41 (s, 1H, ArH), 8.08 (s, 1H, ArH), 8.04 (d, J = 8.24 Hz, 2H, ArH), 7.85 (s, 1H, ArH), 7.76 (s, 1H, ArH),

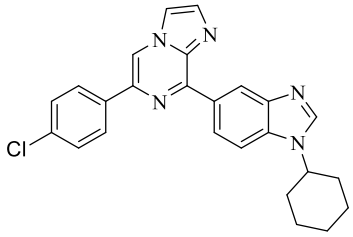

7.58 (d, *J* = 8.72 Hz, 1H, ArH), 7.47 (d, *J* = 8.68 Hz, 2H, ArH), 4.29-4.21 (m, 1H, cyclohex-CH), 2.28 (d, *J* = 11.44 Hz, 2H, cyclohex- CH_2), 2.01 (d, *J* = 12.36 Hz, 2H, cyclohex-CH_2), 1.88-1.78 (m, 2H, cyclohex-CH_2), 1.60-1.49 (m, 2H, cyclohex-CH_2), 1.43-1.25 (m, 2H, cyclohex-CH_2); ^{13}C NMR ($CDCl_3$, 100 MHz): δ (ppm) 149.3, 143.8, 141.4, 138.8, 137.5, 135.2, 135.1, 135.0, 134.4, 130.4, 128.9, 127.3, 124.6, 122.4, 114.3, 113.3, 109.6 (ArC), 55.5 (CH), 33.2 (CH_2), 25.6 (CH_2), 25.3 (CH_2); MS (ESI): m/z 428.4 (M^++1); Anal Calcd for $C_{25}H_{22}ClN_5$: C, 70.17; H, 5.18; N, 16.37; found C, 70.25; H, 5.25; N, 16.34.

6-(4-Bromophenyl)-8-(1-cyclohexyl-1*H*-benzo[*d*]imidazol-5-yl)imidazo[1,2-*a*]pyrazine (19):

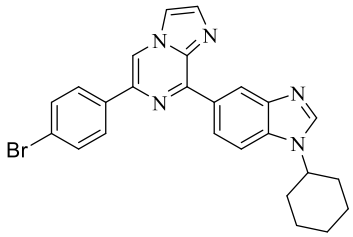

Light green solid; 141.24 mg, 79% yield; R_f 0.5 (40% ethyl acetate in hexane); mp 195-198 °C; ^{1}H NMR ($CDCl_3$, 400 MHz): δ (ppm) 9.30 (d, *J* = 0.92 Hz, 1H, ArH), 8.89 (dd, ^2J = 8.68 Hz, ^3J = 1.36 Hz, 1H, ArH), 8.40 (s, 1H, ArH), 8.09 (s, 1H, ArH), 7.96 (d, *J* = 8.68 Hz, 2H, ArH), 7.84 (d, *J* = 0.92 Hz, 1H, ArH), 7.74 (d, *J* = 0.92 Hz, 1H, ArH), 7.61 (d, *J* = 8.68 Hz, 2H, ArH), 7.57 (s, 1H, ArH), 4.28-4.20 (m, 1H, cyclohex-CH), 2.27 (d, *J* = 9.64 Hz, 2H, cyclohex-CH_2), 2.01 (d, *J* = 11.92 Hz, 2H, cyclohex-CH_2), 1.87-1.77 (m, 2H, cyclohex-CH_2), 1.58-1.49 (m, 2H, cyclohex-CH_2), 1.42-1.25 (m, 2H, cyclohex-CH_2); ^{13}C NMR ($CDCl_3$, 100 MHz): δ (ppm) 149.2, 143.7, 141.4, 138.7, 137.5, 135.6, 135.2, 135.0, 131.8, 130.4, 128.5, 127.6, 126.5, 124.6, 122.7, 122.3, 114.3, 113.3, 109.6 (ArC), 55.5 (CH), 33.2 (CH_2), 25.6 (CH_2), 25.3 (CH_2); MS (ESI): m/z 472.1 (M^++1); Anal Calcd for $C_{25}H_{22}BrN_5$: C, 63.57; H, 4.69; N, 14.83; found C, 63.51; H, 4.74; N, 14.88.

8-(1-Cyclohexyl-1*H*-benzo[*d*]imidazol-5-yl)-6-(2-methoxyphenyl)imidazo[1,2-*a*]pyrazine (20): Light green solid; 128.18 mg, yield 80%; R_f 0.5 (40% ethyl acetate in hexane); mp 195-198 °C; ^{1}H NMR ($CDCl_3$, 400 MHz): δ (ppm) 9.29 (s, 1H, ArH), 8.91 (dd, ^2J = 8.72 Hz, ^3J = 1.40 Hz, 1H, ArH), 8.87 (s, 1H, ArH), 8.46 (dd, ^2J = 7.80 Hz, ^3J = 1.84 Hz, 1H, ArH), 8.06 (s, 1H, ArH), 7.83 (s, 1H, ArH), 7.74 (d, *J* =0.92 Hz, 1H, ArH), 7.57 (d, *J* = 8.68 Hz, 1H, ArH), 7.39-7.35 (m, 1H, ArH), 7.16 (t, *J* = 7.36 Hz, 1H, ArH), 7.04 (d, *J* = 8.24 Hz, 1H, ArH), 4.28-4.20 (m, 1H, cyclohex-CH), 3.96 (s, 3H, CH_3), 2.27 (d, *J* = 11.48 Hz, 2H, cyclohex-CH_2), 2.00 (d, *J* = 13.72 Hz, 2H, cyclohex-CH_2), 1.87-1.76 (m, 2H, cyclohex-

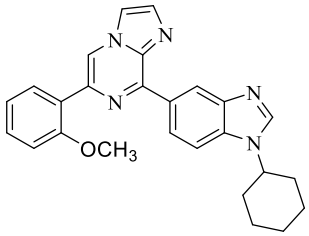

CH_2), 1.58-1.47 (m, 2H, cyclohex-CH_2), 1.37-1.25 (m, 2H, cyclohex-CH_2); ^{13}C NMR ($CDCl_3$, 100 MHz): δ (ppm) 156.7, 148.6, 143.8, 141.2, 138.6, 134.9, 134.8, 130.9, 130.8, 129.3, 125.1, 124.5, 122.1, 121.1, 118.1, 114.1, 111.1, 109.5 (ArC), 55.5 (CH), 55.4 (OCH_3), 33.2 (CH_2), 25.5 (CH_2), 25.3 (CH_2); MS (ESI): m/z 424.3 (M^++1); Anal Calcd for $C_{26}H_{25}N_5O$: C, 73.74; H, 5.95; N, 16.54; found C, 73.80; H, 5.90; N, 16.44.

8-(1-Cyclohexyl-1*H*-benzo[*d*]imidazol-5-yl)-6-(2-fluorophenyl)imidazo[1,2-*a*]pyrazine (21):

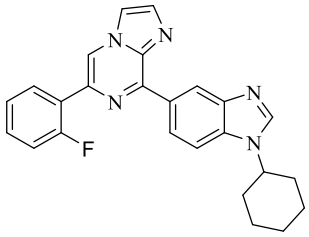

Light green solid; 133.88 mg, 86% yield; R_f 0.4 (40% ethyl acetate in hexane); mp 190-193 °C; ^1H NMR ($CDCl_3$, 400 MHz): δ (ppm) 9.30 (s, 1H, ArH), 8.90 (d, *J* = 8.68 Hz, 1H, ArH), 8.39 (s, 1H, ArH), 8.13-8.05 (m, 3H, ArH), 7.85 (s, 1H, ArH), 7.76 (s, 1H, ArH), 7.58 (d, *J* = 8.72 Hz, 1H, ArH), 7.22-7.16 (m, 2H, ArH), 4.29-4.22 (m, 1H, cyclohex-CH), 2.28 (d, *J* = 12.84 Hz, 2H, cyclohex-CH_2), 2.02 (d, *J* = 13.76 Hz, 2H, cyclohex-CH_2), 1.88-1.78 (m, 2H, cyclohex-CH_2), 1.60-1.49 (m, 2H, cyclohex-CH_2), 1.42-1.25 (m, 2H, cyclohex-CH_2); ^{13}C NMR ($CDCl_3$, 100 MHz): δ (ppm) 149.1, 141.4, 138.7, 137.8, 135.2, 134.9, 132.7, 130.6, 127.9, 127.7, 124.7, 122.2, 115.8, 115.4, 114.2, 113.1, 109.7 (ArC), 55.6 (CH), 33.2 (CH_2), 25.6 (CH_2), 25.3 (CH_2). MS (ESI): m/z 412.3 (M^++1); Anal Calcd for $C_{25}H_{22}FN_5$: C, 72.97; H, 5.39; N, 17.02; found C, 72.95; H, 5.43; N, 17.08.

8-(1-Cyclohexyl-1*H*-benzo[*d*]imidazol-5-yl)-6-(thien-2-yl)imidazo[1,2-*a*]pyrazine (22):

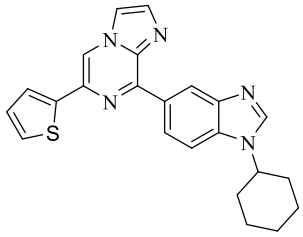

Light green solid; 120.90 mg, 80% yield; R_f 0.3 (40% ethyl acetate in hexane); mp 187-190 °C; ^1H NMR ($CDCl_3$, 400 MHz): δ (ppm) 9.32 (s, 1H, ArH), 8.89 (dd, ^2J = 8.72 Hz, ^3J = 0.92 Hz, 1H, ArH), 8.37 (s, 1H, ArH), 8.08 (s, 1H, ArH), 7.84 (s, 1H, ArH), 7.74 (s, 1H, ArH), 7.60-7.56 (m, 2H, ArH), 7.40 (d, *J* = 5.04 Hz, 1H, ArH), 7.15-7.13 (dd, ^2J = 3.68 Hz, ^3J = 1.36 Hz, 1H, ArH), 4.29-4.22 (m, 1H, cyclohex-CH), 2.28 (d, *J* = 10.08 Hz, 2H, cyclohex-CH_2), 2.02 (d, *J* = 13.28 Hz, 2H, cyclohex-CH_2), 1.89-1.78 (m, 2H, cyclohex-CH_2), 1.60-1.49 (m, 2H, cyclohex-CH_2), 1.42-1.24 (m, 2H, cyclohex-CH_2); ^{13}C NMR ($CDCl_3$, 100 MHz): δ (ppm) 149.1, 138.9, 138.7, 135.4, 135.0, 130.9, 126.6, 124.9, 122.8, 122.0, 114.2, 112.9, 109.8, (ArC), 55.8 (CH), 33.2 (CH_2), 25.6 (CH_2), 25.3 (CH_2); MS (ESI): m/z 400.2 (M^++1); Anal Calcd for $C_{23}H_{21}N_5S$: C, 69.15; H, 5.30; N, 17.53; S, 8.02; found C, 69.17; H, 5.26; N, 17.58; S, 8.08.

8-(1-Cyclohexyl-1*H*-benzo[*d*]imidazol-5-yl)-6-(3-(trifluoromethyl)phenyl)imidazo[1,2-*a*]pyrazine (23): Light green solid; 141.44 mg, 81% yield; R_f 0.6 (40% ethyl acetate in hexane);

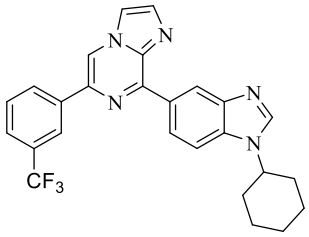

mp 196-199 °C; ^{1}H NMR ($CDCl_3$, 400 MHz): δ (ppm) 9.33 (s, 1H, ArH), 8.89 (dd, ^2J = 8.68 Hz, ^3J = 0.92 Hz, 1H, ArH), 8.50 (s, 1H, ArH), 8.32 (d, J = 6.44 Hz, 2H, ArH), 8.08 (s, 1H, ArH), 7.88 (s, 1H, ArH), 7.80 (s, 1H, ArH), 7.68-7.63 (m, 2H, ArH), 7.60 (d, J = 8.72 Hz, 1H, ArH), 4.30-4.22 (m, 1H, cyclohex-CH), 2.29 (d, J = 11.48 Hz, 2H, cyclohex-CH_2), 2.02 (d, J = 13.76 Hz, 2H, cyclohex-CH_2), 1.89-1.79 (m, 2H, cyclohex-CH_2), 1.61-1.49 (m, 2H, cyclohex-CH_2), 1.43-1.25 (m, 2H, cyclohex-CH_2); ^{13}C NMR ($CDCl_3$, 100 MHz): δ (ppm) 149.6, 143.9, 141.5, 138.9, 137.6, 137.2, 135.4, 135.1, 131.3, 131.0, 130.2, 129.4, 129.3, 125.2, 125.1, 124.5, 122.8, 122.7, 122.5, 114.4, 113.8, 109.7 (ArC), 55.6 (CH), 33.2 (CH_2), 25.6 (CH_2), 25.3 (CH_2); MS (ESI): m/z 462.4 (M^++1); Anal Calcd for $C_{26}H_{22}F_3N_5$: C, 67.67; H, 4.81; N, 15.18; found C, 67.73; H, 4.98; N, 15.35.

2,4-Dibromo-1-nitrobenzene (25): Procedure for synthesis of 2,4-dibromo-1-nitrobenzene (**25**) is similar as that for the synthesis of 1,4-dibromo-2-nitrobenzene (**2**) using 1,3-dibromobenzene (**24**).

5-Bromo-*N*-cyclohexyl/benzyl-2-nitroaniline (26a-b): Procedure for synthesis of 5-bromo-*N*-cyclohexyl-2-nitroaniline (**26a**) and *N*-benzyl-5-bromo-2-nitroaniline (**26b**) is similar as that for the synthesis of 4-bromo-*N*-cyclohexyl-2-nitroaniline (**3**) using 2,4-dibromo-1-nitrobenzene (**25**).

5-Bromo-*N*-cyclohexyl-2-nitroaniline (26a): Yellow solid; 2.36 gm, 74% yield; R_f 0.3 (hexane);

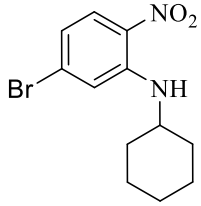

mp 90-93 °C; ^{1}H NMR ($CDCl_3$, 400 MHz): δ (ppm) 8.13 (d, J = 6.88 Hz, 1H, NH), 8.00 (d, J = 9.16 Hz, 1H, ArH), 7.01 (d, J = 1.84 Hz, 1H, ArH), 6.69 (dd, ^2J = 9.16 Hz, ^3J = 2.28 Hz, 1H, ArH), 3.49-3.42 (m, 1H, cyclohex-CH), 2.05-2.02 (m, 2H, cyclohex-CH_2), 1.82-1.74 (m, 2H, cyclohex-CH_2), 1.68-1.64 (m, 1H, cyclohex-CH_2), 1.49-1.28 (m, 5H, cyclohex-CH_2); ^{13}C NMR ($CDCl_3$, 100 MHz): δ (ppm) 144.8, 131.4, 130.3, 128.1, 117.9, 116.4 (ArC), 50.9 (CH), 32.4 (CH_2), 25.3 (CH_2), 24.3 (CH_2).

***N*-Cyclohexyl/benzyl-2-nitro-5-(4,4,5,5-tetramethyl-1,3,2-dioxaborolan-2-yl)aniline (27a-b):** Procedures for synthesis of *N*-cyclohexyl-2-nitro-5-(4,4,5,5-tetramethyl-1,3,2-dioxaborolan-2-yl)aniline (**27a**) and *N*-benzyl-2-nitro-5-(4,4,5,5-tetramethyl-1,3,2-dioxaborolan-2-yl)aniline **(27b)** are similar as that for the synthesis of *N*-cyclohexyl-2-nitro-4-(4,4,5,5-tetramethyl-1,3,2-

dioxaborolan-2-yl)aniline (**4**) from 5-bromo-*N*-cyclohexyl-2-nitroaniline (**26a**) and *N*-benzyl-5-bromo-2-nitroaniline (**26b**), respectively.

***N*-Cyclohexyl-2-nitro-5-(4,4,5,5-tetramethyl-1,3,2-dioxaborolan-2-yl)aniline (27a):** Reddish

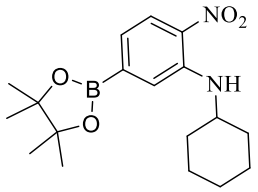

yellow solid; 1.80 gm, 78% yield; R_f 0.5 (10% ethyl acetate in hexane); mp 120-122 ^oC; ^1H NMR ($CDCl_3$, 400 MHz): δ (ppm) 8.13 (d, *J* = 8.68 Hz, 2H, NH & ArH), 7.28 (s, 1H, ArH), 6.96 (d, *J* = 8.72 Hz, 1H, ArH), 3.71-3.63 (m, 1H, cyclohex-CH), 2.07-2.02 (m, 2H, cyclohex- CH_2), 1.83-1.76 (m, 2H, cyclohex-CH_2), 1.67-1.63 (m, 1H, cyclohex-CH_2), 1.53-1.28 (m, 17H, cyclohex-CH_2 & boronate-CH_3); ^{13}C NMR ($CDCl_3$, 100 MHz): δ (ppm) 143.8, 135.5, 132.6, 125.7, 120.8, 119.9 (ArC), 84.3 (C), 50.3 (CH), 32.7 (CH_2), 25.5 (CH_2), 24.7 (CH_3), 24.3 (CH_2). MS (ESI): m/z 346.2 (M^++1); Anal Calcd for $C_{18}H_{27}BN_2O_4$: C, 62.44; H, 7.86; N, 8.09; found C, 62.40; H, 7.80; N, 8.13.

5-(6-Bromoimidazo[1,2-*a*]pyrazin-8-yl)-*N*-cyclohexyl/benzyl-2-nitroaniline (28a-b): Procedures for synthesis of 5-(6-bromoimidazo[1,2-*a*]pyrazin-8-yl)-*N*-cyclohexyl-2-nitroaniline (**28a**) and *N*-benzyl-5-(6-bromoimidazo[1,2-*a*]pyrazin-8-yl)-2-nitroaniline (**28b**) are similar as that for the synthesis of 4-(6-bromoimidazo[1,2-*a*]pyrazin-8-yl)-*N*-cyclohexyl-2-nitroaniline (**6**) from *N*-cyclohexyl-2-nitro-5-(4,4,5,5-tetramethyl-1,3,2-dioxaborolan-2-yl)aniline (**27a**) and *N*-benzyl-2-nitro-5-(4,4,5,5-tetramethyl-1,3,2-dioxaborolan-2-yl)aniline **(27b)**, respectively.

5-(6-Bromoimidazo[1,2-*a*]pyrazin-8-yl)-*N*-cyclohexyl-2-nitroaniline (28a): Reddish solid;

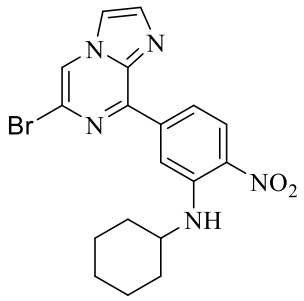

2.09 gm, 70% yield; R_f 0.3 (10% ethyl acetate in hexane); mp 152-154 ^oC; ^1H NMR ($CDCl_3$, 400 MHz): δ (ppm) 8.69 (d, *J* = 1.68 Hz, 1H, ArH), 8.32 (s, 1H, ArH), 8.29 (d, *J* = 8.68 Hz, 1H, ArH), 8.22 (d, *J* = 7.32 Hz, 1H, NH), 7.89 (d, *J* = 0.92 Hz, 1H, ArH), 7.82 (dd, ^2J = 9.16 Hz, ^3J = 1.84 Hz, 1H, ArH), 7.77 (d, *J* = 0.92 Hz, 1H, ArH), 3.79-3.70 (m, 1H, cyclohex-CH), 2.19-2.16 (m, 2H, cyclohex- CH_2), 2.06-2.01 (m, 2H, cyclohex-CH_2), 1.87-1.77 (m, 1H, cyclohex-CH_2), 1.70-1.25 (m, 5H, cyclohex-CH_2); ^{13}C NMR ($CDCl_3$, 100 MHz): δ (ppm) 144.4, 141.1, 136.5, 126.8, 125.8, 122.4, 120.8, 120.0, 119.1, 117.3, 115.1, 114.0 (ArC), 51.3 (CH), 32.7 (CH_2), 25.5 (CH_2), 24.3 (CH_2).

5-(6-Bromoimidazo[1,2-*a*]pyrazin-8-yl)-*N*^{1}-cyclohexyl/benzylbenzene-1,2-diamine (29a-b): Procedures for synthesis of 5-(6-bromoimidazo[1,2-*a*]pyrazin-8-yl)-*N*^{1}-cyclohexylbenzene-1,2-diamine (**29a**) and *N*^{1}-benzyl-5-(6-bromoimidazo[1,2-*a*]pyrazin-8-yl)benzene-1,2-diamine (**29b**)

are similar as that for the synthesis of 4-(6-bromoimidazo[1,2-*a*]pyrazin-8-yl)-N^1-cyclohexylbenzene-1,2-diamine (**7**) from 5-(6-bromoimidazo[1,2-*a*]pyrazin-8-yl)-*N*-cyclohexyl-2-nitroaniline (**28a**) and *N*-benzyl-5-(6-bromoimidazo[1,2-*a*]pyrazin-8-yl)-2-nitroaniline (**28b**), respectively. Compounds **26b-29b** were used further without purification.

6-Bromo-8-(1-cyclohexyl/benzyl-1*H*-benzo[*d*]imidazol-6-yl)imidazo[1,2-*a*]pyrazine (30a-b): Procedures for synthesis of 6-bromo-8-(1-cyclohexyl-1*H*-benzo[*d*]imidazol-6-yl)imidazo[1,2-*a*]pyrazine (**30a**) and 8-(1-benzyl-1*H*-benzo[*d*]imidazol-6-yl)-6-bromoimidazo[1,2-*a*]pyrazine (**30b**) are similar as that for the synthesis of 6-bromo-8-(1-cyclohexyl-1*H*-benzo[*d*]imidazol-5-yl)imidazo[1,2-*a*]pyrazine (**8**) from 5-(6-bromoimidazo[1,2-*a*]pyrazin-8-yl)-N^1-cyclohexylbenzene-1,2-diamine (**29a**) and N^1-benzyl-5-(6-bromoimidazo[1,2-*a*]pyrazin-8-yl)benzene-1,2-diamine (**29b**), respectively.

6-Bromo-8-(1-cyclohexyl-1*H*-benzo[*d*]imidazol-6-yl)imidazo[1,2-*a*]pyrazine (30a): Light

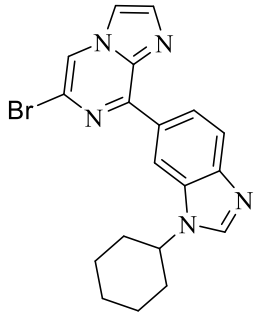

brown solid; 0.91 gm, 90% yield; R_f 0.5 (40% ethyl acetate in hexane); mp 175-178 ^oC; ^1H NMR ($CDCl_3$, 400 MHz): δ (ppm) 9.00 (d, *J* = 1.36, 1H, ArH), 8.72 (dd, ^2J = 8.72 Hz, ^3J = 1.84 Hz, 1H, ArH), 8.23 (s, 1H, ArH), 8.11 (s, 1H, ArH), 7.93 (d, *J* = 8.24 Hz, 1H, ArH), 7.88 (d, *J* = 1.36 Hz, 1H, ArH), 7.72 (d, *J* = 1.36 Hz, 1H, ArH), 4.44-4.36 (m, 1H, cyclohex-CH), 2.30 (d, *J* = 11.48 Hz, 2H, cyclohex-CH_2), 2.01 (d, *J* = 13.76 Hz, 2H, cyclohex-CH_2), 1.88-1.78 (m, 2H, cyclohex-CH_2), 1.64-1.53 (m, 2H, cyclohex-CH_2), 1.43-1.24 (m, 2H, cyclohex-CH_2); ^{13}C NMR ($CDCl_3$, 100 MHz): δ (ppm) 149.5, 145.7, 142.2, 138.6, 135.8, 133.3, 129.3, 124.0, 122.4, 119.8, 117.5, 113.8, 112.5 (ArC), 55.2 (CH), 33.4 (CH_2), 25.5 (CH_2), 25.3 (CH_2). MS (ESI): m/z 395.0 (M^++1); Anal Calcd for $C_{19}H_{18}BrN_5$: C, 57.59; H, 4.58; N, 17.67; found C, 57.48; H, 4.70; N, 17.93.

8-(1-Benzyl-1*H*-benzo[*d*]imidazol-6-yl)-6-bromoimidazo[1,2-*a*]pyrazine (30b): Light brown solid; 0.77 gm, 80% yield; R_f 0.4 (40% ethyl acetate in hexane); mp 182-185 ^oC; ^1H NMR ($CDCl_3$,

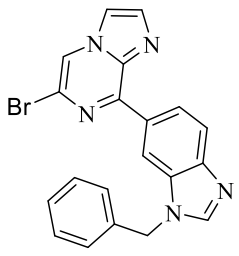

400 MHz): δ (ppm) 8.99 (d, *J* = 1.40 Hz, 1H, ArH), 8.71 (dd, ^2J = 8.68 Hz, ^3J = 1.36 Hz,1H, ArH), 8.20 (s, 1H, ArH), 8.00 (s, 1H, ArH), 7.95 (d, *J* = 8.72 Hz, 1H, ArH), 7.85 (d, *J* = 0.92 Hz, 1H, ArH), 7.70 (d, *J* = 0.92 Hz, 1H, ArH), 7.37-7.28 (m, 5H, ArH), 5.48 (s, 2H, CH_2-benzyl); ^{13}C NMR ($CDCl_3$, 100 MHz): δ (ppm) 149.4, 145.9, 144.9, 138.6, 135.9,

135.2, 134.0, 129.9, 129.0, 128.3, 127.5, 124.2, 122.5, 120.1, 117.5, 113.8, 112.5 (ArC), 48.9 (CH_2-benzyl). MS (ESI): m/z 403.0 (M^++1); Anal Calcd for $C_{20}H_{14}BrN_5$: C, 59.42; H, 3.49; N, 17.32; found C, 59.48; H, 3.60; N, 17.13.

6-Aryl-8-(1-cyclohexyl-1*H*-benzo[*d*]imidazol-6-yl)imidazo[1,2-*a*]pyrazine (31-49): Procedures for synthesis of 6-aryl-8-(1-cyclohexyl-1*H*-benzo[*d*]imidazol-6-yl)imidazo[1,2-*a*]pyrazine **(31-49)** are similar as that for the synthesis of 6-aryl-8-(1-cyclohexyl-1*H*-benzo[*d*]imidazol-5-yl)imidazo[1,2-*a*]pyrazine (**9-23**) from 6-bromo-8-(1-cyclohexyl-1*H*-benzo[*d*]imidazol-5-yl)imidazo[1,2-*a*]pyrazine (**30a**).

8-(1-Cyclohexyl-1*H*-benzo[*d*]imidazol-6-yl)-6-phenylimidazo[1,2-*a*]pyrazine (31): Light

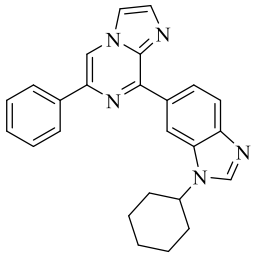

green solid; 111.64 mg, 75% yield; R_f 0.5 (40% ethyl acetate in hexane); mp 194-196 ^oC; ^1H NMR ($CDCl_3$, 400 MHz): δ (ppm) 9.18 (s, 1H, ArH), 8.79 (dd, ^2J = 8.72 Hz, ^3J = 1.84 Hz, 1H, ArH), 8.37 (s, 1H, ArH), 8.10 (s, 1H, ArH), 8.05 (d, *J* = 8.24 Hz, 2H, ArH), 7.95 (d, *J* = 8.68 Hz, 1H, ArH), 7.83 (s, 1H, ArH), 7.73 (s, 1H, ArH), 7.49 (t, *J* = 7.32 Hz, 2H, ArH), 7.40 (t, *J* = 7.32 Hz, 1H, ArH), 4.42-4.34 (m, 1H, cyclohex-CH), 2.28 (d, *J* = 11.92 Hz, 2H, cyclohex-CH_2), 1.98 (d, *J* = 13.28 Hz, 2H, cyclohex-CH_2), 1.87-1.77 (m, 2H, cyclohex-CH_2), 1.60-1.51 (m, 2H, cyclohex-CH_2), 1.38-1.23 (m, 2H, cyclohex-CH_2); ^{13}C NMR ($CDCl_3$, 100 MHz): δ (ppm) 148.6, 145.1, 141.7, 138.6, 138.4, 136.5, 134.8, 133.2, 130.6, 128.6, 128.4, 126.0, 123.6, 119.6, 114.2, 113.4, 112.4 (ArC), 55.1 (CH), 33.3 (CH_2), 25.4 (CH_2), 25.2 (CH_2); MS (ESI): m/z 394.3 (M^++1); Anal Calcd for $C_{25}H_{23}N_5$: C, 76.31; H, 5.89; N, 17.80; found C, 76.42; H, 5.87; N, 17.94.

8-(1-Cyclohexyl-1*H*-benzo[*d*]imidazol-6-yl)-6-(4-methoxyphenyl)imidazo[1,2-*a*]pyrazine (32): Light green solid; 121.76 mg, 76% yield; R_f 0.6 (40% ethyl acetate in hexane); mp 196-198 ^oC; ^1H NMR ($CDCl_3$, 400 MHz): δ (ppm) 9.19 (d, *J* = 1.40, 1H, ArH), 8.78 (dd, ^2J = 8.72 Hz, ^3J = 1.36 Hz, 1H, ArH), 8.35 (s, 1H, ArH), 8.12 (s, 1H, ArH), 8.03 (d, *J* = 8.72 Hz, 2H, ArH), 7.96 (d, *J* = 8.72 Hz, 1H, ArH), 7.85 (d, *J* = 0.92 Hz, 1H, ArH), 7.75 (d, *J* = 0.92 Hz, 1H, ArH), 7.05

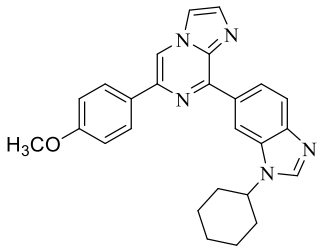

(d, *J* = 9.16 Hz, 2H, ArH), 4.45-4.37 (m, 1H, cyclohex-CH), 3.88 (s, 3H, CH_3), 2.32 (d, *J* = 11.88 Hz, 2H, cyclohex-CH_2), 2.01 (d, *J* = 13.76 Hz, 2H, cyclohex-CH_2), 1.90-1.80 (m, 2H, cyclohex-CH_2), 1.64-1.53 (m, 2H, cyclohex-CH_2), 1.41-1.23 (m, 2H, cyclohex-CH_2); ^{13}C NMR ($CDCl_3$, 100 MHz): δ (ppm) 160.1, 148.8, 145.2,

141.8, 138.7, 138.6, 134.9, 133.3, 130.9, 129.2, 127.4, 123.7, 119.8, 114.2, 114.1, 112.6, 112.5 (ArC), 55.3 (CH), 55.2 (OCH_3), 33.4 (CH_2), 25.6 (CH_2), 25.3 (CH_2); MS (ESI): m/z 424.3 (M^++1); Anal Calcd for $C_{26}H_{25}N_5O$: C, 73.74; H, 5.95; N, 16.54; found C, 73.67; H, 5.78; N, 16.48.

4-(8-(1-Cyclohexyl-1*H*-benzo[*d*]imidazol-6-yl)imidazo[1,2-*a*]pyrazin-6-yl)benzaldehyde (33): Light green solid; 130.75 mg, 82% yield; R_f 0.4 (40% ethyl acetate in hexane); mp 198-201

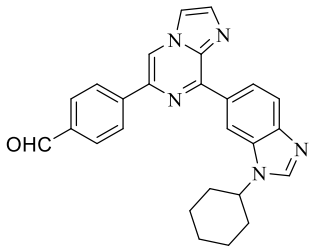

°C; ^{1}H NMR ($CDCl_3$, 400 MHz): δ (ppm) 10.09 (s, 1H, CHO), 9.23 (s, 1H, ArH), 8.76 (dd, ^2J = 8.68 Hz, ^3J = 1.36 Hz, 1H, ArH), 8.56 (s, 1H, ArH), 8.28 (d, J = 8.00 Hz, 2H, ArH), 8.12 (s, 1H, ArH), 8.04 (d, J = 8.24 Hz, 2H, ArH), 7.97 (d, J = 8.72 Hz, 1H, ArH), 7.91 (d, J = 0.92 Hz, 1H, ArH), 7.83 (d, J = 0.92 Hz, 1H, ArH), 4.45-4.37 (m, 1H, cyclohex-CH), 2.33 (d, J = 11.0 Hz, 2H, cyclohex-CH_2), 2.03-1.99 (m, 2H, cyclohex-CH_2), 1.92-1.82 (m, 2H, cyclohex-CH_2), 1.65-1.54 (m, 2H, cyclohex-CH_2), 1.43-1.24 (m, 2H, cyclohex-CH_2); ^{13}C NMR ($CDCl_3$, 100 MHz): δ (ppm) 191.8 (CO), 149.3, 142.5, 142.1, 138.9, 137.2, 136.1, 135.5, 133.4, 130.4, 130.2, 126.6, 123.6, 120.0, 114.7, 114.6, 112.7 (ArC), 55.4 (CH), 33.4 (CH_2), 25.6 (CH_2), 25.4 (CH_2); MS (ESI): m/z 422.5 (M^++1); Anal Calcd for $C_{26}H_{23}N_5O$: C, 74.09; H, 5.50; N, 16.62; found C, 74.42; H, 5.25; N, 16.57.

8-(1-Cyclohexyl-1*H*-benzo[*d*]imidazol-6-yl)-6-(naphthalen-1-yl)imidazo[1,2-*a*]pyrazine (34):

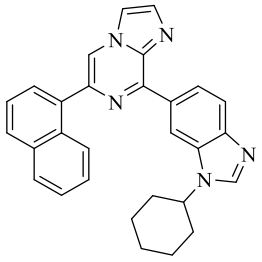

Light green solid; 137.59 mg, 82% yield; R_f 0.4 (40% ethyl acetate in hexane); mp 200-203 °C; ^{1}H NMR ($CDCl_3$, 400 MHz): δ (ppm) 9.09 (d, J = 1.36 Hz, 1H, ArH), 8.82 (dd, ^2J = 8.24 Hz, ^3J = 1.40 Hz, 1H, ArH), 8.30 (s, 1H, ArH), 8.29 (s, 1H, ArH), 8.10 (s, 1H, ArH), 7.98 (d, J = 6.88 Hz, 1H, ArH), 7.94 (s, 1H, ArH), 7.92 (d, J = 8.72 Hz, 1H, ArH), 7.82 (d, J = 0.92 Hz, 1H, ArH), 7.72 (dd, ^2J = 6.88 Hz, ^3J = 0.92 Hz, 1H, ArH), 7.60-7.57 (m, 2H, ArH), 7.55-7.49 (m, 2H, ArH), 4.40-4.32 (m, 1H, cyclohex-CH), 2.29 (d, J = 11.48 Hz, 2H, cyclohex-CH_2), 1.98 (d, J = 13.76 Hz, 2H, cyclohex-CH_2), 1.87-1.77 (m, 2H, cyclohex-CH_2), 1.58-1.47 (m, 2H, cyclohex-CH_2), 1.42-1.25 (m, 2H, cyclohex-CH_2); ^{13}C NMR ($CDCl_3$, 100 MHz): δ (ppm) 148.8, 145.3, 141.9, 140.2, 138.6, 135.1, 134.0, 133.4, 131.7, 130.7, 129.2, 128.4, 127.6, 126.4, 126.0, 125.8, 125.2, 124.0, 119.8, 117.1, 114.1, 112.3 (ArC), 55.3 (CH), 33.4 (CH_2), 25.5 (CH_2), 25.3 (CH_2); MS (ESI): m/z 444.5 (M^++1); Anal Calcd for $C_{29}H_{25}N_5$: C, 78.53; H, 5.68; N, 15.79; found C, 78.23; H, 5.89; N, 15.49.

8-(1-Cyclohexyl-1*H*-benzo[*d*]imidazol-6-yl)-6-(4-fluorophenyl)imidazo[1,2-*a*]pyrazine (35):

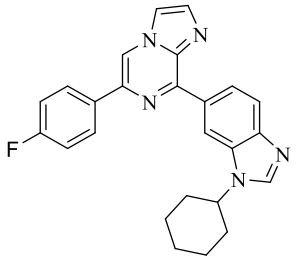

Light green solid; 121.42, 78% yield; R_f 0.5 (40% ethyl acetate in hexane); mp 186-188 ^oC; ^1H NMR ($CDCl_3$, 400 MHz): δ (ppm) 9.20 (d, *J* = 1.40 Hz, 1H, ArH), 8.76 (dd, ^2J = 8.28 Hz, ^3J = 1.40 Hz, 1H, ArH), 8.37 (s, 1H, ArH), 8.11 (s, 1H, ArH), 8.06 (d, *J* = 5.52 Hz, 1H, ArH), 8.04 (d, *J* = 5.48 Hz, 1H, ArH), 7.96 (d, *J* = 8.24 Hz, 1H, ArH), 7.87 (d, *J* = 1.36 Hz, 1H, ArH), 7.77 (d, *J* = 0.92 Hz, 1H, ArH), 7.20 (t, *J* = 8.68 Hz, 2H, ArH), 4.44-4.36 (m, 1H, cyclohex-CH), 2.31 (d, *J* = 11.44 Hz, 2H, cyclohex-CH_2), 2.01 (d, *J* = 13.76 Hz, 2H, cyclohex-CH_2), 1.90-1.80 (m, 2H, cyclohex-CH_2), 1.64-1.52 (m, 2H, cyclohex-CH_2), 1.41-1.24 (m, 2H, cyclohex-CH_2); ^{13}C NMR ($CDCl_3$, 100 MHz): δ (ppm) 164.3, 161.9, 148.9, 145.4, 141.9, 138.7, 137.8, 135.1, 133.3, 132.8, 130.6, 128.0, 127.9, 123.6, 119.9, 115.8, 115.6, 114.2, 113.2, 112.5 (ArC), 55.2 (CH), 33.4 (CH_2), 25.6 (CH_2), 25.3 (CH_2); MS (ESI): m/z 412.3 (M^++1); Anal Calcd for $C_{25}H_{22}FN_5$: C, 72.97; H, 5.39; N, 17.02; found C, 72.72; H, 5.20; N, 16.85.

8-(1-Cyclohexyl-1*H*-benzo[*d*]imidazol-6-yl)-6-(thiophen-3-yl)imidazo[1,2-*a*]pyrazine (36):

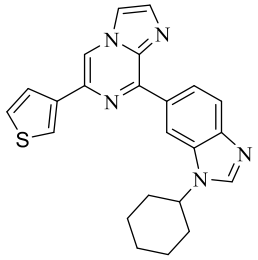

Light green solid; 125.43 mg, 83% yield; R_f 0.4 (40% ethyl acetate in hexane); mp 180-183 ^oC; ^1H NMR ($CDCl_3$, 400 MHz): δ (ppm) 9.15 (d, *J* = 0.92 Hz, 1H, ArH), 8.75 (dd, ^2J = 8.68 Hz, ^3J = 1.36 Hz, 1H, ArH), 8.34 (s, 1H, ArH), 8.10 (s, 1H, ArH), 8.04 (d, *J* = 2.76 Hz, 1H, ArH), 7.96 (d, *J* = 8.72 Hz, 1H, ArH), 7.85 (d, *J* = 0.92 Hz, 1H, ArH), 7.75 (d, *J* = 0.92 Hz, 1H, ArH), 7.62 (dd, ^2J = 5.04 Hz, ^3J = 1.36 Hz, 1H, ArH), 7.47 (dd, ^2J = 5.04 Hz, ^3J = 3.36 Hz, 1H, ArH), 4.44-4.37 (m, 1H, cyclohex-CH), 2.32 (d, *J* = 13.28 Hz, 2H, cyclohex-CH_2), 2.01 (d, *J* = 11.00 Hz, 2H, cyclohex-CH_2), 1.90-1.80 (m, 2H, cyclohex-CH_2), 1.63-1.54 (m, 2H, cyclohex-CH_2), 1.41-1.24 (m, 2H, cyclohex-CH_2); ^{13}C NMR ($CDCl_3$, 100 MHz): δ (ppm) 149.3, 145.6, 142.0, 139.0, 138.9, 135.6, 135.1, 133.5, 130.7, 126.8, 125.1, 123.8, 122.9, 120.0, 114.3, 113.1, 112.6 (ArC), 55.4 (CH), 33.6 (CH_2), 25.7 (CH_2), 25.5 (CH_2); MS (ESI): m/z 400.2 (M^++1); Anal Calcd for $C_{23}H_{21}N_5S$: C, 69.15; H, 5.30; N, 17.53; S, 8.02; found C, 69.47; H, 5.59; N, 17.65; S, 8.40.

8-(1-Cyclohexyl-1*H*-benzo[*d*]imidazol-6-yl)-6-(*m*-tolyl)imidazo[1,2-*a*]pyrazine (37): Light

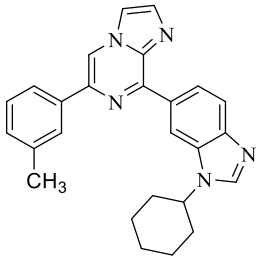

green solid; 121.78 mg, 79% yield; R_f 0.6 (40% ethyl acetate in hexane); mp 182-185 ^oC; ^1H NMR ($CDCl_3$, 400 MHz): δ (ppm) 9.18 (d, *J* = 0.92 Hz, 1H, ArH), 8.81 (dd, ^2J = 8.72 Hz, ^3J = 1.84 Hz, 1H, ArH), 8.43 (s, 1H, ArH), 8.10 (s, 1H, ArH), 7.96 (d, *J* = 8.28 Hz, 1H, ArH), 7.92 (s, 1H, ArH), 7.87 (s, 1H, ArH), 7.84 (s, 1H, ArH), 7.77 (s, 1H, ArH), 7.41 (t, *J* = 7.56 Hz, 2H, ArH), 4.45-4.37 (m, 1H, cyclohex-CH), 2.48 (s, 3H, CH_3), 2.32 (d, *J* = 11.48 Hz, 2H, cyclohex-CH_2), 2.01 (d, *J* = 13.28 Hz, 2H, cyclohex-CH_2), 1.91-1.81 (m, 2H, cyclohex-CH_2), 1.64-1.52 (m, 2H, cyclohex-CH_2), 1.43-1.25 (m, 2H, cyclohex-CH_2); ^{13}C NMR ($CDCl_3$, 100 MHz): δ (ppm) 148.9, 145.4, 141.8, 138.9, 138.8, 138.5, 136.6, 135.0, 133.4, 130.8, 129.4, 128.7, 127.0, 123.8, 123.2, 119.8, 114.2, 113.5, 112.5 (ArC), 55.3 (CH), 33.4 (CH_2), 25.6 (CH_2), 25.4 (CH_2), 21.6 (CH_3); MS (ESI): m/z 408.6 (M^++1); Anal Calcd for: $C_{26}H_{25}N_5$: C, 76.63; H, 6.18; N, 17.19; found C, 76.53; H, 6.14; N, 17.45.

8-(1-Cyclohexyl-1*H*-benzo[*d*]imidazol-6-yl)-6-(4-ethylphenyl)imidazo[1,2-*a*]pyrazine (38):

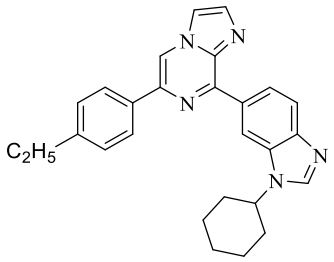

Light green solid; 130.75 mg, 82% yield; R_f 0.6 (40% ethyl acetate in hexane); mp 184-186 ^oC; ^1H NMR ($CDCl_3$, 400 MHz): δ (ppm) 9.18 (d, *J* = 0.88 Hz, 1H, ArH), 8.80 (dd, ^2J = 8.24 Hz, ^3J = 1.36 Hz, 1H, ArH), 8.41 (s, 1H, ArH), 8.10 (s, 1H, ArH), 8.01 (d, *J* = 8.24 Hz, 2H, ArH), 7.96 (d, *J* = 8.72 Hz, 1H, ArH), 7.86 (s, 1H, ArH), 7.77 (s, 1H, ArH), 7.37 (d, *J* = 8.24 Hz, 2H, ArH), 4.45-4.37 (m, 1H, cyclohex-CH), 2.76 (q, *J* = 7.80 Hz, 2H, CH_2), 2.32 (d, *J* = 11.44 Hz, 2H, cyclohex-CH_2), 2.01 (d, *J* = 13.76 Hz, 2H, cyclohex-CH_2), 1.90-1.80 (m, 2H, cyclohex-CH_2), 1.64-1.53 (m, 2H, cyclohex-CH_2), 1.41-1.24 (m, 5H, cyclohex-CH_2, CH_3); ^{13}C NMR ($CDCl_3$, 100 MHz): δ (ppm) 148.9, 145.4, 144.9, 141.8, 138.9, 135.0, 134.2, 133.4, 130.8, 128.4, 126.2, 123.7, 119.8, 114.1, 113.1, 112.4 (ArC), 55.2 (CH), 33.5 (CH_2), 28.6 (CH_2), 25.6 (CH_2), 25.4 (CH_2), 15.5 (CH_3); MS (ESI): m/z 422.5 (M^++1); Anal Calcd for $C_{27}H_{27}N_5$: C, 76.93; H, 6.46; N, 16.61; found C, 76.82; H, 6.31; N, 16.75.

1-(4-(8-(1-Cyclohexyl-1*H*-benzo[*d*]imidazol-6-yl)imidazo[1,2-*a*]pyrazin-6-yl)phenyl)ethan-1-one (39): Light green solid; 131.81 mg, 80% yield; R_f 0.6 (40% ethyl acetate in hexane); mp 201-204 ^oC; ^1H NMR ($CDCl_3$, 400 MHz): δ (ppm) 9.23 (s, 1H, ArH), 8.80 (dd, ^2J = 8.72 Hz, ^3J =

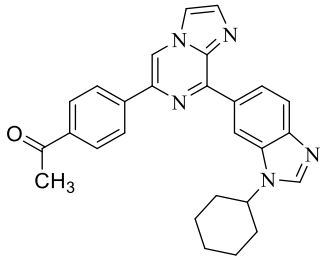

1.40 Hz, 1H, ArH), 8.55 (s, 1H, ArH), 8.22 (d, *J* = 8.00 Hz, 2H, ArH), 8.16 (s, 1H, ArH), 8.12 (d, *J* = 8.00 Hz, 2H, ArH), 7.98 (d, *J* = 8.68 Hz, 1H, ArH), 7.91 (s, 1H, ArH), 7.83 (s, 1H, ArH), 4.47-4.39 (m, 1H, cyclohex-CH), 2.68 (s, 3H, CH_3), 2.34 (d, *J* = 12.36 Hz, 2H, cyclohex-CH_2), 2.03 (d, *J* = 14.20 Hz, 2H, cyclohex-CH_2), 1.92-1.82 (m, 2H, cyclohex-CH_2), 1.65-1.55 (m, 2H, cyclohex-CH_2), 1.42-1.21 (m, 2H, cyclohex-CH_2); ^{13}C NMR ($CDCl_3$, 100 MHz): δ (ppm) 197.7 (C=O), 149.0, 141.0, 138.8, 137.4, 136.8, 135.4, 133.2, 130.7, 128.9, 126.2, 124.0, 123.9, 119.6, 114.6, 112.8 (ArC), 55.5 (CH), 33.4 (CH_2), 26.7 (CH_3), 25.6 (CH_2), 25.3 (CH_2); MS (ESI): m/z 436.4 (M^++1); Anal Calcd for $C_{27}H_{25}N_5O$: C, 74.46; H, 5.79; N, 16.08; found C, 74.36; H, 5.89; N, 16.40.

6-(4-Chlorophenyl)-8-(1-cyclohexyl-1*H*-benzo[*d*]imidazol-6-yl)imidazo[1,2-*a*]pyrazine (40):

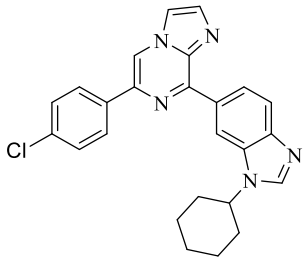

Light green solid; 126.15 mg, 78% yield; R_f 0.6 (40% ethyl acetate in hexane); mp 189-193 °C; ^{1}H NMR ($CDCl_3$, 400 MHz): δ (ppm) 9.18 (s, 1H, ArH), 8.74 (dd, ^2J = 8.68 Hz, ^3J = 1.36 Hz, 1H, ArH), 8.40 (s, 1H, ArH), 8.11 (s, 1H, ArH), 8.01 (d, *J* = 8.24 Hz, 2H, ArH), 7.94 (d, *J* = 8.24 Hz, 1H, ArH), 7.86 (d, *J* = 0.92 Hz, 1H, ArH), 7.76 (d, *J* = 1.08 Hz, 1H, ArH), 7.48 (s, 1H, ArH), 7.45 (s, 1H, ArH), 4.43-4.35 (m, 1H, cyclohex-CH), 2.30 (d, *J* = 11.92 Hz, 2H, cyclohex-CH_2), 2.00 (d, *J* = 13.76 Hz, 2H, cyclohex-CH_2), 1.89-1.78 (m, 2H, cyclohex-CH_2), 1.62-1.52 (m, 2H, Cyclohex-CH_2), 1.40-1.19 (m, 2H, Cyclohex-CH_2); ^{13}C NMR ($CDCl_3$, 100 MHz): δ (ppm) 149.1, 145.4, 142.0, 138.9, 137.7, 135.4, 135.3, 134.7, 133.4, 130.7, 129.1, 127.5, 123.8, 119.9, 114.5, 113.6, 112.7 (ArC), 55.5 (CH), 33.6 (CH_2), 25.7 (CH_2), 25.5 (CH_2); MS (ESI): m/z 428.4 (M^++1); Anal Calcd for $C_{25}H_{22}ClN_5$: C, 70.17; H, 5.18; N, 16.37; found C, 70.25; H, 5.14; N, 16.32.

6-(4-Bromophenyl)-8-(1-cyclohexyl-1*H*-benzo[*d*]imidazol-6-yl)imidazo[1,2-*a*]pyrazine (41):

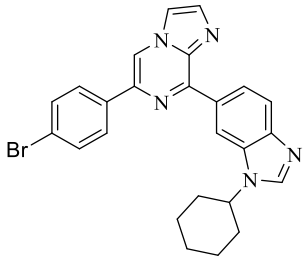

Light green solid; 139.44 mg, 78% yield; R_f 0.6 (40% ethyl acetate in hexane); mp 197-200 °C; ^{1}H NMR ($CDCl_3$, 400 MHz): δ (ppm) 9.20 (s, 1H, ArH), 8.76 (dd, ^2J = 8.24 Hz, ^3J = 1.40 Hz, 1H, ArH), 8.41 (s, 1H, ArH), 8.13 (s, 1H, ArH), 7.95 (d, *J* = 8.68 Hz, 3H, ArH), 7.87 (s, 1H, ArH), 7.77 (s, 1H, ArH), 7.64 (d, *J* = 8.24 Hz, 2H, ArH), 4.44-4.35 (m, 1H, cyclohex-CH), 2.32 (d, *J* = 12.36 Hz, 2H, cyclohex-CH_2), 2.01 (d, *J* = 13.76 Hz, 2H, cyclohex-CH_2), 1.90-1.80 (m, 2H, cyclohex-CH_2), 1.65-1.53 (m, 2H, cyclohex-CH_2), 1.42-

1.21 (m, 2H, cyclohex-CH_2); ^{13}C NMR ($CDCl_3$, 100 MHz): δ (ppm) 149.1, 142.0, 139.0, 137.7, 135.7, 135.3, 132.0, 130.7, 128.6, 127.8, 127.4, 126.8, 123.8, 122.8, 119.9, 114.4, 113.6, 112.6 (ArC), 55.5 (CH), 33.6 (CH_2), 25.7 (CH_2), 25.5 (CH_2); MS (ESI): m/z 472.2 (M^++1); Anal Calcd for $C_{25}H_{22}BrN_5$: C, 63.57; H, 4.69; N, 14.83; found C, 63.27; H, 4.34; N, 14.95.

8-(1-Cyclohexyl-1*H*-benzo[*d*]imidazol-6-yl)-6-(2-methoxyphenyl)imidazo[1,2-*a*]pyrazine (42): Light green solid; 128.17 mg, 80% yield; R_f 0.5 (40% ethyl acetate in hexane); mp 191-194 °C; ^{1}H NMR ($CDCl_3$, 400 MHz): δ (ppm) 9.16 (s, 1H, ArH), 8.88 (s, 1H, ArH), 8.78 (dd, ^2J = 8.72 Hz, ^3J = 1.40 Hz, 1H, ArH), 8.40 (dd, ^2J = 7.80 Hz, ^3J = 1.84 Hz, 1H, ArH), 8.14 (s, 1H, ArH), 7.96 (d, J = 8.28 Hz, 1H, ArH), 7.87 (d, J = 1.40 Hz, 1H, ArH), 7.78 (d, J = 0.92 Hz, 1H, ArH), 7.42-7.38 (m, 1H, ArH), 7.21-7.17 (m, 1H, ArH), 7.07 (d, J = 8.24 Hz, 1H, ArH), 4.46-4.38 (m, 1H, cyclohex-CH), 3.99 (s, 3H, CH_3), 2.32 (d, J = 13.72 Hz, 2H, cyclohex-CH_2), 2.01 (d, J = 13.76 Hz, 2H, cyclohex-CH_2), 1.90-1.80 (m, 2H, cyclohex-CH_2), 1.64-1.53 (m, 2H, cyclohex-CH_2), 1.42-1.21 (m, 2H, cyclohex-CH_2); ^{13}C NMR ($CDCl_3$, 100 MHz): δ (ppm) 156.7, 148.5, 141.6, 138.7, 135.1, 134.9, 133.3, 131.1, 130.9, 129.5, 125.2, 123.8, 121.2, 119.7, 118.3, 114.2, 112.3, 111.2 (ArC), 55.6 (CH), 55.3 (OCH_3), 33.4 (CH_2), 25.6 (CH_2), 25.4 (CH_2); MS (ESI): m/z 424.3 (M^++1); Anal Calcd for $C_{26}H_{25}N_5O$: C, 73.74; H, 5.95; N, 16.54; found C, 73.77; H, 5.72; N, 16.36.

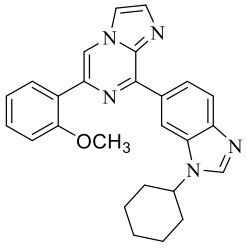

8-(1-Cyclohexyl-1*H*-benzo[*d*]imidazol-6-yl)-6-(2-fluorophenyl)imidazo[1,2-*a*]pyrazine (43): Light green solid; 127.64 mg, 82% yield; R_f 0.4 (40% ethyl acetate in hexane); mp 192-194 °C; ^{1}H NMR ($CDCl_3$, 400 MHz): δ (ppm) 9.22 (d, J = 1.36 Hz, 1H, ArH), 8.76 (dd, ^2J = 8.24 Hz, ^3J = 1.36 Hz, 1H, ArH), 8.69 (s, 1H, ArH), 8.48-8.43 (m, 1H, ArH), 8.15 (s, 1H, ArH), 7.97 (d, J = 8.68 Hz, 1H, ArH), 7.89 (s, 1H, ArH), 7.79 (s, 1H, ArH), 7.69-7.64 (m, 1H, ArH), 7.37-7.35 (m, 1H, ArH), 7.23-7.18 (m, 1H, ArH), 4.46-4.38 (m, 1H, cyclohex-CH), 2.33 (d, J = 11.92 Hz, 2H, cyclohex-CH_2), 2.02 (d, J = 13.72 Hz, 2H, cyclohex-CH_2), 1.91-1.81 (m, 2H, cyclohex-CH_2), 1.64-1.53 (m, 2H, cyclohex-CH_2), 1.42-1.21 (m, 2H, cyclohex-CH_2); ^{13}C NMR ($CDCl_3$, 100 MHz): δ (ppm) 149.1, 141.9, 138.8, 135.3, 133.4, 132.2, 132.1, 130.9, 130.8, 130.0, 129.9, 128.6, 128.5, 124.8, 123.8, 119.9, 117.9, 117.8, 116.3, 114.6, 112.8, (ArC), 55.5 (CH), 33.6 (CH_2), 25.7 (CH_2), 25.5 (CH_2); MS (ESI): m/z 412.3 (M^++1); Anal Calcd for $C_{25}H_{22}FN_5$: C, 72.97; H, 5.39; N, 17.02; found C, 72.73; H, 5.42; N, 17.42.

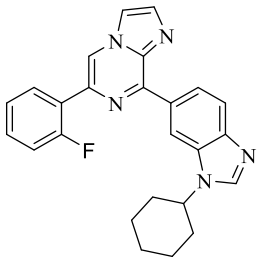

8-(1-Cyclohexyl-1*H*-benzo[*d*]imidazol-6-yl)-6-(thiophen-2-yl)imidazo[1,2-*a*]pyrazine (44):

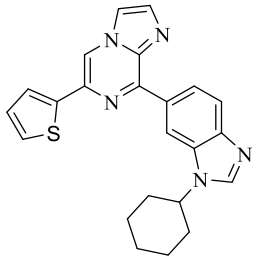

Light green solid; 123.92 mg, 82% yield; R_f 0.4 (40% ethyl acetate in hexane); mp 188-191 °C; ^{1}H NMR ($CDCl_3$, 400 MHz): δ (ppm) 9.18 (s, 1H, ArH), 8.81 (dd, ^2J = 8.72 Hz, ^3J = 1.40 Hz, 1H, ArH), 8.36 (s, 1H, ArH), 8.12 (s, 1H, ArH), 7.95 (d, J = 8.72 Hz, 1H, ArH), 7.84 (s, 1H, ArH), 7.72 (s, 1H, ArH), 7.57 (d, J = 3.64 Hz, 1H, ArH), 7.40 (d, J = 5.04 Hz, 1H, ArH), 7.14 (q, J = 3.68 Hz, 1H, ArH), 4.43-4.35 (m, 1H, cyclohex-CH), 2.32 (d, J = 11.92 Hz, 2H, cyclohex-CH_2), 2.01 (d, J = 13.72 Hz, 2H, cyclohex-CH_2), 1.91-1.81 (m, 2H, cyclohex-CH_2), 1.64-1.52 (m, 2H, cyclohex-CH_2), 1.41-1.23 (m, 2H, cyclohex-CH_2); ^{13}C NMR ($CDCl_3$, 100 MHz): δ (ppm) 148.9, 145.4, 142.1, 141.9, 138.8, 135.3, 134.8, 133.4, 130.5, 128.1, 126.6, 124.0, 123.1, 119.8, 114.4, 112.7, 111.8 (ArC), 55.5 (CH), 33.5 (CH_2), 25.7 (CH_2), 25.5 (CH_2); MS (ESI): m/z 400.2 (M^++1); Anal Calcd for $C_{23}H_{21}N_5S$: C, 69.15; H, 5.30; N, 17.53; S, 8.02; found C, 69.14; H, 5.33; N, 17.32; S, 8.24.

8-(1-Cyclohexyl-1*H*-benzo[*d*]imidazol-6-yl)-6-(3-(trifluoromethyl)phenyl)imidazo[1,2-*a*]pyrazine (45): Light green solid; 148.42 mg, 85% yield; R_f 0.6 (40% ethyl acetate in hexane);

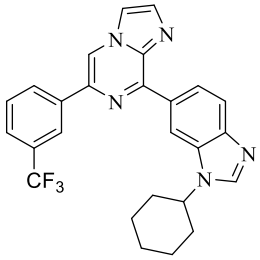

mp 198-201 °C; ^{1}H NMR ($CDCl_3$, 400 MHz): δ (ppm) 9.19 (s, 1H, ArH), 8.85 (dd, ^2J = 8.72 Hz, ^3J = 1.36 Hz, 1H, ArH), 8.52 (s, 1H, ArH), 8.39 (s, 1H, ArH), 8.28 (d, J = 7.80 Hz, 1H, ArH), 8.13 (s, 1H, ArH), 7.98 (d, J = 8.24 Hz, 1H, ArH), 7.91 (s, 1H, ArH), 7.82 (s, 1H, ArH), 7.70-7.62 (m, 2H, ArH), 4.45-4.37 (m, 1H, cyclohex-CH), 2.34 (d, J = 12.36 Hz, 2H, cyclohex-CH_2), 2.03 (d, J = 13.76 Hz, 2H, cyclohex-CH_2), 1.92-1.82 (m, 2H, cyclohex-CH_2), 1.64-1.54 (m, 2H, cyclohex-CH_2), 1.42-1.21 (m, 2H, cyclohex-CH_2); ^{13}C NMR ($CDCl_3$, 100 MHz): δ (ppm) 149.1, 142.1, 138.9, 137.6, 137.2, 135.5, 133.4, 131.5, 131.2, 130.7, 129.4, 129.3, 125.3, 124.1, 123.1, 119.7, 114.7, 114.1, 112.7 (ArC), 55.7 (CH), 33.5 (CH_2), 25.7 (CH_2), 25.4 (CH_2); MS (ESI): m/z 462.4 (M^++1); Anal Calcd for $C_{26}H_{22}F_3N_5$: C, 67.67; H, 4.81; N, 15.18; found C, 67.82; H, 4.99; N, 15.00.

6-Aryl-8-(1-benzyl-1*H*-benzo[*d*]imidazol-6-yl)imidazo[1,2-*a*]pyrazine (46-49): Procedures for synthesis of 6-aryl-8-(1-benzyl-1*H*-benzo[*d*]imidazol-6-yl)imidazo[1,2-*a*]pyrazine **(46-49)** is similar as that for the synthesis of 6-aryl-8-(1-cyclohexyl-1*H*-benzo[*d*]imidazol-5-yl)imidazo[1,2-*a*]pyrazine (**9-23**) from 8-(1-benzyl-1*H*-benzo[*d*]imidazol-6-yl)-6-bromoimidazo[1,2-*a*]pyrazine (**30b**).

8-(1-Benzyl-1*H*-benzo[*d*]imidazol-6-yl)-6-(4-ethylphenyl)imidazo[1,2-*a*]pyrazine (46): Light brown solid; 132.20 mg, 83% yield; R_f 0.3 (40% ethyl acetate in hexane); mp 179-181 ^oC; ^1H NMR ($CDCl_3$, 400 MHz): δ (ppm) 9.08 (s, 1H, ArH), 8.83 (dd, ^2J = 8.24 Hz, ^3J = 1.36 Hz, 1H, ArH), 8.37 (s, 1H, ArH), 8.00 (s, 1H, ArH), 7.97-7.94 (m, 3H, ArH), 7.81 (s, 1H, ArH), 7.73 (s, 1H, ArH), 7.36-7.28 (m, 7H, ArH), 5.48 (s, 2H, benzyl-CH_2), 2.75 (q, J = 7.80 Hz, 2H, ethyl-CH_2), 1.31 (t, J = 7.80 Hz, 3H, ethyl-CH_3); ^{13}C NMR ($CDCl_3$, 100 MHz): δ (ppm) 148.5, 145.4, 144.9, 144.5, 138.7, 135.3, 134.9, 134.0, 131.3, 128.9, 128.3, 128.2, 127.5, 126.1, 124.0, 119.8, 114.1, 113.1, 112.3 (ArC), 48.9 (benzyl-CH_2), 28.6 (ethyl-CH_2), 15.5 (ethyl-CH_3); MS (ESI): m/z 430.6 (M^++1); Anal Calcd for $C_{28}H_{23}N_5$: C, 78.30; H, 5.40; N, 16.31; found C, 78.38; H, 5.28; N, 16.10.

8-(1-Benzyl-1*H*-benzo[*d*]imidazol-6-yl)-6-(*m*-tolyl)imidazo[1,2-*a*]pyrazine (47): Light brown solid; 124.80 mg, 81% yield; R_f 0.3 (40% ethyl acetate in hexane); mp 184-187 ^oC; ^1H NMR ($CDCl_3$, 400 MHz): δ (ppm) 9.08 (d, J = 1.36 Hz, 1H, ArH), 8.82 (dd, ^2J = 8.72 Hz, ^3J = 1.36 Hz, 1H, ArH), 8.40 (s, 1H, ArH), 8.01 (s, 1H, ArH), 7.98 (d, J = 8.72 Hz, 1H, ArH), 7.86 (s, 1H, ArH), 7.83 (s, 1H, ArH), 7.74 (s, 1H, ArH), 7.41-7.28 (m, 7H, ArH), 7.25 (d, J = 7.80 Hz, 1H, ArH), 5.48 (s, 2H, benzyl-CH_2), 2.47 (s, 3H, CH_3); ^{13}C NMR ($CDCl_3$, 100 MHz): δ (ppm) 148.7, 145.5, 144.5, 138.8, 138.4, 136.5, 135.3, 135.0, 134.0, 131.3, 129.4, 129.0, 128.7, 128.2, 127.5, 126.8, 124.0, 123.2, 119.9, 114.2, 113.5, 112.3 (ArC), 48.9 (benzyl-CH_2), 21.6 (CH_3); MS (ESI): m/z 416.5 (M^++1); Anal Calcd for: $C_{27}H_{21}N_5$: C, 78.05; H, 5.09; N, 16.86; found C, 77.95; H, 5.02; N, 17.04.

4-(8-(1-Benzyl-1*H*-benzo[*d*]imidazol-6-yl)imidazo[1,2-*a*]pyrazin-6-yl)benzaldehyde (48): Light brown solid; 125.83 mg, 79% yield; R_f 0.3 (40% ethyl acetate in hexane); mp 182-185 ^oC; ^1H NMR ($CDCl_3$, 400 MHz): δ (ppm) 10.09 (s, 1H, CHO), 9.11 (s, 1H, ArH), 8.83 (d, J = 8.72 Hz, 1H, ArH), 8.53 (s, 1H, ArH), 8.23 (d, J = 8.24 Hz, 2H, ArH), 8.04-7.97 (m, 4H, ArH), 7.87 (s, 1H, ArH), 7.79 (s, 1H, ArH), 7.38-7.30 (m, 5H, ArH), 5.50 (s, 2H, benzyl-CH_2); ^{13}C NMR ($CDCl_3$, 100 MHz): δ (ppm) 191.8 (CO), 149, 145.7, 144.7, 142.3, 138.8, 137.1, 136.0, 135.4, 135.3, 134.0, 130.9, 130.2, 129.0, 128.3, 127.5, 126.5, 123.9, 120.0, 114.8, 114.6,

112.5 (ArC), 49.0 (benzyl-CH_2); MS (ESI): m/z 430.6 (M^++1); Anal Calcd for $C_{27}H_{19}N_5O$: C, 75.51; H, 4.46; N, 16.31; found C, 75.58; H, 4.50; N, 16.30.

8-(1-Benzyl-1*H*-benzo[*d*]imidazol-6-yl)-6-(naphthalen-1-yl)imidazo[1,2-*a*]pyrazine (49):

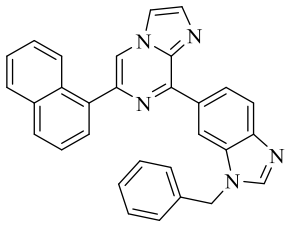

Light brown solid; 137.30 mg, 82% yield; R_f 0.3 (40% ethyl acetate in hexane); mp 183-186 ^oC; ^1H NMR ($CDCl_3$, 400 MHz): δ (ppm) 9.05 (d, *J* = 1.36 Hz, 1H, ArH), 8.82 (dd, ^2J = 8.72 Hz, ^3J = 1.84 Hz, 1H, ArH), 8.26 (s, 1H, ArH), 8.23 (d, *J* = 8.24 Hz, 1H, ArH), 7.98-7.90 (m, 6H, ArH), 7.78 (s, 1H, ArH), 7.67 (d, *J* = 6.88 Hz, 1H, ArH), 7.58-7.54 (m, 2H, ArH), 7.52-7.45 (m, 2H, ArH), 7.31-7.27 (m, 2H, ArH), 7.25-7.23 (m, 1H, ArH), 5.43 (s, 2H, benzyl-CH_2); ^{13}C NMR ($CDCl_3$, 100 MHz): δ (ppm) 148.7, 145.5, 144.5, 140.1, 138.5, 135.3, 135.1, 135.0, 134.0, 133.9, 131.7, 131.2, 129.2, 128.9, 128.4, 128.2, 127.6, 127.5, 126.4, 126.0, 125.7, 125.2, 124.1, 120.0, 117.1, 114.1, 112.2 (ArC), 48.8 (benzyl-CH_2); MS (ESI): m/z 452.5 (M^++1); Anal Calcd for $C_{30}H_{21}N_5$: C, 79.80; H, 4.69; N, 15.51; found C, 79.65; H, 4.55; N, 15.76.

4-bromo-N^1-cyclohexylbenzene-1,2-diamine (50a): 4-Bromo-*N*-cyclohexyl-2-nitroaniline (**3**) (1 g, 3.34 mmol) and sodium dithionite (2.9 g, 16.72 mmol) were charged in THF:water (3:2) mixture. Ammonia solution (3 ml) was added to the reaction mixture at room temperature and further stirred for 1h. The reaction mixture was extracted with ethyl acetate. Ethyl acetate was dried over Na_2SO_4. Crude brown product was directly used for further reaction without purification.

5-Bromo-N^1-cyclohexylbenzene-1,2-diamine (50b): Similar synthesis route has been adopted using 5-bromo-*N*-cyclohexyl-2-nitroaniline (**26a**).

5-Bromo-1-cyclohexyl-1*H*-benzo[*d*]imidazole (51a): 4-Bromo-N^1-cyclohexylbenzene-1,2-diamine (**50a**) (1 g, 3.71 mmol) was stirred with triethylorthoformate (0.550 g, 3.71 mmol) in acetic acid at room temperature for 10 min. Reaction mixture was quenched in water and further treated with $NaHCO_3$ to basify the reaction and extracted using chloroform. Sodium sulphate was used to dry the chloroform layer. Column chromatography was performed to purify the crude product with the help of hexane and ethyl acetate (3:7) as eluent.

6-Bromo-1-cyclohexyl-1*H*-benzo[*d*]imidazole (51b): Similar synthesis route has been adopted using 5-bromo-N^1-cyclohexylbenzene-1,2-diamine (**50b**).

1-Cyclohexyl-5-(4,4,5,5-tetramethyl-1,3,2-dioxaborolan-2-yl)-1*H*-benzo[*d*]imidazole (52a): 5-Bromo-1-cyclohexyl-1*H*-benzo[*d*]imidazole (**51a**) (2 gm, 7.16 mmol), bis(pinacolato)diboron (2.19 gm, 8.60 mmol), potassium acetate (1.05 gm, 10.75 mmol) and palladium(II)bis(triphenylphosphine) dichloride (5.0 mol%) were added in 1,4-dioxane (20 mL). The reaction mixture was refluxed for the period of 12 h until aryl halide got completely consumed as determined by thin layer chromatography. Solvent of reaction was evaporated under reduced pressure followed by addition of 100 ml water to the reaction mixture. The crude product was extracted using chloroform (3 × 50 mL). Extract was dried over anhydrous Na_2SO_4, filtered to obtain the crude product. Crude material was purified *via* column chromatography using ethyl acetate and hexane as solvent system to obtain desired reddish yellow product.

1-Cyclohexyl-6-(4,4,5,5-tetramethyl-1,3,2-dioxaborolan-2-yl)-1*H*-benzo[*d*]imidazole (52b): Similar synthesis route has been adopted using 6-bromo-1-cyclohexyl-1*H*-benzo[*d*]imidazole (**51b**).

6,8-(Bisbenzimidazole)imidazo[1,2-*a*]pyrazine (53-57): 1-Cyclohexyl-5-(4,4,5,5-tetramethyl-1,3,2-dioxaborolan-2-yl)-1*H*-benzo[*d*]imidazole (**52a**) or 1-cyclohexyl-6-(4,4,5,5-tetramethyl-1,3,2-dioxaborolan-2-yl)-1*H*-benzo[*d*]imidazole (**52b**) (1.0 eq), **8/30a/30b** (1.0 eq., 150 mg), K_2CO_3 (1.0 eq.) and $Pd(PPh_3)_4$ (5 mol%) were taken in a mixture of acetonitrile : water (9:1). Reaction mixture was refluxed for 12-15 h under nitrogen until the completion of the reaction (checked by TLC). Solvents were evaporated under reduced pressure. Water (50 ml) was added to the mixture and extracted with chloroform. Chloroform layer was dried over sodium sulphate to get the crude product. Crude was further purified by column chromatography using hexane:ethyl acetate as eluents.

6,8-Bis(1-cyclohexyl-1*H*-benzo[*d*]imidazol-5-yl)imidazo[1,2-*a*]pyrazine (53): Light brown

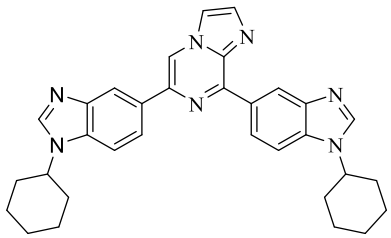

solid; 146.30 mg, 75% yield; R_f 0.5 (80% ethyl acetate in hexane); mp 205-209 ºC; ^{1}H NMR ($CDCl_3$, 400 MHz): δ (ppm) 8.44 (s, 1H, ArH), 8.24 (d, J = 1.36 Hz, 1H, ArH), 8.05 (s, 2H, ArH), 8.03 (s, 1H, ArH), 7.94 (dd, ^2J = 8.72 Hz, ^3J = 1.40 Hz, 1H , ArH), 7.82 (s, 2H, ArH), 7.61 (dd, ^2J = 8.24 Hz, ^3J = 1.36 Hz, 1H, ArH), 7.52 (d, J = 3.68 Hz, 1H, ArH), 7.50 (d, J = 3.20 Hz, 1H, ArH), 4.26-4.18 (m, 2H, 2 x cyclohex-CH), 2.26 (d, J = 12.80 Hz, 4H, 2 x cyclohex-CH_2), 2.01 (d, J = 13.28 Hz, 4H, 2 x cyclohex-CH_2), 1.87-1.76 (m, 4H, 2 x cyclohex-CH_2), 1.57-1.47 (m, 4H, 2 x cyclohex-CH_2),

1.39-1.25 (m, 4H, 2 x cyclohex-CH_2); ^{13}C NMR ($CDCl_3$, 100 MHz): δ (ppm) 144.2, 144.0, 142.5, 141.4, 140.8, 139.4, 137.1, 136.3, 135.8, 134.0, 132.4, 129.3, 122.7, 121.5, 118.8, 117.7, 115.9, 114.1, 110.5, 110.2 (ArC), 55.6 (CH), 55.5 (CH), 33.2 (CH_2), 25.6 (CH_2), 25.5 (CH_2), 25.3 (CH_2), 25.2 (CH_2); MS (ESI): m/z 516.6 (M^++1); Anal Calcd for $C_{32}H_{33}N_7$: C, 74.54; H, 6.45; N, 19.01; found C, 74.92; H, 6.25; N, 19.11.

8-(1-Cyclohexyl-1*H*-benzo[*d*]imidazol-5-yl)-6-(1-cyclohexyl-1*H*-benzo[*d*]imidazol-6-yl)imidazo[1,2-*a*]pyrazine (54): Light brown solid; 158.0 mg, 81% yield; R_f 0.3 (80% ethyl acetate in hexane); mp 203-206 °C; ^1H NMR ($CDCl_3$, 400 MHz): δ (ppm) 9.27 (d, *J* = 1.36 Hz, 1H, ArH), 8.89 (dd, ^2J = 8.72 Hz, ^3J = 1.36 Hz, 1H, ArH), 8.49 (s, 1H, ArH), 8.25 (s, 1H, ArH), 8.10 (d, *J* = 7.80 Hz, 2H, ArH), 7.90-7.84 (m, 3H, ArH), 7.80 (d, *J* = 0.92 Hz, 1H, ArH), 7.61 (d, *J* = 8.72 Hz, 1H, ArH), 4.40-4.33 (m, 1H, cyclohex-CH), 4.31-4.23 (m, 1H, cyclohex-CH), 2.29 (d, *J* = 13.28 Hz, 4H, 2 x cyclohex-CH_2), 2.02-1.97 (m, 4H, 2 x cyclohex-CH_2), 1.89-1.77 (m, 4H, 2 x cyclohex-CH_2), 1.65-1.49 (m, 4H, 2 x cyclohex-CH_2), 1.41-1.25 (m, 4H, 2 x cyclohex-CH_2); ^{13}C NMR ($CDCl_3$, 100 MHz): δ (ppm) 149.4, 144.0, 143.8, 141.4, 141.2, 139.4, 138.8, 135.1, 134.0, 131.7, 130.6, 124.7, 122.3, 120.4, 120.3, 114.2, 113.5, 109.6, 108.4 (ArC), 55.5 (CH), 55.0 (CH), 33.5 (CH_2), 33.2 (CH_2), 25.6 (CH_2), 25.5 (CH_2), 25.3 (CH_2); MS (ESI): m/z 516.6 (M^++1); Anal Calcd for $C_{32}H_{33}N_7$: C, 74.54; H, 6.45; N, 19.01; found C, 74.48; H, 6.39; N, 19.26.

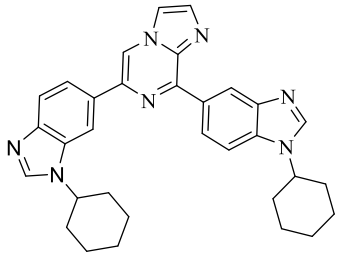

6-(1-Cyclohexyl-1*H*-benzo[*d*]imidazol-5-yl)-8-(1-cyclohexyl-1*H*-benzo[*d*]imidazol-6-yl) imidazo[1,2-*a*]pyrazine (55): Light brown solid; 146.30 mg, 75% yield; R_f 0.5 (80% ethyl acetate in hexane); mp 204-207 °C; ^1H NMR ($CDCl_3$, 400 MHz): δ (ppm) 9.19 (s, 1H, ArH), 8.82 (dd, ^2J = 8.72 Hz, ^3J = 1.36 Hz, 1H, ArH), 8.49 (s, 1H, ArH), 8.47 (d, *J* = 0.92 Hz, 1H, ArH), 8.13-8.08 (m, 3H, ArH), 7.97 (d, *J* = 8.28 Hz, 1H, ArH), 7.88 (d, *J* = 1.36 Hz, 1H, ArH), 7.81 (d, *J* = 0.92 Hz, 1H, ArH), 7.58 (d, *J* =8.24 Hz, 1H, ArH), 4.47-4.35 (m, 1H, cyclohex-CH), 4.30-4.22 (m, 1H, cyclohex-CH), 2.33 (t, *J* = 9.00 Hz, 4H, 2 x cyclohex-CH_2), 2.02-1.99 (m, 4H, 2 x cyclohex-CH_2), 1.91-1.79 (m, 4H, 2 x cyclohex-CH_2), 1.65-1.50 (m, 4H, 2 x cyclohex-CH_2), 1.41-1.25 (m, 4H, 2 x cyclohex-CH_2); ^{13}C NMR ($CDCl_3$, 100 MHz): δ (ppm) 148.9, 145.3, 142.0, 141.3, 139.5, 138.9, 135.0, 133.8, 133.4, 131.3, 130.8, 123.8, 121.6, 119.8, 118.0, 114.2, 113.2, 112.4, 110.4, 108.6 (ArC), 55.6 (CH), 55.2 (CH), 33.5 (CH_2), 33.3

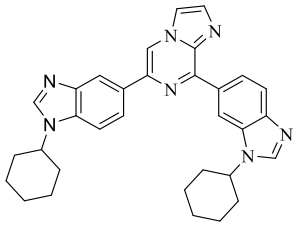

(CH_2), 25.7 (CH_2), 25.6 (CH_2), 25.4 (CH_2), 25.3 (CH_2); MS (ESI): m/z 516.6 (M^++1); Anal Calcd for $C_{32}H_{33}N_7$: C, 74.54; H, 6.45; N, 19.01; found C, 74.39; H, 6.38; N, 18.71.

6,8-Bis(1-yclohexyl-1*H*-benzo[*d*]imidazol-6-yl)imidazo[1,2-*a*]pyrazine (56): Light brown

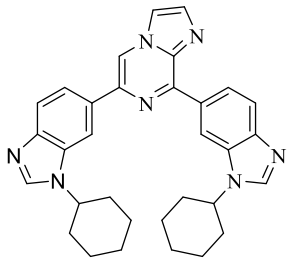

solid; 152.15 mg, 78% yield; R_f 0.5 (40% ethyl acetate in hexane); mp 225-228 ºC; ^{1}H NMR ($CDCl_3$, 400 MHz): δ (ppm) 9.19 (d, *J* = 0.92 Hz, 1H, ArH), 8.77 (dd, ^2J = 8.68 Hz, ^3J = 1.36 Hz, 1H, ArH), 8.50 (s, 1H, ArH), 8.26 (s, 1H, ArH), 8.13 (s, 1H, ArH), 8.09 (s, 1H, ArH), 7.99 (d, *J* = 8.72 Hz, 1H, ArH), 7.92-7.86 (m, 3H, ArH), 7.82 (d, *J* = 0.92 Hz, 1H, ArH), 4.46-4.30 (m, 2H, 2 x cyclohex-CH), 2.32 (d, *J* = 12.36 Hz, 4H, 2 x cyclohex-CH_2), 2.02 (d, *J* = 12.36 Hz, 4H, 2 x cyclohex-CH_2), 1.91-1.82 (m, 4H, 2 x cyclohex-CH_2), 1.63-1.52 (m, 4H, 2 x cyclohex-CH_2), 1.44-1.25 (m, 4H, 2 x cyclohex-CH_2); ^{13}C NMR ($CDCl_3$, 100 MHz): δ (ppm) 149.1, 145.3, 144.1, 141.9, 141.4, 139.4, 138.8, 135.1, 134.0, 133.4, 131.7, 130.8, 127.5, 123.7, 120.4, 119.9, 114.2, 113.6, 112.6, 108.6 (ArC), 55.4 (CH), 55.3 (CH), 33.4 (CH_2), 25.7 (CH_2), 25.6 (CH_2), 25.4 (CH_2), 25.3 (CH_2); MS (ESI): m/z 516.6 (M^++1); Anal Calcd for $C_{32}H_{33}N_7$: C, 74.54; H, 6.45; N, 19.01; found C, 74.65; H, 6.71; N, 19.32.

8-(1-Benzyl-1*H*-benzo[*d*]imidazol-6-yl)-6-(1-cyclohexyl-1*H*-benzo[*d*]imidazol-5-yl)imidazo[1,2-*a*]pyrazine (57): Light green solid; 157.28 mg, 81% yield; R_f 0.5 (90% ethyl

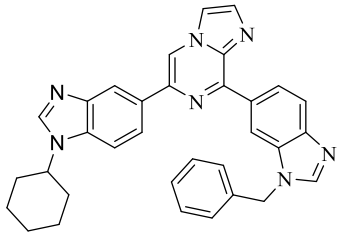

acetate in hexane); mp 131-134 ºC; ^{1}H NMR ($CDCl_3$, 400 MHz): δ (ppm) 9.13 (d, *J* = 0.92 Hz, 1H, ArH), 8.87 (dd, ^2J = 8.72 Hz, ^3J = 1.36 Hz, 1H, ArH), 8.45 (s, 2H, ArH), 8.07 (s, 1H, ArH), 8.06 (dd, ^2J = 8.68 Hz, ^3J = 1.84 Hz, 1H, ArH), 8.00 (s, 1H, ArH), 7.99 (d, *J* = 8.72 Hz, 1H, ArH), 7.83 (d, *J* = 0.92 Hz, 1H, ArH), 7.77 (s, 1H, ArH), 7.55 (d, *J* = 8.24 Hz, 1H, ArH), 7.35-7.30 (m, 5H, ArH), 5.50 (s, 2H, benzyl-CH_2), 4.27-4.20 (m, 1H, cyclohex-CH), 2.28 (d, *J* = 11.00 Hz, 2H, cyclohex-CH_2), 2.02 (d, *J* = 13.76 Hz, 2H, cyclohex-CH_2), 1.88-1.78 (m, 3H, cyclohex-CH_2), 1.59-1.48 (m, 2H, cyclohex-CH_2), 1.40-1.32 (m, 1H, cyclohex-CH_2); ^{13}C NMR ($CDCl_3$, 100 MHz): δ (ppm) 148.5, 145.4, 144.4, 144.1, 141.3, 139.3, 138.7, 135.3, 134.9, 134.0, 133.7, 131.4, 131.1, 129.0, 128.2, 127.6, 124.0, 121.4, 119.9, 117.9, 114.1, 113.2, 112.2, 110.4 (ArC), 55.6 (CH), 48.9 (benzyl-CH_2), 33.2 (CH_2), 25.6 (CH_2), 25.3 (CH_2); MS (ESI): m/z 524.6 (M^++1); Anal Calcd for $C_{33}H_{29}N_7$: C, 75.69; H, 5.58; N, 18.72; found C, 75.63; H, 5.63; N, 18.75.

CHAPTER 3
HYBRIDS OF BENZIMIDAZOLE AND NAPHTHALIMIDE

3.1 Introduction

DNA-damaging agent constitutes a cornerstone of cancer therapy and contributes to the subsistence of cancer patients in binding with drugs having different mode of interaction. However, severe toxicity and drug resistance in clinic is the Achilles' heel of DNA-damaging agents.[91,92] Thus, by targeting DNA-associated processes, enhanced selectivity for cancer cells can be acquired. Naphthalimides are highly versatile functionalized moiety, and continuously receiving attention to bind with DNA,[13] and establishing pronounced therapeutic importance in pharmaceutical and medicinal chemistry.[14,15] Some of the naphthalimides such as mitonafide, amonafide, and aristolochic acid showed effective antitumor activity towards the growth of various murine and human cancer cell lines. These naphthalimides exerted their anticancer function by interacting with DNA and inhibiting directly the function of replication and transcription, and/or topoisomerase (TOPO-II) to stabilize the supramolecular TOPO-II and DNA complex.[16] On account of limited efficacy and central neurotoxicity in solid tumors, the clinical developments of these compounds were regrettably terminated.[93,94] To increase the efficiency and toxicological profile, significant efforts have been attempted for the development of more potent naphthalimides.[95-98] and most of these efforts were concentrated on binding affinity with DNA.[99] On the other hand, benzimidazole is an important structural motif for bioactivity and widely present in broad range of therapeutic drugs[100] having an electron-accepting group (C=N) and an electron-donating group (NH), that could rapidly interact with DNA and other useful biomacromolecules.[101] The biological potential of benzimidazoles against cancer cells has been reported with different mechanism of action. The success of these drugs and many other clinical trial derivatives[102] has provoked wide range of studies to construct more benzimidazole based bioactive molecules in the field of cancer. In view of these investigations, in this chapter, we have introduced benzimidazole fragment at C-4 position of naphthalimide ring to develop novel naphthalimide-benzimidazole conjugates (**Figure 1**). The antitumor screenings with 60 human cancer cell lines were executed to naphthalimide-benzimidazoles**.** Additionally, to study the effect of naphthalimide, the mode of action for anticancer activity was also evaluated through interaction with ct-DNA using different spectroscopic techniques. Cell cycle arrest was also checked to

investigate the effect of benzimidazole using flow cytometer. The transportation behaviour of bovine serum albumin (BSA) to most active derivatives has also been done using UV-visible and fluorescence spectroscopy.

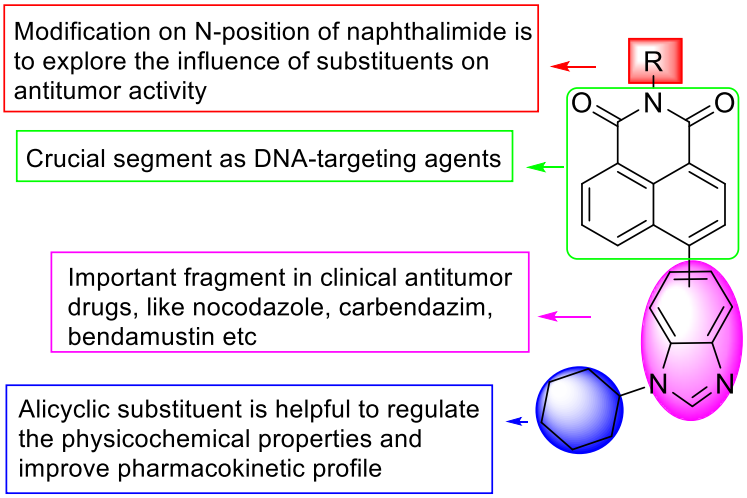

Figure 1. Design of novel naphthalimide-benzimidazole conjugates

3.2 Chemistry

Naphthalimide-benzimidazoles **11-26** have been synthesized via multistep reactions starting with commercial available 1,4- and 1,3-dibromobenzene according to **Scheme 1**. Nitration of 1,4- and 1,3-dibromobenzene **1a-b** with nitric acid and sulphuric acid in the ratio of 4:1, yielded 1,4-dibromo-2-nitro-benzene **2a** and 2,4-dibromo-1-nitro-benzene **2b** in 90% and 95% yields, both of which were subjected to regioselective nucleophilic substitution with cyclohexylamine to afford **3a-b**. Boronation of **3a-b** with bis(pinacolato)diboran in the presence of $Pd(PPh_3)_2Cl_2$ and KOAc, afforded **4a-b**. Suzuki-Miyaura cross-coupling of **4a-b** was carried out with 6-bromo-1*H*,3*H*-benzo[*de*]isochromene-1,3-dione **5** (obtained from bromination of acenaphthene followed by oxidation with potassium dichromate in glacial acetic acid) to obtain **6a-b**. Compound **6a-b** was further reduced with sodium dithionite in the presence of ammonia to afford mixture of **7a-b** and **8a-b** which were subsequently cyclized with triethylorthoformate in acetic acid at room temperature to afford the requisite **9a-b** and **10a-b**, respectively. The yields of both the intermediates were depended upon the amount of ammonia used in reduction. On refluxing of **9a-b** with alkyl and aryl amines in ethanol, compounds **11-26** were achieved in the yields of 71-86%. These novel synthesized compounds were well characterized by NMR and mass spectrometry.

Scheme 1. Synthesis of 6-(1-cyclohexyl-1*H*-benzo[*d*]imidazol-5/6-yl)-2-substituted-1*H*-benzo[*de*]isoquinoline-1,3(2*H*)-dione

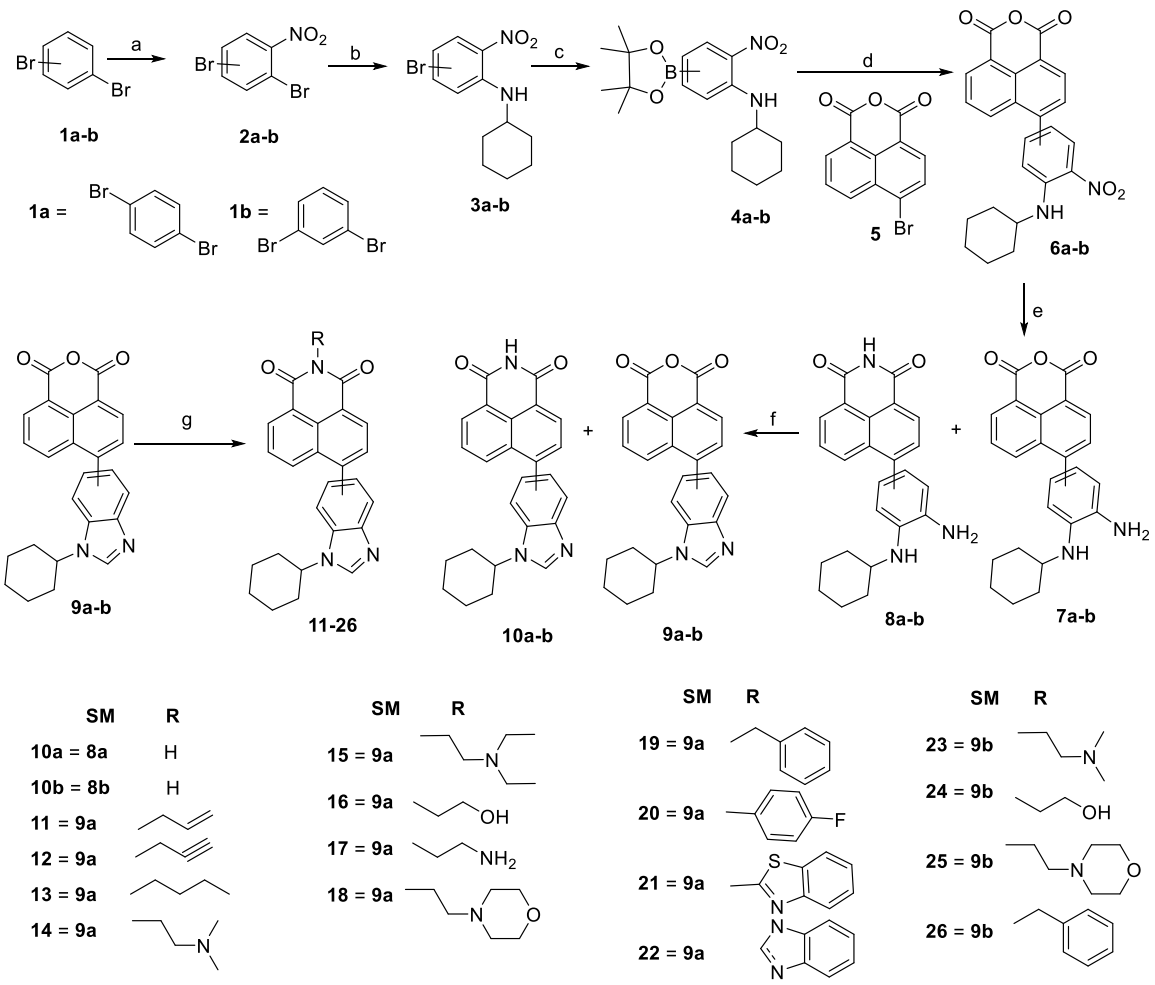

Reagents and conditions: (a) HNO_3, H_2SO_4, DCM, 0 °C, 30 min., 90-95%; (b) Cyclohexyl amine, K_2CO_3, DMF, 100 °C, 18 h, 70-75%; (c) Bis(pinacolato)diboron, $Pd(PPh_3)_2Cl_2$, KOAc, dioxane, reflux, 10 h, 78-82%; (d) $Pd(PPh_3)_4$, K_2CO_3, CH_3CN : water (9:1), N_2, reflux, 10-12 h, 70-73%; (e) $Na_2S_2O_4$, aq. NH_3, THF : water, 1 h, rt; (f) Triethylorthoformate, AcOH, 30 min., rt; (g) RNH_2, ethanol, reflux, 12-15 h, 71-86%

3.3 Biology

3.3.1 Cytotoxicity

We are now interested to find out the effect of alkyl/aryl groups on naphthalimides towards the cytotoxicity. National Cancer Institute (NCI)[71] has selected eighteen naphthalimide-benzimidazoles (**9a-b**, **10b, 11-23, 25** and **26**) for one-dose screening in the panel of 60 human cancer cell lines (**Tables 1-2**). The results indicated that many of these naphthalimides exhibited equal or better cytotoxicity than amonafide or mitonafide (drugs used in clinical trials). A comparison of two isomers of benzimidazole with naphthalimide revealed that derivatives

substituted with aromatic rings were less active than the aliphatic groups. In fact, amongst these eighteen naphthalimide-benzimidazoles, five showed cytotoxic effect in a broad range of cell lines at 10^{-5} M level and two of them showed cytotoxicity with cytostatic and cytotoxic effects against all 58 tested cell lines (**Table 3**).

Table 1. Percent growth inhibition of compounds **9a-b, 10b** and **11-16** at 10^{-5} M concentration

Cell Panel	Cell Line	9a	9b	10b	11	12	13	14	15	16
Leukemia	CCRF-CEM	13.46	0.74	27.58	67.01	30.87	--	63.33	88.63	20.98
	HL-60(TB)	20.74	5.71	27.38	74.51	14.08	0.33	33.55	-15.20	--
	K-562	24.85	17.17	43.49	73.82	NT	14.04	NT	-14.20	NT
	MOLT-4	11.56	8.40	65.32	94.60	27.66	5.30	82.74	-9.62	28.12
	RPMI-8226	24.63	9.04	42.76	70.46	48.67	--	73.24	-32.97	33.73
	SR	22.34	20.64	56.83	60.25	15.27	8.94	61.09	-13.96	15.28
Non-Small	A549/ATCC	--	--	38.72	41.74	2.94	9.19	53.16	81.16	4.44
Cell Lung	EXVX	2.02	2.93	14.96	47.08	21.36	0.22	33.42	84.37	23.65
Cancer	HOP-62	--	4.65	30.45	32.86	10.23	14.77	46.10	91.28	18.08
	HOP-92	15.76	8.35	NT	67.59	63.12	5.42	75.13	-7.68	48.94
	NCI-H226	--	--	19.55	55.15	6.56	--	28.42	-29.93	23.01
	NCI-H23	5.81	11.12	12.04	49.48	8.94	4.03	45.36	79.81	21.39
	NCI-H322M	2.37	12.29	8.91	6.15	--	--	36.99	56.83	8.19
	NCI-H460	13.35	--	39.55	41.76	1.02	--	79.49	-30.87	5.90
	NCI-H522	--	20.09	51.23	48.04	15.71	30.43	43.63	78.66	26.26
Colon	COLO 205	--	--	27.32	52.98	--	5.97	50.74	-20.39	--
Cancer	HCC-2998	12.39	3.46	9.15	24.83	6.52	--	29.51	63.35	6.80
	HCT-116	6.03	5.54	25.47	68.04	23.21	8.30	75.47	-66.14	19.98
	HCT-15	--	--	15.42	55.05	11.33	--	64.12	91.39	1.55
	HT29	11.02	1.93	30.65	76.57	18.58	15.90	68.61	99.26	16.43
	KM12	2.53	3.75	19.23	50.64	12.87	7.86	38.54	75.70	13.32
	SW-620	--	--	25.85	13.74	--	--	65.74	88.83	--
CNS	SF-268	7.89	0.48	16.42	27.64	9.39	--	42.96	60.14	6.06
Cancer	SF-295	--	0.39	12.41	55.45	11.32	3.27	50.25	-41.68	18.07
	SF-539	0.31	--	--	28.57	1.95	--	33.84	-76.24	0.98
	SNB-19	--	--	11.93	23.87	4.39	--	48.12	67.38	1.88
	SNB-75	11.09	12.43	9.95	49.76	14.48	7.72	33.11	95.59	13.35
	U251	--	--	25.94	47.98	8.97	1.68	51.30	85.35	6.83
Melanoma	LOX IMVI	3.26	9.55	22.08	49.71	6.91	--	52.55	-81.64	12.63
	MALME-3M	6.75	5.34	--	44.04	1.20	4.63	23.30	-74.50	--
	M14	--	6.74	--	49.98	3.94	7.88	25.18	-62.81	--
	MDA-MB-435	--	--	--	60.60	--	--	28.79	83.04	--
	SK-MEL-2	--	--	5.34	NT	6.16	NT	11.94	NT	10.51
	SK-MEL-28	--	--	--	23.26	--	--	27.18	-38.21	--

	SK-MEL-5	--	--	19.41	-27.80	36.14	--	41.73	-96.57	37.98
	UACC-257	--	--	38.09	55.43	--	--	--	-14.97	5.54
	UACC-62	11.21	7.70	29.90	56.02	30.72	7.19	40.38	77.99	25.56
Ovarian	IGROV1	10.75	11.58	14.21	32.91	8.28	--	49.80	71.62	3.80
Cancer	OVCAR-3	--	--	1.67	37.57	3.33	--	27.84	55.22	11.09
	OVCAR-4	1.33	--	7.55	67.68	28.49	2.36	45.32	67.05	14.04
	OVCAR-5	4.90	--	--	24.67	--	1.74	38.57	63.60	--
	OVCAR-8	0.40	--	38.43	50.50	10.35	10.08	54.20	74.08	16.77
	NCI/ADR-RES	--	0.57	16.94	60.37	10.84	7.54	58.13	78.15	10.94
	SK-OV-3	--	--	4.00	25.59	--	7.69	11.90	78.81	--
Renal	786-0	0.33	--	12.94	41.20	5.74	--	69.97	-46.10	4.59
Cancer	A498	--	--	22.15	23.10	--	--	41.38	-11.58	--
	ACHN	--	1.50	5.29	44.66	9.66	--	72.71	89.96	5.27
	CAKI-1	NT	NT	36.73	47.85	29.41	6.27	45.99	80.28	22.49
	RXF 393	--	--	5.26	--	--	--	34.74	-11.35	--
	SN12C	--	--	18.07	38.55	10.17	--	59.49	76.17	6.24
	TK-10	--	--	6.54	30.14	--	--	22.67	67.89	--
	UO-31	21.04	25.37	43.11	65.55	37.72	17.88	69.74	-23.74	37.88
Prostate	PC-3	17.63	17.42	42.77	77.16	34.66	5.66	58.13	94.79	14.97
Cancer	DU-145	--	--	10.35	27.43	6.17	--	42.37	71.56	--
Breast	MCF7	8.89	6.45	25.45	62.37	23.38	3.29	53.51	-7.00	2.17
Cancer	MDA-MB-231/ATCC	2.53	--	24.16	42.94	22.90	--	31.86	88.24	28.85
	HS 578T	--	--	12.96	NT	2.02	NT	21.36	NT	5.27
	BT-549	--	--	21.34	83.04	12.45	0.56	19.89	95.43	4.82
	T-47D	17.72	18.92	28.65	88.83	33.06	18.13	46.25	-9.17	32.03
	MDA-MB-468	--	--	14.16	65.41	3.90	--	33.30	-6.34	21.10

-- indicates GI < 10%; NT, not tested; 30-40% growth inhibition; 40-50% growth inhibition; 50-70% growth inhibition; 70-90% growth inhibition; 90-100% growth inhibition; lethal to cancer cells

Table 2. Percent growth inhibition of compounds **17-23** and **25-26** at 10^{-5} M concentration

Cell Panel	Cell Line	17	18	19	20	21	22	23	25	26
Leukemia	CCRF-CEM	4.95	0.16	7.54	14.97	17.00	25.61	84.59	39.35	20.26
	HL-60(TB)	2.08	2.72	--	3.82	24.00	16.39	85.19	53.60	70.50
	K-562	NT	NT	NT	NT	NT	26.95	93.24	56.10	46.18
	MOLT-4	10.81	8.05	7.97	25.94	18.93	30.74	-18.71	88.92	48.79
	RPMI-8226	3.37	16.33	26.70	32.02	24.37	38.69	92.49	59.15	45.09
	SR	0.35	--	--	20.80	19.01	28.69	96.41	54.67	20.35
Non-Small	A549/ATCC	0.79	--	0.79	3.03	--	12.18	96.66	60.79	40.00
Cell Lung	EXVX	12.28	3.35	25.74	29.75	23.59	20.80	70.20	29.70	34.19
Cancer	HOP-62	13.18	8.80	18.24	12.10	18.05	2.81	76.57	37.54	29.29

	HOP-92	11.28	28.53	33.20	47.45	23.98	49.90	NT	NT	NT
	NCI-H226	10.57	--	11.23	19.94	15.86	35.19	74.94	16.59	9.16
	NCI-H23	4.89	--	15.72	18.36	13.65	32.79	69.52	22.11	15.06
	NCI-H322M	10.07	0.05	0.04	--	8.31	26.40	74.71	11.88	9.47
	NCI-H460	--	--	2.54	4.16	5.19	19.27	98.60	59.47	11.87
	NCI-H522	16.09	20.04	16.67	11.80	21.82	30.99	95.35	35.20	48.90
Colon	COLO 205	--	--	--	6.10	10.20	13.91	91.31	33.74	13.58
Cancer	HCC-2998	--	2.74	5.93	9.09	7.02	6.60	60.24	10.99	2.02
	HCT-116	8.12	20.52	25.22	29.74	15.57	28.27	91.40	50.80	28.27
	HCT-15	--	5.32	7.48	22.38	40.46	24.24	87.51	32.20	21.70
	HT29	2.49	16.40	21.18	29.13	16.01	40.51	92.55	39.29	26.71
	KM12	6.65	--	8.80	16.84	16.22	24.64	75.15	29.92	19.54
	SW-620	2.01	--	--	--	--	14.38	78.58	39.61	12.41
CNS	SF-268	6.67	5.51	0.97	7.67	5.91	10.90	64.20	32.93	14.82
Cancer	SF-295	--	--	9.46	5.39	9.55	28.87	76.86	15.42	10.26
	SF-539	--	5.38	--	13.73	4.28	10.32	68.11	17.63	2.35
	SNB-19	--	0.62	--	6.20	5.35	8.67	76.65	30.38	11.24
	SNB-75	15.74	12.54	20.27	23.56	24.80	40.66	59.87	32.80	23.21
	U251	--	--	11.97	17.60	23.07	11.26	87.37	33.09	30.89
Melanoma	LOX IMVI	7.66	0.57	5.17	11.88	15.16	17.80	86.23	26.02	10.30
	MALME-3M	1.08	--	5.46	13.45	7.00	20.24	69.23	5.57	--
	M14	--	8.52	6.35	0.14	6.15	19.80	69.77	11.67	7.08
	MDA-MB-435	--	--	--	--	--	1.57	60.14	14.93	8.51
	SK-MEL-2	8.37	4.67	4.33	--	18.61	NT	NT	--	23.47
	SK-MEL-28	--	--	--	--	3.36	6.11	52.80	1.91	6.80
	SK-MEL-5	3.30	10.70	14.08	27.26	25.42	44.59	78.60	43.79	22.19
	UACC-257	--	--	--	0.03	--	17.42	76.93	49.57	43.09
	UACC-62	10.55	8.33	22.08	20.64	26.99	39.73	75.39	39.94	42.30
Ovarian	IGROV1	9.35	--	4.77	--	7.70	45.49	79.57	21.19	8.52
Cancer	OVCAR-3	--	--	6.44	13.25	10.25	20.70	62.40	15.26	16.18
	OVCAR-4	--	9.68	22.68	27.73	20.93	46.72	69.18	33.78	24.16
	OVCAR-5	--	--	--	1.84	--	29.11	64.20	10.42	5.45
	OVCAR-8	5.02	0.25	7.74	8.27	2.04	14.56	85.33	43.00	26.69
	NCI/ADR-RES	0.96	--	3.58	8.26	8.69	14.23	79.91	32.51	12.43
	SK-OV-3	--	--	--	--	5.01	--	76.95	17.48	11.79
Renal	786-0	0.23	4.92	7.31	12.09	7.03	4.72	80.95	26.75	8.67
Cancer	A498	--	0.98	--	--	--	--	95.31	36.51	9.45
	ACHN	0.04	1.52	12.26	3.26	15.33	24.82	86.22	48.22	11.18
	CAKI-1	22.50	8.36	32.50	20.67	27.23	28.99	74.97	46.36	38.54
	RXF 393	--	--	--	0.92	--	--	73.74	19.02	0.83
	SN12C	3.47	3.11	5.55	11.12	16.29	24.28	80.73	36.84	18.41
	TK-10	--	--	--	4.81	0.38	0.34	73.27	19.03	4.27
	UO-31	35.03	25.88	37.47	48.32	43.79	48.52	97.58	62.22	40.14

Prostate Cancer	PC-3	9.46	3.52	25.57	30.73	28.79	41.58	77.91	50.70	47.92
	DU-145	--	--	1.05	2.42	--	7.85	73.01	10.96	2.12
Breast Cancer	MCF7	1.69	10.51	3.49	24.10	31.03	60.66	87.91	23.87	22.20
	MDA-MB-231/ATCC	14.52	9.39	7.73	21.89	26.04	44.24	66.43	27.06	36.94
	HS 578T	8.01	--	5.70	6.06	7.08	NT	59.18	15.26	13.41
	BT-549	--	15.15	12.58	13.81	4.18	24.15	43.49	22.61	11.11
	T-47D	18.55	11.03	33.98	36.81	27.38	62.90	72.21	41.44	35.45
	MDA-MB-468	7.66	--	12.11	10.22	7.98	55.14	95.67	15.89	8.68

-- indicates GI < 10%; NT, not tested; 30-40% growth inhibition; 40-50% growth inhibition; 50-70% growth inhibition; 70-90% growth inhibition; 90-100% growth inhibition; lethal to cancer cells

Table 3. Overview of the preliminary cytotoxic assay at single dose concentration of 10^{-5} M

Compd	Mean growth percent	[a]Range of growth inhibition	The most sensitive cell lines	[b]Positive cytostatic effect	[c]Positive cytotoxic effect	No. of sensitive cell lines
11	49.68	-27.80 to 94.60	SK-MEL-5 (Melanoma)	26/58	1/58	27/58
14	46.00	50.25 to 83.74	MOLT-4 (Leukemia)	23/59	0/59	23/59
15	78.83	-96.57 to 99.26	SK-MEL-5 (Melanoma)	33/58	25/58	58/58
23	77.95	-18.71 to 98.60	MOLT-4 (Leukemia)	57/58	1/58	58/58
25	32.52	50.70 to 88.92	MOLT-4 (Leukemia)	9/59	0/59	9/59

[a]Negative (-) indicates the cell killed; [b]The ratio between number of cell lines with percent growth from 0 to 50 and total number of cell lines; [c]The ratio between number of cell lines with percent growth of <0 and total number of cell lines

Compounds **15** and **23** fulfilled the selection criteria set by NCI for antiproliferative activity in this assay and thus, selected for further evaluation at the full panel of cancer cell lines at five dose concentrations (10^{-4}–10^{-8} M). Three parameters for each cell lines *viz.* GI_{50}, TGI and LC_{50} have been reported for derivatives **15** and **23** towards cytotoxicity and average of mean graph midpoint (MG-MID) was determined for these parameters. *In vitro* evaluation of these compounds indicated that derivatives **15** and **23** exhibited cytotoxicity towards most of the human cell lines, showing MG-MID GI_{50} values of 1.43 and 1.83 μM, respectively (**Table 4**). Both the derivatives showed particular efficacy against colon and leukemia subpanels having GI_{50} values in the range of 0.42-1.03 μM. The most sensitive leukemia and colon cell lines are MOLT-4 (GI_{50} = 0.44-0.47 μM) and HCT-116 (GI_{50} = 0.40-0.42 μM) for derivative **15,** and SR (GI_{50} = 0.41-0.49 μM) and

HT-29 (GI_{50} = 0.54-0.93 μM) in case of compound **23**, respectively. Moreover, derivative **15** exhibited good selectivity towards HOP-92 (GI_{50} = 0.37 μM) of non-small cell lung cancer, UO-31 (GI_{50} = 0.58 μM) of renal cancer and BT-549 (GI_{50} = 0.92 μM) of breast cancer while compound **23** showed selectivity towards LOX IMVI (GI_{50} = 0.82 μM) of melanoma cancer and ACHN (GI_{50} = 0.53 μM) of renal cancer. Thus, in 5-benzimidazole series, (diethylamino)ethyl (**15**) indicated the better cytotoxicity while in 6-benzimidazole series, (dimethylamino)ethyl (**23**) exhibited good activity. Overall, the naphthalimide substituted with 5-benzimidazole (**15**) led to more potency than the 6-benzimidazole analogue (**23**). These results were also compared with clinical trial drugs, amonafide (NSC: 308847), a naphthalimide derivative and marketed drug nocadozaole (NSC: 238159), a benzimidazole analogue. It has been observed that compounds **15** and **23** are more active than amonafide but less potent than nocadozaole towards cancer cell lines.

Table 4. GI_{50} (μM), TGI (μM) and LC_{50} (μM) of derivatives **15** and **23** *in vitro* tumor cell lines

Compd	Activiy (μM)	I	II	III	IV	V	VI	VII	VIII	IX	MG-MID[a]
15	**GI_{50}**	1.09	1.50	1.18	1.36	1.67	1.61	1.32	1.61	1.56	1.43
	TGI	4.94	3.39	3.07	2.89	3.15	4.14	3.39	3.93	3.97	3.65
	LC_{50}	[b]	10.8	6.74	5.72	5.85	13.8	11.2	53.2	5.84	14.1
23	**GI_{50}**	1.21	1.63	1.29	2.02	1.98	1.92	1.39	2.38	2.68	1.83
	TGI	7.87	6.19	8.89	11.6	5.47	12.1	7.05	9.62	14.2	9.24
	LC_{50}	[b]	44.6	58.5	55.3	35.6	67.2	29.5	53.1	66.4	51.3
Amonafide	**GI_{50}**	2.09	3.35	2.93	4.15	3.43	4.24	2.76	2.57	3.96	3.32
Nocodazole	**GI_{50}**	0.18	0.39	0.09	0.25	0.22	0.34	0.86	0.28	0.23	0.60

Leukemia (I), non-small cell lung cancer (II), colon cancer (III), CNS cancer (IV), melanoma (V), ovarian cancer (VI), renal cancer (VII), prostate cancer (VIII), breast cancer (IX), [a](MG_MID): The average sensitivity of all cell lines towards the test agent (μM), [b]Compounds showed values > 100 μM.

3.3.2 DNA interaction studies

The binding properties of DNA with compounds **15** and **23** as a model of naphthalimide-benzimidazole conjugates have been studied with calf thymus (ct)-DNA using UV-visible and fluorescence spectroscopy as well as circular dichroism experiment.

3.3.2.1 UV-visible spectroscopic studies

In order to provide evidence for the possibility of binding of naphthalimide-benzimidazoles to calf-thymus DNA, UV-visible titrations of solution of **15** and **23** with DNA were performed. The absorption spectra of compounds **15** and **23** exhibited absorption band at 370 nm in phosphate buffer (*p*H 7.4) at room temperature. The changes observed in the absorption spectra of compounds **15** and **23** (20.0 μM) with incremental addition of ct-DNA (0-110 μM for **15**; 0-85 μM for **23**) showed hypochromism at 370 nm (29.92 % for **15** and 20% for **23**), indicating the interaction of derivatives with double-helical ct-DNA (**Figure 2a-b**). The absorption intensity at 370 nm was decreased due to the fact that purine and pyrimidine bases of DNA are exposed because of binding of planar naphthalimide moiety with DNA. To access the stability of adduct formed between DNA and substrate, Benesi-Hildebrand equation[73] has been used to calculate the intrinsic binding constant (K_b) for compounds **15** and **23** (**Figure 2c**) and were found to be 3.62×10^5 M^{-1} and 2.23×10^5 M^{-1}, respectively. The results indicated that compound **15** with (diethylamino)ethyl showed stronger interaction with ct-DNA than compound **23**.

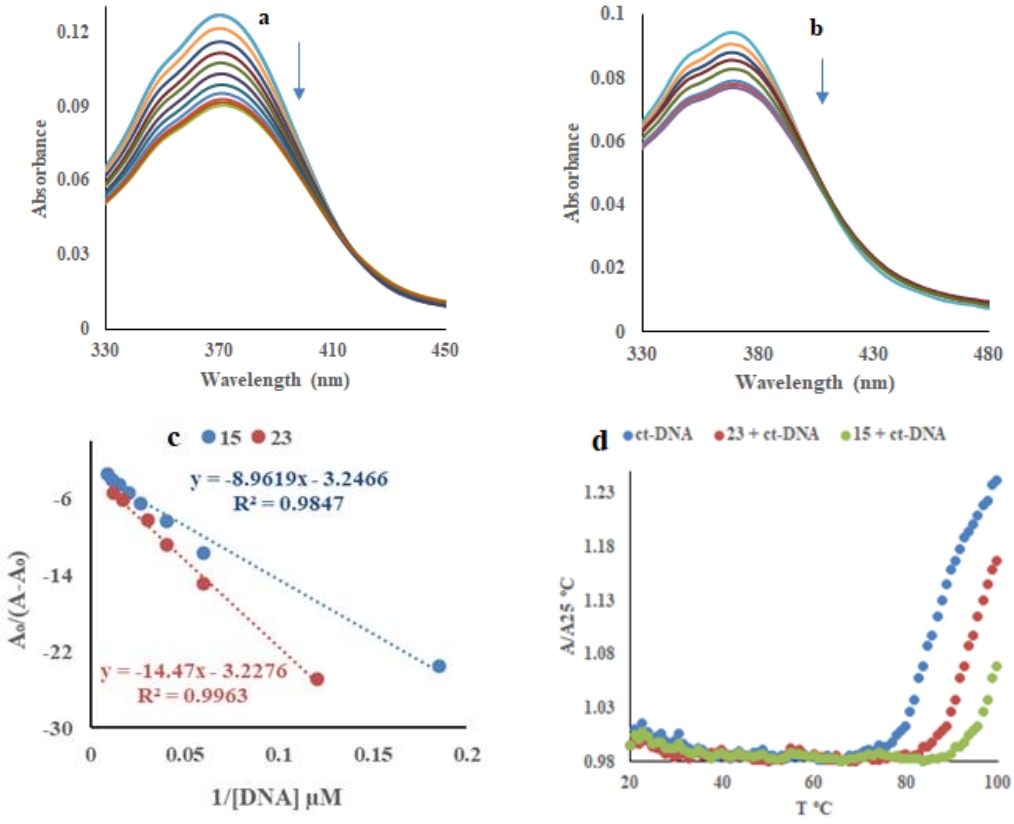

Figure 2. Absorption spectra of compounds (a) **15,** (b) **23**, (c) Benesi-Hildebrand plot and (d) Thermal denaturation plots of ct-DNA in the absence and presence of compounds **15** and **23**

3.3.2.2 Thermal denaturation studies

Thermal behaviour of DNA in the presence of **15** and **23** might be given an insight into DNA conformation changes on rising the temperature, and thus offered information about the interaction strength of compounds with DNA. The thermal denaturation experiment was carried out for DNA in the absence of compounds that revealed melting temprature (T_m) value of 75.6 ± 0.2 ˚C under given experimental conditions, while the melting temperature of DNA in the presence of compounds **15** and **23** were successively increased to 89.8 ± 0.2 ˚C and 81.5 ± 0.3 ˚C, respectively (**Figure 2d**). The observed changes in UV-visible and T_m were consistent with antitumor activity, with potency improving from compound **23** to **15**.

3.3.2.3 Fluorescence studies

Fluorescence emission of compounds **15** and **23** (5.0 μM) showed a band at around 530 nm, at the excitation of 370 nm. Quenching of fluorescent intensity of compounds **15** (56.16 % at 298 K, 54.38 % at 308 K and 39.11 % at 318 K) and **23** (55.10 % at 298 K, 36.30 % at 308 K and 29.37 % at 318 K) at three different temperatures has been observed while maximum emission wavelength was slightly blue shifted to 20 nm with increase in the concentration of ct-DNA (**Figure 3**). Quantitative estimation of quenching with DNA in terms of fluorescence quenching data was done by Stern-Volmer equation,[75] where K_{sv} and K_q have been calculated at different temperatures (**Table 5**). It has been observed that K_{sv} and K_q were decreased on increasing the temperature, indicated that the mechanism of quenching might be a static process. Moreover, the K_q is much larger than diffusion controlled (1.0×10^{10} M^{-1} s^{-1}),[77] also suggested that interaction involved the stating quenching. To calculate the binding constant (K_b) and the average number of binding sites per DNA molecule (n) of compound-DNA interaction, fluorescence titrations were performed at different temperatures using modified Stern-Volmer equation.[78] The values of K_b were observed to decrease with increasing temperature for compounds **15** and **23**, indicating a reduction in the stability of DNA-compound adduct at higher temperatures. The values of n have been obtained for both the compounds from the slope, which were found to be close to one.

The non-covalent interactions between small molecule and ct-DNA are hydrogen bonding, electrostatic forces, hydrophobic interactions and van der Waals forces.[79] To determine these binding forces, thermodynamic parameters such as entropy change (ΔS), enthalpy change (ΔH) and free energy change (ΔG) have been calculated using van't Hoff equation (**Table 6**). The observed negative values of ΔG for compounds revealed that the binding process is spontaneous

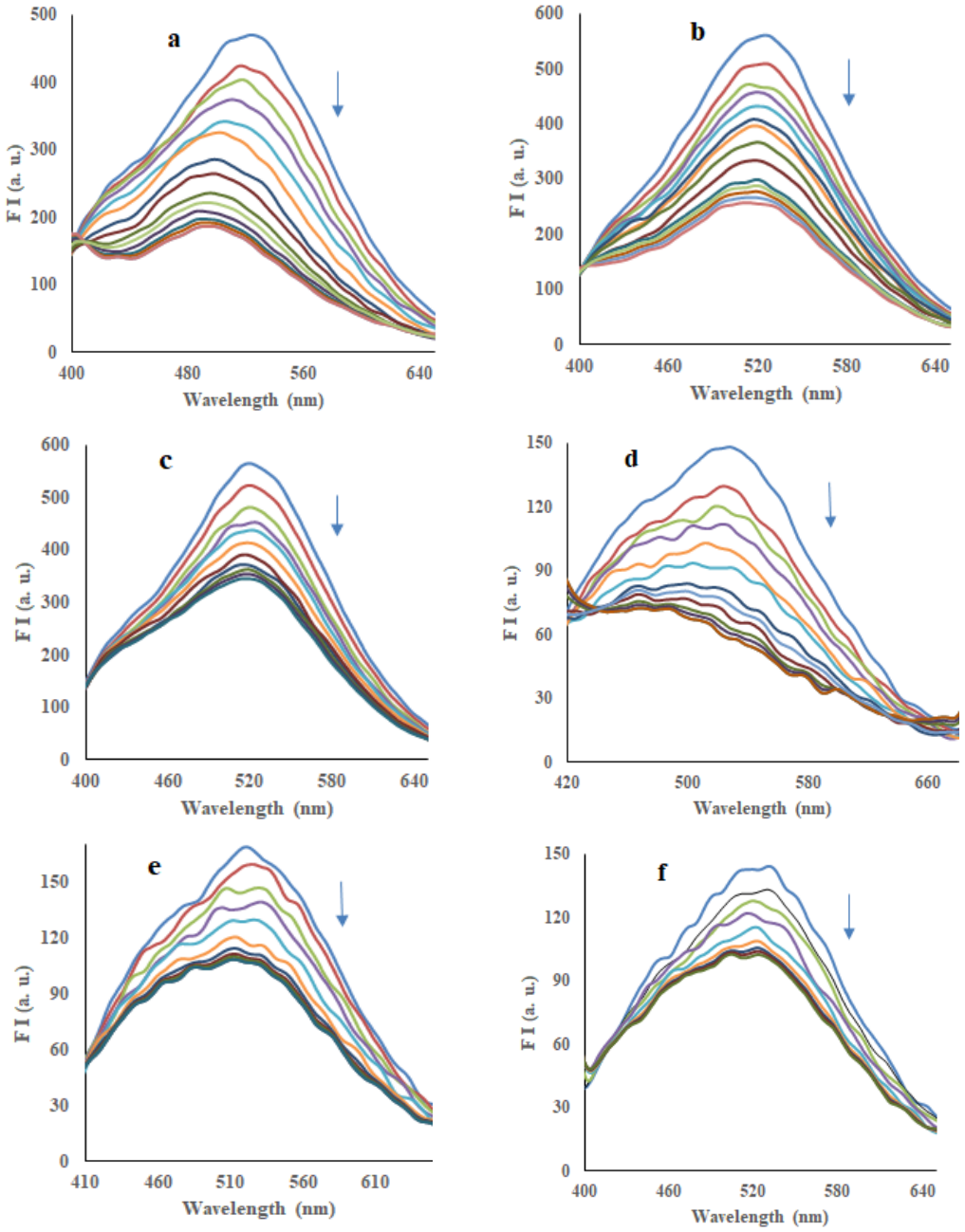

Figure 3. Emission spectra of compound **15** in the presence of ct-DNA at (a) 298 K, (b) 308 K and (c) 318 K; Emission spectra of compound **23** in the presence of ct-DNA at (d) 298 K, (e) 308 K and (f) 318 K

and favorable. The type of interaction between compound and DNA has been identified by evaluating the values of ΔH and ΔS and in the present study found to be -38.59 kcal M^{-1} and -102.75 cal M^{-1} K^{-1} for compound **15**, and -27.36 kcal M^{-1} and -67.40 cal M^{-1} K^{-1} for compound **23**, respectively. The negative values of ΔH and ΔS for **15** and **23** indicated that the interaction with

DNA is mainly enthalpy driven by which hydrogen bonding and van der Waals contacts atributed towards the stability of complexes.

Table 5. Quenching and binding parameters for the interaction of compounds **15** and **23** with ct-DNA at three different temperatures

Compd	T (K)	K_{SV} ($\times10^4$) (M^{-1})	K_q ($\times10^{12}$) ($M^{-1}s^{-1}$)	R^2	K_b ($\times10^5$) (M^{-1})	N	R^2
15	298	4.72	4.72	0.9563	9.26	1.37	0.9856
	308	2.92	2.92	0.9597	0.49	1.06	0.9609
	318	1.72	1.72	0.9805	0.15	0.97	0.9686
23	298	5.98	5.98	0.9479	2.83	1.18	0.9352
	308	2.26	2.26	0.9497	0.29	1.03	0.9770
	318	1.88	1.88	0.9894	0.15	0.98	0.9931

R^2 is the correlation coefficients

Table 6. Thermodynamic parameters for the interaction of compounds **15** and **23** with ct-DNA at three different temperatures

Compd	T (K)	ΔH (kcal M^{-1})	ΔS (cal M^{-1} K^{-1})	ΔG (kcal M^{-1})	R^2
15	298	-38.59	-102.75	-7.97	0.9502
	308			-6.94	
	318			-5.91	
23	298	-27.36	-67.40	-7.27	0.9178
	308			-6.60	
	318			-5.92	

R^2 is the correlation coefficients

3.3.2.4 Competitive displacement assay

To investigate the mode of binding of **15** and **23** to ct-DNA, a competitive binding experiment with ethidium bromide (EB) was performed. EB acts as one of the sensitive fluorescent probes having a planar structure that interacts with DNA by an intercalative mode.[80] Ethidium bromide shows an emission maximum at 600 nm on excitation at 520 nm. Fluorescence spectra of fixed concentration of EB-DNA complex (3 μM : 30 μM) in the presence of increasing concentration of compounds (**15**: 0-150 μM; **23**: 0-120 μM) in phosphate buffer (*p*H 7.4) were recorded (**Figure 4**). On subsequent addition of compound, a decrease in fluorescence emission (**15**: 62.03% and **23**: 55.72%) at 600 nm of EB-DNA complex was observed, indicated that these compounds were effectively competing with EB for the occupation at the same binding sites on DNA through intercalation.

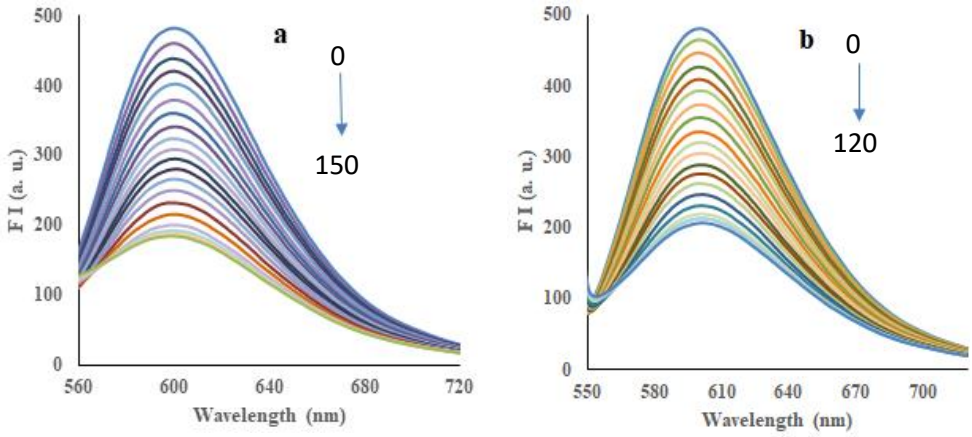

Figure 4. Emission spectra of EB-DNA complex in the absence and presence of the compounds (a) **15** and (b) **23** in phosphate buffer at *p*H 7.4

3.3.2.5. Circular Dichroism (CD)

In order to get insight into the variations of properties induced by small molecule binding, CD spectroscopy is helpful in analysing the changes in DNA structure during DNA-drug interactions. CD spectrum of DNA consists of a negative band at 247 nm because of helicity and a positive band at 277 nm due to base stacking, which are characteristics of DNA in the right handed B form.[81] On the addition of compounds **15** and **23**, the intensities of positive and negative bands of DNA increased significantly; this observation is a strong indicator of classical intercalation (**Figure 5a)**. Moreover, these compounds did not yield any positive induced CD (ICD) band at the region of (λ) 350 and 400 nm, instead, a weak negative ICD band was observed, thus, excluding binding into the minor groove of ct-DNA.[82,83] This data shows good agreement with increasing T_m and decreasing EB fluorescence intensity.

3.3.3 Cell cycle analysis

Numerous anticancer compounds exhibit their effect by blockade of cell cycle process at a particular phase.[103] We hypothesized that naphthalimide-benzimidazole conjugates have the mechanism of action that they also arrest the process of mitosis due to the presence of benzimidazole moiety. To test this hypothesis, we performed the cell cycle distribution using flow cytometer with compounds **15** and **23** on MDA-MB-468 breast cancer cells. In our study, MDA-MB-468 cells were treated with compounds **15** and **23** at 1 μM concentration for 24 h along with control (**Figure 5b**). The results indicated that compound **15** had no significant effect at cell cycle whereas compound **23** arrested the cell cycle at G_2/M phase (**Figure 5c-d**, **Table 7**). In the vehicle

treated group, about 13.47% of MDA-MB-468 cells were distributed in G2/M phase. Only compound **23** increased the proportion of cells in G2/M phase. About 25.23% of cells were found in G2/M phase when treated with 1 μM of compound **23** for 24 h.

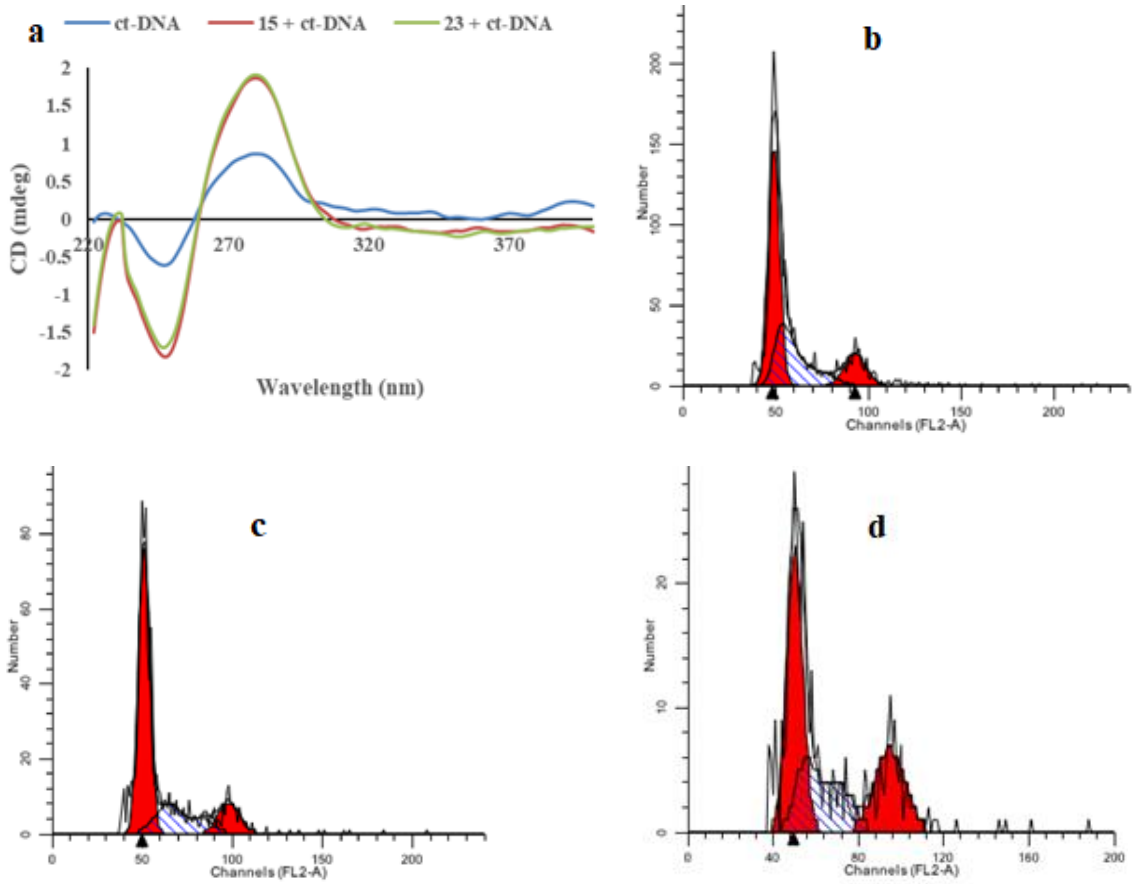

Figure 5. (a) CD spectra of free ct-DNA (40 μM) (blue line), **15**-DNA complex (red line) and **23**-DNA complex (green line) at ratio $r_{[compound/ct\text{-}DNA]}$ = 0.025 in Tris HCl buffer (*p*H 7.4); Flow cytometry analysis on cell cycle progression on MDA-MB-468 (breast cancer) cell line: (b) control, (c) compound **15** and (d) compound **23**

Table 7. Cell cycle distribution of MDA-MB-468 cell line treated with compounds **15** and **23**.

Compd	Sub G_1%	G_0/G_1%	S%	G_2/M%
Control	1.88	51.98	32.67	13.47
15	1.91	62.55	22.01	13.53
23	1.88	44.05	28.84	25.23

3.3.4 BSA binding studies

Binding of a prospective drug to plasma protein is recognized as a crucial step in accessing its bioavailability,[104] and the reports on plasma protein binding are required in screening potential

therapeutic agents.[105] Albumin binding, in particular, plays a decisive role for *in vivo* bioavailability of any drug. Within this rationale, we examined the interaction of naphthalimide-benzimidazoles with bovine serum albumin (BSA), structural homology with human serum albumin (HSA), using absorption and emission spectroscopy.

3.3.4.1 UV-visible spectroscopic studies

UV-visible spectrum of BSA showed an intense absorption band at about 279 nm in phosphate buffer at *p*H 7.4, mainly due to presence of tyrosine (Tyr), tryptophan (Trp) and phenylalanine (Phe) residues. On subsequent addition of compounds **15** and **23** (0-15 μM) to BSA solution (7.0 μM), gradual increase in intensity of band at 279 nm along with enhancement of new band at 370 nm was observed (**Figure 6a-b**). These variations originated from conformational changes and polarity of microenvironment around aromatic residues of BSA. Moreover, absorption maxima of BSA remains unchanged, suggested that interactions between compounds and BSA are non-covalent in nature and likely to occur through π-π stacking between aromatics of naphthalimide-benzimidazole and phenyl rings of Trp, Tyr and Phe residues located in the binding cavity of BSA. Binding constants (K_b) for the interaction of compounds with BSA have been calculated using Benesi-Hildebrand equation[73] and were found to be 6.96 × 10^4 M^{-1} for **15** and 5.64 × 10^4 M^{-1} for **23**, signifying better binding affinity of compound **15** with serum albumin than **23**.

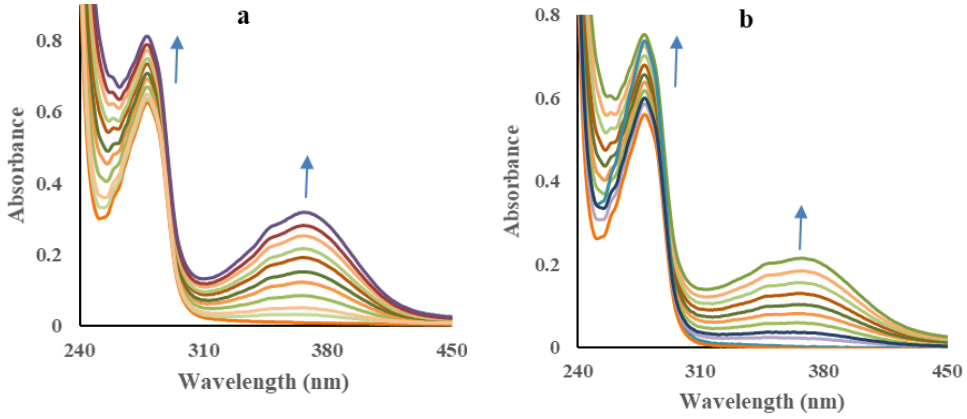

Figure 6. Absorption spectra of BSA in the presence of compounds (a) **15,** (b) **23** in phosphate buffer (*p*H 7.4) at 298 K

3.3.4.2 Fluorescence studies

The emission of BSA is observed from two Trp residues; one is located on the surface and the other residue present in the hydrophobic pocket of protein molecule.[106] **Figure 7a-b** depicted that on progressive addition of different concentration of compounds (0-45 μM) to BSA (7.0 μM), the

emission spectrum of Trp residue of serum protein at around 350 nm was gradually quenched (82.49% for **15** and 79.11% for **23**) with the appearance and enhancement of new band at 485 nm. The λ_{max} of the emission of Trp residues in BSA was also blue shifted from 350 nm (in free BSA) to 330 nm. This suggests that the emitting Trp residue(s) in the complex of compound-BSA are in less polar or more hydrophobic environment as compared with free BSA.

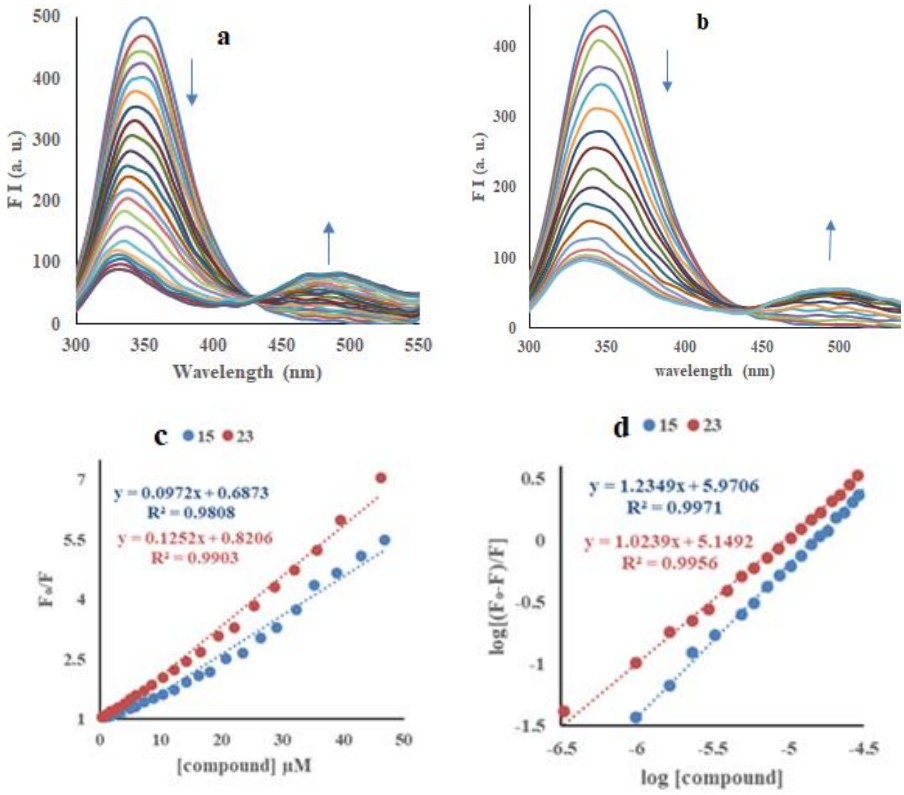

Figure 7. Emission spectra of BSA in the presence of compounds (a) **15,** (b) **23** in phosphate buffer (*p*H 7.4) at 298 K, (c) Stern-Volmer and (d) Modified Stern-Volmer Plots of compounds **15** and **23**

The steady-state fluorescence quenching of Trp emission in serum albumin with addition of compound has been characterized by Stern-Volmer equation[75] that showed the relation between the quenching extent for each compound and the strength of their interactions with BSA. The values of Stern-Volmer constant (K_{SV}) and bimolecular quenching constant (K_q) were calculated from the slope of linear portion of regression curve (**Table 8**, **Figure 7c**). A linear Stern-Volmer plot was obtained with compounds **15** and **23,** suggested that solely one type of quenching or binding process occur, either stating or dynamic quenching. The values obtained for bimolecular quenching constant (K_q) of compounds **15** (1.41×10^{13} $M^{-1}s^{-1}$) and **23** (1.52×10^{13} $M^{-1}s^{-1}$) were

much greater than the diffusion control limiting value of 1×10^{10} M^{-1} s^{-1}, which is the largest possible value reported in aqueous medium.[77] Thus, the binding of compounds to BSA probably involves the static quenching with formation of complex at ground state.

Modified Stern-Volmer equation[78] has been used to determine the binding constants (K_b) and the average number of binding sites (n) for compound-BSA complexes (**Figure 7d**). These complexes exhibited excellent binding parameters, suggesting their binding to the albumins and their possible transfer as well as their release ability upon arrival at their target sites. As these values are significantly lower than 10^{15} M^{-1}, which is the value of the association constant of protein albumin with diverse compounds, their interactions are considered significant among the known non-covalent ones.[107]

Table 8. Quenching and binding parameters for interaction of BSA with compounds **15** and **23**

Compd	K_{sv} ($\times 10^5$) (M^{-1})	K_q ($\times 10^{13}$) ($M^{-1}s^{-1}$)	R^2	K_b ($\times 10^5$) (M^{-1})	N	R^2
15	1.41	1.41	0.9808	9.34	1.23	0.9971
23	1.52	1.52	0.9903	1.41	1.02	0.9956

R^2 is the correlation coefficients

3.4 Conclusion

A series of isomeric benzimidazole with substituted naphthalimides has been synthesized in moderate to good yields and studied their effects on cytotoxicity. Both the isomeric groups of 18 compounds were assessed over 60 human tumor cell line panel at 10^{-5} M concentration, where most of the examined compounds showed superior activity. Compounds **15** and **23** were identified excellent activity against leukemia and colon cancer subpanels at five dose concentration levels. The interaction between these compounds with DNA was studied by UV-visible, fluorescence and CD spectroscopy as well as DNA melting experiment. The results suggested that fluorescence of compounds **15** and **23** has been quenched significantly by DNA and the probable mechanism was a static quenching process. The association constant (K_b) value between compound and DNA has been found to be in the order of 10^5 mol^{-1}, which is better than other reported DNA intercalators. The thermodynamic parameters, ΔH^o and ΔS^o, were calculated in the range of -38.59 to -27.36 kcal M^{-1} and -102.75 to -67.40 cal M^{-1} K^{-1}, respectively, indicated that the binding of compounds to DNA were driven mainly by hydrogen bonds and van der Waals interactions. The mechanism of action studies with cell cycle arrest confirmed that compound **23** maintained their ability to arrest cells in G2/M phase and induce cell apoptosis. Compounds **15** and **23** have also been

effectively bound to BSA protein with good binding constant values of 9.34 x 10^5 M^{-1} and 1.41 x 10^5 M^{-1}, respectively, determined through emission spectroscopy.

3.5 Experimental section

All commercially available compounds (Spectrochem, Aldrich, Merck etc.) were used without purification. Melting points were determined in an open capillary and were uncorrected. ^{1}H and ^{13}C NMR spectra have been performed on Jeol ECS 400 NMR spectrophotometer, which were operated at 400 MHz for ^{1}H nuclei and 100 MHz for ^{13}C nuclei, using $CDCl_3$ as solvent. Chemical shifts are reported in parts per million (ppm) with TMS as an internal reference. Water Micromass-Q-T of Micro has been used to determine the mass spectra. CHN analysis was done using Thermo Scientific (Flash 2000) analyser. Reactions have been observed by TLC with plate coated with silica gel HF-254 and column chromatography was done with silica gel 60-120/100-200 mesh. UV-visible absorption and fluorescence emission spectra were measured with 1 cm quartz cell. Shimadzu-2400 PC spectrometer instrument was used to determine the UV-visible spectra. Emission spectra were recorded with Varian Cary Eclipse fluorescence spectrometer. Circular dichroism spectra were recorded with an Applied Photophysics CD spectrophotometer.

Dibromonitrobenzene (2a-b):[90] Dibromobenzene (**1a-b**) (5 g, 21.27 mmol) in dichloromethane (15 ml) and sulphuric acid (10 ml) was treated with cooled solution of nitric acid and sulphuric acid (4:1) at 0˚C for 30 min. The reaction mixture was allowed to warm at room temperature with stirring. On completion of reaction (monitored by TLC), quenched the reaction mixture with ice. The precipitate formed was collected and dried in an oven to afford desired product **(2a-b)** in 90-95% yields.

5-Bromo-*N*-cyclohexyl-2-nitroaniline (3b): 1,3-Dibromonitrobenzene (3 g, 10.71 mmol), cyclohexyl amine (1.27 g, 12.85 mmol) and K_2CO_3 (1.47 g, 10.71 mmol) were taken in DMF (20 ml) in 100 ml dried round bottom flask and stirred the reaction mixture at 100˚C for 18 h. On completion of reaction, 50 mL water was added and extracted with ethyl acetate. The extract was then dried over anhydrous sodium sulphate, filtered and concentrated to get the crude product. The residue was column purified on silica gel (Hexane/EtOAc = 20:1) to obtain the desired product.

5-Bromo-*N*-cyclohexyl-2-nitroaniline (3b): Yellow solid; 70% yield; mp 90-93 ºC; ^{1}H NMR

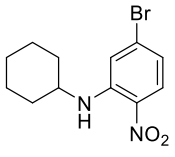

($CDCl_3$, 400 MHz): δ (ppm) 8.13 (d, *J* = 6.88 Hz, 1H, NH), 8.00 (d, *J* = 9.16 Hz, 1H, ArH), 7.01 (d, *J* = 1.84 Hz, 1H, ArH), 6.69 (dd, ^2J = 9.16 Hz, ^3J = 2.28 Hz, 1H, ArH), 3.49-3.42 (m, 1H, cyclohex-CH), 2.05-2.02 (m, 2H, cyclohex-

CH_2), 1.82-1.74 (m, 2H, cyclohex-CH_2), 1.68-1.64 (m, 1H, cyclohex-CH_2), 1.49-1.28 (m, 5H, cyclohex-CH_2); ^{13}C NMR ($CDCl_3$, 100 MHz): δ (ppm) 144.8, 131.4, 130.3, 128.1, 117.9, 116.4 (ArC), 50.9 (CH), 32.4 (CH_2), 25.3 (CH_2), 24.3 (CH_2).

***N*-Cyclohexyl-2-nitro-4/5-(4,4,5,5-tetramethyl-1,3,2-dioxaborolan-2-yl)aniline (4a-b):** 4/5-Bromo-*N*-cyclohexyl-2-nitroaniline (**3a-b**) (2.0 g, 6.68 mmol), bis(pinacolato)diboron (2.03 g, 8.01 mmol), KOAc (0.98 g, 10.01 mmol), palladium(II)bis(triphenylphosphine) dichloride (5.0 mol%) in 1,4-dioxane (30 mL) were charged in 100 ml oven-dried round bottom flask. The reaction mixture was refluxed for 10 h until the halide was completely consumed as determined by TLC. The mixture was then cooled to room temperature. Solvent of reaction was concentrated under reduced pressure and the crude was extracted with chloroform and water (3 × 50 mL). The extract was dried over anhydrous Na_2SO_4, filtered and concentrated. The crude material obtained was column purified on silica gel using ethyl acetate and hexane to obtain the desired reddish yellow product.

***N*-Cyclohexyl-2-nitro-4-(4,4,5,5-tetramethyl-1,3,2-dioxaborolan-2-yl)aniline (4a):** Reddish

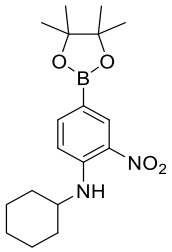

yellow solid; 82% yield; mp 125-127 °C; ^{1}H NMR ($CDCl_3$, 400 MHz): δ (ppm) 8.63 (d, *J* = 1.36 Hz, 1H, ArH), 8.29 (d, *J* = 6.88 Hz, 1H, NH), 7.75 (dd, ^2J = 8.68 Hz, ^3J = 0.92 Hz, 1H, ArH), 6.83 (d, *J* = 8.72 Hz, 1H, ArH), 3.58-3.51 (m, 1H, cyclohex-CH), 2.06-2.03 (m, 2H, cyclohex-CH_2), 1.82-1.76 (m, 2H, cyclohex-CH_2), 1.67-1.63 (m, 1H, cyclohex-CH_2), 1.48-1.23 (m, 17H, cyclohex -CH_2 & boronate-CH_3); ^{13}C NMR ($CDCl_3$, 100 MHz): δ (ppm) 146.1, 141.3, 134.5, 131.4, 113.2 (ArC), 83.7 (C), 50.8 (CH), 32.5 (CH_2), 25.4 (CH_2), 24.7 (CH_3), 24.4 (CH_2).

***N*-Cyclohexyl-2-nitro-5-(4,4,5,5-tetramethyl-1,3,2-dioxaborolan-2-yl)aniline (4b):** Reddish yellow solid; 78% yield; mp 120-122 °C; ^{1}H NMR ($CDCl_3$, 400 MHz): δ (ppm) 8.13 (d, *J* = 8.68

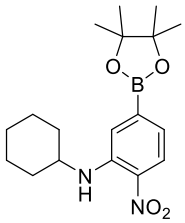

1H, ArH), 3.71-3.63 (m, 1H, cyclohex-CH), 2.07-2.02 (m, 2H, cyclohex-CH_2), 1.83-1.76 (m, 2H, cyclohex-CH_2), 1.67-1.63 (m, 1H, cyclohex- CH_2), 1.53-1.28 Hz, 2H, NH & ArH), 7.28 (s, 1H, ArH), 6.96 (d, *J* = 8.72 Hz, (m, 17H, cyclohex-CH_2 & boronate-CH_3); ^{13}C NMR ($CDCl_3$, 100 MHz): δ (ppm) 143.8, 135.5, 132.6, 125.7, 120.8, 119.9 (ArC), 84.3 (C), 50.3 (CH), 32.7 (CH_2), 25.5 (CH_2), 24.7 (CH_3), 24.3 (CH_2).

6-(4/3-(Cyclohexylamino)-3/4-nitrophenyl)-1*H*,3*H*-benzo[*de*]isochromene-1,3-dione (6a-b): To a solution of 6-bromo-1*H*,3*H*-benzo[*de*]isochromene-1,3-dione (**5**) (2 g, 7.22 mmol) in a

mixture of acetonitrile and water (9:1) in 100 ml round bottom flask, *N*-cyclohexyl-2-nitro-4/5-(4,4,5,5-tetramethyl-1,3,2-dioxaborolan-2-yl)aniline (**4a-b**) (2.51 g, 7.22 mmol) and K_2CO_3 (1.0 g, 7.22 mmol) were added under inert atmosphere. Then, $Pd(PPh_3)_4$ (5 mol%) was added with continued N_2 purging and refluxed the reaction mixture for 10-12 h. On completion of reaction (determined by TLC), solvents were evaporated under reduced pressure followed by water (50 ml) was added and then extracted with chloroform. Chloroform layer was dried over sodium sulphate. The crude product has further been purified by column chromatography with hexane and ethyl acetate to get the yellowish solid product.

6-(4-(Cyclohexylamino)-3-nitrophenyl)-1*H*,3*H*-benzo[*de*]isochromene-1,3-dione (6a):

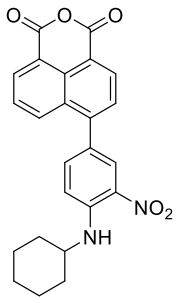

Reddish yellow solid; 70% yield; mp 83-86 ^oC; ^1H NMR ($CDCl_3$, 400 MHz): δ (ppm) 8.67-8.63 (m, 2H, ArH), 8.42 (dd, ^2J = 8.72 Hz, ^3J = 0.92 Hz, 1H, ArH), 8.39 (d *J* = 2.28 Hz, 1H, ArH), 8.35 (d, *J* = 7.36 Hz, 1H, ArH), 7.82-7.78 (m, 1H, ArH), 7.76 (d, *J* = 7.76 Hz, 1H, ArH), 7.61 (dd, ^2J = 8.72 Hz, ^3J = 1.84 Hz, 1H, ArH), 7.11 (d, *J* = 9.16 Hz, 1H, NH), 3.68-3.59 (m, 1H, Cyclohex-CH), 2.16-2.12 (m, 2H, Cyclohex-CH_2), 1.89-1.82 (m, 2H, Cyclohex-CH_2), 1.73-1.69 (m, 1H, Cyclohex-CH_2), 1.53-1.43 (m, 4H, Cyclohex-CH_2), 1.41-1.33 (m, 1H, Cyclohex-CH_2); ^{13}C NMR ($CDCl_3$, 100 MHz): δ (ppm) 160.6, 160.4, 146.3, 144.6, 137.0, 133.5, 133.4, 133.1, 131.4, 131.0, 130.0, 128.2, 128.0, 127.4, 124.2, 118.9, 117.4, 114.9 (ArC), 51.3 (CH), 32.6 (CH_2), 25.4 (CH_2), 24.5 (CH_2).

6-(3-(Cyclohexylamino)-4-nitrophenyl)-1*H*,3*H*-benzo[*de*]isochromene-1,3-dione (6b): Reddish yellow solid; 73% yield; mp 81-84 ^oC; ^1H NMR ($CDCl_3$, 400 MHz): δ (ppm) 8.65 (t, *J* = 6.44 Hz, 2H, ArH), 8.35 (t, *J* = 7.32 Hz, 2H, ArH), 8.31 (d, *J* = 7.80 Hz, 1H, ArH), 7.83-7.78 (m,

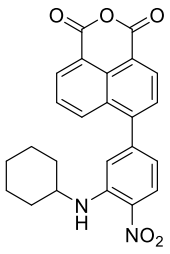

2H, ArH), 6.99 (s, 1H, NH), 6.72 (dd, ^2J = 8.72 Hz, ^3J = 1.36 Hz, 1H, ArH), 3.60-3.52 (m, 1H, cyclohex-CH), 2.10-2.06 (m, 2H, cyclohex-CH_2), 1.82-1.77 (m, 2H, cyclohex-CH_2), 1.68-1.62 (m, 1H, cyclohex-CH_2), 1.50-1.32 (m, 5H, cyclohex-CH_2); ^{13}C NMR ($CDCl_3$, 100 MHz): δ (ppm) 160.3, 160.1, 146.7, 145.7, 144.5, 133.5, 132.8, 131.3, 130.5, 129.8, 127.8, 127.7, 127.5, 118.8, 118.4, 116.1, 115.2 (ArC), 51.0 (CH), 32.6 (CH_2), 25.4 (CH_2), 24.3(CH_2).

6-(3/4-Amino-4/3-(cyclohexylamino)phenyl)-1*H*,3*H*-benzo[*de*]isochromene-1,3-dione (7a-b) and 6-(3/4-amino-4/3-(cyclohexylamino)phenyl)-1*H*-benzo[*de*]isoquinoline-1,3(2*H*)-dione (8a-b): A 100 ml round bottom flask was charged with 6-(4/3-(cyclohexylamino)-3/4-

nitrophenyl)-1*H*,3*H*-benzo[*de*]isochromene-1,3-dione (**6a-b**) (2 g, 4.80 mmol) and sodium dithionite (4.18 g, 24.03 mmol) in THF:water (3:2). Ammonia solution (5 ml) has been added to the reaction mixture and stirred for 1 h at room temperature. Completion of reaction was monitored by TLC and the reaction mixture was extracted with ethyl acetate. Ethyl acetate layer was dried over Na_2SO_4, filtered and concentrated to get the crude product. Mixture of crude brown product (**7** and **8**) was directly used further without purification.

6-(1-Cyclohexyl-1*H*-benzo[*d*]imidazol-5/6-yl)-1*H*,3*H*-benzo[*de*]isochromene-1,3-dione (9a-b) and 6-(1-cyclohexyl-1*H*-benzo[*d*]imidazol-5/6-yl)-1*H*-benzo[*de*]isoquinoline-1,3(2*H*)-dione (10a-b): Mixture of 6-(3/4-amino-4/3-(cyclohexylamino)phenyl)-1*H*,3*H*-benzo[*de*]isochromene-1,3-dione (**7a-b**) and 6-(3/4-amino-4/3-(cyclohexylamino)phenyl)-1*H*-benzo[*de*]isoquinoline-1,3(2*H*)-dione (**8a-b**) (1 mmol) was stirred with triethylorthoformate (1 mmol) in acetic acid (30 ml) for 30 min at room temperature. The reaction mixture was then poured into water and then treated with $NaHCO_3$ followed by extracted with chloroform. Sodium sulphate was used to dry the chloroform layer. Crude was purified by column chromatography using ethyl acetate and hexane as elutents to obtain light brown solid.

6-(1-Cyclohexyl-1*H*-benzo[*d*]imidazol-5-yl)-1*H*,3*H*-benzo[*de*]isochromene-1,3-dione (9a):

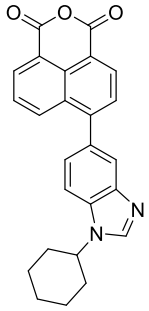

Light brown solid; 72% yield; mp 191-193 ^oC; ^1H NMR ($CDCl_3$, 400 MHz): δ (ppm) 8.65 (d, *J* = 7.32 Hz, 1H, ArH), 8.62 (d, *J* = 7.32 Hz, 1H, ArH), 8.46 (d, *J* = 8.68 Hz, 1H, ArH), 8.16 (s, 1H, ArH), 7.92 (s, 1H, ArH), 7.81 (d, *J* = 7.32 Hz, 1H, ArH), 7.74 (t, *J* = 8.44 Hz, 1H, ArH), 7.66 (d, *J* = 8.24 Hz, 1H, ArH), 7.45 (dd, ^2J = 8.28 Hz, ^3J = 1.40 Hz, 1H, ArH), 4.36-4.28 (m, 1H, cyclohex-CH), 2.33 (d, *J* = 11.00 Hz, 2H, cyclohex-CH_2), 2.08-2.03 (m, 2H, cyclohex-CH_2), 1.95-1.85 (m, 3H, cyclohex-CH_2), 1.64-1.52 (m, 2H, cyclohex-CH_2), 1.44-1.32 (m, 1H, cyclohex-CH_2); ^{13}C NMR ($CDCl_3$, 100 MHz): δ (ppm) 160.8, 160.5, 149.1, 143.8, 141.7, 134.5, 133.6, 133.2, 132.9, 131.9, 130.8, 130.4, 128.6, 127.1, 124.3, 121.6, 118.7, 117.1, 110.5 (ArC), 55.7 (cyclohex-CH), 33.2 (cyclohex-CH_2), 25.5 (cyclohex-CH_2), 25.2 (cyclohex-CH_2); MS (ESI): m/z 397.0 (M^++1); Anal Calcd for $C_{25}H_{20}N_2O_3$: C, 75.74; H, 5.09; N, 7.07; found C, 75.78; H, 5.05; N, 7.09.

6-(1-Cyclohexyl-1*H*-benzo[*d*]imidazol-6-yl)-1*H*,3*H*-benzo[*de*]isochromene-1,3-dione (9b) : Light brown solid; 70% yield; mp 193-196 ^oC; ^1H NMR ($CDCl_3$, 400 MHz): δ (ppm) 8.69 (d, *J* = 7.80 Hz, 1H, ArH), 8.67 (dd, ^2J = 7.32 Hz, ^3J = 0.92 Hz, 1H, ArH), 8.42 (d, *J* = 7.76 Hz, 1H, ArH),

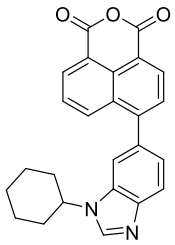

8.15 (s, 1H, ArH), 7.97 (d, *J* = 8.24 Hz, 1H, ArH), 7.85 (d, *J* = 7.76 Hz, 1H, ArH), 7.79-7.75 (m, 1H, ArH), 7.56 (s, 1H, ArH), 7.41 (dd, ^{2}J = 8.24 Hz, ^{3}J = 1.36 Hz, 1H, ArH), 4.30-4.22 (m, 1H, cyclohex-CH), 2.29 (d, *J* = 11.00 Hz, 2H, cyclohex-CH_2), 2.01-1.96 (m, 2H, cyclohex-CH_2), 1.90-1.80 (m, 3H, cyclohex-CH_2), 1.56-1.45 (m, 2H, cyclohex-CH_2), 1.42-1.30 (m, 1H, cyclohex-CH_2); ^{13}C NMR ($CDCl_3$, 100 MHz): δ (ppm) 160.8, 160.6, 149.1, 141.7, 134.4, 133.4, 132.9, 132.1, 131.9, 130.8, 130.6, 128.7, 128.5, 128.4, 127.3, 124.1, 120.4, 118.8, 117.4, 111.4 (ArC), 55.6 (cyclohex-CH), 33.3 (cyclohex-CH_2), 25.6 (cyclohex-CH_2), 25.2 (cyclohex-CH_2); MS (ESI): m/z 397.0 (M^++1); Anal Calcd for $C_{25}H_{20}N_2O_3$: C, 75.74; H, 5.09; N, 7.07; found C, 75.72; H, 5.11; N, 7.05.

6-(1-Cyclohexyl-1*H*-benzo[*d*]imidazol-5-yl)-1*H*-benzo[*de*]isoquinoline-1,3(2*H*)-dione (10a) :

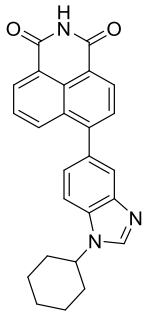

Light yellow solid; 20% yield; mp 208-211 ^{o}C; ^{1}H NMR ($CDCl_3$, 400 MHz): δ (ppm) 8.86 (s, 1H, NH), 8.66 (d, *J* = 7.32 Hz, 1H, ArH), 8.63 (d, *J* = 7.32 Hz, 1H, ArH), 8.39 (d, *J* = 8.72 Hz, 1H, ArH), 8.15 (s, 1H, ArH), 7.96 (s, 1H, ArH), 7.79 (d, *J* = 7.32 Hz, 1H, ArH), 7.71 (t, *J* = 7.80 Hz, 1H, ArH), 7.62 (d, *J* = 8.24 Hz, 1H, ArH), 7.44 (d, *J* = 8.24 Hz, 1H, ArH), 4.34-4.26 (m, 1H, cyclohex-CH), 2.32 (d, *J* = 12.80 Hz, 2H, cyclohex-CH_2), 2.05 (d, *J* = 13.20 Hz, 2H, cyclohex-CH_2), 1.94-1.85 (m, 3H, cyclohex-CH_2), 1.62-1.52 (m, 2H, cyclohex-CH_2), 1.42-1.32 (m, 1H, cyclohex-CH_2); ^{13}C NMR ($CDCl_3$, 100 MHz): δ (ppm) 164.2, 164.0, 148.2, 143.8, 141.6, 133.7, 133.4, 132.7, 130.9, 130.7, 130.6, 130.0, 128.2, 126.6, 124.6, 122.5, 121.8, 121.1, 110.3 (ArC), 55.7 (cyclohex-CH), 33.3 (cyclohex-CH_2), 25.6 (cyclohex-CH_2), 25.3 (cyclohex-CH_2); MS (ESI): m/z 396.1 (M^++1); Anal Calcd for $C_{25}H_{21}N_3O_2$: C, 75.93; H, 5.35; N, 10.63; found C, 75.91; H, 5.37; N, 10.68.

6-(1-Cyclohexyl-1*H*-benzo[*d*]imidazol-6-yl)-1*H*-benzo[*de*]isoquinoline-1,3(2*H*)-dione (10b) :

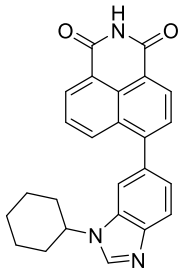

Light yellow solid; 25% yield; mp 213-216 ^{o}C; ^{1}H NMR ($CDCl_3$, 400 MHz): δ (ppm) 8.78 (s, 1H, NH), 8.67-8.63 (m, 2H, ArH), 8.35 (d, *J* = 8.24 Hz, 1H, ArH), 8.14 (s, 1H, ArH), 7.97 (d, *J* = 8.24 Hz, 1H, ArH), 7.81 (d, *J* = 7.80 Hz, 1H, ArH), 7.74 (t, *J* = 7.80 Hz, 1H, ArH), 7.55 (s, 1H, ArH), 7.41 (d, *J* = 7.80 Hz, 1H, ArH), 4.29-4.21 (m, 1H, cyclohex-CH), 2.29 (d, *J* = 11.00 Hz, 2H,

cyclohex -CH_2), 2.01-1.96 (m, 2H, cyclohex-CH_2), 1.89-1.79 (m, 3H, cyclohex-CH_2), 1.55-1.42 (m, 2H, cyclohex-CH_2), 1.37-1.30 (m, 1H, cyclohex-CH_2); ^{13}C NMR ($CDCl_3$, 100 MHz): δ (ppm) 164.1, 163.8, 148.3, 133.6, 133.2, 131.9, 131.0, 130.8, 130.5, 129.9, 128.5, 128.4, 128.2, 126.8, 124.3, 122.6, 121.3, 120.3, 111.4 (ArC), 55.6 (cyclohex-CH), 33.3 (cyclohex-CH_2), 25.6 (cyclohex-CH_2), 25.2 (cyclohex-CH_2); MS (ESI): m/z 396.1 (M^++1); Anal Calcd for $C_{25}H_{21}N_3O_2$: C, 75.93; H, 5.35; N, 10.63; found C, 75.89; H, 5.39; N, 10.61.

2-Aryl/alkyl-6-(1-cyclohexyl-1*H*-benzo[*d*]imidazol-yl)-1*H*-benzo[*de*]isoquinoline-1,3(2*H*)-dione (11-26): 6-(3/4-Amino-4/3-(cyclohexylamino)phenyl)-1*H*,3*H*-benzo[*de*]isochromene-1,3-dione (**7a-b**) (1 mmol) and corresponding amines (1.2 mmol) in 5 ml ethanol were taken in oven dried round bottom flask and refluxed the reaction mixture for 12-15 h. After the completion of the reaction, solvent was evaporated under pressure followed by water (50 ml) was added and extracted with chloroform. Chloroform layer was dried over sodium sulphate. Crude product was further column purified using ethyl acetate and hexane as eluents to get the desired solid products.

2-Allyl-6-(1-cyclohexyl-1*H*-benzo[*d*]imidazol-5-yl)-1*H*-benzo[*de*]isoquinoline-1,3(2*H*)-dione (11): Reddish brown solid; 76% yield; mp 261-263 °C; ^{1}H NMR ($CDCl_3$, 400 MHz): δ (ppm) 8.68

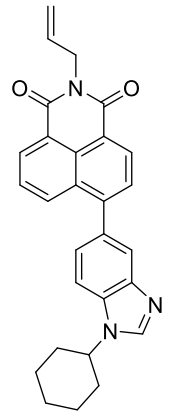

(d, *J* = 7.80 Hz, 1H, ArH), 8.65 (d, *J* = 7.32 Hz, 1H, ArH), 8.36 (d, *J* = 8.68 Hz, 1H, ArH), 8.12 (s, 1H, ArH), 7.95 (s, 1H, ArH), 7.77 (d, *J* = 7.76 Hz, 1H, ArH), 7.70-7.67 (m, 1H, ArH), 7.61 (d, *J* = 8.24 Hz, 1H, ArH), 7.44 (dd, ^2J = 8.24 Hz, ^3J = 1.40 Hz,1H, ArH), 6.08-5.98 (m, 1H, allyl-CH), 5.36 (dd, ^2J = 17.44 Hz, ^3J = 1.40 Hz,1H, allyl-CH_2), 5.24 (dd, ^2J = 10.08 Hz, ^3J = 0.92 Hz,1H, allyl-CH_2), 4.85 (d, *J* = 5.52 Hz, 2H, allyl-CH_2), 4.33-4.26 (m, 1H, cyclohex-CH), 2.32 (d, *J* = 11.00 Hz, 2H, cyclohex-CH_2), 2.05 (d, *J* = 13.32 Hz, 2H, cyclohex-CH_2), 1.93-1.83 (m, 3H, cyclohex-CH_2), 1.62-1.51 (m, 2H, cyclohex-CH_2), 1.43-1.32 (m, 1H, cyclohex-CH_2); ^{13}C NMR ($CDCl_3$, 100 MHz): δ (ppm) 164.1, 163.9, 147.5, 143.8, 141.5, 133.4, 132.7, 132.0, 131.2, 130.9, 130.3, 128.7, 128.4, 128.2, 126.7, 124.6, 122.6, 121.7, 121.2, 117.3, 110.3 (ArC), 55.7 (cyclohex-CH), 42.3 (allyl-CH_2), 33.3 (cyclohex-CH_2), 25.6 (cyclohex-CH_2), 25.3 (cyclohex-CH_2); MS (ESI): m/z 436.1 (M^++1); Anal Calcd for $C_{28}H_{25}N_3O_2$: C, 77.22; H, 5.79; N, 9.65; found C, 77.20; H, 5.80; N, 9.63.

6-(1-Cyclohexyl-1*H*-benzo[*d*]imidazol-5-yl)-2-(prop-2-yn-1-yl)-1*H*-benzo[de]isoquinoline-1,3(2*H*)-dione (12) : Yellow solid; 82% yield; mp 258-261 °C; ^{1}H NMR ($CDCl_3$, 400 MHz): δ (ppm) 8.71 (d, *J* = 7.80 Hz, 1H, ArH), 8.68 (d, *J* = 7.36 Hz, 1H, ArH), 8.37 (d, *J* = 8.28 Hz, 1H,

ArH), 8.13 (s, 1H, ArH), 7.94 (s, 1H, ArH), 7.79 (d, *J* = 7.32 Hz, 1H, ArH), 7.71 (t, *J* = 8.24 Hz, 1H, ArH), 7.62 (d, *J* = 8.28 Hz, 1H, ArH), 7.44 (dd, ^{2}J = 8.24 Hz, ^{3}J = 0.92 Hz,1H, ArH), 5.00 (d,

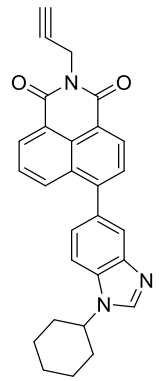

J = 2.72 Hz, 2H, propagyl-CH_2), 4.33-4.26 (m, 1H, cyclohex-CH), 2.32 (d, *J* = 11.00 Hz, 2H, cyclohex-CH_2), 2.21 (t, *J* = 2.32 Hz, 1H, propagyl-CH), 2.05-2.02 (m, 2H, cyclohex-CH_2), 1.94-1.83 (m, 3H, cyclohex-CH_2), 1.62-1.51 (m, 2H, cyclohex-CH_2), 1.43-1.35 (m, 1H, cyclohex-CH_2); ^{13}C NMR ($CDCl_3$, 100 MHz): δ (ppm) 163.6, 163.3, 147.9, 143.9, 141.6, 133.5, 132.6, 131.5, 131.2, 130.4, 128.7, 128.2, 126.7, 124.6, 122.4, 121.8, 121.0, 110.3 (ArC), 78.6 (propargyl-C), 70.4 (propargyl-CH), 55.7 (cyclohex-CH), 33.3 (cyclohex-CH_2), 29.4 (propargyl-CH_2), 25.6 (cyclohex-CH_2), 25.3 (cyclohex-CH_2); MS (ESI): m/z 434.1 (M^++1); Anal Calcd for $C_{28}H_{23}N_3O_2$: C, 77.58; H, 5.35; N, 9.69; found C, 77.61; H, 5.32; N, 9.68.

2-Butyl-6-(1-cyclohexyl-1*H*-benzo[*d*]imidazol-5-yl)-1*H*-benzo[*de*]isoquinoline-1,3(2*H*)-dione (13): White solid; 86% yield; mp 254-257 ºC; ^{1}H NMR ($CDCl_3$, 400 MHz): δ (ppm) 8.66 (d, *J* =

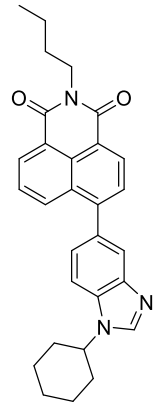

7.80 Hz, 1H, ArH), 8.63 (dd, ^{2}J = 7.32 Hz, ^{3}J = 0.92 Hz, 1H, ArH), 8.34 (dd, ^{2}J = 8.24 Hz, ^{3}J = 0.92 Hz, 1H, ArH), 8.12 (s, 1H, ArH), 7.95 (s, 1H, ArH), 7.77 (d, *J* = 7.32 Hz, 1H, ArH), 7.69 (t, *J* = 7.32 Hz, 1H, ArH), 7.61 (d, *J* = 8.72 Hz, 1H, ArH), 7.44 (dd, ^{2}J = 8.68 Hz, ^{3}J = 1.36 Hz, 1H, ArH), 4.33-4.25 (m, 1H, cyclohex-CH), 4.24 (t, *J* = 7.32 Hz, 2H, butyl-CH_2), 2.32 (d, *J* = 11.44 Hz, 2H, cyclohex-CH_2), 2.06-2.00 (m, 2H, cyclohex-CH_2), 1.93-1.83 (m, 3H, cyclohex-CH_2), 1.77-1.71 (m, 2H, cyclohex-CH_2), 1.61-1.35 (m, 5H, cyclohex- CH_2 & butyl-CH_2), 1.01 (t, 3H, *J* = 7.32 Hz, butyl-CH_3); ^{13}C NMR ($CDCl_3$, 100 MHz): δ (ppm) 164.3, 164.1, 147.3, 143.9, 141.5, 133.4, 132.9, 132.8, 131.0, 130.7, 130.3, 128.6, 128.1, 126.6, 124.6, 122.8, 121.8, 121.4, 110.2 (ArC), 55.7 (cyclohex-CH), 40.2 (butyl-CH_2), 33.3 (cyclohex-CH_2), 30.1 (butyl-CH_2), 25.6 (cyclohex-CH_2), 25.3 (cyclohex-CH_2), 20.3 (butyl-CH_2), 13.8 (butyl-CH_3); MS (ESI): m/z 452.1 (M^++1); Anal Calcd for $C_{29}H_{29}N_3O_2$: C, 77.14; H, 6.47; N, 9.31; found C, 77.18; H, 6.51; N, 9.38.

6-(1-Cyclohexyl-1*H*-benzo[*d*]imidazol-5-yl)-2-(2-(dimethylamino)ethyl)-1*H*-benzo[*de*] isoquinoline-1,3(2*H*)-dione (14): Light yellow solid; 80% yield; mp 260-263 ºC; ^{1}H NMR ($CDCl_3$, 400 MHz): δ (ppm) 8.59 (d, *J* = 7.76 Hz, 1H, ArH), 8.56 (d, *J* = 6.88 Hz, 1H, ArH), 8.33 (d, *J* = 8.28 Hz, 1H, ArH), 8.13 (s, 1H, ArH), 7.90 (s, 1H, ArH), 7.73 (d, *J* = 7.32 Hz, 1H, ArH),

7.65 (t, *J* = 8.24 Hz, 1H, ArH), 7.60 (d, *J* = 8.24 Hz, 1H, ArH), 7.39 (d, *J* = 8.24 Hz, 1H, ArH), 4.73 (t, *J* = 6.64 Hz, 2H, ethyl-CH_2), 4.33-4.25 (m, 1H, cyclohex-CH), 3.86 (t, *J* = 6.40 Hz, 2H, ethyl-CH_2), 3.51 (s, 6H, N-CH_3), 2.31 (d, *J* = 11.00 Hz, 2H, cyclohex-CH_2), 2.04 (d, *J* = 13.32 Hz, 2H, cyclohex-CH_2), 1.93-1.78 (m, 3H, cyclohex-CH_2), 1.61-1.51 (m, 2H, cyclohex- CH_2), 1.42-1.33 (m, 1H, cyclohex-CH_2); ^{13}C NMR ($CDCl_3$, 100 MHz): δ (ppm) 164.2, 164.0, 148.1, 143.8, 141.6, 133.6, 133.5, 132.4, 131.5, 131.2, 130.3, 128.6, 128.3, 126.8, 124.6, 122.0, 121.7, 120.5, 110.4 (ArC), 66.5 (ethyl-CH_2), 57.7 (N-CH_3), 55.7 (cyclohex-CH), 34.8 (ethyl-CH_2), 33.3 (cyclohex-CH_2), 25.6 (cyclohex-CH_2), 25.3 (cyclohex-CH_2); MS (ESI): m/z 467.1 (M^++1); Anal Calcd for $C_{29}H_{30}N_4O_2$: C, 74.65; H, 6.48; N, 12.01; found C, 74.62; H, 6.51; N, 12.05.

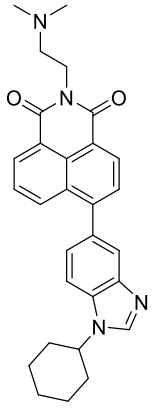

6-(1-Cyclohexyl-1*H*-benzo[*d*]imidazol-5-yl)-2-(2-(diethylamino)ethyl)-1*H*-benzo[*de*] isoquinoline-1,3(2*H*)-dione (15): Light yellow solid; 81% yield; mp 265-268 ^{o}C; ^{1}H NMR ($CDCl_3$, 400 MHz): δ (ppm) 8.66 (d, *J* = 7.36 Hz, 1H, ArH), 8.63 (d, *J* = 7.32 Hz, 1H, ArH), 8.35 (d, *J* = 8.24 Hz, 1H, ArH), 8.12 (s, 1H, ArH), 7.94 (s, 1H, ArH), 7.77 (d, *J* = 7.80 Hz, 1H, ArH), 7.69 (t, *J* = 7.80 Hz, 1H, ArH), 7.61 (d, *J* = 8.28 Hz, 1H, ArH), 7.44 (d, *J* = 8.24 Hz, 1H, ArH), 4.37 (t, *J* = 7.36 Hz, 2H, ethyl-CH_2), 4.32-4.25 (m, 1H, cyclohex-CH), 2.90 (t, *J* = 7.76 Hz, 2H, ethyl-CH_2), 2.78 (q, *J* = 7.32 Hz, 4H, ethyl-CH_2), 2.32 (d, *J* = 11.48 Hz, 2H, cyclohex-CH_2), 2.05 (d, *J* = 13.32 Hz, 2H, cyclohex-CH_2), 1.93-1.83 (m, 3H, cyclohex-CH_2), 1.62-1.50 (m, 2H, cyclohex-CH_2), 1.43-1.34 (m, 1H, cyclohex-CH_2), 1.17 (t, *J* = 6.88 Hz, 6H, ethyl-CH_3); ^{13}C NMR ($CDCl_3$, 100 MHz): δ (ppm) 164.3, 164.1, 147.5, 143.9, 141.5, 133.4, 133.1, 132.7, 131.1, 130.8, 130.3, 128.6, 128.2, 126.6, 124.6, 122.6, 121.7, 121.2, 110.2 (ArC), 55.7 (cyclohex-CH_2), 49.4 (ethyl-CH_2), 47.5 (ethyl-CH_2), 37.4 (ethyl-CH_2), 33.3 (cyclohex-CH_2), 25.6 (cyclohex-CH_2), 25.3 (cyclohex-CH_2), 11.86 (ethyl-CH_3); MS (ESI): m/z 495.1 (M^++1); Anal Calcd for $C_{31}H_{34}N_4O_2$: C, 75.28; H, 6.93; N, 11.33; found C, 75.25; H, 6.90; N, 11.36.

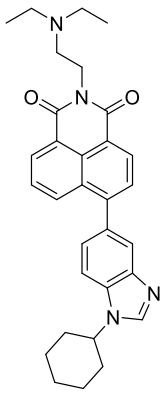

6-(1-Cyclohexyl-1*H*-benzo[*d*]imidazol-5-yl)-2-(2-hydroxyethyl)-1*H*-benzo[*de*]isoquinoline-1,3(2*H*)-dione (16): Light brown solid; 76% yield; mp 275-278 ^{o}C; ^{1}H NMR ($CDCl_3$, 400 MHz): δ (ppm) 8.67 (d, *J* = 7.32 Hz, 1H, ArH), 8.64 (dd, ^2J = 7.36 Hz, ^3J = 0.92 Hz, 1H, ArH), 8.36 (d, *J* = 8.72 Hz, 1H, ArH), 8.12 (s, 1H, ArH), 7.94 (s, 1H, ArH), 7.77 (d, *J* = 7.76 Hz, 1H, ArH), 7.70

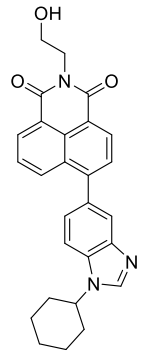

(t, *J* = 8.24 Hz, 1H, ArH), 7.61 (d, *J* = 8.24 Hz, 1H, ArH), 7.44 (dd, ^{2}J = 8.72 Hz, ^{3}J = 1.40 Hz, 1H, ArH), 4.51 (t, *J* = 4.05 Hz, 2H, ethyl-CH_2), 4.32-4.26 (m, 1H, cyclohex-CH), 4.02 (t, *J* = 5.04 Hz, 2H, ethyl-CH_2), 2.31 (d, *J* = 11.00 Hz, 2H, cyclohex-CH_2), 2.05-2.02 (m, 2H, cyclohex- CH_2), 1.93-1.83 (m, 3H, cyclohex-CH_2), 1.61-1.52 (m, 2H, cyclohex-CH_2), 1.42-1.35 (m, 1H, cyclohex-CH_2); ^{13}C NMR ($CDCl_3$, 100 MHz): δ (ppm) 165.3, 165.1, 147.8, 143.7, 141.6, 133.4, 132.5, 131.4, 131.1, 130.2, 128.7, 128.2, 126.7, 124.6, 122.4, 121.7, 120.9, 110.3 (ArC), 61.7 (ethyl-CH_2), 55.2 (cyclohex-CH), 42.8 (ethyl-CH_2), 33.3 (cyclohex-CH_2), 25.6 (cyclohex-CH_2), 25.3 (cyclohex-CH_2); MS (ESI): m/z 440.0 (M^++1); Anal Calcd for $C_{27}H_{25}N_3O_3$: C, 73.79; H, 5.73; N, 9.56; found C, 73.84; H, 5.79; N, 9.59.

2-(2-Aminoethyl)-6-(1-cyclohexyl-1*H*-benzo[*d*]imidazol-5-yl)-1*H*-benzo[*de*]isoquinoline-1,3(2*H*)-dione (17): Brown solid; 71% yield; mp 270-273 °C; ^{1}H NMR ($CDCl_3$, 400 MHz): δ

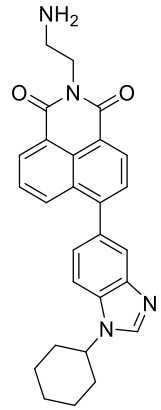

(ppm) 8.53-8.47 (m, 2H, ArH), 8.23 (t, *J* = 8.72 Hz, 1H, ArH), 8.11 (s, 1H, ArH), 7.93 (s, 1H, ArH), 7.68 (d, *J* = 6.40 Hz, 1H, ArH), 7.60-7.56 (m, 2H, ArH), 7.43 (d, *J* = 8.72 Hz, 1H, ArH), 4.31-4.19 (m, 5H, cyclohex-CH, ethyl-CH_2), 2.31 (d, *J* = 9.60 Hz, 2H, cyclohex-CH_2), 2.05 (d, *J* = 13.76 Hz, 2H, cyclohex-CH_2), 1.92-1.82 (m, 3H, cyclohex-CH_2), 1.61-1.51 (m, 2H, cyclohex-CH_2), 1.41-1.32 (m, 1H, cyclohex-CH_2); ^{13}C NMR ($CDCl_3$, 100 MHz): δ (ppm) 164.4, 164.1, 147.6, 143.8, 141.5, 133.3, 133.0, 131.1, 130.7, 130.4, 128.6, 128.2, 126.8, 124.3, 122.7, 121.4, 120.3, 111.3 (ArC), 56.1 (ethyl-CH_2), 55.5 (cyclohex-CH), 37.1 (ethyl-CH_2), 33.3 (cyclohex-CH_2), 25.6 (cyclohex-CH_2), 25.2 (cyclohex-CH_2); MS (ESI): m/z 439.0 (M^++1); Anal Calcd for $C_{27}H_{26}N_4O_2$: C, 73.95; H, 5.98; N, 12.78; found C, 73.91; H, 5.92; N, 12.74.

6-(1-Cyclohexyl-1*H*-benzo[*d*]imidazol-5-yl)-2-(2-morpholinoethyl)-1*H*-benzo[*de*]isoquinoline-1,3(2*H*)-dione (18): Brown solid; 81% yield; mp 259-262 °C; ^{1}H NMR ($CDCl_3$, 400 MHz): δ (ppm) 8.66 (d, *J* = 7.32 Hz, 1H, ArH), 8.63 (dd, ^{2}J = 7.36 Hz, ^{3}J = 0.92 Hz, 1H, ArH), 8.36 (dd, ^{2}J = 8.24 Hz, ^{3}J = 0.92 Hz, 1H, ArH), 8.12 (s, 1H, ArH), 7.95 (s, 1H, ArH), 7.78 (d, *J* = 7.32 Hz, 1H, ArH), 7.70 (t, *J* = 8.72 Hz, 1H, ArH), 7.62 (d, *J* = 8.28 Hz, 1H, ArH), 7.44 (dd, ^{2}J = 8.24 Hz, ^{3}J = 0.92 Hz, 1H, ArH), 4.40 (t, *J* = 6.88 Hz, 2H, ethyl-CH_2), 4.33-4.26 (m, 1H, cyclohex-CH), 3.71 (t, *J* = 4.60 Hz, 4H, morph-CH_2), 2.76 (t, *J* = 7.32 Hz, 2H, ethyl-CH_2), 2.63 (bs, 4H, morph-CH_2), 2.32 (d, *J* = 11.44 Hz, 2H, cyclohex-CH_2), 2.05-2.02 (m, 2H, cyclohex-

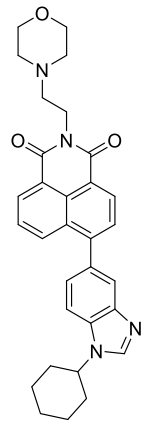

CH_2), 1.94-1.85 (m, 3H, cyclohex-CH_2), 1.61-1.52 (m, 2H, cyclohex-CH_2), 1.42-1.35 (m, 1H, cyclohex-CH_2); ^{13}C NMR ($CDCl_3$, 100 MHz): δ (ppm) 164.4, 164.1, 147.5, 143.9, 141.6, 133.4, 133.1, 132.7, 131.1, 130.8, 130.3, 128.7, 128.2, 126.7, 124.6, 122.7, 121.8, 121.3, 110.3 (ArC), 66.9 (morph-CH_2), 56.1 (ethyl-CH_2), 55.7 (cyclohex-CH), 53.7 (morph-CH_2), 37.1 (ethyl-CH_2), 33.3 (cyclohex-CH_2), 25.6 (cyclohex-CH_2), 25.3 (cyclohex-CH_2); MS (ESI): m/z 509.1 (M^++1); Anal Calcd for $C_{31}H_{32}N_4O_3$: C, 73.21; H, 6.34; N, 11.02; found C, 73.18; H, 6.31; N, 11.05.

2-Benzyl-6-(1-cyclohexyl-1*H*-benzo[*d*]imidazol-5-yl)-1*H*-benzo[*de*]isoquinoline-1,3(2*H*)-dione (19): Off white solid; 83% yield; mp 261-263 ºC; ^{1}H NMR ($CDCl_3$, 400 MHz): δ (ppm)

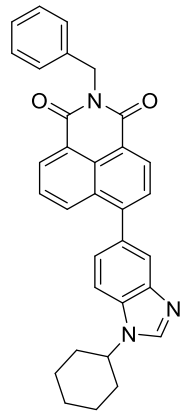

8.67 (d, *J* = 7.36 Hz, 1H, ArH), 8.64 (dd, ^2J = 7.32 Hz, ^3J = 0.92 Hz, 1H, ArH), 8.34 (d, *J* = 8.24 Hz, 1H, ArH), 8.12 (s, 1H, ArH), 7.93 (s, 1H, ArH), 7.76 (d, *J* = 7.32 Hz, 1H, ArH), 7.68 (t, *J* = 7.32 Hz, 2H, ArH), 7.60-7.55 (m, 3H, ArH), 7.43 (dd, ^2J = 8.24 Hz, ^3J = 0.92 Hz, 1H, ArH), 7.32 (t, *J* = 7.36 Hz, 2H, ArH), 5.41 (s, 2H, benzyl-CH_2), 4.32-4.24 (m, 1H, cyclohex-CH), 2.31 (d, *J* = 12.84 Hz, 2H, cyclohex-CH_2), 2.04-2.01 (m, 2H, cyclohex-CH_2), 1.92-1.82 (m, 3H, cyclohex-CH_2), 1.61-1.50 (m, 2H, cyclohex-CH_2), 1.42-1.37 (m, 1H, cyclohex-CH_2); ^{13}C NMR ($CDCl_3$, 100 MHz): δ (ppm) 164.3, 164.1, 147.5, 143.8, 141.5, 137.2, 133.1, 132.7, 132.0, 131.9, 131.3, 131.0, 130.3, 128.7, 128.3, 128.1, 127.3, 126.6, 124.6, 122.6, 121.7, 121.2, 110.3 (ArC), 55.7 (cyclohex-CH), 43.5 (benzyl-CH_2), 33.3 (cyclohex-CH_2), 25.6 (cyclohex-CH_2), 25.2 (cyclohex-CH_2); MS (ESI): m/z 486.1 (M^++1); Anal Calcd for $C_{32}H_{27}N_3O_2$: C, 79.15; H, 5.60; N, 8.65; found C, 79.11; H, 5.65; N, 8.61.

6-(1-Cyclohexyl-1*H*-benzo[*d*]imidazol-5-yl)-2-(4-fluorophenyl)-1*H*-benzo[*de*]isoquinoline-1,3(2*H*)-dione (20): Brown solid; 78% yield; mp 262-264 ºC; ^{1}H NMR ($CDCl_3$, 400 MHz): δ (ppm) 8.70 (d, *J* = 7.32 Hz, 1H, ArH), 8.68 (dd, ^2J = 7.32 Hz, ^3J = 0.88 Hz, 1H, ArH), 8.42 (dd, ^2J = 8.24 Hz, ^3J = 0.92 Hz, 1H, ArH), 8.13 (s, 1H, ArH), 7.97 (d, *J* = 0.88 Hz, 1H, ArH), 7.81 (d, *J* = 7.36 Hz, 1H, ArH), 7.73 (t, *J* = 8.72 Hz, 1H, ArH), 7.63 (d, *J* = 8.24 Hz, 1H, ArH), 7.46 (dd, ^2J = 8.68 Hz, ^3J = 1.84 Hz, 1H, ArH), 7.35-7.30 (m, 2H, ArH), 7.27-7.23 (m, 2H, ArH), 4.34-4.26 (m, 1H, cyclohex-CH), 2.33 (d, *J* = 11.88 Hz, 2H, cyclohex-CH_2), 2.06 (d, *J* = 13.76 Hz, 2H,

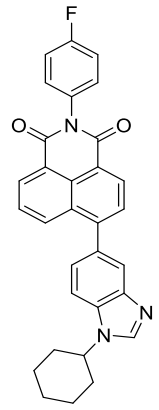

cyclohex-CH_2), 1.94-1.84 (m, 3H, cyclohex-CH_2), 1.63-1.51 (m, 2H, cyclohex-CH_2), 1.43-1.35 (m, 1H, cyclohex-CH_2); ^{13}C NMR ($CDCl_3$, 100 MHz): δ (ppm) 164.5, 164.3, 148.0, 143.9, 141.6, 133.5, 133.4, 132.6, 131.6, 131.3, 131.1, 130.5, 130.4, 130.3, 129.0, 128.3, 126.8, 124.6, 122.7, 121.8, 121.2, 116.5, 116.2, 110.3 (ArC), 55.7 (cyclohex-CH), 33.3 (cyclohex-CH_2), 25.6 (cyclohex-CH_2), 25.3 (cyclohex-CH_2); MS (ESI): m/z 490.1 (M^++1); Anal Calcd for $C_{31}H_{24}FN_3O_2$: C, 76.06; H, 4.94; N, 8.58; found C, 76.11; H, 4.97; N, 8.61.

2-(Benzo[*d*]thiazol-2-yl)-6-(1-cyclohexyl-1*H*-benzo[*d*]imidazol-5-yl)-1*H*-benzo[*de*]isoquinoline-1,3(2*H*)-dione (21): Light yellow solid; 75% yield; mp 269-272 ^{o}C; ^{1}H

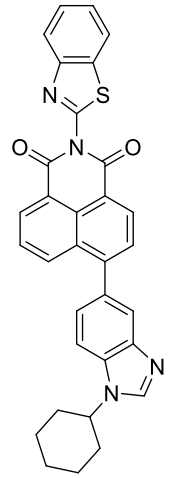

NMR ($CDCl_3$, 400 MHz): δ (ppm) 8.74 (d, *J* = 7.32 Hz, 1H, ArH), 8.71 (dd, ^2J = 7.32 Hz, ^3J = 0.92 Hz, 1H, ArH), 8.45 (dd, ^2J = 8.72 Hz, ^3J = 1.40 Hz, 1H, ArH), 8.17 (d, *J* = 7.80 Hz, 1H, ArH), 8.14 (s, 1H, ArH), 7.97 (d, *J* = 7.32 Hz, 2H, ArH), 7.82 (d, *J* = 7.80 Hz, 1H, ArH), 7.75 (t, *J* = 7.32 Hz, 1H, ArH), 7.63 (d, *J* = 8.04 Hz, 1H, ArH), 7.58-750 (m, 2H, ArH), 7.48-7.45 (m, 1H, ArH), 4.34-4.26 (m, 1H, cyclohex-CH), 2.32 (d, *J* = 11.00 Hz, 2H, cyclohex-CH_2), 2.05 (d, *J* = 14.24 Hz, 2H, cyclohex-CH_2), 1.94-1.84 (m, 3H, cyclohex-CH_2), 1.62-1.52 (m, 2H, cyclohex-CH_2), 1.42-1.33 (m, 1H, cyclohex-CH_2); ^{13}C NMR ($CDCl_3$, 100 MHz): δ (ppm) 163.8, 163.6, 155.8, 150.4, 148.6, 143.9, 141.7, 136.7, 134.2, 133.5, 132.5, 132.0, 131.6, 130.6, 129.2, 128.4, 126.8, 126.3, 126.0, 124.6, 124.2, 122.1, 121.8, 120.6, 110.4 (ArC), 55.7 (cyclohex-CH), 33.3(cyclohex-CH_2), 25.6 (cyclohex-CH_2), 25.3 (cyclohex-CH_2); MS (ESI): m/z 529.1 (M^++1); Anal Calcd for $C_{32}H_{24}N_4O_2S$: C, 72.71; H, 4.58; N, 10.60; S, 6.06; found C, 72.66; H, 4.65; N, 10.71; S, 6.09.

3-(1-Cyclohexyl-1*H*-benzo[*d*]imidazol-5-yl)-7*H*-benzo[*de*]benzo[4,5]imidazo[2,1-*a*]isoquinolin-7-one (22): Yellow solid; 80% yield; mp 281-283 ^{o}C; ^{1}H NMR ($CDCl_3$, 400 MHz): δ (ppm) 8.87 (t, *J* = 8.24 Hz, 1H, ArH), 8.82 (t, *J* = 7.80 Hz, 1H, ArH), 8.58-8.55 (m, 1H, ArH), 8.43-8.24 (m, 1H, ArH), 8.13 (d, *J* = 2.28 Hz, 1H, ArH), 7.99 (d, *J* = 3.68 Hz, 1H, ArH), 7.90-7.87 (m, 1H, ArH), 7.81 (q, *J* = 4.12 Hz, 1H, ArH), 7.73-7.67 (m, 1H, ArH), 7.63 (dd, ^2J = 8.24 Hz, ^3J = 3.20 Hz, 1H, ArH), 7.50-7.45 (m, 3H, ArH), 4.34-4.26 (m, 1H, cyclohex-CH), 2.33 (d, *J* = 11.44 Hz, 2H, cyclohex-CH_2), 2.05 (d, *J* = 13.72 Hz, 2H, cyclohex-CH_2), 1.93-1.85 (m, 3H, cyclohex-

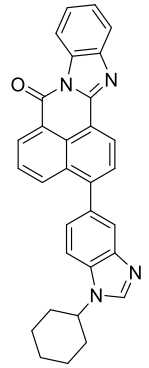

CH_2), 1.63-1.51 (m, 2H, cyclohex-CH_2), 1.43-1.35 (m, 1H, cyclohex- CH_2); ^{13}C NMR ($CDCl_3$, 100 MHz): δ (ppm) 160.8, 160.7, 149.5, 148.6, 145.3, 143.9, 141.6, 134.3, 133.3, 132.9, 131.7, 131.6, 131.2, 131.0, 128.6, 128.3, 127.0, 126.7, 125.7, 125.1, 124.9, 121.9, 119.8, 115.8, 110.2 (ArC), 55.7 (cyclohex-CH), 33.3 (cyclohex-CH_2), 25.6 (cyclohex-CH_2), 25.3 (cyclohex-CH_2); MS (ESI): m/z 469.0 (M^++1); Anal Calcd for $C_{31}H_{24}N_4O$: C, 79.46; H, 5.16; N, 11.96; found C, 79.55; H, 5.13; N, 11.99.

6-(1-Cyclohexyl-1*H*-benzo[*d*]imidazol-6-yl)-2-(2-(dimethylamino)ethyl)-1*H*-benzo[*de*]isoquinoline-1,3(2*H*)-dione (23): Light yellow solid; 81% yield; mp 260-263 ^oC; ^1H

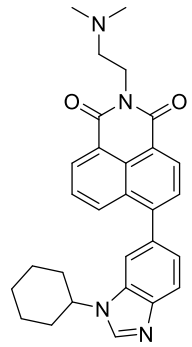

NMR ($CDCl_3$, 400 MHz): δ (ppm) 8.66 (d, *J* = 7.32 Hz, 1H, ArH), 8.64 (d, *J* = 7.32 Hz, 1H, ArH), 8.30 (d, *J* = 7.80 Hz, 1H, ArH), 8.12 (s, 1H, ArH), 7.94 (d, *J* = 8.24 Hz, 1H, ArH), 7.78 (d, *J* = 7.80 Hz, 1H, ArH), 7.71 (t, *J* = 8.24 Hz, 1H, ArH), 7.54 (d, *J* = 0.68 Hz, 1H, ArH), 7.40 (dd, ^2J = 8.28 Hz, ^3J = 0.92 Hz, 1H, ArH), 4.44 (t, *J* = 6.68 Hz, 2H, ethyl-CH_2), 4.28-4.21 (m, 1H, cyclohex-CH), 2.88 (t, *J* = 7.12 Hz, 2H, ethyl-CH_2), 2.49 (s, 6H, N-CH_3), 2.28 (d, *J* = 11.00 Hz, 2H, cyclohex-CH_2), 2.00 (d, *J* = 13.72 Hz, 2H, cyclohex-CH_2), 1.89-1.79 (m, 3H, cyclohex-CH_2), 1.56-1.44 (m, 2H, cyclohex-CH_2), 1.40-1.31 (m, 1H, cyclohex-CH_2); ^{13}C NMR ($CDCl_3$, 100 MHz): δ (ppm) 164.4, 164.2, 147.6, 143.7, 141.5, 133.3, 133.0, 131.2, 130.8, 130.4, 128.7, 128.2, 126.8, 124.3, 122.6, 121.3, 120.2, 111.4 (ArC), 56.5 (ethyl-CH_2), 55.5 (cyclohex-CH), 45.1 (N-CH_3), 37.3 (ethyl-CH_2), 33.3 (cyclohex-CH_2), 25.5 (cyclohex-CH_2), 25.2 (cyclohex-CH_2); MS (ESI): m/z 467.1 (M^++1); Anal Calcd for $C_{29}H_{30}N_4O_2$: C, 74.65; H, 6.48; N, 12.01; found C, 74.71; H, 6.41; N, 12.12.

6-(1-Cyclohexyl-1*H*-benzo[*d*]imidazol-6-yl)-2-(2-hydroxyethyl)-1*H*-benzo[*de*]isoquinoline-1,3(2*H*)-dione (24): Brown solid; 76% yield; mp 275-278 ^oC; ^1H NMR ($CDCl_3$, 400 MHz): δ

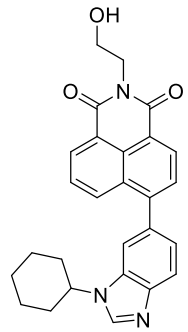

(ppm) 8.57-8.48 (m, 2H, ArH), 8.20-8.15 (m, 2H, ArH), 7.94 (d, *J* = 8.68 Hz, 1H, ArH), 7.70 (d, *J* = 7.36 Hz, 1H, ArH), 7.64-7.59 (m, 1H, ArH), 7.54 (s, 1H, ArH), 7.41 (d, *J* = 9.16 Hz, 1H, ArH), 4.31-4.18 (m, 5H, cyclohex-CH & ethyl-CH_2), 2.29 (d, *J* = 11.00 Hz, 2H, cyclohex-CH_2), 1.99 (d, *J* = 13.28 Hz,, 2H, cyclohex-CH_2), 1.89-1.78 (m, 3H, cyclohex-CH_2), 1.55-1.47 (m, 2H, cyclohex-CH_2), 1.45-1.42 (m, 1H, cyclohex-CH_2); ^{13}C NMR ($CDCl_3$, 100 MHz): δ (ppm)

165.4, 165.2, 147.9, 141.4, 133.6, 132.7, 131.4, 131.1, 130.3, 128.5, 128.2, 126.8, 124.4, 122.3, 121.7, 120.7, 110.1 (ArC), 61.8 (ethyl-CH_2), 55.7 (cyclohex-CH), 42.8 (ethyl-CH_2), 33.3 (cyclohex-CH_2), 25.6 (cyclohex-CH_2), 25.2 (cyclohex-CH_2); MS (ESI): m/z 440.0 (M^++1); Anal Calcd for $C_{27}H_{25}N_3O_3$: C, 73.79; H, 5.73; N, 9.56; found C, 73.72; H, 5.78; N, 9.64.

6-(1-Cyclohexyl-1*H*-benzo[*d*]imidazol-6-yl)-2-(2-morpholinoethyl)-1*H*-benzo[*de*]isoquinoline-1,3(2*H*)-dione (25): Light brown solid; 83% yield; mp 259-262 °C; ^{1}H

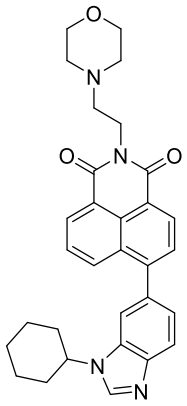

NMR ($CDCl_3$, 400 MHz): δ (ppm) 8.67 (d, *J* = 7.32 Hz, 1H, ArH), 8.65 (d, *J* = 7.32 Hz, 1H, ArH), 8.32 (d, *J* = 8.24 Hz, 1H, ArH), 8.13 (s, 1H, ArH), 7.96 (d, *J* = 8.24 Hz, 1H, ArH), 7.79 (d, *J* = 7.36 Hz, 1H, ArH), 7.73 (t, *J* = 7.32 Hz, 1H, ArH), 7.54 (s, 1H, ArH), 7.41 (d, *J* = 8.24 Hz, 1H, ArH), 4.41 (t, *J* = 6.64 Hz, 2H, ethyl-CH_2), 4.29-4.21 (m, 1H, cyclohex-CH), 3.72 (t, *J* = 4.60 Hz, 4H, morph-CH_2), 2.77 (t, *J* = 6.64 Hz, 2H, ethyl-CH_2), 2.64 (bs, 4H, morph-CH_2), 2.29 (d, *J* = 11.44 Hz, 2H, cyclohex-CH_2), 2.00 (d, *J* = 13.76 Hz, 2H, cyclohex-CH_2), 1.89-1.80 (m, 3H, cyclohex-CH_2), 1.56-1.44 (m, 2H, cyclohex-CH_2), 1.37-1.33 (m, 1H, cyclohex-CH_2); ^{13}C NMR ($CDCl_3$, 100 MHz): δ (ppm) 164.3, 164.1, 147.6, 143.8, 141.5, 133.6, 133.3, 133.0, 131.1, 130.7, 130.4, 128.6, 128.2, 126.8, 124.3, 122.7, 121.4, 120.3, 111.3 (ArC), 66.9 (morph-CH_2), 56.1 (ethyl-CH_2), 55.5 (cyclohex-CH), 53.7 (morph-CH_2), 37.1 (ethyl-CH_2), 33.3 (cyclohex-CH_2), 25.6 (cyclohex-CH_2), 25.2 (cyclohex-CH_2); MS (ESI): m/z 509.1 (M^++1); Anal Calcd for $C_{31}H_{32}N_4O_3$: C, 73.21; H, 6.34; N, 11.02; found C, 73.18; H, 6.42; N, 11.02.

2-Benzyl-6-(1-cyclohexyl-1*H*-benzo[*d*]imidazol-6-yl)-1*H*-benzo[*de*]isoquinoline-1,3(2*H*)-dione (26): Off whie solid; 77% yield; mp 266-269 °C; ^{1}H NMR ($CDCl_3$, 400 MHz): δ (ppm) 8.68

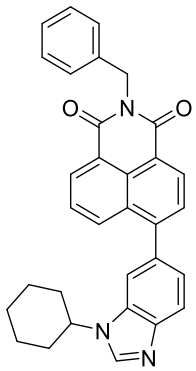

(d, *J* = 7.32 Hz, 1H, ArH), 8.66 (d, *J* = 7.76 Hz, 1H, ArH), 8.30 (d, *J* = 8.24 Hz, 1H, ArH), 8.12 (s, 1H, ArH), 7.95 (d, *J* = 8.72 Hz, 1H, ArH), 7.78 (d, *J* = 7.80 Hz, 1H, ArH), 7.72 (t, *J* = 8.72 Hz, 1H, ArH), 7.57 (t, *J* = 7.32 Hz, 3H, ArH), 7.40 (d, *J* = 8.24 Hz, 1H, ArH), 7.34 (t, *J* = 7.36 Hz, 3H, ArH), 5.42 (s, 2H, benzyl-CH_2), 4.28-4.20 (m, 1H, cyclohex-CH), 2.28 (d, *J* = 11.44 Hz, 2H, cyclohex-CH_2), 1.99 (d, *J* = 13.72 Hz, 2H, cyclohex-CH_2), 1.88-1.78 (m, 3H, cyclohex-CH_2), 1.55-1.44 (m, 2H, cyclohex-CH_2), 1.37-1.33 (m, 1H, cyclohex-CH_2); ^{13}C NMR ($CDCl_3$, 100 MHz): δ (ppm) 164.3, 164.1, 147.6, 141.5, 137.2, 133.3, 133.0, 131.4, 130.9, 130.3, 128.8, 128.4, 128.2, 127.4, 126.7, 124.3, 122.7, 121.3, 120.2, 111.2

(ArC), 55.5 (cyclohex-CH), 43.5 (benzyl-CH_2), 33.3 (cyclohex-CH_2), 25.6 (cyclohex-CH_2), 25.2 (cyclohex-CH_2); MS (ESI): m/z 486.1 (M^++1); Anal Calcd for $C_{32}H_{27}N_3O_2$: C, 79.15; H, 5.60; N, 8.65; found C, 79.13; H, 5.61; N, 8.78.

CHAPTER 4
HYBRIDS OF NAPHTHALIMIDE AND PHENANTHRO[9,10-*d*]IMIDAZOLE

4.1 Introduction

Many heterocyclic molecules have been synthesized with naphthalimide as a key moiety which were recognized as potential anticancer agents.[108] Planar structure of naphthalimide derivatives favor to intercalate into base pairs of DNA[108] and exhibit excellent antitumor activity. DNA plays an important role in cell growth and cell division. Consequently, DNA remains to be one of the key molecular objectives in the designing of an effective anticancer agent. In our research group, derivatives of naphthalimide-benzimidazole, conjugates have been designed, synthesized and studied for their effect on antiproliferative activity and results revealed that these derivatives were found more potent than amonafide.[109] Phenanthro[9,10-*d*]imidazole derivatives have also been proved to exhibit good activity *in vitro* and bind to DNA.[53,110] Li and co-workers have designed and synthesized a series of polyglycol side chain substituted phenanthro-imidazole as anticancer agent.[54] Moody and co-workers have synthesized a series of phenanthro[9,10-*d*]imidazoles that showed *in vitro* potency against human melanoma, breast and colon cancer cell lines as well as inhibition of pathway of molecular chaperone heat shock protein 70 (Hsp70) in cells.[53]

In the present case, a new series of naphthalimide-based molecules comprising phenanthro[9,10-*d*]imidazole, connected by phenyl ring spacer was designed and synthesized. These compounds were further evaluated *in vitro* for anticancer activity Moreover, interactions with ct-DNA and human serum albumin (HSA) were studied by UV-visible, fluorescence and CD spectroscopy as well as DNA viscosity measurement.

4.2 Chemistry

Conjugates of naphthalimide and phenanthroimidazole were synthesized by multiple step according to **Scheme 1**. Commercial available acenaphthene (**1**) was treated with *N*-bromosuccinimide in DMF at room temperature to afford 5-bromo acenaphthene (**2**) in 94% yield. Oxidation of bromo acenaphthene was accomplished with sodium dichromate in acetic acid to obtain 6-bromo-1*H*,3*H*-benzo[*de*]isochromene-1,3-dione (**3**) in 72% yield. Condensation of 4-formylphenylboronic acid (**4**) with 9,10-phenanthrenequinone (**5**) in the presence of ammonium acetate in acetic acid gave (4-(1*H*-phenanthro[9,10-*d*]imidazol-2-yl)phenyl)boronic acid (**6**) in

58% yield. Suzuki-Miyaura cross-coupling reaction of (4-(1*H*-phenanthro[9,10-*d*]imidazol-2-yl)phenyl)boronic acid (**6**) with 6-bromo-1*H*,3*H*-benzo[*de*]isochromene-1,3-dione (**3**) in the presence of $Pd(PPh_3)_4$ and K_2CO_3 in CH_3CN and water mixture (9:1) gave 6-(4-(1*H*-phenanthro[9,10-*d*]imidazol-2-yl)phenyl)-1*H*,3*H*-benzo[*de*]isochromene-1,3-dione (**7)** in 72% yield. Appearance of aromatic protons of naphthalimide and phenanthroimidazole in the range of δ 8.78-7.65 ppm in proton NMR spectrum confirmed the formation of intermediate **7**. Intermediate **7** was refluxed with various aliphatic and aromatic amines in ethanol for 7-9 h to afford compounds **8-21** in 78-91% yields. Characteristic signals of allyl group (multiplet of one protons at δ 5.95-5.89 ppm representing CH of allyl, multiplet of two protons at δ 5.14-5.10 ppm representing CH_2 of allyl and broad singlet of two protons at δ 4.63 ppm representing CH_2 of allyl) in ^1H NMR along with aromatic signals confirmed the formation of compound **8**. All the synthesized compounds were well characterized by NMR and mass spectrometry.

Scheme 1. Synthesis of 6-(4-(1*H*-phenanthro[9,10-*d*]imidazol-2-yl)phenyl)-2-substituted-1*H*-benzo[*de*]isoquinoline-1,3(2*H*)-dione

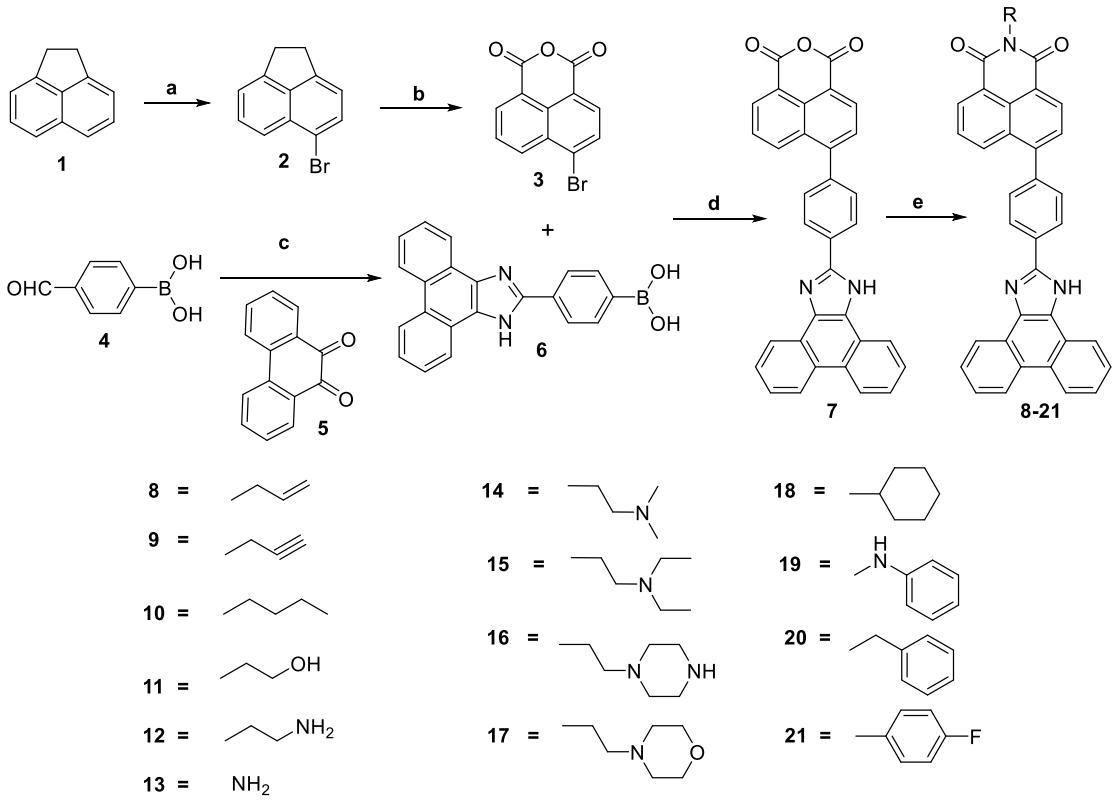

Reagents and conditions: (a) NBS, DMF, rt, 3 h, 94%; (b) Sodium dichromate, AcOH, reflux, 2.5 h, 72%; (c) Ammonium acetate, AcOH, reflux, 10 h, 58%; (d) $Pd(PPh_3)_4$, K_2CO_3, CH_3CN : water (9:1), N_2, reflux, 12 h, 72%; (e) RNH_2, ethanol, reflux, 7-9 h, 78-91%

4.3 Biology

4.3.1 Cytotoxicity

The selected compounds (14 in no.) were evaluated for their *in vitro* cytotoxic activity against 9 panels of human cell lines (leukemia, non-small cell lung, colon, CNS, melanoma, ovarian, renal, prostate and breast) having 58 different cancer cell lines at National Cancer Institute (NCI),[84] USA at the dose of 10 μM (**Tables 1-2**). Among all the tested compounds, 1-ethylpiperazine substituted, compound **16**, found to be most active compound of the series with the range of growth inhibition -55.78-94.53. Compound **16** has been found sensitive against 14 cancer cell lines out of 56 tested cell lines and found most susceptible against LOXIMVI of melanoma panel of cancer cell lines. Compound **16** has been found cytotoxic against K-562 (leukemia), HCT-116 (colon cancer), LOXIMVI (melanoma), OVCAR-4 (ovarian cancer) and MCF-7 (breast cancer) cell lines. Compound **16** showed cytostatic effect against CCRF-CEM (leukemia), SR (leukemia), NCI-H460 (non-small cell lung cancer), HCT-15 (colon cancer), HT29 (colon cancer), KM12 (colon cancer), SW-620 (colon cancer), OVCAR-8 (ovarian cancer) and DU-145 (prostate cancer). Compound **16** found to be least active against full panel of CNS and renal cancer cell lines. Compound **14** substituted with *N*,*N*-dimethylethylamine showed cytostatic activity towards K-562 (leukemia), SR (leukemia), 786-0 (renal cancer) and MCF7 (breast cancer) cell lines.

Table 1. Cytotoxicity of compounds **8-14** at 10 μM concentration

Panel	Cell Line	8	9	10	11	12	13	14
Leukemia	CCRF-CEM	3.30	13.83	7.81	10.30	15.21	16.29	44.56
	HL-60(TB)	--	27.06	25.96	27.24	33.99	10.77	9.35
	K-562	8.67	23.09	18.41	22.43	16.72	23.40	71.51
	MOLT-4	9.55	13.60	10.69	19.52	21.14	12.87	15.97
	RPMI-8226	--	NT	--	NT	NT	NT	45.12
	SR	6.10	26.89	28.12	2.51	31.01	37.80	61.45
Non-Small	A549/ATCC	7.03	6.83	11.84	17.58	9.89	5.23	9.56
Cell Lung	EXVX	2.00	18.56	18.69	26.95	13.97	5.39	6.13
Cancer	HOP-92	20.96	25.15	8.09	4.66	2.60	21.42	28.17
	NCI-H226	--	3.44	2.48	5.16	4.91	2.09	--
	NCI-H23	--	2.01	2.51	1.46	--	1.18	--
	NCI-H322M	--	9.22	6.49	22.02	17.63	--	--
	NCI-H460	--	14.65	15.54	23.99	17.39	--	--
	NCI-H522	9.72	12.22	10.38	20.57	6.08	10.01	5.83
Colon	COLO 205	--	8.31	7.55	12.37	9.04	--	--
Cancer	HCC-2998	--	3.92	1.48	4.81	6.68	--	--
	HCT-116	--	8.44	13.08	20.95	16.80	4.19	34.92

	HCT-15	--	24.55	23.30	29.95	29.21	2.38	--
	HT29	--	--	6.39	2.36	17.50	--	18.90
	KM12	--	15.82	10.76	10.19	10.48	4.65	24.23
	SW-620	--	0.79	1.53	1.67	1.66	0.80	14.01
CNS	SF-268	--	--	--	4.49	2.35	0.37	--
Cancer	SF-295	--	2.88	1.83	3.39	3.25	1.05	--
	SF-539	4.39	5.61	--	13.64	2.46	14.02	7.28
	SNB-19	--	3.86	--	6.75	8.72	--	--
	SNB-75	--	--	--	7.42	9.13	1.56	--
	U251	0.93	15.82	17.41	18.87	21.34	0.39	4.48
Melanoma	LOX IMVI	0.30	37.22	3.03	32.52	30.55	0.40	42.01
	MALME-3M	--	6.25	--	1.01	2.89	8.23	--
	MDA-MB-435	--	--	--	2.41	7.34	--	--
	SK-MEL-2	--	--	--	2.26	--	--	--
	SK-MEL-28	--	--	0.91	3.19	--	--	--
	SK-MEL-5	NT	NT	NT	2.78	4.27	NT	--
	UACC-257	--	0.95	--	1.76	--	--	--
	UACC-62	--	13.01	--	11.50	5.93	--	--
Ovarian	IGROV1	0.54	6.38	2.73	21.52	13.13	1.56	3.72
Cancer	OVCAR-3	--	8.21	--	7.60	--	--	--
	OVCAR-4	--	3.27	1.72	7.68	17.91	--	--
	OVCAR-5	--	10.23	3.66	15.53	16.61	--	--
	OVCAR-8	--	--	--	5.03	6.21	0.48	47.97
	NCI/ADR-RES	--	--	--	2.74	2.05	2.42	11.86
	SK-OV-3	--	--	--	4.11	--	--	--
Renal	786-0	5.01	5.06	--	16.13	16.74	13.12	81.77
Cancer	A498	7.12	--	2.71	8.20	3.62	13.81	--
	ACHN	--	--	--	9.60	11.38	--	--
	CAKI-1	4.90	11.35	6.45	10.29	6.74	8.34	12.01
	SN12C	1.95	0.50	--	10.03	9.20	11.38	2.58
	TK-10	1.60	13.70	17.56	22.90	16.91	--	--
	UO-31	5.25	11.91	11.28	23.82	14.44	6.63	3.23
Prostate	PC-3	2.89	21.89	16.87	21.56	21.70	6.97	12.14
Cancer	DU-145	--	7.48	--	6.43	4.25	--	--
Breast	MCF7	11.18	19.97	17.86	21.50	21.70	11.28	63.84
Cancer	MDA-MB-231/ATCC	--	13.63	5.45	17.01	8.15	1.04	10.92
	HS 578T	--	--	--	7.24	--	--	--
	BT-549	--	4.34	--	17.63	15.48	12.55	--
	T-47D	1.89	21.05	9.53	32.64	21.41	15.14	13.27
	MDA-MB-468	--	3.36	--	2.95	9.21	--	--

-- indicates GI < 10%; NT, not tested; 30-40% growth inhibition; 40-50% growth inhibition; 50-70% growth inhibition; 70-90% growth inhibition

Table 2. Cytotoxicity of compounds **15-21** at 10 μM concentration

Panel	Cell line	15	16	17	18	19	20	21
Leukemia	CCRF-CEM	23.10	62.54	5.86	8.95	10.67	1.23	16.18
	HL-60(TB)	39.79	17.53	9.70	33.95	4.98	0.69	36.84
	K-562	31.05	-10.20	11.75	10.99	21.31	2.09	26.17
	MOLT-4	26.53	46.58	7.69	14.82	11.62	--	22.79
	RPMI-8226	15.37	NT	8.62	--	22.53	--	NT
	SR	48.00	94.01	17.55	29.72	19.85	--	41.01
Non-Small	A549/ATCC	19.35	29.28	4.44	4.39	13.84	--	13.95
Cell Lung	EXVX	19.52	2.97	11.23	15.93	22.85	3.56	19.89
Cancer	HOP-62	--	37.87	--	0.08	3.82	--	--
	HOP-92	10.33	13.79	10.70	--	38.28	--	--
	NCI-H226	9.46	5.12	1.39	10.24	11.15	--	6.29
	NCI-H23	--	16.72	1.52	--	5.23	--	--
	NCI-H322M	2.94	24.74	3.99	2.70	18.09	--	8.82
	NCI-H460	23.99	58.76	--	20.47	4.01	--	29.83
	NCI-H522	7.58	8.16	5.47	4.98	21.04	6.07	10.69
Colon	COLO 205	19.84	38.14	--	11.71	2.65	--	12.34
Cancer	HCC-2998	6.91	14.54	2.74	--	--	--	3.74
	HCT-116	22.83	-12.29	--	15.62	6.51	--	34.26
	HCT-15	33.92	59.08	--	30.73	7.25	--	42.12
	HT29	14.54	94.53	5.58	6.01	--	--	14.88
	KM12	11.76	78.36	--	18.90	12.89	2.94	13.14
	SW-620	7.10	74.85	--	5.86	--	--	5.41
CNS	SF-268	4.35	--	--	--	14.18	--	1.23
Cancer	SF-295	3.42	--	5.76	5.46	5.16	--	8.58
	SF-539	7.40	26.23	0.96	5.38	16.71	--	1.50
	SNB-19	4.41	--	--	2.70	1.79	--	4.79
	SNB-75	2.85	--	--	--	16.30	--	0.68
	U251	14.33	37.89	3.56	10.42	10.36	--	17.98
Melanoma	LOX IMVI	35.16	-55.78	0.34	30.42	21.11	--	36.05
	MALME-3M	--	14.63	8.46	--	14.32	--	--
	MDA-MB-435	--	--	--	1.35	2.89	0.45	5.65
	SK-MEL-28	--	--	--	2.38	6.38	--	1.70
	UACC-257	--	--	3.49	--	6.38	--	--
	UACC-62	1.34	--	--	8.47	19.66	--	8.31
Ovarian	IGROV1	16.12	27.60	3.20	7.33	39.51	--	13.56
Cancer	OVCAR-3	4.06	8.47	--	8.12	3.91	--	7.48
	OVCAR-4	7.84	-23.24	--	9.57	4.76	--	17.05
	OVCAR-5	--	--	--	1.41	12.12	--	9.17
	OVCAR-8	7.99	79.76	3.65	--	7.82	--	4.87
	NCI/ADR-RES	0.40	42.17	--	--	2.42	--	4.35
	SK-OV-3	--	--	--	5.72	10.76	--	6.26
Renal	786-0	37.61	47.58	8.85	--	9.97	--	4.30

Cancer	A498	--	--	8.79	--	11.19	--	--
	ACHN	1.02	28.33	--	--	10.83	--	9.43
	CAKI-1	13.66	8.62	--	5.22	31.80	--	12.60
	SN12C	7.23	6.55	8.74	3.10	14.76	--	4.82
	TK-10	19.50	--	--	13.46	0.03	--	18.91
	UO-31	14.36	5.85	5.32	17.77	40.58	--	18.52
Prostate Cancer	PC-3	27.95	33.39	1.52	18.64	19.17	--	18.48
	DU-145	2.11	57.46	--	1.12	--	--	4.15
Breast Cancer	MCF7	29.57	-6.70	10.17	15.04	43.21	6.19	24.73
	MDA-MB-231/ATCC	11.76	36.67	--	6.77	21.73	--	4.05
	HS 578T	1.81	--	--	--	9.80	--	--
	BT-549	15.49	4.64	2.37	--	5.19	--	4.13
	T-47D	2.86	32.50	8.72	16.54	35.45	--	13.99
	MDA-MB-468	--	18.49	--	--	8.09	--	--

-- indicates GI < 10%; NT, not tested; 30-40% growth inhibition; 40-50% growth inhibition; 50-70% growth inhibition; 70-90% growth inhibition; 90-100% growth inhibition; lethal to cancer cells

4.3.2 DNA interaction studies

To evaluate the interaction between naphthalimide-1*H*-phenanthro[9,10-*d*]imidazole conjugates with DNA, binding studies of compound **16**, the most potent derivative among the present series, with ct-DNA were performed using UV-visible, fluorescence and CD spectroscopy as well as DNA viscosity measurement.

4.3.2.1 UV-Vis absorption spectroscopy

UV-Vis absorption spectroscopy of compound **16** was carried out in the presence and absence of ct-DNA. Absorption spectra of free compound **16** (20 μM) in phosphate buffer (*p*H 7.2) at 298 K showed intense bands at 415 nm, 330 nm and 268 nm. On incremental addition of ct-DNA upto saturation (0-15 μM), absorption spectra noticeably showed the occurrence of hyperchromism in all three bands (**Figure 1**). The hyperchromicity may be as a consequence of external contact (groove or electrostatic binding).[111] Moreover, the absence of isosbestic points in the absorption spectra pointed out that the complex formation had noncovalent interactions.[112] For a qualitative determination of interaction between compound **16** and ct-DNA, the binding constant (K_b) was calculated using Benesi-Hildebrand equation[73] and found to be 7.81×10^4 M^{-1}. The calculated K_b value at 298 K (order of 10^3 or 10^4)[113] was smaller than that reported for a typical classic intercalator (order of 10^5).[114] Furthermore, by comparison with K_b value of other DNA groove binders, the binding mode between compound **16** and DNA was inferred to be groove binding.

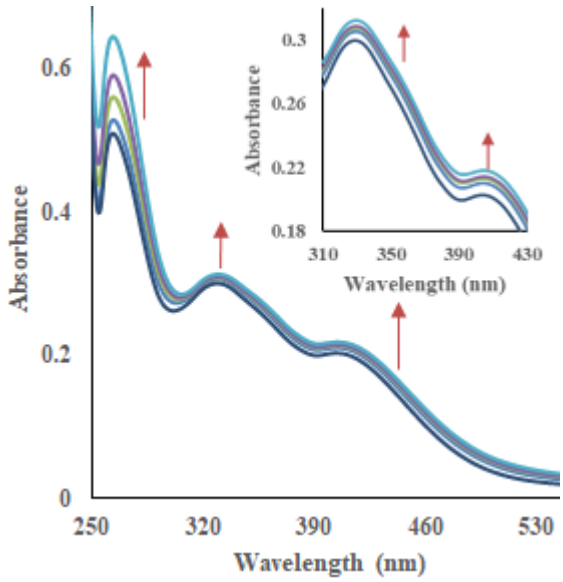

Figure 1. UV-visible absorption compound **16** in the presence of increasing concentrations of ct-DNA in phosphate buffer (*p*H 7.2) at 298 K

4.3.2.2 Fluorescence emission spectroscopy

To get further insight into the interaction between compound **16** and ct-DNA, and to determine effect of temperature on interactions, fluorescence emission spectrum of compound **16** was recorded at three different temperatures (298 K, 308 K and 318 K). Compound **16** displayed a strong emission band at 390 nm after excitation at 330 nm. The fluorescence intensity of compound **16** (5 μM) decreases gradually on incremental addition of ct-DNA (0-60 μM) in phosphate buffer (*p*H 7.2) at three different temperatures, i.e. 298 K, 308 K and 318 K (**Figure 2a-c**), which indicates the good interactions of compound **16** and ct-DNA. With the objective to elaborate the quenching process, a quenching constant (K_{sv}) was obtained from Stern-Volmer equation[75] (**Figure 2d**) and found to be in the range of 2.00–4.44 × 10^3 M^{-1} (**Table 3)** at three different temperatures. In general, a decrease in K_{sv} value can be detected with increasing temperature at static quenching, however, an opposite trend will be detected for dynamic quenching.[77] In the present case, K_{sv} values decreased with increasing temperature, indicating the quenching may be regulated by static quenching with the formation of complex between compound **16** and ct-DNA. The values of quenching rate constant (K_q) was calculated in the range of 2.00-4.44 × 10^{11} M^{-1} s^{-1} (**Table 3**). The higher value was detected for dynamic quenching rate constant than the limiting diffusion constant for biomolecules (≈ 1.0 × 10^{10} M^{-1} s^{-1}),[76] further confirmed the static quenching mechanism in compound **16** and ct-DNA.

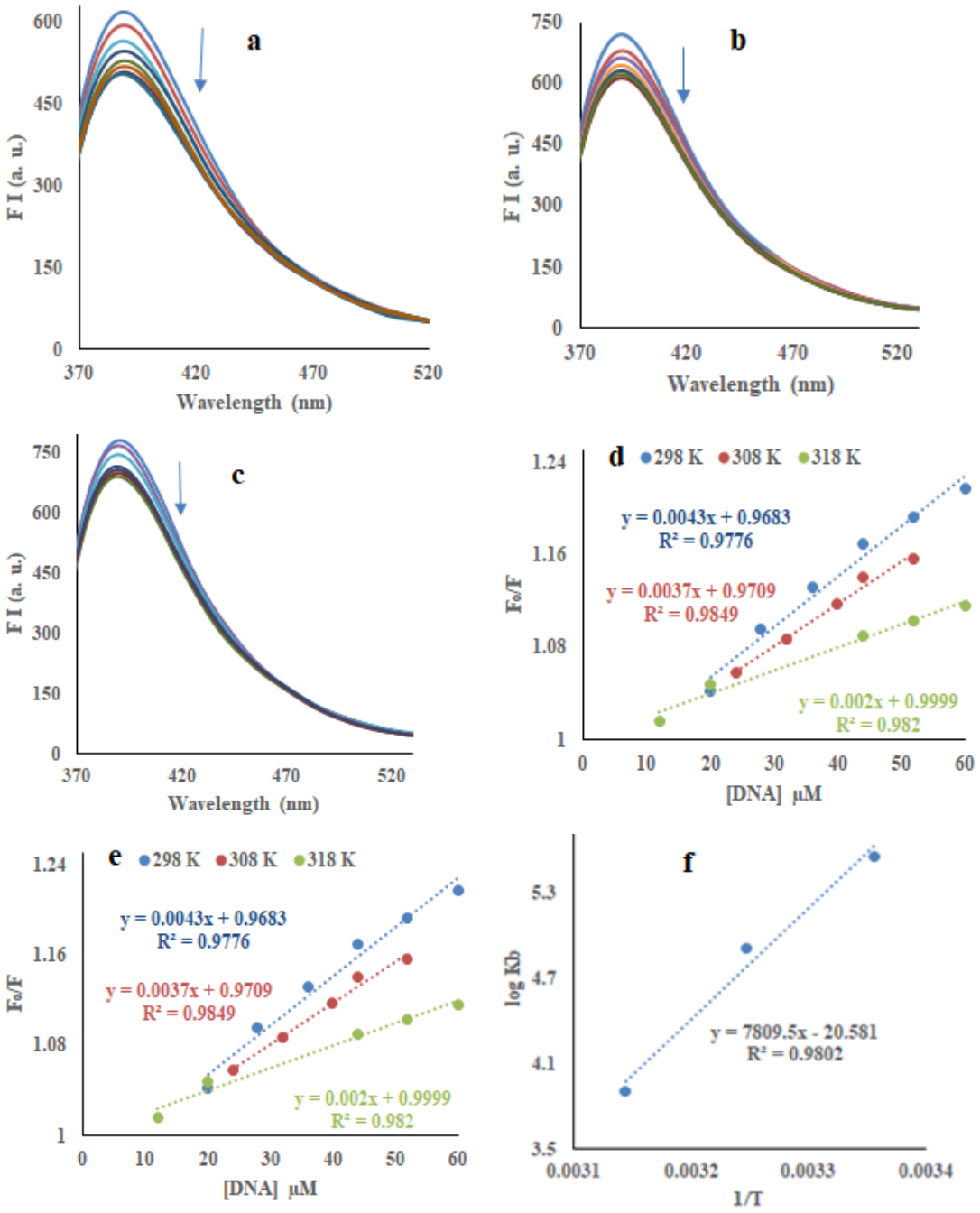

Figure 2. (a) Emission spectra (λ_{ex} = 330 nm) of compound **16** in presence of increasing concentrations of ct-DNA in phosphate buffer (*p*H 7.2) at (a) 298 K, (b) 308 K, (c) 318 K, (d) Stern-Volmer, (e) Modified Stern-Volmer and (f) Van't Hoff plots of emission spectra of compound **16** in the absence and presence of ct-DNA at various temperatures (298 K, 308 K and 318 K)

The values of the binding constant (K_b) and number of binding sites (n) were calculated by modified Stern-Volmer plot (**Figure 2e**) and found to be in the range of 0.80-36.29 × 10^4 M^{-1} and

1.13-1.46, respectively (**Table 3**). The values of enthalpy change (ΔH) and entropy change (ΔS) were calculated from the van't Hoff plot (**Figure 2f**) and found to be -35.70 kcal M^{-1} and -94.08 cal $M^{-1}K^{-1}$, respectively. The free energy change (ΔG) was calculated and determined from (-)7.66 to (-)5.78 kcal M^{-1} (**Table 4**). The negative values of ΔG indicated favorable and spontaneous binding process of compound **16** with ct-DNA. The negative value of ΔH exhibited that an exothermic process played the key role in the complex formation between compound **16** and ct-DNA. The negative value of ΔS is typical regarded for the hydrogen bonding and van der Waals contact in the binding of compound **16** to DNA.

Table 3. Interaction parameters of compound **16** with ct-DNA at three different temperatures (298 K, 308 K and 318 K)

T (K)	K_{sv} ($\times 10^3$) M^{-1}	K_q ($\times 10^{11}$) $M^{-1}s^{-1}$	R^2	K_b ($\times 10^4$) M^{-1}	n	R^2
298	4.44	4.44	0.9776	36.29	1.46	0.9502
308	3.81	3.81	0.9849	8.12	1.32	0.9896
318	2.00	2.00	0.9820	0.80	1.13	0.9548

R^2 is the correlation coefficient

Table 4. Thermodynamic parameters of compound **16** with ct-DNA at three different temperatures (298 K, 308 K and 318 K)

T (K)	ΔH (kcal M^{-1})	ΔS (cal $M^{-1}K^{-1}$)	ΔG (kcal M^{-1})	R^2
298	-35.70	-94.08	-7.66	0.9802
308			-6.72	
318			-5.78	

R^2 is the correlation coefficient

4.3.2.3 Competitive displacement assay

To find the binding mode of compound **16** with ct-DNA, competitive displacement assay was carried out using Hoechst dye and ethidium bromide. Complex of Hoechst dye with ct-DNA displayed an emission peak at around 460 nm, after excitation at 345 nm.[115] A significant decrease in fluorescence intensity of Hoechst-DNA complex (3 μM : 30 μM) was detected upon incremental addition of compound **16** (**Figure 3a**) in phosphate buffer (*p*H 7.2) at 298 K, probably due to replacement of the groove-bound Hoechst from the ct-DNA by compound **16**. The K_{sv} value was calculated from Stern-Volmer equation, with the help of Stern-Volmer plot (**Figure 3b**) and found to be 1.55×10^5 M^{-1}.

Compound **16** has two planer moieties in its structure due to which there are some chances of intercalation. Thus, we have carried out the competitive displacement assay with ethidium bromide.[80] Emission band of ethidium bromide-DNA complex (3 μM : 30 μM) at 602 nm upon excitation at 520 nm, was gradually quenched when titrated with incremental addition of compound **16** (0-90 μM) (**Figure 3c**). The value of K_{sv} was calculated by Stern-Volmer plot (**Figure 3d**) and found to be 1.36×10^4 M^{-1}. Quenching in emission band at 602 nm as well as lower value of K_{sv} displayed possibility of partial intercalation of compound **16** with ct-DNA.

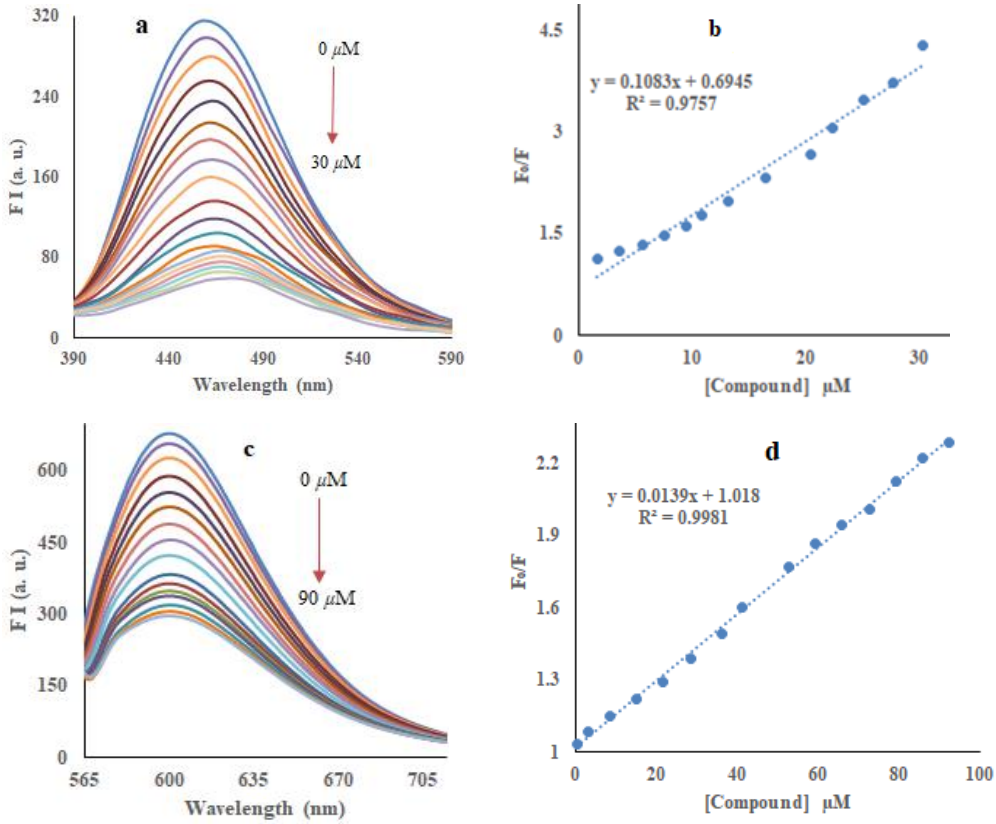

Figure 3. Emission spectra of (a) Hoechst-ct-DNA complex and (b) Ethidium bromide-ct-DNA complex (3 μM : 30 μM) in presence of increasing concentrations of compound **16** in phosphate buffer (*p*H 7.2) at 298 K, Stern-Volmer plots of emission spectra of (c) Hoechst-ct-DNA complex and (d) ethidium bromide-ct-DNA complex in the absence and presence of compound **16**

4.3.2.4 DNA melting studies

DNA melting studies were performed to further evaluate the binding mode of compound **16** with ct-DNA. Melting temperature (T_m) of DNA is a temperature at which point half of the DNA transforms into a single stranded form. Intercalation stabilizes the DNA double helix structure and causes an increase in the value of T_m whereas groove binding does not cause any significant change

in T_m.[74] The values of T_m for ct-DNA in the absence and presence of compound **16** were found to be 78.1 °C and 80.1 °C, respectively. The ΔT_m value of ct-DNA was increased by only 2 °C upon addition of compound **16,** supporting the groove binding as a mode of interaction (**Figure 4a**).

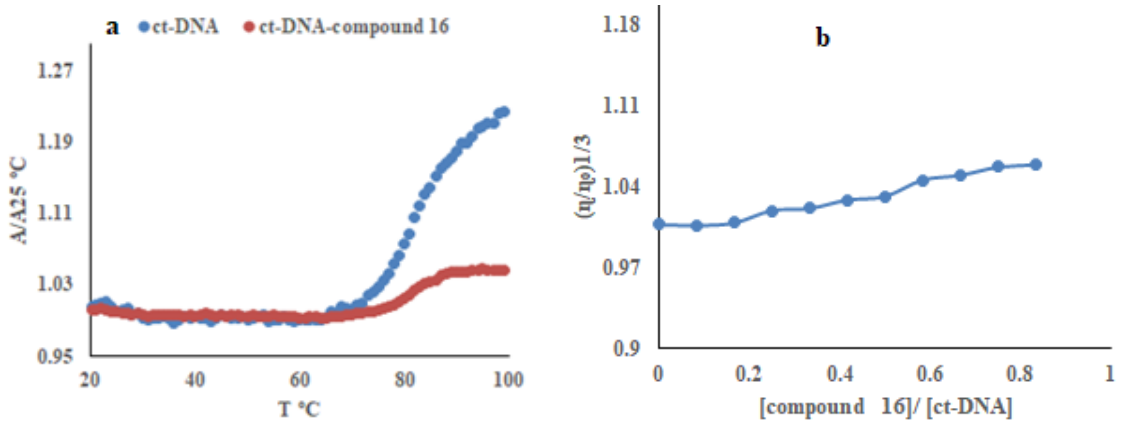

Figure 4. (a) Melting curves of ct-DNA at 260 nm in the absence (blue) and the presence (red) of the compound **16** and (b) effect of the addition of compound **16** on the relative viscosity of ct-DNA at 298 K

4.3.2.5 Viscosity measurments

Generally, groove binding causes a minor change in the viscosity of DNA solution whereas intercalation of small molecule causes significant rise in the viscosity as a result lengthening of DNA.[116] In present experiment, addition of compound **16** to ct-DNA displayed no significant change in the relative viscosity of ct-DNA solution. A relative viscosity plot of $(\eta/\eta_o)^{1/3}$ versus [compound **16**]/[ct-DNA] ratio was obtained (**Figure 4b**). These outcomes further gave evidence regarding the groove binding of compound **16** to ct-DNA.

4.3.2.6 Iodide quenching studies

Potassium iodide (KI) quenching study is an additional technique which gives valuable evidence about the binding mode of any molecule with DNA. The iodide ions can drive the emission quenching of fluorescent compounds in aqueous solution.[117] In this study, compound **16** (5 μM) and compound **16**-ct-DNA complex (5 μM : 60 μM) were titrated with incremental addition of KI solution (**Figure 5a-b**). Stern-Volmer quenching constant (K_{sv}) was calculated by plotting Stern-Volmer plot (**Figure 5c**) in the absence and presence of ct-DNA. The values of K_{sv} were found to be 1.15×10^3 M^{-1} and 1.39×10^3 M^{-1} in the absence and presence of ct-DNA, respectively. The value of K_{sv} for compound **16** was not much affected with the presence of ct-DNA, indicated that mode of interaction is happened preferably by groove binding.

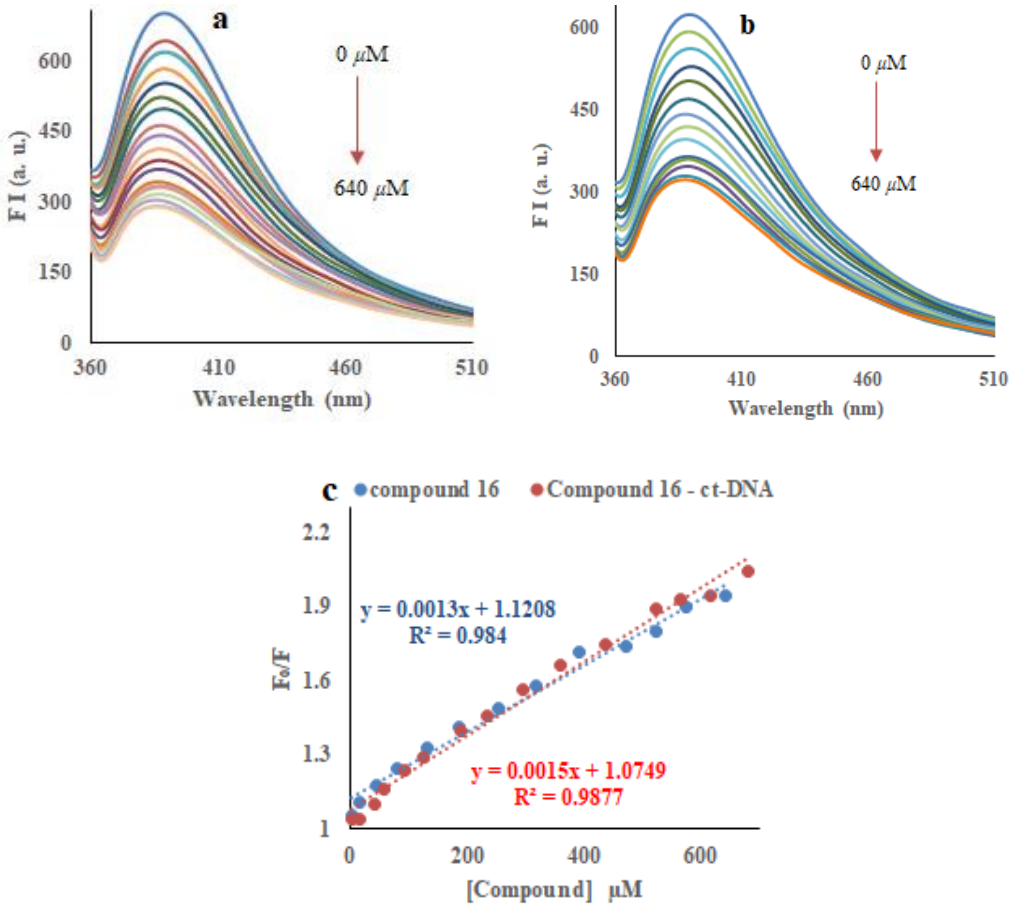

Figure 5. Emission spectra of (a) compound **16**, (b) compound **16**-ct-DNA complex in presence of increasing concentrations of KI in phosphate buffer (*p*H 7.2) at 298 K, and (c) Stern-Volmer plots of emission spectra of compound **16** and compound **16**-ct-DNA complex in the absence and presence of KI

4.3.3 HSA binding studies

To ensure the availability of drug to the target site, there should be good interactions between drug and protein, hence, responsible for transportation. Human serum albumin (HSA) is involved in the transport of drug inside human body.[118] The binding interactions of compound **16** with HSA have been examined by absorption and emission experiments.

4.3.3.1 UV-Vis absorption spectroscopy

UV-Vis absorption spectroscopy is a very simple method to discover the complex formation between a small molecule and protein. UV spectrum of HSA (20 μM) with incremental addition of compound **16** (0-7 μM) was noted in phosphate buffer (*p*H 7.2) at 298 K (**Figure 6a**). Addition of compound **16** drives the enhancement in the absorption peak of HSA at 280 nm, and appearance

of two new weak absorption peaks at 330 nm and 415 nm, which are related to compound **16**. These outcomes indicated that there were significant interactions between compound **16** and HSA. The binding constant (K_b) was calculated to be 0.51 × 10^5 M^{-1} using Benesi-Hildebrand plot (**Figure 6b**).[73]

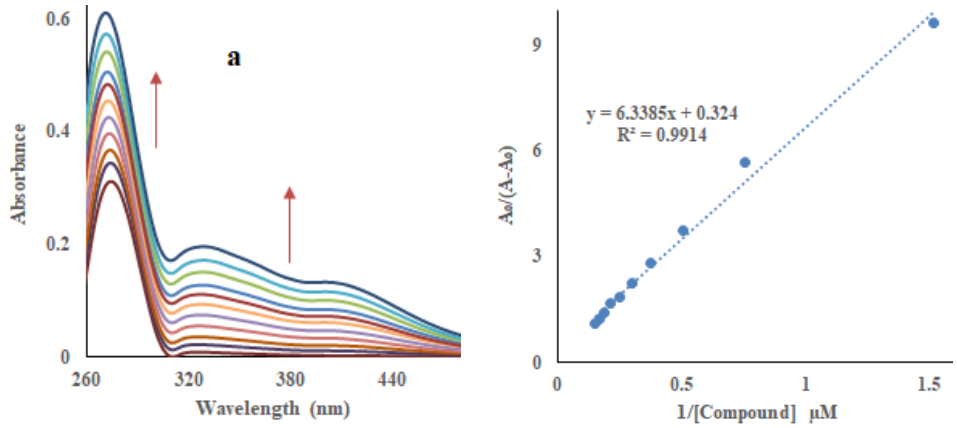

Figure 6. (a) UV-visible absorption and (b) Benesi-Hildebrand plot of HSA (8 μM) in presence of increasing concentrations of compound **16** in phosphate buffer (*p*H 7.2) at 298 K

4.3.3.2 Fluorescence emission spectroscopy

Fluorescence spectrum of HSA is giving emission peak at about 350 nm (λ_{ex} = 280 nm) due to the presence of tryptophan, tyrosine and phenylalanine residues.[119] Gradually quenching was observed in emission peak of HSA (8 μM) at 350 nm upon incremental addition of compound **16** in phosphate buffer (*p*H 7.2) at three different temperatures (298 K, 308 K and 318 K) (**Figure 7a-c**), indicating strong interaction between HSA and compound **16**.

Stern-Volmer and modified Stern-Volmer equations[76,77] were used to calculate the quenching and binding constants. The values of Stern-Volmer quenching constant (K_{sv}) and the quenching rate constant (K_q) were calculated in the range of 6.03-7.60 × 10^5 M^{-1} and 6.03-7.60 × 10^{13} M^{-1} s^{-1}, respectively (**Table 5**, **Figure 7d**). Decrease in the K_{sv} values have been detected with increments in the temperature and higher values were detected for dynamic quenching rate constant than limiting diffusion constant (≈ 1.0 × 10^{10} M^{-1} s−1).[78] All above-mentioned results indicated that quenching mechanism in HSA and compound **16** interaction was static quenching.

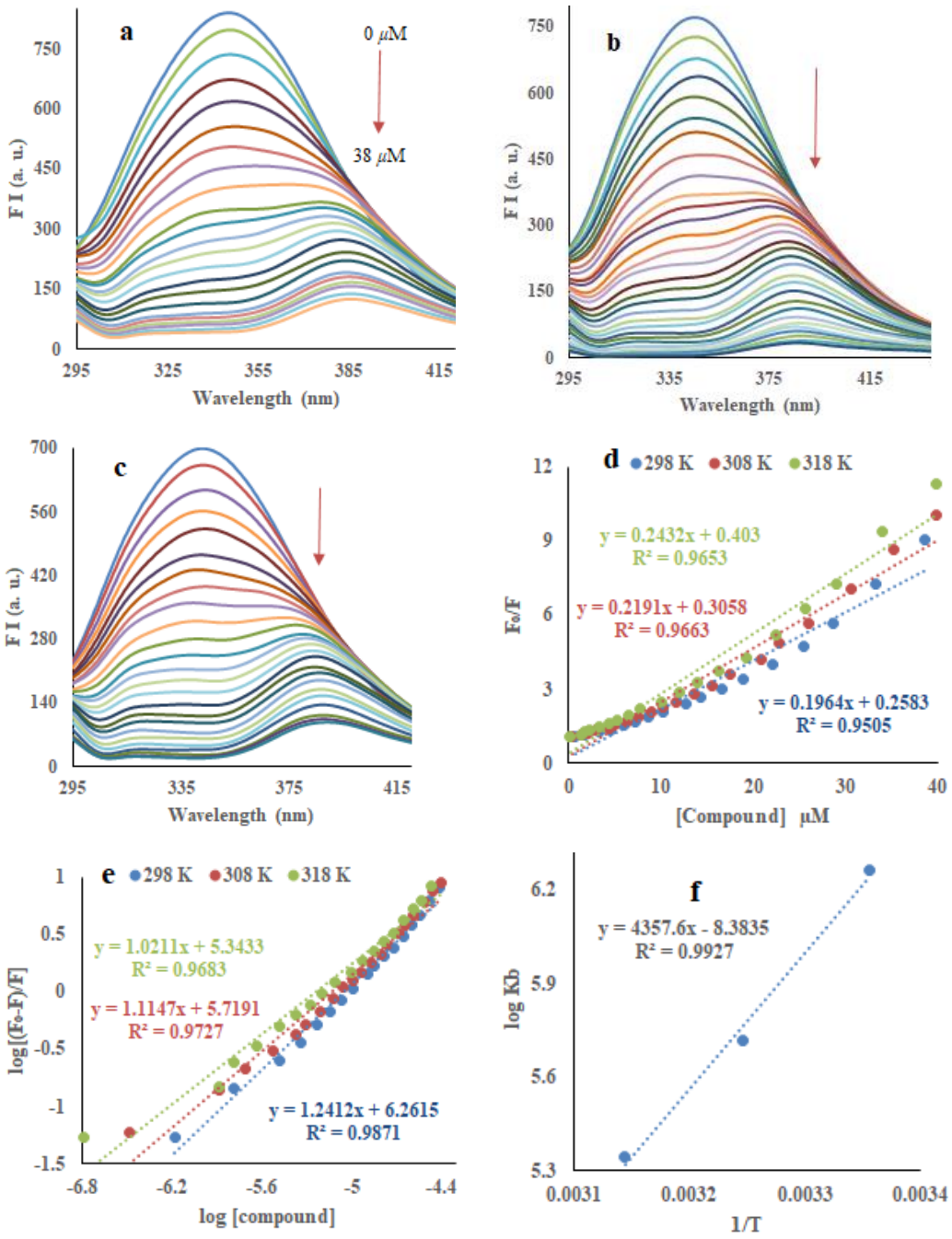

Figure 7. Emission spectra of HSA in presence of increasing concentrations of compound **16** in phosphate buffer (*p*H 7.2) at (a) 298 K, (b) 308 K, (c) 318 K, (d) Stern-Volmer plots, (e) Modified Stern-Volmer plots and (f) Van't Hoff plots of emission spectra of HSA in the absence and presence of compound **16** at various temperatures

Table 5. Interaction parameters of HSA with compound **16** at three different temperatures (298 K, 308 K and 318 K)

T (K)	K_{sv} ($\times 10^5$) M^{-1}	K_q ($\times 10^{13}$) $M^{-1}s^{-1}$	R^2	K_b ($\times 10^6$) M^{-1}	n	R^2
298	7.60	7.60	0.9505	1.82	1.24	0.9871
308	7.16	7.16	0.9663	0.52	1.11	0.9727
318	6.03	6.03	0.9653	0.22	1.02	0.9683

R^2 is the correlation coefficient

The modified Stern-Volmer equation was used to evaluate the binding constants (K_b) and the number of binding sites (n) (**Figure 7e**). The values of K_b and n were found in the range of 0.22-1.82 × 10^5 M^{-1} and 1.02-1.24, respectively, exhibiting strong binding interactions between HSA and compound **16**. Moreover, it was clear that values of K_b have been decreased upon increasing the temperature of HSA solution, showing the stability of HSA-compound **16** complex was reduced with the enhancement in temperatures (**Table 5**).

The binding forces (van der Waals forces, electrostatic forces, hydrogen bonds and hydrophobic interactions) were determined by van't Hoff equation. The enthalpy change (ΔH) and the entropy change (ΔS) were evaluated by plotting van't Hoff plot at three different temperatures (298 K, 308 K and 318 K) (**Figure 7f**). The free energy change (ΔG) was calculated using enthalpy change and entropy change (**Table 6**). The negative values of the ΔG and ΔH (-19.92 kcal M^{-1}) revealed that the binding process was spontaneous and exothermic in nature while the negative value of ΔS (-38.32 cal M^{-1} K^{-1}) credited to hydrogen bonding and van der Waals contact between compound **16** and HSA.

Table 6. Thermodynamic parameters of HSA with compound **16** at three different temperatures (298 K, 308 K and 318 K)

T (K)	ΔH (kcal M^{-1})	ΔS (cal $M^{-1}K^{-1}$)	ΔG (kcal M^{-1})	R^2
298	-19.92	-38.32	-8.49	0.9927
308			-8.11	
318			-7.73	

R^2 is the correlation coefficient

4.3.3.3 Synchronous fluorescence spectroscopic studies

Synchronous fluorescence spectrum is one of the most effective ways to discover the microenvironment of the amino acid residues in human serum albumin on determining the

fluorescence wavelength shift.[121] The changes in the polarity nearby the chromosphere result into position shift of the maximum emission wavelength of molecule. The difference among excitation and emission wavelengths ($\Delta\lambda = \lambda_{emi}-\lambda_{exc}$) reveals the spectra of different nature of the chromophores. In synchronous fluorescence study of HSA, 15 nm and 60 nm values of $\Delta\lambda$ give the characteristic information about tyrosine (Tyr) and tryptophan (Trp) residues, respectively.[122]

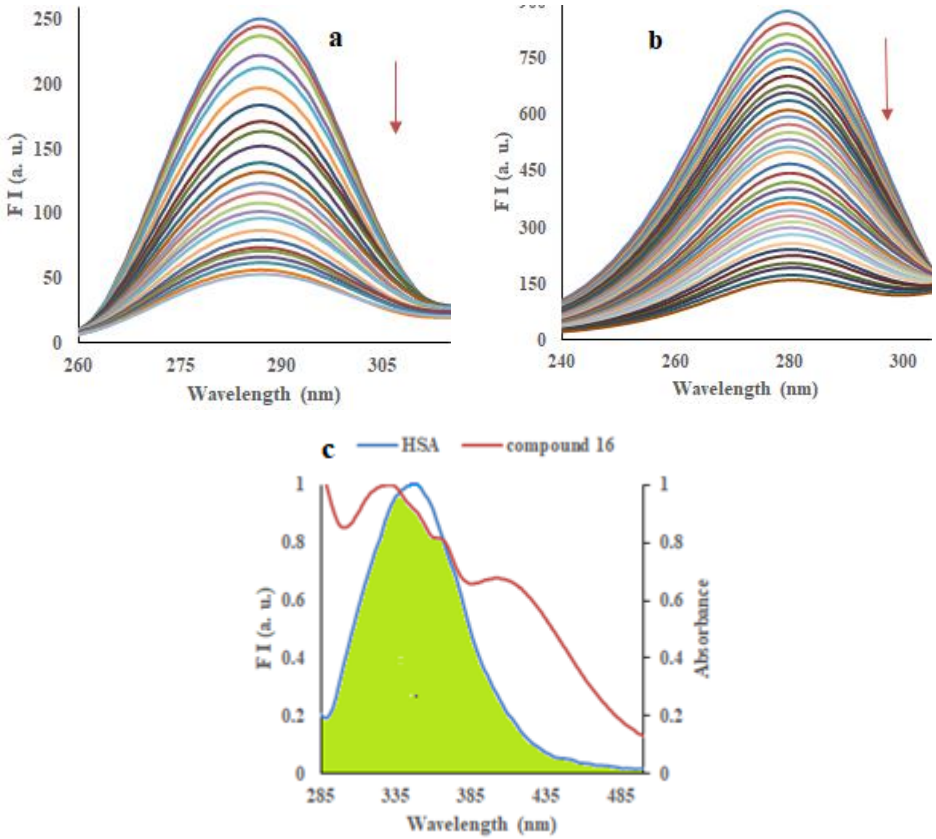

Figure 8. Synchronous emission spectra of HSA (a) $\Delta\lambda$= 15 nm, (b) $\Delta\lambda$ = 60 nm in increasing concentrations of compound **16** and (c) overlap of the fluorescence emission spectrum of HSA (blue) with UV-Vis spectrum of compound **16** (red)

Addition of compound **16** to HSA solution at both $\Delta\lambda$ (15 nm and 60 nm) showed significantly decrease in emission intensity (**Figure 8a-b**). Results had revealed that both Tyr and Trp residues contributed equally to the quenching of the HSA emission and HSA molecule underwent conformational changes around both Tyr and Trp residues upon binding to compound **16**.

4.3.3.4 Energy transfer of compound 16 with HSA

According to the Förster's non-radioactive energy transfer (FRET) theory, energy transfer will takes place if there is the occurrence of overlapping between the absorption band of acceptor

(compound **16**) and the emission band of donor (HSA) (**Figure 8c**).[122] The binding distance between HSA and compound **16** (R: the critical binding distance; r: binding distance), the efficiency of energy transfer (E) and the overlap integral value (*J*) were calculated using dipole orientation factor (k^2) = 2/3, the refractive index of the medium (η) = 1.336, and fluorescence quantum yield of the donor (Φ) = 0.15.[123-125] The values of E, R, *J*, r were calculated to be 94%, 0.57 nm, 1.24×10^{-18} cm^3 L M^{-1} and 0.37 nm, respectively. The binding distance (r) was below 8 nm and satisfied the required condition 0.5 R < r < 2 R[126] for energy transfer. Therefore, there is a high probability of the energy transfer occurred between compound **16** and HSA.

4.4 Molecular docking

The experimental observations were substantiated through molecular docking studies. The preferred binding sites of compound **16** with DNA have been analyzed which play important role in the molecular recognition of nucleic acid and in the rational design of new chemotherapeutic drugs.[127] In our experiment, molecular modeling of compound **16** with DNA was performed using AutoDock program,[88] in order to predict the preferred orientation along with suitable binding sites of the molecule within DNA duplex. The optimized cluster was ranked by energy level in the best

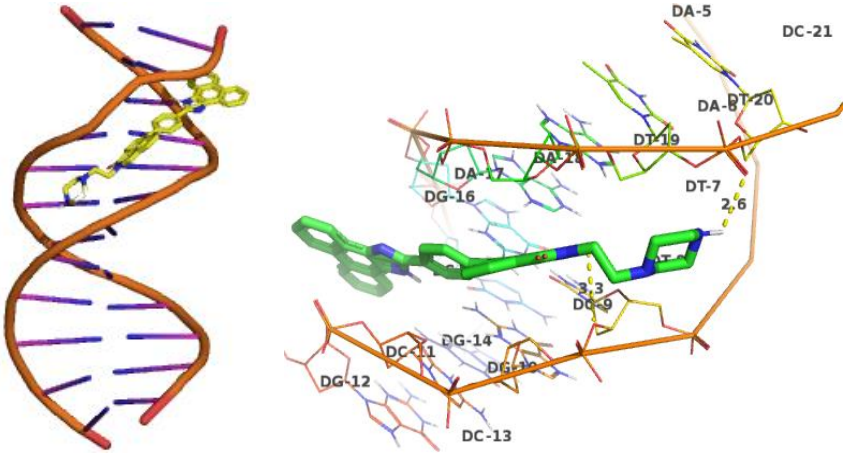

Figure 9. Molecular docking of DNA (1BNA) with compound **16** obtained using Discovery Studio conformation of ligand-DNA modeled structure, and the minimum binding energy of DNA with compounds **16** showed -12.2 kcal mol^{-1}. The binding model of compound **16** with DNA (PdB: 1BNA)[89] has been shown in **Figure 9**. Oxygen atom of naphthalimide ring of compound **16** showed H-bonding (bond length = 2.6 Å) with sugar backbone of DNA attached with cytosine (DC-9, A chain). Similarly, nitrogen atom of piperazine formed H-bonding (bond length = 2.6 Å) with phosphate backbone associated with thymine (DT20 of B chain). Additionally, naphthalimide

and phenanthro[9,10-*d*]imidazole rings showed electrostatic and hydrophobic interactions with DNA.

4.5 Conclusion

Derivatives of naphthalimide-1*H*-phenanthro[9,10-*d*]imidazole conjugate have been synthesized in good yields by Suzuki-Miyaura coupling of key intermediates 6-bromo-1*H*,3*H*-benzo[*de*]isochromene-1,3-dione and (4-(1*H*-phenanthro[9,10-*d*]imidazol-2-yl)phenyl)boronic acid. Compound **16**, substituted with 1-ethylpiperazine, demonstrated excellent cytotoxicity against about 14 human cancer cell lines. DNA interaction studies proposed that the fluorescence of compounds **16** was quenched efficiently and probably quenching phenomenon occurred through the static quenching process. Compound **16** was interacted through groove binding with partial intercalation. The binding results were supported by Hoechst competitive assay, ethidium bromide assay, circular dichroism, DNA melting experiment, DNA viscosity measurements and iodide quenching studies. Furthermore, the interaction of compounds **16** with human serum albumin was evaluated through UV-vis and fluorescence emission spectroscopy with relatively higher binding constant ($K_b = 7.60 \times 10^5\ M^{-1}$).

4.6 Experimental section

Commercially available compounds (Aldrich, Merck, Spectrochem etc.) were used without further purification. Recorded melting points were uncorrected and measured in open capillaries. ^{1}H and ^{13}C NMR characterizations were performed on Jeol ECS 400 NMR spectrometer, operated at 400 MHz for ^{1}H nuclei and 100 MHz for ^{13}C nuclei, taking $CDCl_3$, DMSO-d_6 and TFA as solvents. Chemical shifts were reported in parts per million (ppm) and TMS was used as an internal reference. Coupling constants (*J*) were reported in hertz (Hz). Mass spectra of compounds were performed at Water Micromass-Q-T. Elemental analyses have been done with Thermo Scientific (Flash 2000) analyzer. Purification of synthesized compounds was done through column chromatography with the help of silica gel having mesh size of 60-120/100-200 using hexane/ethyl acetate and chloroform/methanol polarity systems. UV-Vis studies were carried out on a Shimadzu UV-2600 machine using slit width of 1.0 nm and matched quartz cells. Emission spectra were determined on a Varian Cary Eclipse fluorescence spectrometer. CD spectra were carried out on Applied Photophysics CD spectrophotometer. Absorption and fluorescence scans were saved as ACS II files and further processed in Excel™ to produce all graphs shown.

5-Bromo-1,2-dihydroacenaphthylene (2):[128] *N*-Bromosuccinimide (2.54 g, 14.28 mmol) was added portion-wise to the suspension of acenaphthene (**1**) (2 g, 12.98 mmol) in dimethylformamide (20 ml) at room temperature. Reaction was stirred at room temperature for 3 h and progress of the reaction was monitored using thin layer chromatography (TLC). After completion, the reaction mixture was quenched by pouring into ice. The precipitated product was filtered and washed thoroughly with water. Air dried the crude to obtained the desired light brown solid product (**2**) in 2.92 g, 94% yield; R_f 0.6 (hexane); mp 52-55 ^oC.

6-Bromo-1*H*,3*H*-benzo[d*e*]isochromene-1,3-dione (3):[129] Sodium dichromate (10 g) was added portion wise to the solution of 5-bromo-1,2-dihydroacenaphthylene (**2**) (2 g, 5.58 mmol) in acetic acid (50 ml) at 0 °C. After completion of the addition, reaction was transferred to reflux for 2.5 h. Reaction mixture was poured into ice and precipitate was filtered and washed thoroughly with water. White solid product (**3**) was obtained in 1.75 g, 72% yield; R_f 0.5 (hexane); mp 222-225 ^oC.

(4-(1*H*-Phenanthro[9,10-*d*]imidazol-2-yl)phenyl)boronic acid (6): 4-Formylphenylboronic acid (**4**) (1 g, 6.67 mmol), phenanthrene-9,10-dione (**5**) (1.52 g, 7.33 mmol) and ammonium acetate (10.26 g, 133.34 mmol) were refluxed in acetic acid (30 ml) for 10 h. Reaction mixture was quenched by pouring into ice and precipitate was filtered and washed with water to obtain light yellow product (**6**) in 1.12 g, 58% yield; R_f 0.6 (hexane : ethyl acetate; 7:3); mp 278-281 ^oC.

6-(4-(1*H*-Phenanthro[9,10-*d*]imidazol-2-yl)phenyl)-1*H*,3*H*-benzo[*de*]isochromene-1,3-dione (7): Suzuki-Miyaura coupling between 6-bromo-1*H*,3*H*-benzo[*de*]isochromene-1,3-dione (**3**) (1 g, 3.61 mmol) and (4-(1*H*-phenanthro[9,10-*d*]imidazol-2-yl)phenyl)boronic acid (**6**) (1.22 g, 3.61 mmol) was carried out using potassium carbonate (0.5 g, 3.61 mmol) and $Pd(PPh_3)_4$ (5 mol%) in acetonitrile and water mixture (9:1). Reaction was refluxed for 12 h under nitrogen. After completion, solvents were evaporated under reduced pressure. Water (100 ml) was added to the reaction mixture and extracted using chloroform. Chloroform layer was dried over sodium sulphate to get the crude product. Crude was further purified by column chromatography using ethyl acetate:methanol (9.5:0.5) as eluents. Light yellow solid; 72% yield; R_f 0.5 (5% methanol in ethyl acetate); mp 288-291 ^oC; ^1H NMR (DMSO-d_6 + $CDCl_3$, 400 MHz): δ (ppm) 8.78 (d, J = 8.24

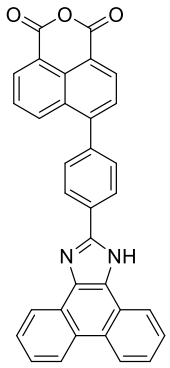

Hz, 2H, ArH), 8.60-8.53 (m, 6H, ArH), 8.43 (d, *J* = 8.56 Hz, 1H, ArH), 7.90 (d, *J* = 7.56 Hz, 1H, ArH), 7.86 (t, *J* = 7.88 Hz, 1H, ArH), 7.76 (d, *J* = 8.20 Hz, 2H, ArH), 7.72 (t, *J* = 7.28 Hz, 2H, ArH), 7.65 (t, *J* = 7.40 Hz, 2H, ArH); ^{13}C NMR (DMSO-d_6 + $CDCl_3$, 100 MHz): δ (ppm) 160.7, 148.9, 146.6, 139.1, 132.9, 131.3, 130.9, 130.5, 129.9, 128.0, 127.2, 127.0, 126.7, 125.3, 122.3, 122.2, 121.1; MS (ESI): m/z 491.5 (M^++1); Anal Calcd for: $C_{33}H_{18}N_2O_3$: C, 80.80; H, 3.70; N, 5.71; found C, 80.87; H, 3.65; N, 5.80.

2-Substituted-6-(4-(1*H*-phenanthro[9,10-*d*]imidazol-2-yl)phenyl)-1*H*-benzo[*de*]isoquinoline-1,3(2*H*)-dione (8-21): 6-(4-(1*H*-Phenanthro[9,10-*d*]imidazol-2-yl)phenyl)-1*H*,3*H*-benzo[*de*]isochromene-1,3-dione (**7**) (100 mg, 0.20 mmol) was refluxed with various alkyl and aryl amines (0.24 mmol) for 7-9 h in ethanol (5 ml). Precipitate was filtered and washed thoroughly with ethanol. Further, crude product was purified by column chromatography using ethyl acetate and methanol as eluents to get desired products.

2-Allyl-6-(4-(1*H*-phenanthro[9,10-*d*]imidazol-2-yl)phenyl)-1*H*-benzo[*de*]isoquinoline-1,3(2*H*)-dione (8): Light yellow solid; 91% yield; R_f 0.6 (5% methanol in ethyl acetate); mp 291-

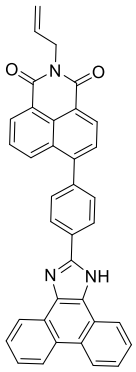

293 °C; ^{1}H NMR (DMSO-d_6, 400 MHz): δ (ppm) 8.80 (s (br), 2H, ArH), 8.54-8.46 (m, 6H, ArH), 8.31 (d, *J* = 8.24 Hz, 1H, ArH), 7.85-7.60 (m, 8H, ArH), 5.95-5.89 (m, 1H, allyl-CH), 5.14-5.10 (m, 2H, allyl-CH_2), 4.63 (s (br), 2H, allyl-CH_2); ^{13}C NMR (DMSO-d_6, 100 MHz): δ (ppm) 163.6, 163.4, 148.9, 146.0, 139.3, 133.2, 132.7, 131.4, 131.0, 130.9, 129.6, 128.5, 128.1, 127.7, 126.9, 122.8, 122.5, 121.7, 116.8 (ArC), 42.3 (allyl-CH_2); MS (ESI): m/z 530.1 (M^++1); Anal Calcd for: $C_{36}H_{23}N_3O_2$: C, 81.65; H, 4.38; N, 7.93; found C, 81.78; H, 4.30; N, 7.88.

6-(4-(1*H*-Phenanthro[9,10-*d*]imidazol-2-yl)phenyl)-2-(prop-2-yn-1-yl)-1*H*-benzo[*de*] isoquinoline-1,3(2*H*)-dione (9): Light yellow solid; 82% yield; R_f 0.6 (5% methanol in ethyl acetate); mp 294-297 °C; ^{1}H NMR (DMSO-d_6 + TFA 400 MHz): δ (ppm) 8.57 (d, *J* = 7.00 Hz, 1H, ArH), 8.35 (d, *J* = 7.52 Hz, 1H, ArH), 8.30 (d, *J* = 8.12 Hz, 2H, ArH), 8.16 (d, *J* = 8.32 Hz, 2H, ArH), 8.05 (t, *J* = 8.00 Hz, 3H, ArH), 7.61-7.50 (m, 7H, ArH), 7.42 (d, *J* = 7.52 Hz, 1H,

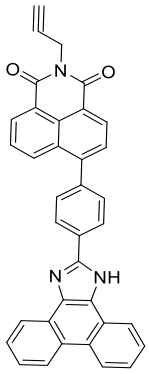

ArH), 5.02 (d, *J* = 2.40 Hz, 2H, propargyl-CH_2), 2.31 (t, *J* = 2.36 Hz, 1H, propargyl-CH); ^{13}C NMR (DMSO-d_6 + TFA, 100 MHz): δ (ppm) 159.5, 159.1, 158.7, 158.3, 147.6, 145.6, 132.7, 131.6, 131.2, 131.1, 129.7, 129.6, 128.8, 128.6, 128.1, 128.1, 127.3, 124.5, 122.7, 122.7, 122.6, 121.8, 117.1, 114.2 (ArC), 79.5 (propargyl-C), 29.7 (propargyl-CH_2); MS (ESI): m/z 528.1 (M^++1); Anal Calcd for: $C_{36}H_{21}N_3O_2$: C, 81.96; H, 4.01; N, 7.96; found C, 81.85; H, 4.15; N, 7.80.

2-Butyl-6-(4-(1*H*-phenanthro[9,10-*d*]imidazol-2-yl)phenyl)-1*H*-benzo[*de*]isoquinoline-1,3(2*H*)-dione (10): Yellow solid; 91% yield; R_f 0.6 (5% methanol in ethyl acetate); mp 288-291

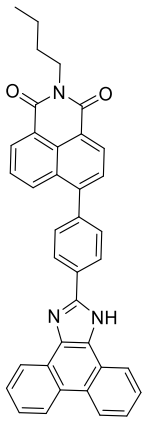

^{o}C; ^{1}H NMR ($CDCl_3$ + TFA, 400 MHz): δ (ppm) 8.50 (d, *J* = 7.24 Hz, 1H, ArH), 8.28 (d, *J* = 9.04 Hz, 3H, ArH), 8.21 (d, *J* = 8.08 Hz, 2H, ArH), 8.09 (d, *J* = 7.72 Hz, 2H, ArH), 7.95 (d, *J* = 8.44 Hz, 1H, ArH), 7.56-7.46 (m, 7H, ArH), 7.32 (d, *J* = 7.52 Hz, 1H, ArH), 4.24 (t, *J* = 7.68 Hz, 2H, butyl-CH_2), 1.78-1.70 (m, 2H, butyl-CH_2), 1.53-1.44 (m, 2H, butyl-CH_2), 1.04 (t, *J* = 7.28 Hz, 3H, butyl-CH_3); ^{13}C NMR (DMSO-d_6 + $CDCl_3$, 100 MHz): δ (ppm) 163.9, 163.7, 148.9, 146.0, 131.1, 130.5, 129.8, 128.1, 127.1, 126.8, 125.4, 123.8, 122.8, 122.4, 121.8 (ArC), 30.2 (butyl-CH_2), 20.4 (butyl-CH_2), 14.1 (butyl-CH_3); MS (ESI): m/z 546.2 (M^++1); Anal Calcd for: $C_{37}H_{27}N_3O_2$: C, 81.45; H, 4.99; N, 7.70; found C, 81.34; H, 4.87; N, 7.61.

2-(2-Hydroxyethyl)-6-(4-(1*H*-phenanthro[9,10-*d*]imidazol-2-yl)phenyl)-1*H*-benzo[*de*] isoquinoline-1,3(2*H*)-dione (11): Light brown solid; 82% yield; R_f 0.3 (5% methanol in

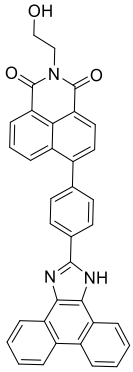

ethyl acetate); mp 290-293 ^{o}C; ^{1}H NMR (DMSO-d_6 + $CDCl_3$, 400 MHz): δ (ppm) 8.77 (d, *J* = 6.76 Hz, 2H, ArH), 8.60-8.54 (m, 6H, ArH), 8.36 (d, *J* = 6.40 Hz, 1H, ArH), 7.81-7.63 (m, 8H, ArH), 4.81 (s (br) 1H, OH), 4.28 (s (br), 2H, ethyl-CH_2), 3.76 (s (br), 2H, ethyl-CH_2); ^{13}C NMR (DMSO-d_6 + $CDCl_3$, 100 MHz): δ (ppm) 164.0, 163.8, 148.9, 145.9, 139.2, 131.0, 131.0, 130.6, 129.8, 128.6, 128.0, 127.4, 127.2, 126.8, 125.5, 123.0, 122.4, 121.9 (ArC), 58.6 (ethyl-CH_2), 42.3 (ethyl-CH_2); MS (ESI): m/z 534.1 (M^++1); Anal Calcd for: $C_{35}H_{23}N_3O_3$: C, 78.78; H, 4.34; N, 7.88; found C, 78.83; H, 4.39; N, 7.71.

2-(2-Aminoethyl)-6-(4-(1*H*-phenanthro[9,10-*d*]imidazol-2-yl)phenyl)-1*H*-benzo[*de*] isoquinoline-1,3(2*H*)-dione (12): Light brown solid; 78% yield; R_f 0.3 (5% methanol in ethyl

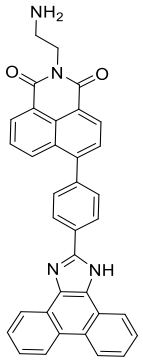

acetate); mp 289-292 °C; ^{1}H NMR (DMSO-d_6, 400 MHz): δ (ppm) 8.81 (bs, 2H, ArH), 8.53-8.28 (m, 6H, ArH), 8.14 (d, J = 6.24 Hz, 1H, ArH), 7.72-7.60 (m, 8H, ArH), 4.16-3.90 (m, 4H, 2 × ethyl-CH_2); ^{13}C NMR (DMSO-d_6, 100 MHz): δ (ppm) 149.3, 130.9, 130.7, 128.3, 128.1, 127.9, 127.7, 127.6, 126.9, 126.7, 126.4, 125.8, 125.5, 125.2, 124.4, 123.9, 122.5, 121.6 (ArC), 63.3 (ethyl-CH_2), 54.0 (ethyl-CH_2); MS (ESI): m/z 533.1 (M^++1); Anal Calcd for: $C_{35}H_{24}N_4O_2$: C, 78.93; H, 4.54; N, 10.52; found C, 78.90; H, 4.41; N, 10.67.

2-Amino-6-(4-(1*H*-phenanthro[9,10-*d*]imidazol-2-yl)phenyl)-1*H*-benzo[*de*]isoquinoline-1,3(2*H*)-dione (13): Reddish brown solid; 83% yield; R_f 0.4 (5% methanol in ethyl acetate); mp

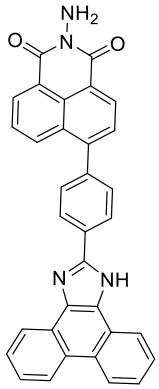

291-293 °C; ^{1}H NMR (DMSO-d_6, 400 MHz): δ (ppm) 8.74 (d, J = 8.04 Hz, 2H, ArH), 8.66-8.61 (m, 3H, ArH), 8.57 (d, J = 7.84 Hz, 3H, ArH), 8.39 (d, J = 8.48 Hz, 1H, ArH), 7.84-7.77 (m, 2H, ArH), 7.75-7.68 (m, 4H, ArH), 7.65 (t, J = 7.68 Hz, 2H, ArH), 5.80 (s, 2H, NH_2); ^{13}C NMR (DMSO-d_6 + $CDCl_3$, 100 MHz): δ (ppm) 160.7, 148.9, 146.6, 139.1, 132.9, 131.3, 131.0, 130.9, 130.5, 129.9, 128.0, 127.2, 127.0, 126.7, 125.3, 122.3, 122.2, 121.1 (ArC); MS (ESI): m/z 505.1 (M^++1); Anal Calcd for: $C_{33}H_{20}N_4O_2$: C, 78.56; H, 4.00; N, 11.10; found C, 78.72; H, 4.22; N, 11.01.

2-(2-(Dimethylamino)ethyl)-6-(4-(1*H*-phenanthro[9,10-*d*]imidazol-2-yl)phenyl)-1*H*-benzo[*de*]isoquinoline-1,3(2*H*)-dione (14): Light yellow solid; 88% yield; R_f 0.3 (5% methanol

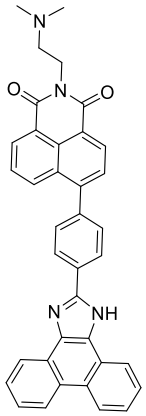

in ethyl acetate); mp 295-298 °C; ^{1}H NMR (DMSO-d_6 + $CDCl_3$, 400 MHz): δ (ppm) 8.74 (s (br), 2H, ArH), 8.65 (s (br), 1H, ArH), 8.55-8.50 (m, 5H, ArH), 8.33 (d, J = 8.40 Hz, 1H, ArH), 7.80-7.75 (m, 2H, ArH), 7.72-7.67 (m, 4H, ArH), 7.64 (t, J = 7.48 Hz, 2H, ArH), 4.26 (t, J = 6.60 Hz, 2H, ethyl-CH_2), 2.62 (t, J = 6.80 Hz, 2H, ethyl-CH_2), 2.30 (s, 6H, 2 × CH_3); ^{13}C NMR (DMSO-d_6 + $CDCl_3$, 100 MHz): δ (ppm) 163.8, 163.6, 148.9, 146.0, 139.2, 137.6, 132.4, 131.1, 130.9, 130.7, 130.6, 129.7, 128.5, 128.0, 127.3, 127.1, 126.8, 125.5, 125.4, 124.0, 123.6, 122.7, 122.4, 121.7 (ArC), 56.9 (ethyl-CH_2), 45.9 (CH_3), 38.1 (ethyl-CH_2); MS (ESI): m/z 560.6 (M^++1); Anal Calcd for: $C_{37}H_{28}N_4O_2$: C, 79.27; H, 5.03; N, 9.99; found C, 79.32; H, 5.13; N, 9.87.

2-(2-(Diethylamino)ethyl)-6-(4-(1*H*-phenanthro[9,10-*d*]imidazol-2-yl)phenyl)-1*H*-benzo[*de*]isoquinoline-1,3(2*H*)-dione (15): Light yellow solid; 86% yield; R_f 0.2 (5% methanol

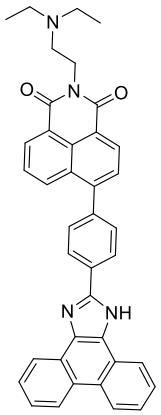

in ethyl acetate); mp 293-296 °C; ^{1}H NMR (DMSO-d_6 + $CDCl_3$, 400 MHz): δ (ppm) 8.76 (d, *J* = 7.76 Hz, 2H, ArH), 8.60-8.54 (m, 6H, ArH), 8.36 (d, *J* = 8.44 Hz, 1H, ArH), 7.83-7.77 (m, 2H, ArH), 7.73-7.68 (m, 4H, ArH), 7.65 (t, *J* = 7.56 Hz, 2H, ArH), 4.24 (t, *J* = 7.24 Hz, 2H, ethyl-CH_2), 2.75 (t, *J* = 6.92 Hz, 2H, ethyl-CH_2), 2.64 (q, *J* = 6.60 Hz, 4H, 2 × ethyl-CH_2), 1.06 (t, *J* = 6.88 Hz, 6H, 2 × ethyl-CH_3); ^{13}C NMR (DMSO-d_6 + $CDCl_3$, 100 MHz): δ (ppm) 163.9, 163.7, 148.9, 146.0, 139.2, 131.0, 130.5, 129.8, 128.6, 128.0, 127.3, 127.2, 126.8, 125.4, 122.8, 122.4, 121.8 (ArC), 49.9 (ethyl-CH_2), 47.5 (ethyl-CH_2), 38.1 (ethyl-CH_2), 12.5 (ethyl-CH_3); MS (ESI): m/z 589.2 (M^++1); Anal Calcd for: $C_{39}H_{32}N_4O_2$: C, 79.57; H, 5.48; N, 9.52; found C, 79.66; H, 5.70; N, 9.41.

6-(4-(1*H*-Phenanthro[9,10-*d*]imidazol-2-yl)phenyl)-2-(2-(piperazin-1-yl)ethyl)-1*H*-benzo[*de*] isoquinoline-1,3(2*H*)-dione (16): Light reddish solid; 83% yield; R_f 0.3 (5% methanol in ethyl

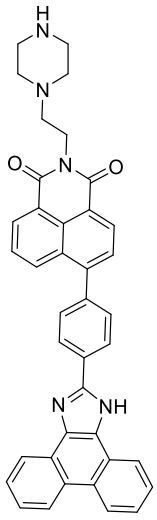

acetate); mp 292-295 °C; ^{1}H NMR (DMSO-d_6 + $CDCl_3$, 400 MHz): δ (ppm) 8.76 (d, *J* = 8.24 Hz, 2H, ArH), 8.61-8.54 (m, 6H, ArH), 8.36 (d, *J* = 8.64 Hz, 1H, ArH), 7.83-7.77 (m, 2H, ArH), 7.74-7.68 (m, 4H, ArH), 7.64-7.59 (m, 2H, ArH), 4.30 (t, *J* = 6.92 Hz, 2H, ethyl-CH_2), 2.79 (t, *J* = 4.44 Hz, 4H, pip-CH_2), 2.65 (t, *J* = 7.16 Hz, 2H, ethyl-CH_2), 2.51 (s (br), 4H, pip-CH_2); ^{13}C NMR (DMSO-d_6 + $CDCl_3$, 100 MHz): δ (ppm) 163.8, 163.6, 148.9, 146.0, 139.2, 132.5, 132.0, 131.9, 131.1, 131.0, 130.7, 130.5, 129.8, 128.9, 128.8, 128.6, 128.0, 127.4, 127.2, 126.8, 125.5, 123.8, 122.8, 122.4, 121.8 (ArC), 56.3 (ethyl-CH_2), 54.7 (pip-CH_2), 46.1 (pip-CH_2), 37.4 (ethyl-CH_2); MS (ESI): m/z 602.2 (M^++1); Anal Calcd for: $C_{39}H_{31}N_5O_2$: C, 77.85; H, 5.19; N, 11.64; found C, 77.72; H, 5.04; N, 11.77.

2-(2-Morpholinoethyl)-6-(4-(1*H*-phenanthro[9,10-*d*]imidazol-2-yl)phenyl)-1*H*-benzo[*de*]isoquinoline-1,3(2*H*)-dione (17): Light yellow solid; 84% yield; R_f 0.4 (5% methanol in ethyl acetate); mp 290-293 °C; ^{1}H NMR (DMSO-d_6, 400 MHz): δ (ppm) 8.85 (d, *J* = 8.00 Hz, 2H, ArH), 8.57-8.48 (m, 6H, ArH), 8.36 (d, *J* = 8.64 Hz, 1H, ArH), 7.90-7.84 (m, 2H, ArH), 7.80 (d, *J* = 8.28 Hz, 2H, ArH), 7.74 (t, *J* = 6.76 Hz, 2H, ArH), 7.64 (t, *J* = 7.52 Hz, 2H, ArH), 4.20 (t, *J* = 6.80 Hz, 2H, ethyl-CH_2), 3.51 (t, *J* = 4.32 Hz, 4H, morph-CH_2), 2.58 (t, *J* = 7.00 Hz, 2H, ethyl-

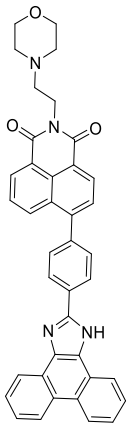

CH_2), 2.47 (merged with solvent, 4H, morph-CH_2); ^{13}C NMR (DMSO-d_6 + $CDCl_3$, 100 MHz): δ (ppm) 163.9, 163.7, 148.9, 146.1, 141.6, 139.2, 139.2, 138.2, 137.7, 131.3, 131.0, 130.7, 129.9, 128.7, 128.3, 127.7, 127.4, 126.8, 125.5, 122.5, 121.9 (ArC), 66.7 (morph-CH_2), 56.2 (morph-CH_2), 53.9 (ethyl-CH_2), 37.3 (ethyl-CH_2); MS (ESI): m/z 603.2 (M^++1); Anal Calcd for: $C_{39}H_{30}N_4O_3$: C, 77.72; H, 5.02; N, 9.30; found C, 77.80; H, 5.00; N, 9.44.

2-Cyclohexyl-6-(4-(1*H*-phenanthro[9,10-*d*]imidazol-2-yl)phenyl)-1*H*-benzo[*de*]isoquinoline-1,3(2*H*)-dione (18): yellow solid; 87% yield; R_f 0.5 (5% methanol in ethyl acetate); mp 290-293

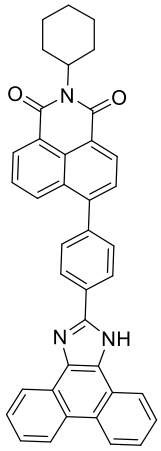

°C; ^{1}H NMR (DMSO-d_6, 400 MHz): δ (ppm) 8.87 (d, *J* = 7.32 Hz, 2H, ArH), 8.59 (d, *J* = 6.20 Hz, 2H, ArH), 8.48 (d, *J* = 6.48 Hz, 4H, ArH), 8.23 (d, *J* = 5.68 Hz, 1H, ArH), 8.02-7.61 (m, 8H, ArH), 4.89 (t, *J* = 10.80 Hz, 1H, cyclohex-CH), 1.82 (d, *J* = 10.04 Hz, 2H, cyclohex-CH_2), 1.68 (d, *J* = 8.60 Hz, 3H, cyclohex-CH_2), 1.38-1.29 (m, 2H, cyclohex-CH_2), 1.22-0.87 (m, 2H, cyclohex-CH_2); ^{13}C NMR (DMSO-d_6, 100 MHz): δ (ppm) 164.2, 164.0, 159.0, 158.6, 147.9, 144.9, 141.3, 131.3, 131.3, 130.8, 129.8, 129.4, 128.7, 128.7, 128.4, 128.3, 128.1, 127.3, 124.7, 123.5, 122.7 (ArC), 53.5 (cyclohex-CH), 29.2 (cyclohex-CH_2), 26.6 (cyclohex-CH_2), 25.7 (cyclohex-CH_2); MS (ESI): m/z 572.2 (M^++1); Anal Calcd for: $C_{39}H_{29}N_3O_2$: C, 81.94; H, 5.11; N, 7.35; found C, 81.91; H, 5.18; N, 7.25.

6-(4-(1*H*-Phenanthro[9,10-*d*]imidazol-2-yl)phenyl)-2-(phenylamino)-1*H*-benzo[*de*]isoquinoline-1,3(2*H*)-dione (19): Light reddish solid; 88% yield; R_f 0.4 (5% methanol

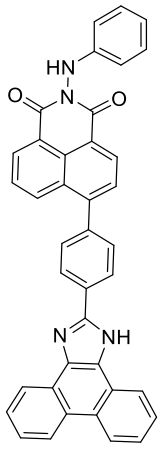

in ethyl acetate); mp 294-297 °C; ^{1}H NMR (DMSO-d_6, 400 MHz): δ (ppm) 8.77-8.65 (m, 5H, ArH), 8.59 (d, *J* = 7.36 Hz, 2H, ArH), 8.45 (d, *J* = 8.56 Hz, 1H, ArH), 8.22 (s, 1H, NH), 7.88-7.81 (m, 2H, ArH), 7.78 (d, *J* = 1.54 Hz, 1H, ArH), 7.74-7.69 (m, 4H, ArH), 7.66-7.61 (m, 3H, ArH), 7.22 (t, *J* = 7.48 Hz, 2H, ArH), 6.88 (t, *J* = 8.12 Hz, 2H, ArH); ^{13}C NMR (DMSO-d_6 + $CDCl_3$, 100 MHz): δ (ppm) 163.3, 163.1, 147.2, 139.1, 137.7, 133.2, 131.9, 131.4, 131.1, 130.4, 130.2, 129.1, 128.5, 128.4, 128.3, 128.1, 128.0, 127.4, 127.3, 127.2, 126.9, 126.8, 125.5, 125.3, 123.9, 123.4, 122.9, 122.4, 122.3, 121.8, 120.7, 113.5 (ArC); MS (ESI): m/z 581.1 (M^++1); Anal Calcd for: $C_{39}H_{24}N_4O_2$: C, 80.67; H,

4.17; N, 9.65; found C, 80.52; H, 4.11; N, 9.78.

2-Benzyl-6-(4-(1*H*-phenanthro[9,10-*d*]imidazol-2-yl)phenyl)-1*H*-benzo[*de*]isoquinoline-1,3(2*H*)-dione (20): Light yellow solid; 88% yield; R_f 0.6 (5% methanol in ethyl acetate); mp 292-295 °C; ^{1}H NMR (DMSO-d_6 + $CDCl_3$, 400 MHz): δ (ppm) 8.76-8.71 (m, 2H, ArH), 8.67 (d, *J* = 7.76 Hz, 1H, ArH), 8.60 (d, *J* = 7.56 Hz, 1H, ArH), 8.56 (d, *J* = 8.20 Hz, 4H, ArH), 8.37 (d, *J* = 8.52 Hz, 1H, ArH), 7.84 (d, *J* = 7.52 Hz, 1H, ArH), 7.80 (t, *J* = 8.04 Hz, 1H, ArH), 7.73-7.68 (m, 4H, ArH), 7.64-7.59 (m, 2H, ArH), 7.46 (d, *J* = 7.36 Hz, 2H, ArH), 7.33 (t, *J* = 7.68 Hz, 2H, ArH), 7.26 (t, *J* = 7.68 Hz, 1H, ArH), 5.34 (s, 2H, benzyl-CH_2); ^{13}C NMR (DMSO-d_6 + $CDCl_3$, 100 MHz): δ (ppm) 163.9, 163.7, 148.8, 146.3, 139.1, 137.6, 132.7, 131.4, 131.0, 130.5, 129.8, 128.6, 128.3, 128.1, 128.0, 127.4, 127.2, 127.1, 126.8, 125.6, 125.4, 124.0, 123.6, 122.9, 122.7, 122.4, 121.6 (ArC), 43.4 (benzyl -CH_2); MS (ESI): m/z 580.1 (M^++1); Anal Calcd for: $C_{40}H_{25}N_3O_2$: C, 82.88; H, 4.35; N, 7.25; found C, 82.80; H, 4.30; N, 7.32.

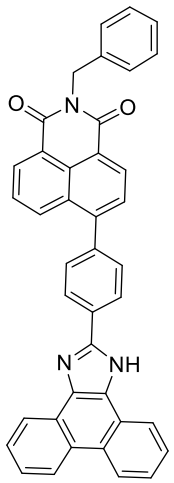

2-(4-Fluorophenyl)-6-(4-(1*H*-Phenanthro[9,10-*d*]imidazol-2-yl)phenyl)-1*H*-benzo[*de*]isoquinoline-1,3(2*H*)-dione (21): Light brown solid; 82% yield; R_f 0.4 (5% methanol in ethyl acetate); mp 296-299 °C; ^{1}H NMR (DMSO-d_6, 400 MHz): δ (ppm) 8.92 (t, *J* = 11.04 Hz, 2H, ArH), 8.62-8.57 (m, 2H, ArH), 8.54-8.44 (m, 4H, ArH), 8.34 (t, *J* = 8.08 Hz, 1H, ArH), 8.03-7.96 (m, 1H, ArH), 7.92-7.85 (m, 4H, ArH), 7.83-7.77 (m, 3H, ArH), 7.73 (t, *J* = 8.00 Hz, 2H, ArH), 7.47-7.43 (m, 1H, ArH), 7.37 (t, *J* = 8.72 Hz, 1H, ArH); ^{13}C NMR (DMSO-d_6, 100 MHz): δ (ppm) 164.2, 164.0, 161.2, 161.0, 159.4, 159.1, 158.7, 158.3, 147.7, 146.2, 140.9, 133.4, 133.1, 132.5, 131.2, 129.6, 128.8, 128.3, 128.2, 127.4, 124.7, 122.7, 119.9, 119.1 (ArC); MS (ESI): m/z 584.1 (M^++1); Anal Calcd for: $C_{39}H_{22}FN_3O_2$: C, 80.26; H, 3.80; F, 3.26; N, 7.20; found C, 80.38; H, 3.62; F, 3.36; N, 7.11.

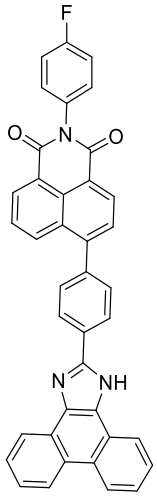

CHAPTER 5
HYBRIDS OF PHENANTHRO[9,10-*d*]IMIDAZOLE AND OTHER HETEROCYCLIC MOIETIES

5.1 Introduction

The development of diverse and novel small heterocyclic scaffold is causing higher attention in the medicinal and biological systems.[130-132] This may attribute to growing necessity in assembling libraries of complex substances that is evaluated as lead compounds in drug discovery and development. Polycyclic aromatic hydrocarbons (PAH) are extremely important structural units in a variety of pharmaceutically active substances,[133-137] owing to rigid structures that have a role in the progress of antitumor agents due to their ability to insert between stacked base pairs of DNA and thus act as intercalators.[138] Introduction of appropriate side chains to these planar polycyclic heterocycles further increase the interactions with important macromolecules.[139] Many heterocyclic compounds were synthesized using phenanthroline as core moiety, some of which having substituted and unsubstituted aryl rings at C2- and/or NH-position(s) of imidazole ring that were identified as potent antitumor agents.[140,141] Phenanthrene-imida-/oxa-zole also showed favorable properties such as high extinction coefficient, ease of synthesis, stability and superior absorption and emission properties,[142] which was commonly utilized in various optical sensors and probes. To the best of our knowledge, only few literature reports are available for anticancer activity of phenanthrene-imida-/oxa-zole moieties. In the framework of our program to develop the potentially bioactive heterocyclic compounds and in continuation with our on-going interests in this field,[32,33,68] in the present work, we have designed and synthesized a series of compounds with different substitution of aromatic ring at C2 position which might be able to form H-bond and π-interaction with various biomacromolecules, that may increase the binding affinity with DNA and thus, improve antiproliferative activity. The planarity of this series of compounds is important to intercalate into the base pairs of DNA double helix, causing miscoding that results in cell death.

A facile procedure has been trailed for the synthesis of 2-(aryl)-1*H*-phenanthro[9,10-*d*]imidazole/oxazole *via* condensation of 9,10-phenanthrenedione with various aryl aldehydes followed by substitution with various heterocyclic moieties. Synthesized compounds were subjected to cytotoxic assay in 60 human cancerous cell lines. Interactions of these compounds were further studied with human and calf thymus (Ct) DNA for intercalation mode of binding as

well as BSA and HSA for protein transport. Moreover, molecular modelling was used to gain further understanding into the binding mode of phenanthroline derivatives in the active site of DNA.

5.2 Chemistry

A series of 1*H*-phenanthro[9,10-*d*]imidazole/oxazole and 7*H*-acenaphtho[1,2-*d*]imidazole derivatives has been synthesized with substitution at C2 position possessing various aromatic rings like thiazolidine, phenol, salicylaldehyde, pyrene, naphthalimide etc (**Schemes 1-4)**. Accordingly, 2-substituted 1*H*-phenanthro[9,10-*d*]imidazole (**3**) and phenanthro[9,10-*d*]oxazole **(4)** were synthesized by heating the phenanthrene-9,10-dione (**1**) with substituted aromatic aldehydes (**2a-h**) at 100 ^{o}C for 2-5 h in the presence of ammonium acetate and acetic acid (**Scheme 1**). In all reactions, 2-substituted 1*H*-phenanthro[9,10-*d*]imidazole (**3a-h**) and phenanthro[9,10-*d*]oxazole **(4a-c)** were obtained in moderate to good yields. Among the aryl aldehydes, 5-bromosalicylaldehyde was most reactive and the corresponding product 4-bromo-2-(1*H*-phenanthro[9,10-*d*]imidazol-2-yl)phenol (**3e**) was obtained in comparatively high yield (65%). On the other hand, condensation with pyren-1-aldehyde was sluggish and low yielding. All products were completely characterized before proceeding further.

Scheme 1. Synthesis of 2-(subsitituted aryl)-1*H*-phenanthro[9,10-*d*]imidazole/oxazole (**3a-h** and **4a-c**).

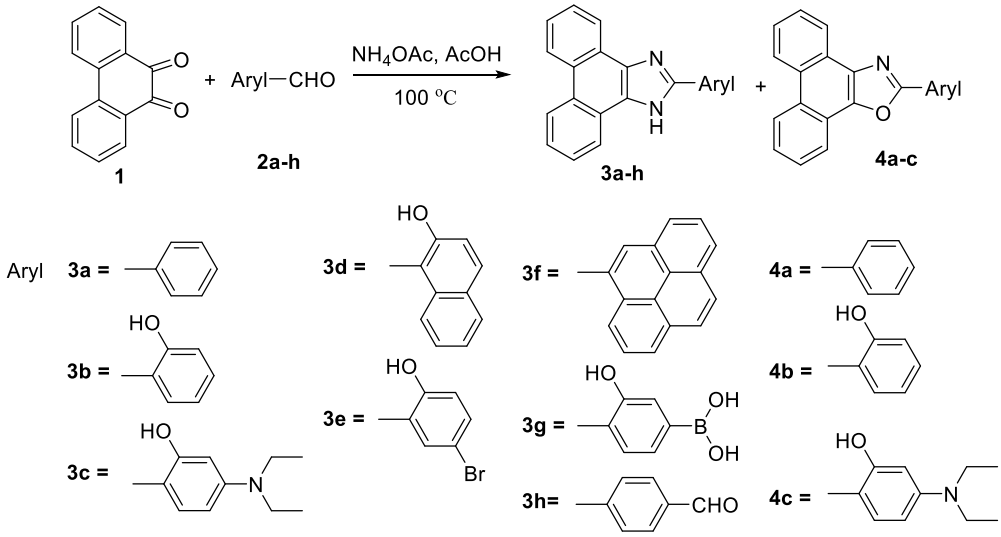

4-(1*H*-Phenanthro[9,10-*d*]imidazol-2-yl)benzaldehyde (**3h**) was further used for reaction with 2-amino-benzo[*de*]isoquinoline-1,3-dione (**5**) and thiazolidine-2,4-dione (**7**) in ethanol for 3-

4 h to obtain **6** and **8** in 62% and 60% yields, respectively. The series of benzimidazoles were formed by condensation of **3h** with 4-benzoyl-1,2-diaminobenzene (**9**) and 1,2-diamino-anthracene-9,10-dione (**11**) at 60 ^{o}C in nitrobenzene for 2 h to obtain (2-(4-(1*H*-phenanthro[9,10-*d*]imidazol-2-yl)phenyl)-1*H*-benzo[*d*]imidazol-6-yl)(phenyl)methanone (**10)** and 2-(4-(1*H*-phenanthro[9,10-*d*]imidazol-2-yl)phenyl)-3*H*-anthra[1,2-*d*]imidazole-6,11-dione (**12)** in 65% and 61% yields, respectively (**Scheme 2**).

Scheme 2. Synthesis of naphthalimide (**6**), thiazolidine (**8**) and benzimidazoles (**10** and **12**) of 4-(1*H*-phenanthro[9,10-*d*]imidazol-2-yl)benzaldehyde (**3h**)

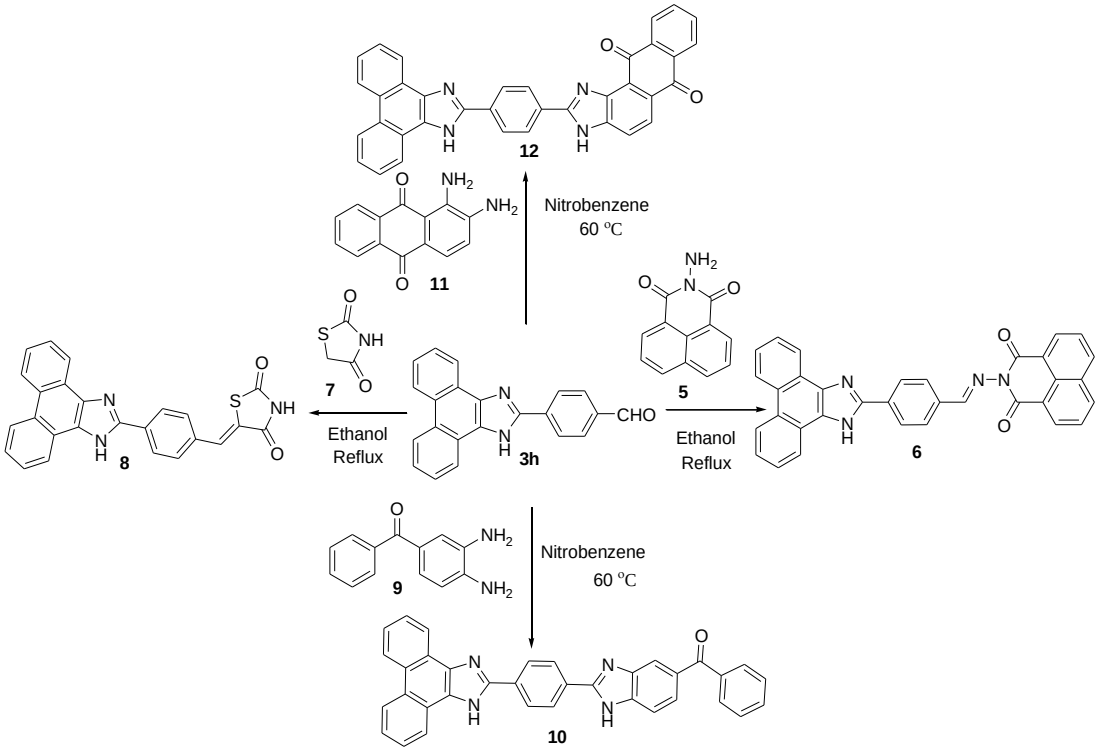

2,3-Diaryl 1*H*-phenanthro[9,10-*d*]imidazole was obtained with phenanthrene-9,10-dione (**1**), employing aniline and benzaldehyde in the presence of ammonium acetate and acetic acid and the corresponding product, 1,2-diphenyl-1*H*-phenanthro[9,10-*d*]imidazole (**14**) was obtained in 57% yield (**Scheme 3**). For SAR studies involving variation of imidazole moiety, 2-(7-phenyl-7*H*-acenaphtho[1,2-*d*]imidazol-8-yl)phenol (**16**) and 4-(7*H*-acenaphtho[1,2-*d*]imidazol-8-yl)benzaldehyde (**17**) were prepared in 64% and 52% yields by condensation of acenaphthylene-1,2-dione with respective salicylaldehyde, and terephthaldehyde, in the presence of ammonium acetate and acetic acid as shown in **Scheme 4**. Compounds have been purified by column

chromatography and purity of all the derivatives were checked by HPLC. The purity of these compounds has been determined to be ≥ 95%.

Scheme 3. Synthesis of 1,2-diphenyl-1*H*-phenanthro[9,10-*d*]imidazole (**14**)

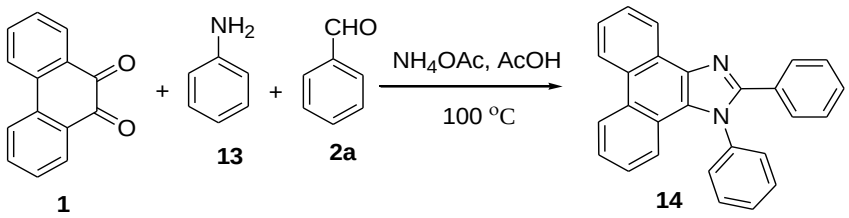

Scheme 4. Synthesis of 2-(7-phenyl-7*H*-acenaphtho[1,2-*d*]imidazol-8-yl)phenol (**16**) and 4-(7*H*-acenaphtho[1,2-*d*]imidazol-8-yl)benzaldehyde (**17**)

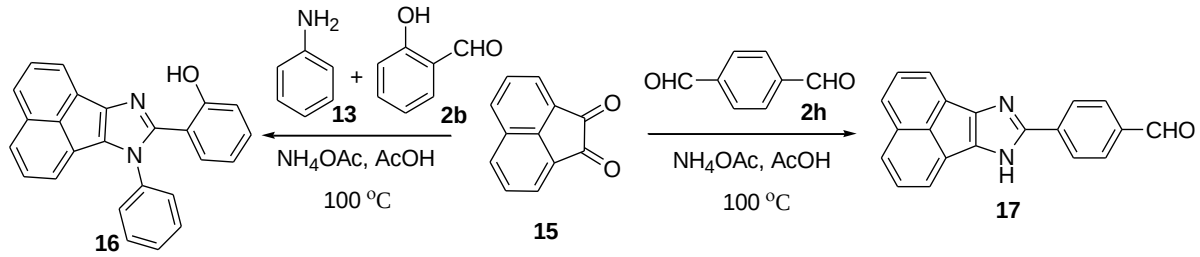

5.3 Biology

5.3.1 Cytotoxicity

5.3.1.1 Cytotoxicity against human cancer cells

Derivatives of 1*H*-phenanthro[9,10-*d*]imidazole/oxazole (**3b, 3c, 3f, 4b, 4c, 8** and **12**) and 4-(7*H*-acenaphtho[1,2-*d*]imidazol-8-yl)benzaldehyde (**17**) were chosen by National Cancer Institute,USA on account of variations in structure for cytotoxicity. These compounds were evaluated *in vitro* for cytotoxicity against cancer cells in a panel of 60-human cell lines at a single dose of 10 μM concentration, and the percentages of growth inhibition over these cell lines were determined (**Table 1**).[71]

Preliminary *in vitro* anticancer screening revealed that derivatives **3f**, **4c** and **17** showed moderate inhibition, while compound **8** indicated more than 50% growth inhibition for most of the cancer cell lines and in some cases, exhibited better growth inhibition than 5-fluorouracil (5-FU). 1*H*-Phenanthro[9,10-*d*]imidazole/oxazole derivatives **3b, 3c, 4b** and **12** showed lower activity for cancer cell lines and were considered to be the least effective. 1*H*-Phenanthro[9,10-*d*]imidazole **3f** showed selectivity towards non-small cell lung cancer cell lines NCI-H226 and breast cancer cell lines MDA-MB-468 with growth inhibition (GI) values of 76.22% and 78.07%, respectively while only OVCAR-4 was selective to **12** with GI value of 88.98%. Similarly, 2-phenanthro[9,10-

d]oxazole having 5-diethylamino-2-hydroxyphenyl group **4c** at 2-position showed selectivity towards leukemia cancer cell lines (K-562; GI = 79.67%, SR; GI = 72.39%), colon cancer cell lines (HCT-15; GI = 65.06%, HT-29; GI = 64.35%, KM12; 55.56%) and melanoma cancer cell lines (LOX IMVI; GI = 75.33%). Derivatives of 7*H*-acenaphtho[1,2-*d*]imidazol-8-yl with benzaldehyde (**17**) displayed selective potency towards breast cancer cell lines MCF7 and T-47D with GI values of 51.61% and 57.05%, respectively. 1*H*-Phenanthro[9,10-*d*]imidazole with thiazolidine-2,4-dione group (**8**) showed broad spectrum of cytotoxicity compared to other derivatives in most of the cancer cell panels. Compound **8** showed excellent inhibition against leukemia cancer cell lines CCRF-CEM (65.23%), HL-60(TB) (57.70%), K-562 (68.08%), RPMI-8226 (66.09%) and SR (79.21%), colon cancer cell lines HCT-116 (65.54%) and HCT-15 (50.01%), melanoma cancer cell lines MDA-MB-435 (67.42%), renal cancer cell lines A498 (92.98%), prostate cancer cell lines PC-3 (51.87%) and breast cancer cell lines BT-549 (63.72%) and MDA-MB-468 (51.74%).

Table 1. Percent growth inhibition of compounds **3b-c, 3f, 4b-c, 8, 12** and **17** on the panel of 60 human tumor cell lines at 10 μM concentration

Panel	Cell lines	3b	3c	3f	4b	4c	8	12	17	5-FU
Leukemia	CCRF-CEM	--	--	10.31	17.88	41.37	65.23	--	11.09	57.1
	HL-60(TB)	--	--	--	11.98	31.39	57.70	--	--	47.9
	K-562	12.13	20.51	--	11.86	79.67	68.08	--	16.50	42.3
	MOLT-4	--	--	26.75	--	39.03	47.12	12.38	20.51	43.1
	RPMI-8226	13.33	--	10.55	24.49	44.56	66.09	10.37	22.81	41.4
	SR	10.82	15.79	23.68	26.32	72.39	79.21	11.44	15.97	24.8
Non-small	EXVX	19.36	18.23	--	21.25	20.24	11.51	10.28	22.99	NT
Cell Lung	HOP-92	16.43	24.20	27.07	16.21	10.99	21.41	--	14.01	50.6
Cancer	NCI-H226	11.55	--	76.22	14.18	--	--	--	12.45	69.5
	NCI-H23	10.68	--	--	14.52	13.50	28.97	--	14.86	39.0
	NCI-460	--	-	--	30.41	15.00	19.73	--	23.63	NT
	NCI-522	--	10.43	17.47	--	19.76	47.59	--	--	58.0
Colon	COLO 205	--	--	--	14.27	12.78	--	--	--	NT
Cancer	HCC-2998	--	--	--	--	18.74	--	--	12.84	L
	HCT-116	12.32	--	16.65	19.25	16.63	65.54	--	19.24	17.8
	HCT-15	--	13.85	--	--	65.06	50.01	--	23.72	26.5
	HT29	--	--	--	--	64.35	24.02	--	--	NT
	KM12	--	--	13.51	--	55.56	43.92	--	13.04	40.7
	SW-620	--	--	--	31.55	31.43	22.83	--	--	--
CNS	SF-268	--	--	14.56	10.18	11.98	12.31	--	13.27	59.0
Cancer	SF-295	--	--	--	--	--	16.26	--	--	69.0

	SNB-19	--	--	--	--	--	18.07	--	--	NT
	SNB-75	11.1	--	--	10.31	--	--	10.03	--	65.9
	U251	--	--	--	17.98	15.6	30.30	--	--	50.3
Melanoma	LOX IMVI	--	11.74	13.70	--	75.33	36.69	--	25.82	30.4
	MALME-3M	--	--	--	--	--	14.85	--	--	58.2
	M14	--	--	--	--	12.40	47.88	--	--	NT
	MDA-MB-435	--	--	--	--	--	67.42	--	--	NT
	SK-MEL-28	--	--	--	--	--	19.07	--	--	19.5
	UACC-62	10.10	20.14	38.38	11.64	11.15	30.28	--	19.80	39.7
Ovarian Cancer	IGROV1	23.53	--	13.23	25.87	19.22	--	--	28.87	51.2
	OVCAR-3	--	--	--	--	10.26	21.28	--	12.27	47.4
	OVCAR-4	--	--	--	23.56	--	--	88.98	27.42	59.4
	OVCAR-8	--	--	--	10.96	15.00	21.68	--	--	NT
	NCI/ADR-RES	--	--	--	--	11.04	--	--	--	47.6
	SK-OV-3	--	10.12	--	--	--	--	--	--	77.5
Renal Cancer	786-0	--	--	--	--	12.22	48.01	--	--	NT
	A498	--	--	36.26	--	--	92.98	--	--	L
	ACHN	11.69	--	10.35	--	23.11	33.35	--	--	39.3
	RXF 393	--	--	--	--	16.65	19.08	--	--	NT
	SN12C	24.36	--	--	17.00	--	--	--	--	54.0
	UO-31	37.89	24.42	37.19	39.05	35.16	25.52	22.61	33.35	41.3
Prostate Cancer	PC-3	11.77	--	21.16	22.22	20.31	51.87	--	21.13	58.2
Breast Cancer	MCF7	26.33	23.75	23.08	37.58	43.24	46.15	--	51.61	11.5
	MDA-MB-231/ATCC	23.78	19.44	23.21	18.28	35.24	15.55	14.43	25.57	78.1
	HS 578T	--	--	--	10.50	10.04	17.56	--	--	L
	BT-549	--	--	--	--	--	63.72	--	--	37.8
	T-47D	36.40	17.10	39.97	21.10	31.38	38.46	--	57.05	56.7
	MDA-MB-468	--	--	78.07	17.03	15.77	51.74	--	30.9	NT

-- indicates GI < 10%; NT, not tested; L, lethal to the cancer cell line; 30-40% growth inhibition; 40-50% growth inhibition; 50-70% growth inhibition; 70-90% growth inhibition; 90-100% growth inhibition

5.3.1.2 Cytotoxicity against human normal cells

Cytotoxicity of compound **8** in human cancer cell line (A549/ATCC) and normal cell line (Hek293) was determined by means of colorimetric assay (MTT assay). The cytotoxicity of compound **8** to A549/ATCC at 10^{-4}, 10^{-5}, 10^{-6}, 10^{-7} and 10^{-8} μM concentration has been found to be 90%, 78%, 75%, 59% and 42%, respectively (**Figure 1a**). Compound **8** exhibited excellent

growth inhibition activity against A549/ATCC with IC_{50} value of 1.70 μM. To evaluate the safety, the cytotoxic effect of active derivative **8** on human normal cell lines (Hek293) was also carried out. It has been observed that derivative **8** showed only 15%, 9%, 6%, 5% and 4% cytotoxicity to Hek293 cells at the concentration level of 10^{-4}, 10^{-5}, 10^{-6}, 10^{-7} and 10^{-8} μM, respectively (**Figure 1b**). The compound showed only 15% toxicity to Hek293 cells even at 100 μM concentration. These data revealed that derivative **8** had low cytotoxicity towards mammalian cells, indicating that the bioactive compound **8** was able to selectively kill cancer cells.

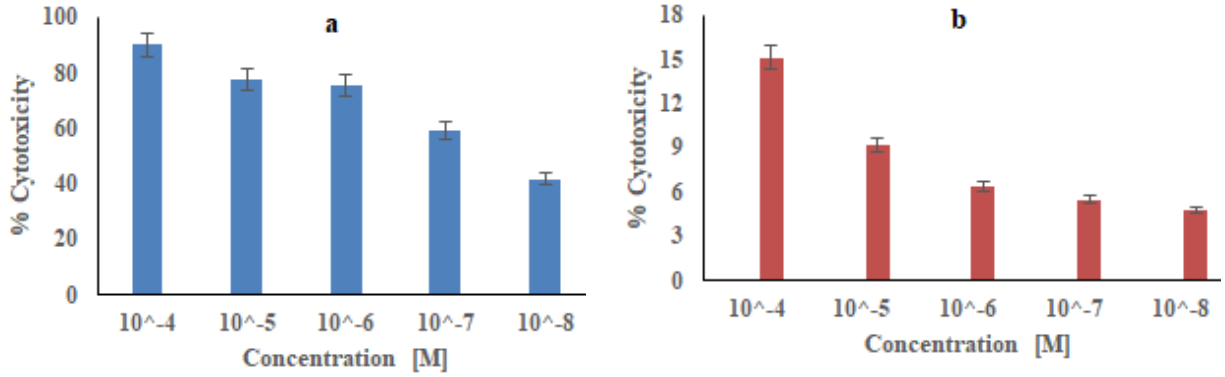

Figure 1. Effect of cytotoxicity of compound **8** on (a) human cancer cell line A549/ATCC and (b) human normal cell line Hek293

5.3.2 DNA binding studies

In order to determine the interaction of compound with DNA, binding properties of most active compound **8** have been assessed using UV-visible and fluorescence spectrophotometer.

5.3.2.1 Calf thymus DNA binding studies

5.3.2.1.1 UV-vis absorption spectroscopy

Upon incremental addition of ct-DNA (0-40 μM) to compound **8** (20 μM), the intensity of the absorption band of compound **8** at 398 nm decreases (**Figure 2a**). The observed hypochromic shift upon addition of DNA results from intercalation. The binding constant of compound **8** with ct-DNA (K_b) has been investigated with Benesi-Hildebrand equation[73] that was found to be 2.95×10^6 M^{-1} (**Figure 2b**). The free energy of interaction (ΔG_{obs}) has also been calculated from binding constant and was found to be -6.09 kcal mol^{-1}, indicating the favorable and spontaneous nature of binding process.

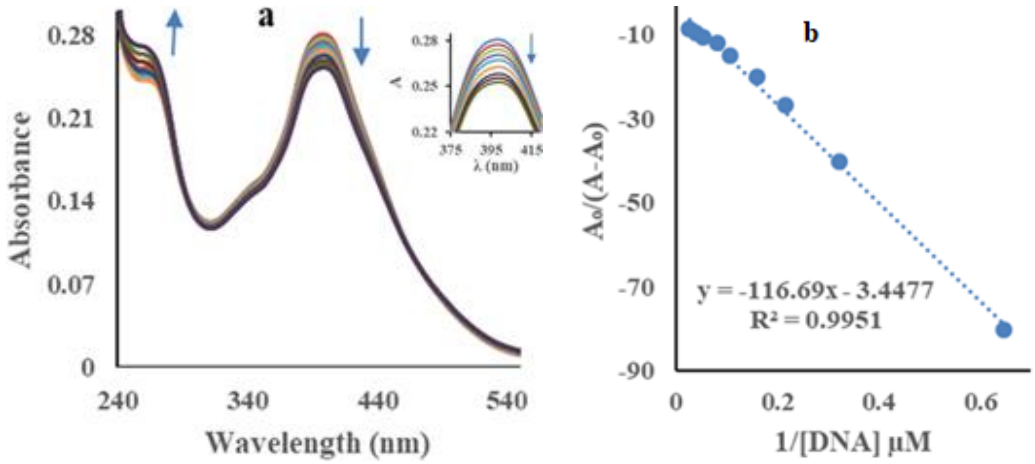

Figure 2. (a) Absorption spectra of compound **8** in the presence of the ct-DNA and (b) Benesi-Hildebrand plot of compound **8** for absorption spectroscopy of ct-DNA

5.3.2.1.2 DNA melting studies

Thermal denaturation experiment has been performed to support the intercalative nature of interaction between compound **8** and ct DNA. The melting curve indicated that upon addition of compound **8** (83.1 ^{o}C), the thermal melting temperature of ct-DNA (76 ^{o}C) increased by 7.1 ^{o}C. Therefore, both UV-visible titrations and thermal denaturation experiment designated strong intercalative binding of compound **8** into the base pairs of ct-DNA.

5.3.2.1.3 Fluorescence emission spectroscopy

To further understand the interactions, fluorescence based spectroscopic technique was employed. Studies have been implemented by keeping the concentration of compound **8** constant (20 μM) and varying the concentrations of ct-DNA (0-20 μM). The emission spectrum of compound **8** upon excitation at 400 nm exhibited a peak at 468 nm (**Figure 3a**). On increasing the concentration of ct-DNA to compound **8** resulted in enhancement of fluorescence at 468 nm, suggesting the interaction between compound **8** and ct-DNA. In order to study the enhancement process and to distinguish the possible enhancement mechanism, quantitative estimation in terms of fluorescence change has been determined using the Stern-Volmer equation.[75] Linear Stern-Volmer plot (**Figure 3b**) shows that there is only one type of binding occurred whether static or dynamic. The average fluorescence lifetime is usually 10^{-8} s[76] in the absence of DNA and therefore, the value of K_q has been found to be 1.88×10^{11} M^{-1} s^{-1} (**Table 2**). Since K_q value is much greater than typically observed dynamic enhancement (~2×10^{10} M^{-1} s^{-1}),[77] interaction probably involves the static enhancement with formation of complex at ground state. The binding constant (K_b) and the number of binding sites

(n) were analyzed by modified Stern-Volmer (MSV) equation.[78] As shown in **Figure 3c**, the values of n and K_b were calculated to be 1.44 and 1.95 × 10^5 M^{-1}, respectively (**Table 2**). ΔG_{obs} has been calculated to be -7.21 kcal mol^{-1}, indicating the favorable and spontaneous nature of binding process.

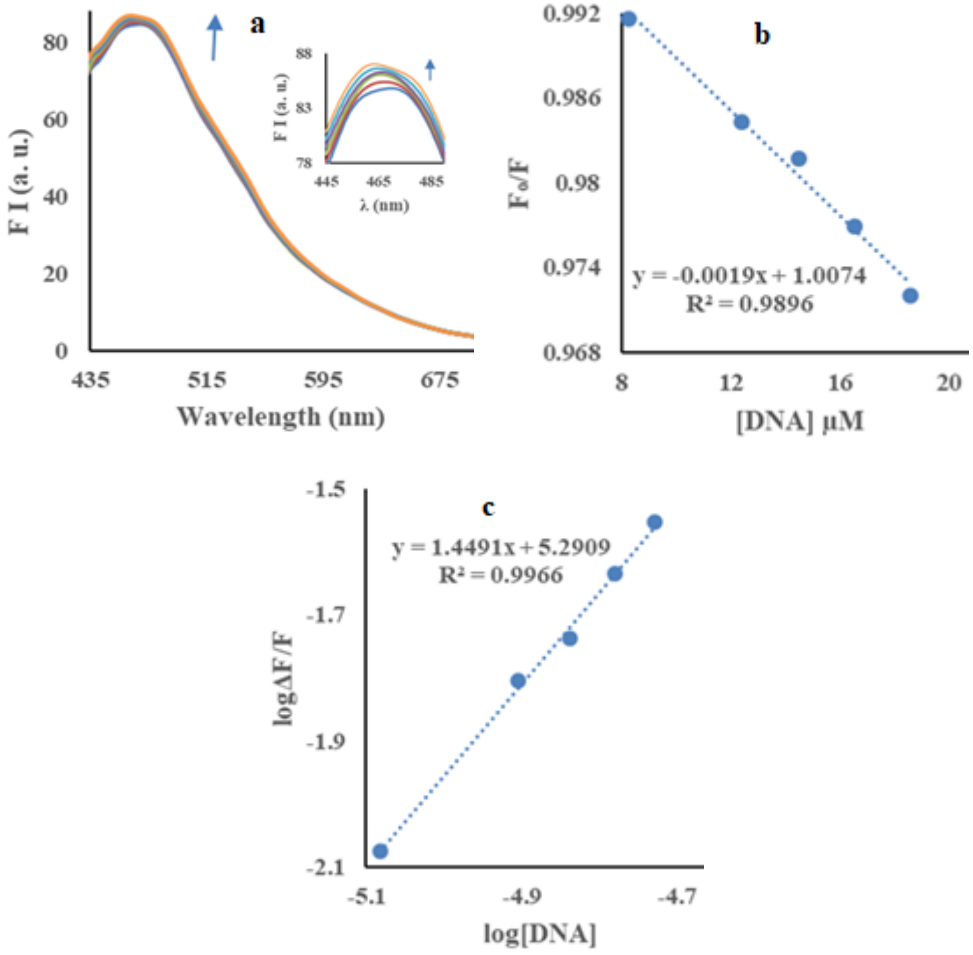

Figure 3. (a) Emission spectra of compound **8** in the presence of ct-DNA, (b) Stern-Volmer and (c) Modified Stern-Volmer plots for the observed fluorescence enhancement on addition of ct-DNA to compound **8**

Table 2. Quenching and binding parameters for the interaction of DNA and EB-DNA complex with compound **8**

	T (K)	K_{SV} (×10^4) (M^{-1})	K_q (×10^{12}) ($M^{-1}S^{-1}$)	R^2	K_b (×10^5 M^{-1})	n	R^2
DNA	298	0.188	0.188	0.9896	1.95	1.44	0.9966
EB-DNA	298	6.53	6.53	0.9958	1.00	1.05	0.9943

R^2 is correlation coefficient

5.3.2.1.4 Competitive displacement assay

Further, to confirm the intercalative mode of compound **8** with DNA, ethidium bromide (EB) competitive displacement assay was performed. The complex of EB with DNA exhibited the emission band at 600 nm. On subsequent addition of compound **8** to the EB-DNA complex, quenching in emission band at 600 nm was observed (**Figure 4a**), indicated that compound **8** displaced EB from DNA through intercalation binding mode. K_{SV} (Stern-Volmer quenching constant), K_q (bimolecular quenching constant), K_b (binding constant) and n (number of binding sites) were calculated using Stern-Volmer and modified Stern-Volmer equations and were found to the values of 6.53×10^4 M^{-1}, 6.53×10^{12} $M^{-1}s^{-1}$, 1.00×10^5 M^{-1} and 1.05, respectively (**Table 2, Figure 4b-c**).

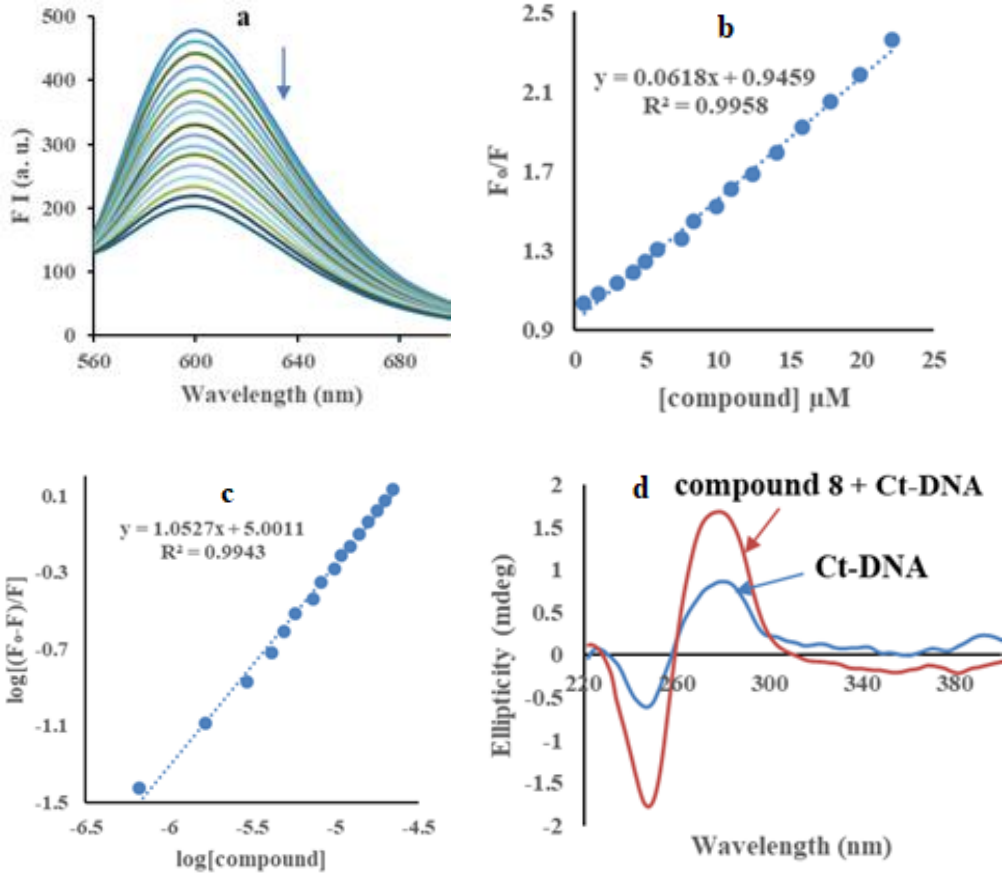

Figure 4. (a) Effect of incremental addition of compound **8** to ct-DNA-EB complex (40 μM-4 μM), (b) Stern-Volmer plot, (c) Modified Stern-Volmer plot of compound **8**-EB-ct-DNA complex and (d) CD spectrum of free ct-DNA (40 μM) (blue line) and compound **8**-ct-DNA complex (red line) at ratio $r_{[compound/ct\text{-}DNA]} = 0.025$

5.3.2.1.5 Circular dichroism (CD)

The conformational changes of ct-DNA with compound **8** were also investigated through circular dichroism (CD) spectroscopy. Upon binding to ct-DNA, compound **8** eventually acquired induced CD spectrum (ICD), from which mutual orientation of the molecule could be derived, therefore, giving useful information about modes of binding. The effect of compound **8** on conformation of secondary structure of DNA was assessed at a fixed concentration of ct-DNA (40 μM) and compound **8** (1 μM). Addition of compound **8** resulted in decrease in intensity of CD band at (λ) 250 nm and increase of CD band at (λ) 281 nm (**Figure 4d**). The induced CD (ICD) band between (λ) 300 and 400 nm has not been observed but slightly shifted towards the negative end, thus excluding binding into the minor groove of ct-DNA.[82,86] The results obtained for compound **8** together with no change in ICD band indicating the intercalative mode of binding.

5.3.2.2 Human DNA binding studies

5.3.2.2.1 UV-vis absorption spectroscopy

Compound **8** showed the highest cytotoxicity and strong intercalation with ct-DNA and thus, further used as a model to investigate the interaction with human DNA. In the UV-visible spectral analysis of **8** with human DNA, a characteristic hypochromic shift at 398 nm was observed, consistent with intercalation (**Figure 5a**). Titration experiment indicated that the examined compound showed binding constant of 5.24 x 10^6 M^{-1} (**Figure 5b**)**,** for intercalation with human DNA, that is about 2-fold greater than that with calf-thymus DNA (2.95 x 10^6 M^{-1}).

5.3.2.2.2 Fluorescence emission spectroscopy

Emission spectrum was recorded by keeping the constant concentration of compound **8** (20 μM) and varying the concentrations of human DNA (0-40 μM). Enhanced fluorescence intensity at 498 nm was obtained with increasing DNA concentration, indicating a deep intercalation of **8** with human DNA (**Figure 5c**). The values of K_{SV} and K_q were calculated using the Stern-Volmer equation and found to be 3.46 × 10^3 M^{-1} and 3.46 × 10^{11} M^{-1} s^{-1}, respectively (**Figure 5d**). Since K_q value is much greater than typically observed for dynamic enhancement (~2 × 10^{10} M^{-1} s^{-1}), interaction probably involves the static enhancement with formation of complex at ground state. The binding constant (K_b) and the number of binding sites (n) were calculated using modified Stern-Volmer equation and found to be 7.09 × 10^5 M^{-1} and 1.51, respectively (**Figure 5e**).

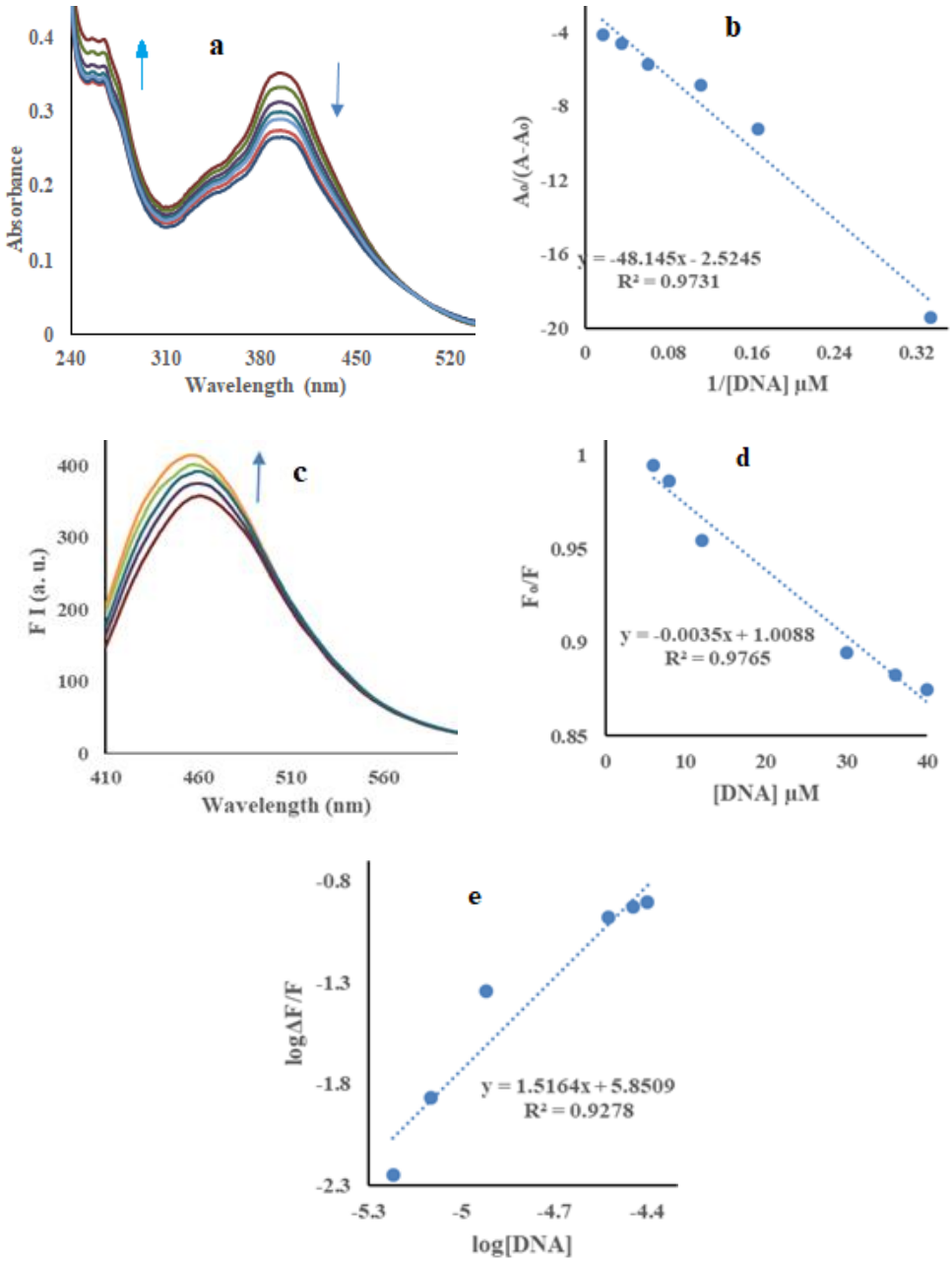

Figure 5. (a) Absorption spectra of compound **8** in the presence of the human DNA, (b) Benesi-Hildebrand plot, (c) Emission spectra of compound **8** in the presence of the human DNA, (d) Stern-Volmer plot and (e) Modified Stern-Volmer plot

5.3.3 Serum albumin binding studies

A great deal of research has been reported in the literature for the interaction of compounds with human and bovine serum albumins.[143,144] The novelty of the present study is based upon the fact that phenanthrene imidazole[145] acts as potential selective drug, which can easily transport with

serum albumin to the target site. Thus, we have analyzed the interaction between the most active compound **8** with BSA and HSA *via* absorption and emission spectroscopic methods.

5.3.3.1 Bovine serum albumin (BSA) binding studies

5.3.3.1.1 UV-vis absorption spectroscopy

Solution of bovine serum albumin shows an absorption band at 280 nm which could be assigned to the polarity of the microenvironment around tyrosine and tryptophan residues of BSA.[87] As shown in **Figure 6a**, with increasing concentration of compound **8** (0-10 μM) to the BSA solution (8 μM), the absorption intensity at 280 nm increases with generation of a new band at 400 nm. This observation confirmed that compound **8** showed worthy interaction with BSA. A relatively high binding constant of $6.57 \times 10^4\ M^{-1}$ has been calculated using Benesi-Hildebrand equation[73] (**Figure 6b**) for compound **8**-BSA system which is acceptable for drug-carrier complexes in blood.

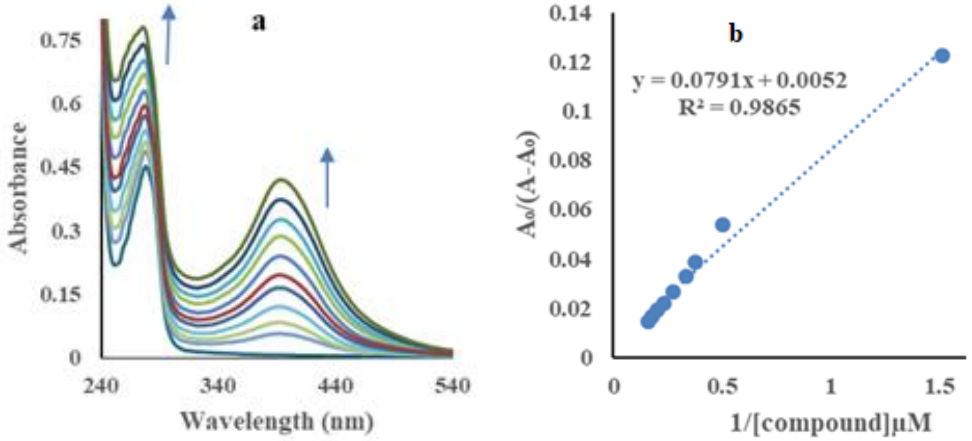

Figure 6. (a) Absorption spectra of BSA with varying concentration compound **8** in phosphate buffer and (b) Benesi-Hildebrand plot of BSA-compound **8** complex

5.3.3.1.2 Fluorescence emission spectroscopy

The interaction of BSA with compound **8** has also been evaluated by emission spectroscopy with incremental addition of compound **8** (0-10 μM) at three different temperatures (298K, 308K and 318K) (**Figure 7a-c)**. BSA exhibits an intense emission band at ~350 nm on excitation at 280 nm. With increasing concentration of compound **8**, a remarkable decrease in fluorescence intensity along with appearance of new band at 510 nm with increase in intensity was observed. These results indicated that compound **8** interacts with BSA and quenches its intrinsic fluorescence. The quenching mechanism has also been discussed with Stern-Volmer equation[75] at three different temperatures (**Figure 7d**). Stern-Volmer quenching constant (K_{SV}) and quenching rate constant

(K_q) were calculated to be in the range of 8.42-3.51 × 10^5 M^{-1} and 8.42-3.51 × 10^{13} $M^{-1}s^{-1}$, respectively at different temperatures (**Table 3**). Since the values of K_q are significant greater than typically observed dynamic quenching (~2 × 10^{10} M^{-1} s^{-1}),[77] interaction probably involves the static quenching with formation complex at ground state. The binding constant (K_b) and number of binding sites (n) could be determined using the modified Stern-Volmer analysis (**Figure 7e, Table 3**).[78] The magnitude of the binding constant has been decreased with increasing the temperature which is due to decrease in the stability of BSA-compound **8** complex system.

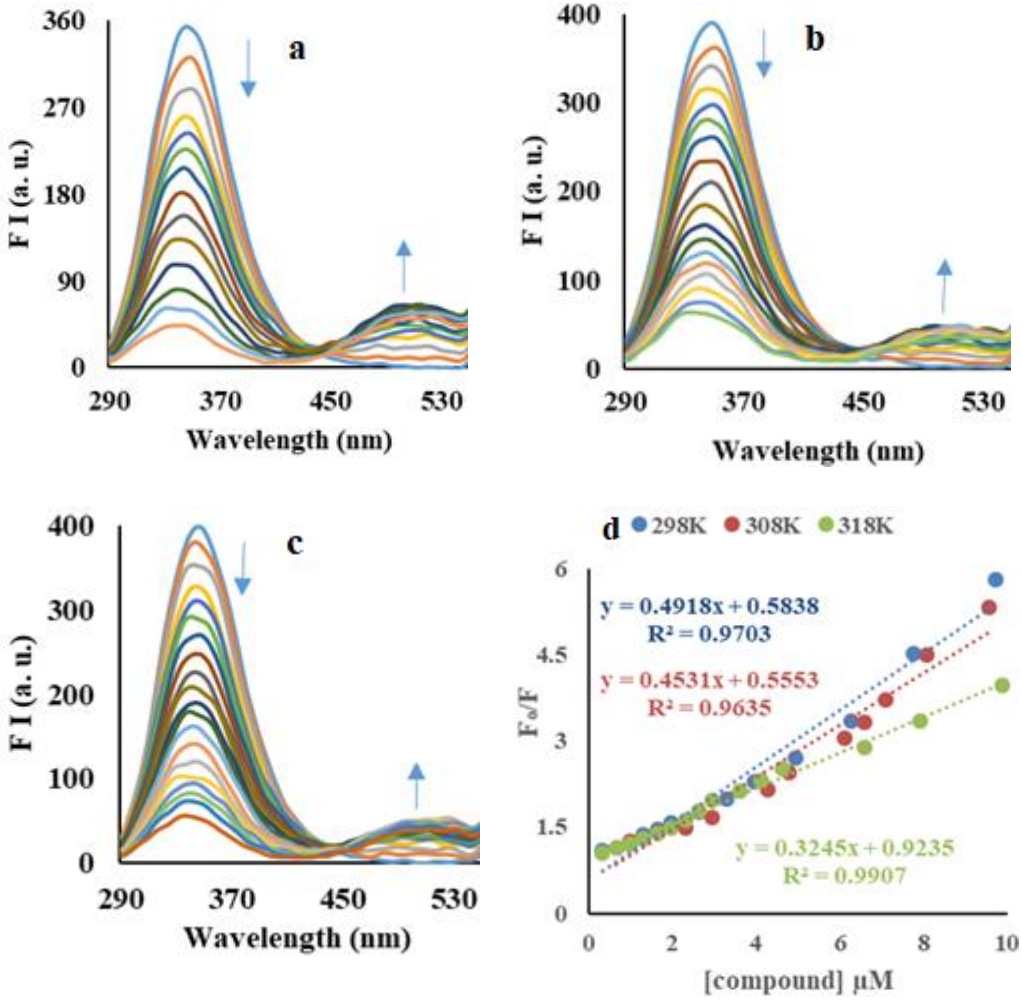

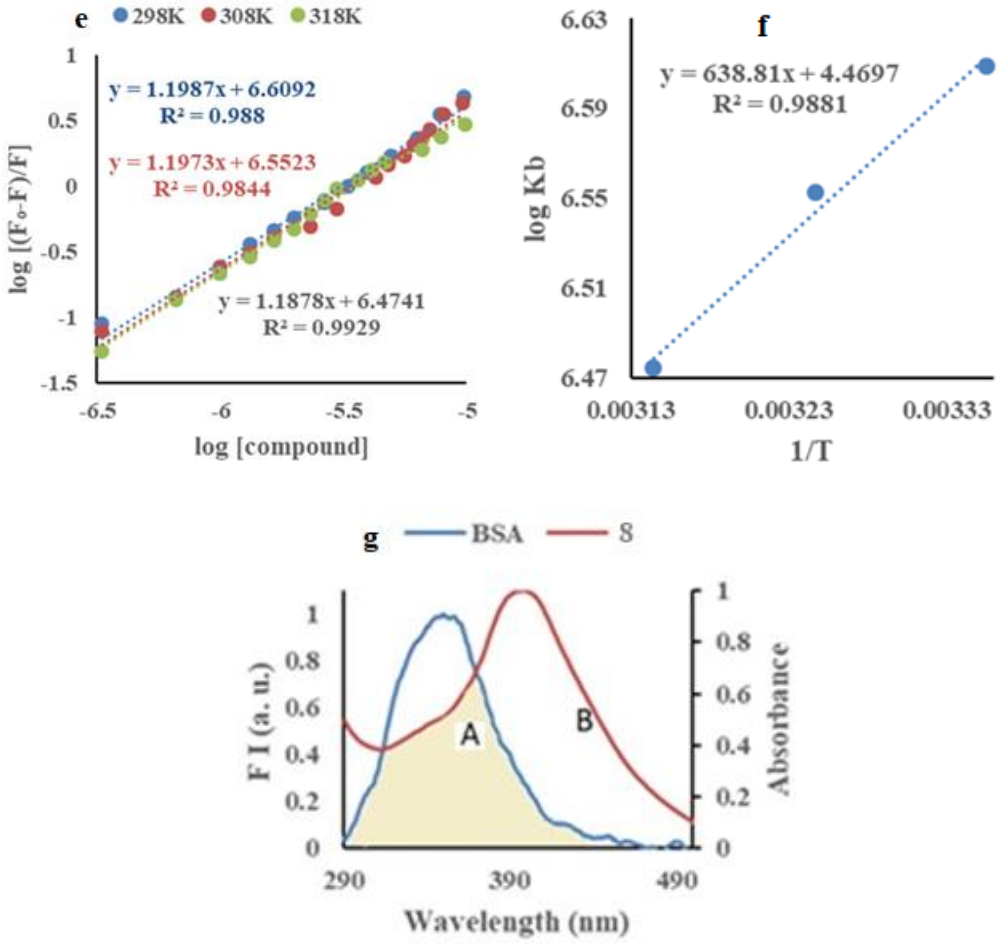

Figure 7. (a) Emission spectra of BSA with varying concentration compound **8** in phosphate buffer at different temperatures (a) 298 K, (b) 308 K, (c) 318 K, (d) Stern-Volmer plot, (e) Modified Stern-Volmer Plot, (f) Van't Hoff plot of BSA at different temperatures and (g) Overlap of the fluorescence emission spectrum of BSA (A, blue) with UV-Visible absorption spectrum of compounds **8** (B, red)

Table 3. Quenching and binding parameters for the interaction of compound **8** with BSA

T (K)	K_{SV} ($\times 10^5$) (M^{-1})	K_q ($\times 10^{13}$) ($M^{-1}S^{-1}$)	R^2	K_b ($\times 10^6$ M^{-1})	n	R^2
298	8.42	8.42	0.9703	4.06	1.19	0.9880
308	8.15	8.15	0.9635	3.56	1.19	0.9844
318	3.51	3.51	0.9907	2.97	1.18	0.9929

R^2 is the correlation coefficients

In order to identify the type of interacting forces such as van der Waals interactions, electrostatic interactions, hydrogen bonds and hydrophobic forces that acted between the

compound **8** and BSA, thermodynamic parameters *viz.*, changes in free energy (ΔG), enthalpy (ΔH) and entropy (ΔS) for the interaction have been investigated using van't Hoff equation (**Figure 7f, Table 4**). Accordingly, the negative value of ΔH showed that the process of binding is mainly enthalpy driven and involves the hydrogen bonding interaction. The positive value of ΔS indicated hydrophobic interaction as a leading action for binding of compound **8** with BSA and contributes to stability of the succeeding complex. Moreover, the negative values of ΔG at different temperatures revealed the favorable and spontaneous nature of binding process.

Table 4. Thermodynamic parameters for the binding of compound **8** to BSA at various temperatures.

T (K)	ΔH (Kcal M^{-1})	ΔS (cal M^{-1} K^{-1})	ΔG (Kcal M^{-1})	R^2
298	-2.92	20.43	-9.00	0.9881
308			-9.21	
318			-9.41	

R^2 is the correlation coefficient

5.3.3.1.3 Energy transfer of compound 8 with BSA

To further check the vicinity of derivative **8** with BSA (distance between compound and BSA), Forster's resonance energy transfer (FRET) was verified. According to FRET phenomenon, the energy transfer (E) occurs when the electronic absorption spectrum of acceptor (derivative **8**) overlaps with the emission spectrum of donor (BSA). **Figure 7g** showed overlap pattern of the emission spectrum of BSA (A) with absorption spectrum of compound **8** (B). Using $k^2 = 2/3$, $\eta = 1.336$, and $\Phi = 0.15$,[146-149] the following parameters were calculated: $J = 6.71 \times 10^{-14}$ cm^3 L mol^{-1}, $R_o = 1.10$ nm, $E = 0.61$, and $r = 1.02$ nm. Thus, the donor-to-acceptor distance (r) is smaller than 10 nm which indicated that energy transfer occurred from BSA to compound **8** with high probability.

5.3.3.2 Human serum albumin (HSA) binding studies

5.3.3.2.1 UV-vis absorption spectroscopy

UV-visible absorption spectroscopy was also used to estimate the mode of binding between compound **8** and HSA. On subsequent addition of compound **8**, the peak intensity present at 280 nm due to aromatic rings of Trp-214, Tyr-411 and Phe residues in HSA, increased with the generation and enhancement of new band at 400 nm (**Figure 8a**). The binding constant of

compound **8** and HSA has been found to be 9.35 x 10^4 M^{-1} (**Figure 8b**) which is more than that with BSA.

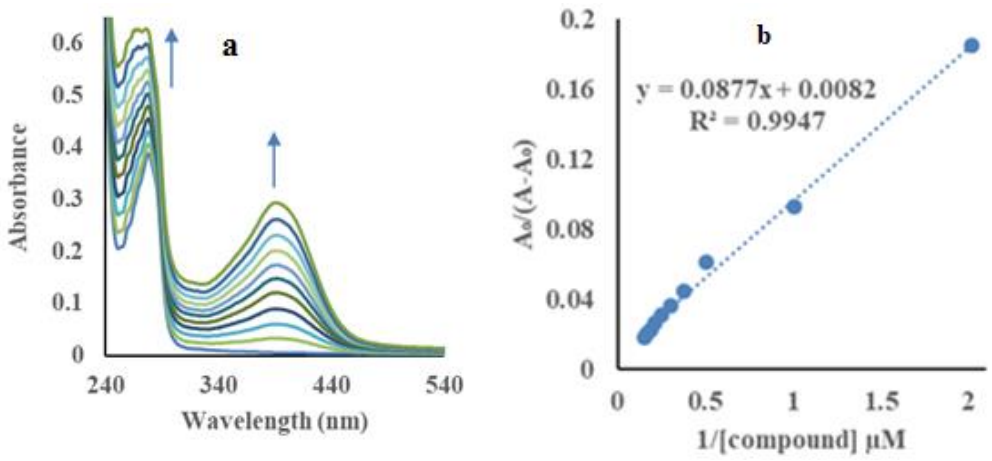

Figure 8. (a) Absorption spectrum and (b) Benesi-Hildebrand plot of HSA with varying concentration compound **8** in phosphate buffer at 298K

5.3.3.2.2 Fluorescence emission spectroscopy

Human serum albumin possesses potent fluorescence emission with a peak intensity of 348 nm corresponding to Trp-214 residue. With increasing the concentration of compound **8**, there is consistent decrease in intensity of this typical emission band (**Figure 9a**) but the maximum emission wavelength of HSA remains unchanged. This suggested that Trp-214 did not undergo any change in polarity and hence compound **8** was likely to interact *via* hydrophobic region located in HSA. The values of K_{SV} and K_q for the interaction of compound **8** with HSA were calculated to be 3.01 × 10^6 M^{-1} and 3.01 × 10^{14} $M^{-1}s^{-1}$, respectively (**Figure 9b**). The K_q value obtained at 298 K was in the range of 10^{12}-10^{14} M^{-1} s^{-1}, that exceeded the diffusion controlled rate constants of various quenchers with a biopolymer (2.0 x 10^{10} M^{-1} s^{-1}), indicated that the quenching was not initiated by the dynamic diffusion process but occurred in the static formation in **8**-HSA complex. The binding constant (K_b) and number of binding sites (n) were determined with modified Stern-Volmer analysis (**Figure 9c**) and found to be 7.29 × 10^6 M^{-1} and 1.24, respectively which showed that high affinity binding site was present in the interaction of compound **8** with HSA.

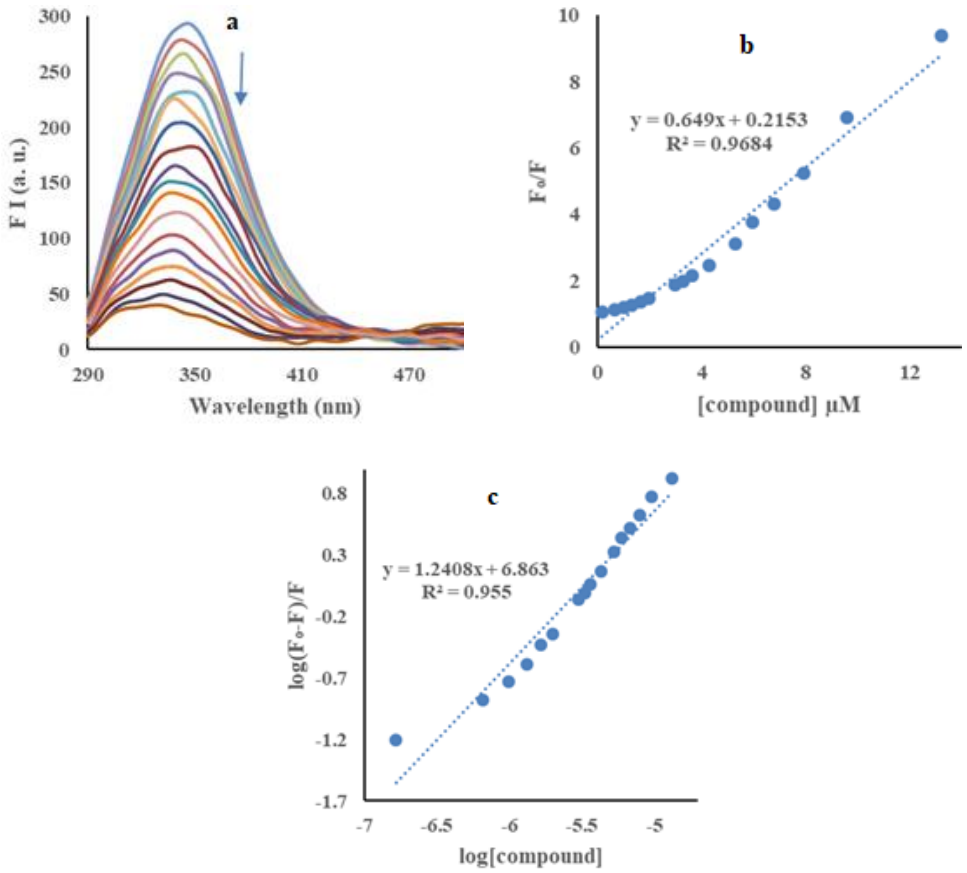

Figure 9. (a) Emission spectra of HSA with varying concentration compound **8** in phosphate buffer at 298K**,** (b) Stern-Volmer and (c) Modified Stern-Volmer Plots of HSA

5.4 Molecular docking

To understand the interaction mode and free energy of binding, molecular docking was performed using Autodock 4.0 between compound **8** and DNA (PDB ID: 1BNA).[88,89] The optimized cluster was ranked by energy level in the best conformation of ligand-DNA modeled structures, and the minimum binding energy of DNA with compound **8** has been observed as -10.6 kcal/mol (**Figure 10**). Docking of compound **8** in DNA (1BNA) showed hydrogen bonding interaction of oxygen of thiazolidine-2,4-dione with DG2 (*d* = 2.6 Å), DG4 (*d* = 3.2 Å) and DC3 (*d* = 3.3 Å) of DNA. Similarly, compound **8** also exhibited hydrogen bonding interaction of NH group of thiazolidine-2,4-dione with DC3 of DNA (*d* = 2.4 Å). NH group of phenanthroimidazole also showed interaction with DC21 of DNA, with hydrogen bonding distance of 2.7 Å (**Table 5**).

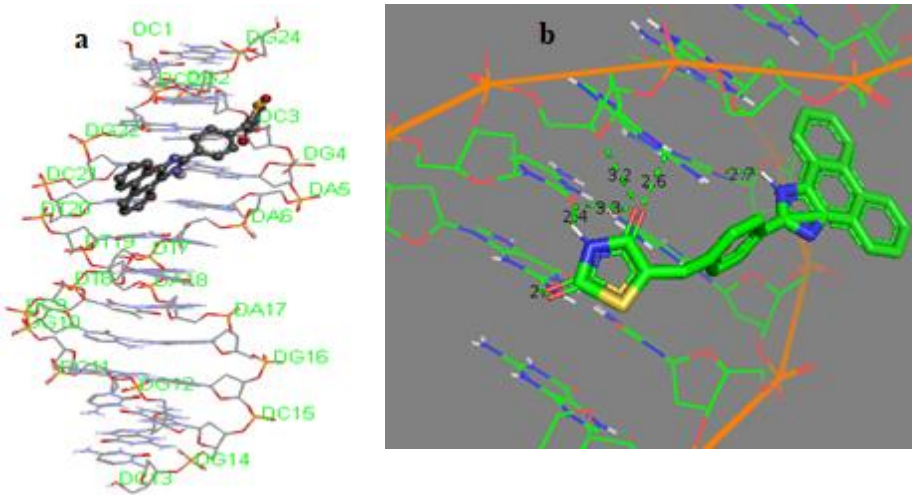

Figure 10. Docked poses of compound **8** bound to DNA (PDB ID: 1BNA). (a) Lowest energy conformation; (b) H-bonding interactions between compound **8** and DNA

Table 5. The hydrogen bonding of compounds **8** with DNA docked into 1BNA

Ligand	DNA	H-Bonding (Å)
Oxygen of thiazolidine-2,4-dione ring	DG2	2.6
Oxygen of thiazolidine-2,4-dione ring	DG4	3.2
Oxygen of thiazolidine-2,4-dione ring	DC3	3.3
NH of thiazolidine-2,4-dione ring	DC3	2.4
NH of phenanthroimidazole	DC21	2.7

5.5 Conclusion

A series of 1*H*-phenanthro[9,10-*d*]imidazole/oxazole and 7*H*-acenaphtho[1,2-*d*]imidazole were synthesized and evaluated for cytotoxicity. Compound **8** with thiazolidine moiety at C-2 position of 1*H*-phenanthro[9,10-*d*]imidazole exhibited better growth inhibitory activity for most of the cancer cell panels than other derivatives. In addition, MTT assay was used for the evaluation of the cytotoxicity effects of the compound **8** which showed 90% inhibition to cancer cell lines and only 15% inhibition to normal cells at high dose concentration. The specific interaction of compound **8** with calf thymus and human DNA displayed that compound **8** could intercalate into DNA to form **8**-DNA complex which might further block DNA replication to exert their powerful antiproliferative activity. Binding investigations revealed that HSA and BSA could generate fluorescent quenching by **8** as a result of formation of ground-state complexes, and the calculated

parameters indicated that the binding process was spontaneous. Hydrophobic interactions and hydrogen bonds played an important role in the binding of compound **8** to serum albumins, while electrostatic interactions might also be involved in the binding process. The binding constant values also revealed that compound **8** showed better interactions with human DNA and HSA than their respective calf thymus DNA and BSA. These initial promising outcomes of antiproliferative activity and docking of active compound can present promising frameworks in the area of medicinal chemistry and might lead to discovery of strong anti-tumour candidates.

5.6 Experimental section

Melting points were observed in open capillaries and were uncorrected. All commercially available compounds (Spectrochem, Aldrich, Merck etc.) were used without further purification. ^{1}H and ^{13}C NMR spectra were performed on Jeol ECS 400 NMR spectrometer, operated at 400 MHz for ^{1}H nuclei and 100 MHz for ^{13}C nuclei, using $CDCl_3$ and DMSO-d_6 as solvents. Chemical shifts are reported in parts per million (ppm) with TMS as an internal reference. Mass spectra of the synthesized compounds were observed at Water Micromass-Q-T of Micro. CHN analyses have been done with Thermo Scientific (Flash 2000) analyser. Reactions were examined with thin layer chromatography (TLC) and silica plate coated with silica gel HF-254 and column chromatography was executed with silica gel 60-120/100-200 mesh. Hexane/ethyl acetate and chloroform/methanol were the implemented solvent systems. Absorption and emission spectra have been measured with 1 cm quartz cell. UV-Visible spectra were recorded on Shimadzu-2400 PC spectrometer. Emission spectra were recorded with Varian Cary Eclipse fluorescence spectrometer.

2-(Subsitituted aryl)-1*H*-phenanthro[9,10-*d*]imidazole/oxazole (3a-h and 4a-c): Substituted benzaldehyde (1 mmol), 9,10-phenanthroquinone (1 mmol) and ammonium acetate (10 mmol) in acetic acid were heated at 100 ^{o}C for 2-5 h. After completion of reaction, solution was quenched with water; precipitated solid was filtered and washed with water. The crude product was further purified with column chromatography using hexane:ethyl acetate as eluents.

2-Phenyl-1*H*-phenanthro[9,10-*d*]imidazole (3a): Compound **3a** was prepared according to the general procedure, and the title compound was isolated as light brown solid (55% yield). Spectral data obtained were in good agreement with those reported in literature.[150]

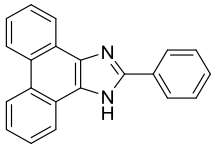

2-(1*H*-*P*henanthro[9,10-*d*]imidazol-2-yl)phenol (3b): Compound **3b** was prepared according

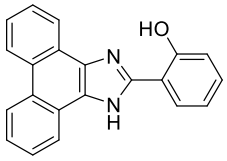

to the general procedure, and the title compound was isolated as white solid (53% yield). Spectral data obtained were in good agreement with those reported in literature.[151]

5-(Diethylamino)-2-(1*H*-phenanthro[9,10-*d*]imidazol-2-yl)phenol (3c): Compound **3c** was

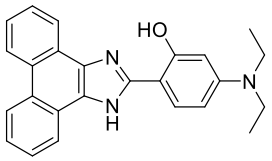

prepared according to the general procedure, and the title of compound was isolated as light brown solid (54% yield). Spectral data obtained were in good agreement with those reported in literature.[140]

1-(1*H*-Phenanthro[9,10-*d*]imidazol-2-yl)naphthalen-2-ol (3d): Light brown solid; yield 61%;

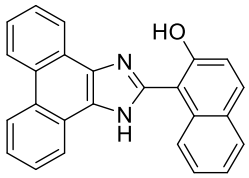

mp 191-193 ^{o}C; ^{1}H NMR ($CDCl_3$, 400 MHz): δ (ppm) 8.77 (d, *J* = 8.36 Hz, 2H, ArH), 8.64 (d, *J* = 8.40 Hz, 2H, ArH), 8.55 (d, *J* = 8.40 Hz, 1H, ArH), 7.88 (t, *J* = 6.84 Hz, 2H, ArH), 7.73-7.61 (m, 5H, ArH), 7.44-7.37 (m, 2H, ArH); ^{13}C NMR ($CDCl_3$, 100 MHz): δ (ppm) 155.9, 147.3, 130.9, 130.4, 128.1, 127.9, 127.6, 126.9, 126.5, 124.8, 123.8, 122.9, 122.8, 121.8, 118.6, 106.3 (ArC); MS (ESI): m/z 361.3 (M^++1); Anal Calcd for $C_{25}H_{16}N_2O$: C, 83.31; H, 4.47; N, 7.77; found C, 83.20; H, 4.45; N, 7.81.

4-Bromo-2-(1*H*-phenanthro[9,10-*d*]imidazol-2-yl)phenol (3e): Brownish solid; yield 65%; mp

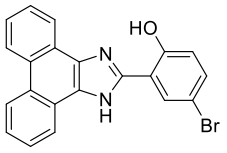

191-193 ^{o}C; ^{1}H NMR ($CDCl_3$ + DMSO-d_6, 400 MHz): δ (ppm) 8.80 (t, *J* = 9.92 Hz, 2H, ArH), 8.53 (t, *J* = 8.40 Hz, 2H, ArH), 8.44 (d, *J* = 2.28 Hz, 1H, ArH), 7.75 (t, *J* = 7.64 Hz, 2H, ArH), 7.68-7.63 (m, 2H, ArH), 7.43 (dd, ^{2}J = 8.40 Hz, ^{3}J = 2.28 Hz, 1H, ArH), 7.01 (d, *J* = 8.40 Hz, 1H, ArH); ^{13}C NMR ($CDCl_3$ + DMSO-d_6, 100 MHz): δ (ppm) 171.9, 156.6, 147.7, 132.8, 127.9, 127.5, 127.0, 126.8, 126.3, 125.6, 125.3, 123.7, 123.3, 121.9, 121.7, 121.6, 119.1, 114.7, 110.0 (ArC); MS (ESI): m/z 391.5 (M^++1); Anal Calcd for $C_{21}H_{13}BrN_2O$: C, 64.80; H, 3.37; N, 7.20; found C, 64.51; H, 3.55; N, 7.11.

2-(Pyren-1-yl)-1*H*-phenanthro[9,10-*d*]imidazole (3f): Compound **3f** was prepared according

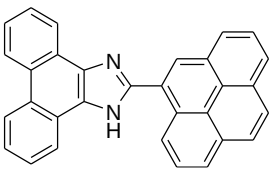

to the general procedure, and the title of compound was isolated as pale yellow solid (45% yield). Spectral data obtained were in good agreement with those reported in literature.[152]

(3-Hydroxy-4-(1*H*-phenanthro[9,10-*d*]imidazol-2-yl)phenyl)boronic acid (3g): Brownish solid; yield 60%; mp 278-281 ^{o}C ^{1}H NMR ($CDCl_3$ + DMSO-d_6, 400 MHz): δ (ppm) 8.75 (d, *J* =

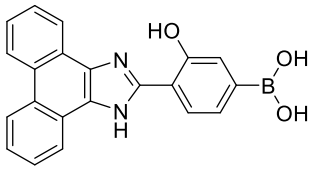

7.64 Hz, 2H, ArH), 8.66 (d, *J* = 6.88 Hz, 2H, ArH), 8.32 (d, *J* = 8.40 Hz, 2H, ArH), 8.05 (d, *J* = 8.40 Hz, 2H, ArH), 7.83 (t, *J* = 7.40 Hz, 1H, ArH), 7.72 (t, *J* = 6.84 Hz, 2H, ArH); ^{13}C NMR ($CDCl_3$ + DMSO-d_6, 100 MHz): δ (ppm) 149.6, 134.9, 131.8, 130.2, 128.1, 127.2, 125.5, 124.3, 124.2, 123.8, 122.4 (ArC); MS (ESI): m/z 355.2 (M^++1); Anal Calcd for $C_{21}H_{15}BN_2O_3$: C, 71.22; H, 4.27; N, 7.91; found C, 71.29; H, 4.22; N, 7.78.

4-(1*H*-Phenanthro[9,10-*d*]imidazol-2-yl)benzaldehyde (3h): Compound **3h** was prepared according to the general procedure, and the title of compound was isolated as yellow solid (62% yield). Spectral data obtained were in good agreement with those reported in literature.[141]

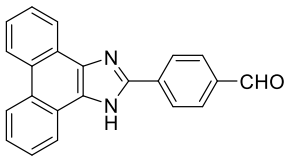

2-Phenylphenanthro[9,10-*d*]oxazole (4a): Compound **4a** was prepared according to the general procedure, and the title of compound was isolated as light brown solid (30% yield). Spectral data obtained were in good agreement with those reported in literature.[153]

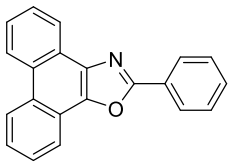

2-(Phenanthro[9,10-*d*]oxazol-2-yl)phenol (4b): Light brown solid; yield 25%; mp 255-258 ^{o}C; ^{1}H NMR ($CDCl_3$, 400 MHz): δ (ppm) 11.55 (s, 1H, OH), 8.74 (t, *J* = 8.24 Hz, 2H, ArH), 8.49 (d, *J* = 7.80 Hz, 1H, ArH), 8.33 (d, *J* = 7.80 Hz, 1H, ArH), 8.16-8.14 (m, 1H, ArH), 7.77-7.67 (m, 4H, ArH), 7.48-7.44 (m, 1H, ArH), 7.19 (d, *J* = 8.68 Hz, 1H, ArH), 7.09-7.05 (m, 1H, ArH); ^{13}C NMR ($CDCl_3$ + DMSO-d_6, 100 MHz): δ (ppm) 161.3, 157.4, 142.9, 132.9, 128.8, 128.5, 127.4, 126.7, 126.4, 124.4, 123.6, 123.4, 122.3, 120.5, 120.0, 119.6, 116.9, 110.5 (ArC); MS (ESI): m/z 312.3 (M^++1); Anal Calcd for $C_{21}H_{13}NO_2$: C, 81.01; H, 4.21; N, 4.50; found C, 81.12; H, 4.26; N, 4.55.

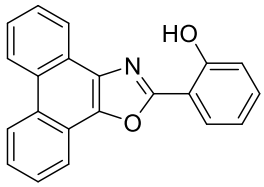

5-(Diethylamino)-2-(phenanthro[9,10-*d*]oxazol-2-yl)phenol (4c): Light brown solid; yield 32%; mp 281-283 ^{o}C; ^{1}H NMR ($CDCl_3$, 400 MHz): δ (ppm) 11.51 (s, 1H, OH), 8.77 (m, 2H, ArH), 8.51 (d, *J* = 7.36 Hz, 1H, ArH), 8.33 (d, *J* = 7.80 Hz, 1H, ArH), 7.96 (d, *J* = 8.72 Hz, 1H, ArH), 7.77-7.66 (m, 4H, ArH), 6.42 (d, *J* = 10.96 Hz, 1H, ArH), 6.36 (d, *J* = 2.32 Hz, 1H, ArH), 3.48 (q, *J* = 6.84 Hz, 4H, CH_2-ethyl), 1.28 (t, *J* = 14.20 Hz, 6H, CH_3-ethyl); ^{13}C NMR ($CDCl_3$ + DMSO-d_6, 100 MHz): δ (ppm) 159.1, 150.5, 149.8, 127.5, 126.8, 124.9,

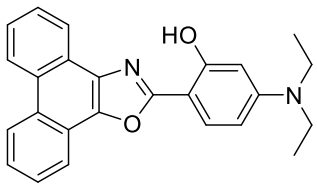

123.4, 121.9, 103.4, 101.0, 98.0 (ArC), 44.1 (CH_2-ethyl), 12.6 (CH_3-ethyl); MS (ESI): m/z 383.2 (M^++1); Anal Calcd for $C_{25}H_{22}N_2O_2$: C, 78.51; H, 5.80; N, 7.32; found C, 78.78; H, 5.65; N, 7.16.

2-((4-(1*H*-Phenanthro[9,10-*d*]imidazol-2-yl)benzylidene)amino)-1*H*-benzo[*de*]isoquinoline-1,3(2*H*)-dione (6) and 5-(4-(1*H*-phenanthro[9,10-*d*]imidazol-2-yl)benzylidene)thiazolidine-2,4-dione (8): Mixture of 4-(1*H*-phenanthro[9,10-*d*]imidazol-2-yl)benzaldehyde (**3h**) (200 mg, 621 mmol) and 2-amino-1*H*-benzo[*de*]isoquinoline-1,3(2*H*)-dione (**5**) (131 mg, 621 mmol) or thiazolidine-2,4-dione (**7**) (73 mg, 621 mmol) in ethanol was refluxed for 3-4 h. Precipitated solid product was filtered and then washed with ethanol.

2-((4-(1*H*-Phenanthro[9,10-*d*]imidazol-2-yl)benzylidene)amino)-1*H*-benzo[*de*]isoquinoline-1,3(2*H*)-dione (6): Yellow solid; yield 62%; mp 291-293 ^oC; ^1H NMR ($CDCl_3$ + DMSO-d_6, 400

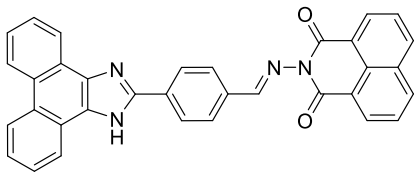

MHz): δ (ppm) 10.06 (s, 1H, CH=N), 8.80-8.76 (m, 3H, ArH), 8.60 (t, *J* = 6.88 Hz, 2H, ArH), 8.53-8.48 (m, 3H, ArH), 8.42 (d, *J* = 7.64 Hz, 1H, ArH), 8.37 (d, *J* = 8.40 Hz, 1H, ArH), 8.19 (d, *J* = 8.40 Hz, 1H, ArH), 8.09 (d, *J* = 8.40 Hz, 1H, ArH), 7.85-7.78 (m, 2H, ArH), 7.73-7.68 (m, 2H, ArH), 7.66-7.61 (m, 2H, ArH); ^{13}C NMR ($CDCl_3$ + DMSO-d_6, 100 MHz): δ (ppm) 171.5 (C=N), 160.8 (C=O), 147.9, 135.1, 135.0, 133.9, 131.8, 131.6, 131.3, 130.7, 129.9, 128.5, 127.9, 127.8, 127.6, 127.3, 126.6, 124.5, 124.0, 122.7 (ArC); MS (ESI): m/z 517.1 (M^++1); Anal Calcd for $C_{34}H_{20}N_4O_2$: C, 79.06; H, 3.90; N, 10.85; found C, 79.01; H, 3.65; N, 10.86.

(*Z*)-5-(4-(1*H*-Phenanthro[9,10-*d*]imidazol-2-yl)benzylidene)thiazolidine-2,4-dione (8):

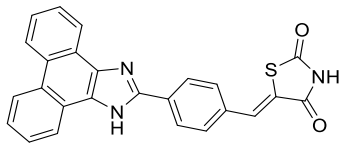

Radish solid; yield 60%; mp 283-286 ^oC; ^1H NMR ($CDCl_3$ + DMSO-d_6, 400 MHz): δ (ppm) 8.86 (d, *J* = 8.40 Hz, 2H, ArH), 8.56 (d, *J* = 6.88 Hz, 2H, ArH, NH), 8.43 (d, *J* = 8.40 Hz, 2H, ArH), 7.84 (s, 1H, CH=C), 7.81 (d, *J* = 8.40 Hz, 2H, ArH), 7.76 (t, *J* = 6.60 Hz, 2H, ArH), 7.66 (t, *J* = 7.64 Hz, 2H, ArH); ^{13}C NMR ($CDCl_3$ + DMSO-d_6, 100 MHz): δ (ppm) 167.9, 167.5 (CO), 148.1, 134.5, 133.5, 131.6, 131.0, 130.7, 127.8, 127.3 126.6, 125.6, 124.0, 122.1 (ArC); MS (ESI): m/z 422.1 (M^++1); Anal Calcd for $C_{25}H_{15}N_3O_2S$: C, 71.24; H, 3.59; N, 9.97; S, 7.61; found C, 71.11; H, 3.72; N, 9.71; S, 7.68.

(2-(4-(1*H*-Phenanthro[9,10-*d*]imidazol-2-yl)phenyl)-1*H*-benzo[*d*]imidazol-5-yl)(phenyl)methanone (10) and 2-(4-(1*H*-phenanthro[9,10-*d*]imidazol-2-yl)phenyl)-3*H*-

anthra[1,2-*d*]imidazole-6,11-dione (12): 4-(1*H*-Phenanthro[9,10-*d*]imidazol-2-yl)benzaldehyde (**3h**) (200 mg, 0.621 mmol) and (3,4-diaminophenyl)(phenyl)methanone (**9**) (131 mg, 0.621 mmol) or 1,2-diaminoanthracene-9,10-dione (**11**) (147 mg, 0.621 mmol) was heated in nitrobenzene at 60 ^{o}C for 2 h. Reaction was then quenched with 50 ml diethyl ether. Precipitated solid product was filtered and washed with diethyl ether. Crude product was purified with column chromatography using ethyl acetate and hexane.

(2-(4-(1*H*-Phenanthro[9,10-*d*]imidazol-2-yl)phenyl)-1*H*-benzo[*d*]imidazol-6-yl)(phenyl)methanone (10): Brown solid; yield 65%; mp 278-281 ^{o}C; ^{1}H NMR ($CDCl_3$ + DMSO-

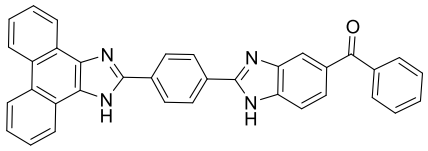

d$_6$, 400 MHz): δ (ppm) 8.75 (d, *J* = 7.64 Hz, 2H, ArH), 8.65 (m, 2H, ArH), 8.54 (d, *J* = 8.40 Hz, 2H, ArH), 8.43 (d, *J* = 8.40 Hz, 2H, ArH), 7.82-7.80 (m, 3H, ArH), 7.73-7.68 (m, 3H, ArH), 7.65-7.61 (m, 4H, ArH), 7.56 (t, *J* = 7.64 Hz, 2H, ArH); ^{13}C NMR ($CDCl_3$ + DMSO-*d*$_6$, 100 MHz): δ (ppm) 195.7 (CO), 148.1, 137.9, 131.8, 131.4, 131.0, 129.4, 129.2, 127.7, 127.5, 126.8, 126.4, 126.2, 126.1, 124.8, 124.7, 123.0, 121.8 (ArC); MS (ESI): m/z 515.8 (M^++1); Anal Calcd for $C_{35}H_{22}N_4O$: C, 81.69; H, 4.31; N, 10.89; found C, 81.82; H, 4.29; N, 10.71.

2-(4-(1*H*-Phenanthro[9,10-*d*]imidazol-2-yl)phenyl)-3*H*-anthra[1,2-*d*]imidazole-6,11-dione (12): Compound 12 was prepared according to the general procedure, and the title of product

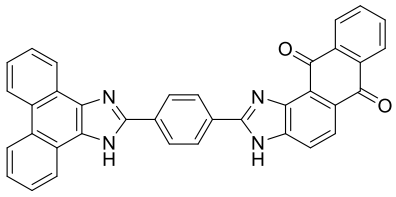

was isolated as cremish white solid (61% yield). Spectral data obtained were in good agreement with those reported in literature.[154]

1,2-Diphenyl-1*H*-phenanthro[9,10-*d*]imidazole (14). The title compound **14** was synthesized

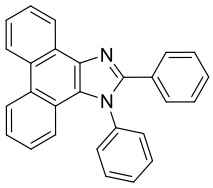

according to the reported procedure from reaction of diketone (**1**), benzaldehyde (**2a**), aniline (**13**) and ammonium acetate in acetic acid and the product was isolated as white solid (57% yield). Spectral data obtained were in good agreement with those reported in literature.[156]

2-(7-Phenyl-7*H*-acenaphtho[1,2-*d*]imidazol-8-yl)phenol (16): Acenaphthylen-1,2-dione (**15**) (200 mg, 1.09 mmol) was slowly added to the mixture of salicylaldehyde (**2b**) (133 mg, 1.09 mmol), aniline (**13**) (101 mg, 1.09 mmol) and ammonium acetate (740 mg, 9.6 mmol) in glacial acetic acid. Reaction mixture was stirred and heated at 100 ˚C for 12 h. On cooling, the solution

was quenched with water and then filtered the precipitated solid. The crude product was further dried and purified using column chromatography using hexane and ethyl acetate as eluents.

2-(7-Phenyl-7*H*-acenaphtho[1,2-*d*]imidazol-8-yl)phenol (16): Brownish solid; yield 64%; mp

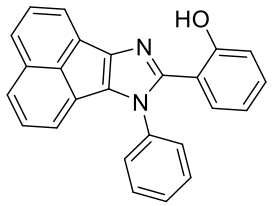

277-280 ^{o}C; ^{1}H NMR ($CDCl_3$, 400 MHz): δ (ppm) 8.00 (dd, ^{2}J = 8.24 Hz, ^{3}J = 1.84 Hz, 2H, ArH), 7.90 (d, J = 6.64 Hz, 2H, ArH), 7.84 (t, J = 3.68 Hz, 2H, ArH), 7.81 (d, J = 7.32 Hz, 2H, ArH), 7.61-7.56 (m, 3H, ArH), 7.41-7.37 (m, 2H, ArH), 7.13 (d, J = 8.24 Hz, 1H, ArH), 7.03-6.99 (m, 1H, ArH); ^{13}C NMR ($CDCl_3$, 100 MHz): δ (ppm) 157.9, 148.4, 144.7, 138.2, 131.6, 130.4, 130.1, 129.6, 129.5, 127.9, 127.4, 127.0, 126.9, 126.7, 126.4, 125.9, 121.2, 119.2, 118.1, 117.8, 113.7 (ArC); MS (ESI): m/z 361.7 (M^{+}+1); Anal Calcd for $C_{25}H_{16}N_2O$: C, 83.31; H, 4.47; N, 7.77; found C, 83.39; H, 4.24; N, 7.43.

4-(7*H*-Acenaphtho[1,2-*d*]imidazol-8-yl)benzaldehyde (17): A mixture of terephthaldehyde (**2h**) (147 mg, 1.09 mmol), acenaphthylen-1,2-dione (**15**) (200 mg, 1.09 mmol) and ammonium acetate (840 mg, 10.09 mmol) in glacial acetic acid (5 mL) was heated for 30 min to 100 ^{o}C. Reaction mixture was cooled and quenched with water. Solid was filtered and washed with excess of water. The crude was further dried, and then purified with column chromatography using hexane:ethyl acetate as eluents to get the pure product.

4-(7*H*-Acenaphtho[1,2-*d*]imidazol-8-yl)benzaldehyde (17): Brown solid; yield 52%; mp 285-

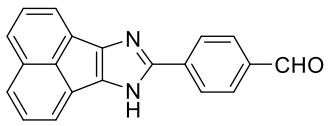

288 ^{o}C; ^{1}H NMR ($CDCl_3$ + DMSO-d_6, 400 MHz): δ (ppm) 10.03 (s, 1H, CHO), 8.27 (d, J = 8.24 Hz, 2H, ArH), 7.97 (d, J = 8.68 Hz, 2H, ArH), 7.74 (d, J = 8.24 Hz, 4H, ArH), 7.57 (d, J = 8.24 Hz, 2H, ArH); MS (ESI): m/z 297.5 (M^{+}+1); Anal Calcd for $C_{20}H_{12}N_2O$: C, 81.07; H, 4.08; N, 9.45; found C, 81.21; H, 4.09; N, 9.44.

CHAPTER 6
HYBRIDS OF NAPHTHALIMIDE, BENZOTHIAZOLE AND INDOLE

6.1 Introduction

With the changes in climate, cancer is becoming a major problem in public health. Cancer can be described as abnormal and uncontrolled growth of cells which spread to nearby organs by circulatory system.[156,157] A standard antitumor drug should selectively express cytotoxicity for cancer cells without harming normal cells, otherwise it led to severe side effects.[158] Existing cancer therapies i.e. radiotherapy, surgery and chemotherapy become ineffective due to multidrug resistance. Also, current drugs for cancer therapies have several problems like poor oral bioavailability and pharmacodynamic properties.[159] Moreover, different kinds of cancers can't be cured with single anticancer drug, particularly at late-stage of disease.[160,161] These situations are motivating the researchers to develop new drug candidates with necessary characteristics of cancer chemotherapy with least side effects and higher therapeutic effect with minimum doses. Compounds comprising heteroatoms show wide range of properties and application and well-studied for various biological activity. Nearly about 60% available cancer drugs contain heterocyclic moieties.[162,163]

Naphthalimde compounds are group of well-established DNA intercalators and some compounds (Amonafide, Mitonafide and UNBS5162) have reached in different phases of clinical trials (**Figure 1**). UNBS5162, a potent anticancer agent, was enter in phase I trial but terminated because of its unexpected prolonged QTc intervals.[165] These results showed that naphthalimide derivatives are potential anticancer agent and alterations in side chain, as well as change in substituents on the ring of naphthalimide moiety can improve selectivity and safety.[109,166,167]

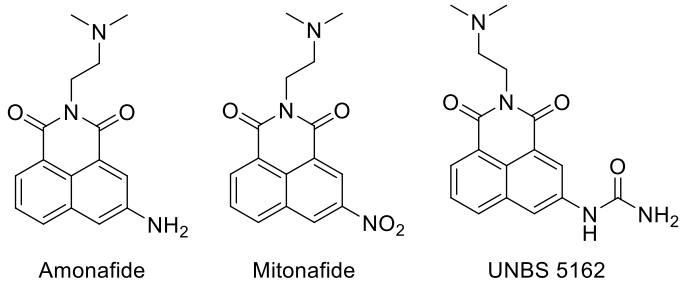

Figure 1. Naphthalimide based anticancer agents

Benzothiazole moiety based compounds were reported to show an extensive varieties of biological activities.[168-177] These benzothiazole compounds exhibited excellent anticancer activity.[178-180] Structure-activity relationships (SAR) for benzothiazole derivatives displayed that substitution of phenyl ring with alkyl as well as aryl chains improved the cytotoxicity towards cancer cell lines (**Figure 2**).[181,182]

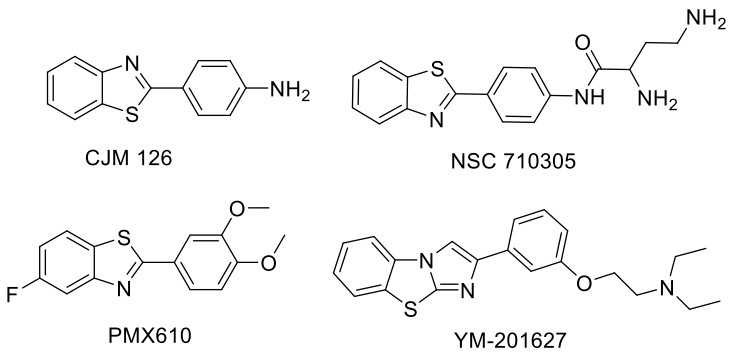

Figure 2. Some clinical benzothiazole based anticancer drugs

Indole based heterocyclic compounds also gained significant attention due to their wide range of biological activity and pharmacological properties.[183] Several indole derivatives were found as potent anticancer agents[184-186] as well as the presence of indole in numerous derivatives, were used in antimalarial,[187-189] antitubercular,[190,191] antimicrobial, [192a-b] and antiinflammatory[193-195] activities. Vincristine and vinblastine, potential anticancer agents are the indole based inhibitors of tubulin protein increase the importance of indole scaffold in anticancer field (**Figure 3**).[36,196a-b]

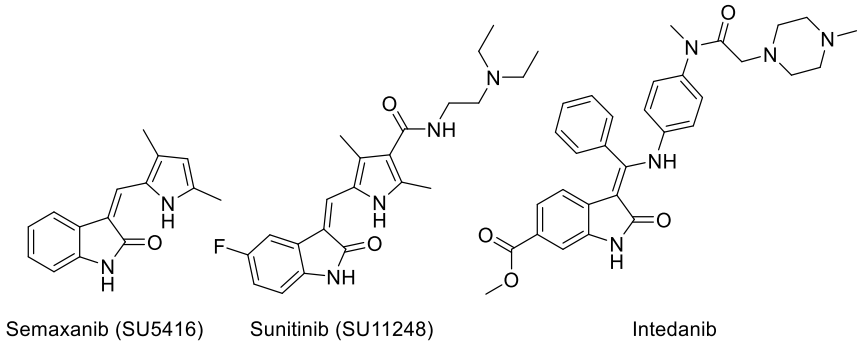

Figure 3. Some commercial anticancer drugs with indole moiety

As a result of interesting biological activities with heterocyclic scaffolds of naphthalimide, benzothiazole and indole, we decided to develop a new series of conjugates by comprising these three pharmacophoric moieties in a single molecule. The synthesized derivatives possessed variable substitutions, which were planned to achieve the aim of the target cytotoxicity.These newly synthesized compounds were characterized by NMR and mass spectrometry and further

evaluated for their cytotoxicity against human cancer cell lines A549 (lung), MCF7 (breast) and HeLa (cervix), and normal cell lines Hek293 (Kidney).

6.2 Chemistry

Conjugates of indole, benzothiazole and naphthalimide were synthesized as depicted in **Scheme 1**. Commercially available 5-bromo indole **1** was subjected to react with Vilsmeier-Haack reagent ($POCl_3$ and DMF) to get 5-bromo-1*H*-indole-3-carbaldehyde **2**. Singlet at δ 9.97 ppm in ^{1}H NMR spectrum and signal at δ 184.9 ppm in ^{13}C NMR spectrum corresponding to proton and carbon of carbaldehyde, respectively, confirmed the formation of **2**. Compound **2** was then treated with allyl bromide in acetone- NaOH (aq.) at room temperature to give brown color solid of 1-allyl-5-bromo-1*H*-indole-3-carbaldehyde **3** in 86% yield. Characteristic signals of allyl group (multiplet of one proton at δ 6.04-5.94 ppm representing CH of allyl, two doublets of two protons at δ 5.33 and 5.18 ppm representing CH_2 of allyl and multiplet of two protons at δ 4.76-4.74 ppm representing N-CH_2 of allyl) confirmed the formation of compound **3**. Further, compound **3** was reacted with 2-aminothiophenol in the presence of nitrobenzene at 80 °C for 8 h afforded reddish color solid of 2-(1-allyl-5-bromo-1*H*-indol-3-yl)benzo[*d*]thiazole **4** in 62% yield. Formation of compound **4** was confirmed by the disappearance of carbaldehyde singlet at δ 9.97 ppm in ^{1}H NMR spectrum and appearance of four protons of benzothiazole ring in the range of δ 8.62-7.24 ppm. Boronate of compound **4** was synthesized using bis(pinacolato)diboron in the presence of bis(triphenylphosphine)palladium chloride and potassium acetate in refluxing dioxane for 3 h. Compound **5** was further subjected to Suzuki-Miyaura cross coupling with 6-bromo-1*H*,3*H*-benzo[*de*]isochromene-1,3-dione **6**. Suzuki coupling gave the light yellow colored solid of 6-(1-allyl-3-(benzo[*d*]thiazol-2-yl)-1*H*-indol-5-yl)-1*H*,3*H*-benzo[*de*]isochromene-1,3-dione **7** in the presence of tetrakis(triphenylphosphine) palladium (0) and potassium carbonate in acetonitrile-water conditions. The ^{1}H NMR spectrum of compound **7** revealed the presence of signals of naphthalimide moiety in the range of δ 8.72-7.32 ppm. The mass spectrum of compound **7** showed the signal at m/z 487.1 (M^++1) further confirmed the formation of this compound. Finally compounds **8-22** were synthesized in 68-75% yield by the condensation of various amines i.e. allyl, butyl, propagyl, cyclohexyl, ethanol amine etc. with compound **7** in the presence of ethanol at reflux condition. Syntheses of all compounds were confirmed by NMR spectroscopy and mass spectrometry.

Scheme 1. Synthesis of 6-(1-allyl-3-(benzo[*d*]thiazol-2-yl)-1*H*-indol-5-yl)-2-substituted-1*H*-benzo[*de*]isoquinoline-1,3(2*H*)-dione

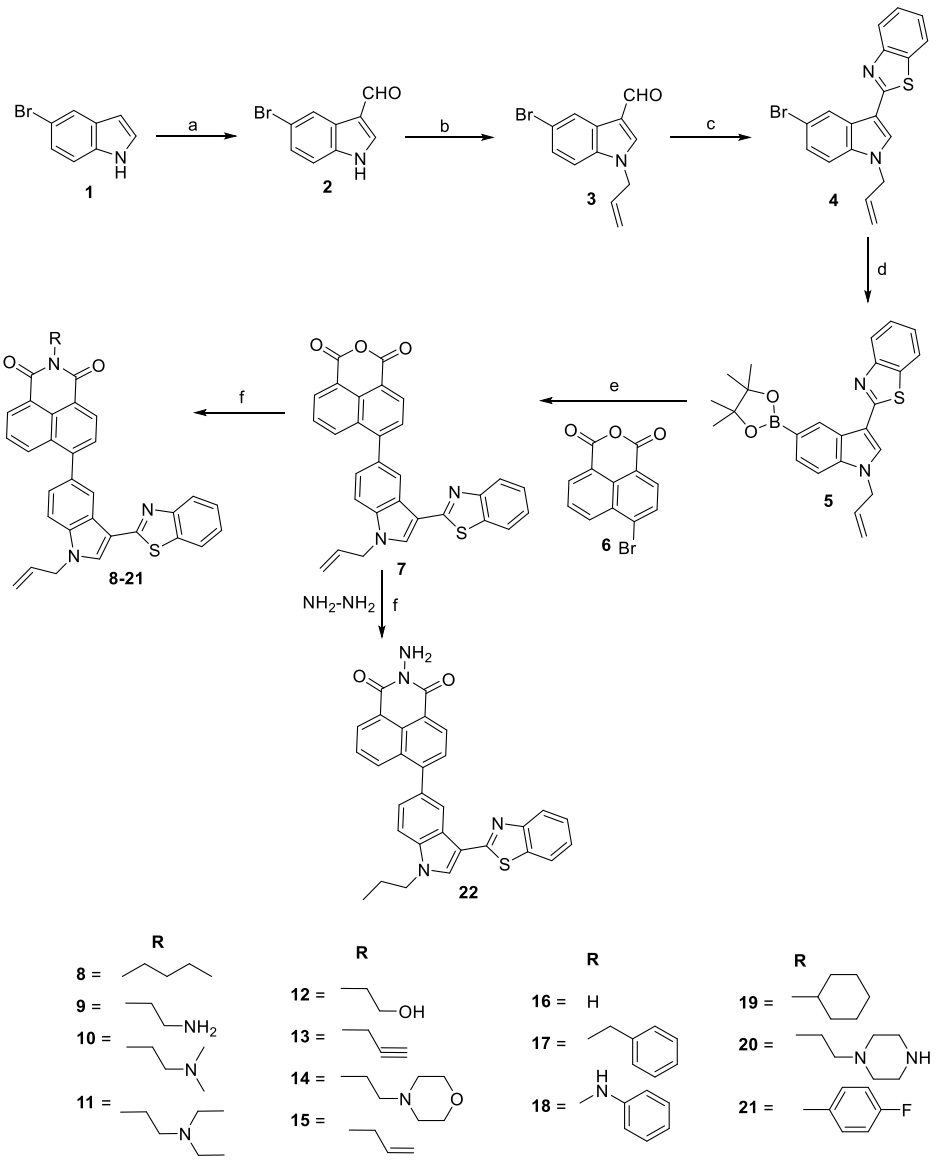

Reagents and conditions: (a) $POCl_3$, DMF, 0 °C, 1 h., 93%; (b) Allyl bromide, acetone-aq. NaOH, RT, 2 h, 86%; (c) 2-Aminothiophenol, nitrobenzene, 80 °C, 8 h, 62%; (d) Bis(pinacolato)diboron, $Pd(PPh_3)_2Cl_2$, KOAc, dioxane, reflux, 3 h; (e) $Pd(PPh_3)_4$, K_2CO_3, CH_3CN : water (9:1), N_2, reflux, 5 h, 55%; (f) RNH_2, ethanol, reflux, 4-6 h, 68-75%

6.3 Biology

6.3.1 Cytotoxicity against human cancer cells

Compounds **7-22** were tested for their cytotoxicity against A549 (Lung), MCF7 (Breast) and HeLa (cervix) human cancer cell lines at 1.0, 10 and 100 μM concentrations. Compounds exhibited more sensitivity towards A549 than MCF7 and HeLa cancer cells at all said concentrations.

Ethanolamine substituted compound **12** reveals potent cytotoxicity against A549 cancer cells having IC_{50} value of 140 nM. Propargylamine substituted derivative **13** shows excellent cytotoxicity for A549 with IC_{50} value of 314 nM. Compound **15** substituted with allyl showed IC_{50} value of 1.89 μM for A549, 0.38 μM for MCF7 and 2.71 μM for HeLa cancer cells, found effective against all tested cancer cells (**Table 1**).

Table 1. Cytotoxicity of compounds (**7**-**22**) against A549, MCF7 and HeLa cancer cell lines.

Compound	**IC_{50} (μM)**		
	A549	**MCF7**	**HeLa**
7	**0.45**	6.94	7.18
8	1.19	7.69	5.52
9	3.06	4.17	4.02
10	1.02	3.31	3.40
11	**0.81**	3.57	3.07
12	**0.14**	3.81	3.76
13	**0.31**	3.49	3.64
14	1.11	3.69	3.93
15	1.89	**0.38**	2.71
16	1.91	3.57	3.61
17	2.01	4.39	4.17
18	**0.96**	3.58	3.96
19	1.47	1.65	3.33
20	**0.76**	3.35	3.45
21	**0.63**	4.10	3.96
22	**0.84**	5.84	8.59

6.3.2 Cytotoxicity against human normal cells

To evaluate the safety, the cytotoxic effect of all compounds (**7**-**22**) against Hek293 (Kidney) human noncancerous cell line was also carried out by means of colorimetric assay (MTT assay) at the concentration level of 100 μM. Results showed that compound **20** exhibited maximum growth inhibition by 18% followed by compound **9**, which displayed growth inhibition by 17% (**Figure**

4). These results indicated that all derivatives had low cytotoxicity towards normal mammalian cells, signifying that the all synthesized compounds were able to selectively kill cancer cells.

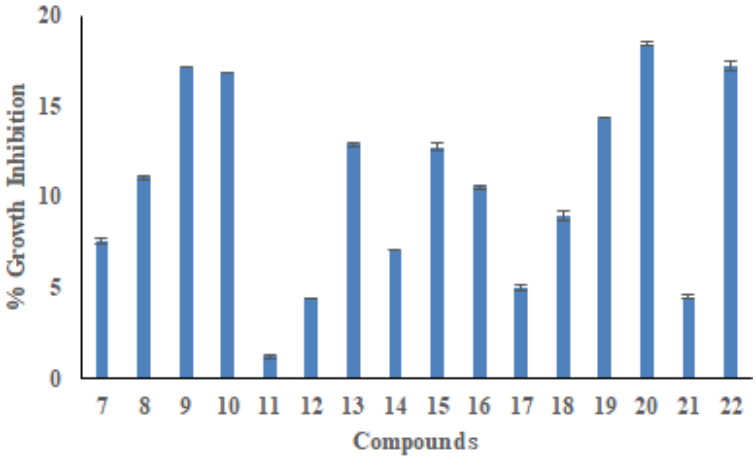

Figure 4. Effect of cytotoxicity of compounds (**7-22**) on human normal cell line Hek293

6.4 Conclusion

A series of conjugates with three biological active pharmacophores of naphthalimide, benzothiazole and indole substituted with different aliphatic and aromatic amines (**7-22**) has been synthesized in moderate to good yields. Compounds **7-22** were tested for their cytotoxicity against A549 (Lung), MCF7 (Breast) and HeLa (cervix) human cancer cells at three different concentrations of 1.0, 10 and 100 μM and showed cytotoxicity in the range of IC_{50} values of 0.14-8.59 μM, indicating that compounds showed excellent activity towards these cancer cell lines. Cytotoxicity studies against normal mammalian kidney cells Hek293 indicated that all synthesized compounds were able to selectively kill cancer cells.

6.5 Experimental section

All commercially available compounds (Aldrich, Merck, Spectrochem etc.) were used without further purification. All the recorded melting points were uncorrected and measured in open capillaries. All ^{1}H and ^{13}C NMR characterizations were performed on Jeol ECS 400 NMR spectrometer, which was operated at 400 MHz for ^{1}H nuclei and 100 MHz for ^{13}C nuclei, taking $CDCl_3$ as solvent. Chemical shifts are reported in parts per million (ppm) and TMS was used as an internal reference. Coupling constants (*J*) were reported in hertz (Hz). The synthesized compounds were characterized by mass spectra using Water Micromass-Q-T of Micro. Elemental analysis has been done with Thermo Scientific (Flash 2000) analyzer. Purification of synthesized

compounds was done through column chromatography with the help of silica gel having mesh size of 60-120 using hexane/ethyl acetate and chloroform/methanol in various polarity systems.

5-Bromo-1*H*-indole-3-carbaldehyde (2): 5-Bromoindole **1** (2 g, 10.30 mmol) was taken in dry round bottom flask (RBF). Vilsmeier-Haack reagent [*N*,*N*-dimethyl formamide (DMF) and phosphorus oxychloride ($POCl_3$)] was added to RBF dropwise at room temperature. Reaction mixture was stirred for 1 h at room temperature and progress of reaction was monitored with the help of thin layer chromatography (TLC). Reaction mixture was poured on crushed ice and neutralizes the solution with aqueous NaOH. Precipitated solid was filtered and washed thoroughly with water. Air dried the precipitate to obtain the desired white solid product in 2.15 g; 94 % yield; R_f 0.5 (20% ethyl acetate in hexane); mp 55-58 °C; ^{1}H NMR ($CDCl_3$, 400 MHz): δ 9.97 (s, 1H, CHO), 8.41 (s, 1H, NH), 7.85 (d, *J* = 3.16 Hz, 1H, ArH), 7.38-7.35 (m, 3H, ArH); ^{13}C NMR ($CDCl_3$, 100 MHz): δ 184.9 (*C*HO), 137.3, 135.9, 126.6, 126.1, 124.2, 118.3, 115.9, 113.6 (Ar*C*).

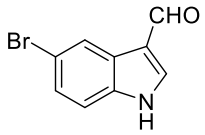

1-Allyl-5-bromo-1*H*-indole-3-carbaldehyde (3): To synthesize 1-allyl-5-bromo-1*H*-indole-3-carbaldehyde (**3**), an oven dried RBF having 10 ml of acetone-aqueous NaOH was charged with 5-bromo-1*H*-indole-3-carbaldehyde (**2**) (2 g, 9.00 mmol). Allyl bromide (1.6 g, 13.50 mmol) was added to reaction mixture and stirred at room temperature for 2 h. Progress of reaction was monitored through TLC. Acetone was evaporated and water was added to the reaction mixture. Precipitated brown solid was filtered, washed with water and air dried to obtain the desired product in 2.09 g; 89 % yield; R_f 0.6 (10% ethyl acetate in hexane); mp 66-69 °C; ^{1}H NMR ($CDCl_3$, 400 MHz): δ 9.95 (s, 1H, CHO), 8.46 (d, *J* = 1.84 Hz, 1H, ArH), 7.70 (s, 1H, ArH), 7.41 (dd, ^2J = 8.72 Hz, ^3J = 1.88 Hz, 1H, ArH), 7.22 (d *J* = 8.72 Hz, 1H, ArH), 6.04-5.94 (m, 1H, allyl-CH), 5.33 (d, *J* = 10.40 Hz, 1H, allyl-CH_2), 5.18 (d, *J* = 16.88 Hz, 1H, allyl-CH_2), 4.76-4.74 (m, 2H, allyl-CH_2); ^{13}C NMR ($CDCl_3$, 100 MHz): δ 184.4 (*C*HO), 138.9, 135.9, 131.4, 127.1, 126.9, 124.8, 119.4, 117.7, 116.7, 111.8 (Ar*C*), 49.8 (allyl-*C*H_2).

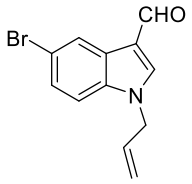

2-(1-Allyl-5-bromo-1*H*-indol-3-yl)benzo[*d*]thiazole (4): An oven dried RBF was charged with 1-allyl-5-bromo-1*H*-indole-3-carbaldehyde (**3**) (1 g, 3.78 mmol) followed by addition of nitrobenzene. 2-Aminothiophenol (475 mg, 3.78 mmol) was added and stirred the reaction at 80 °C for 8 h. 30 ml of hexane was added to the reaction mixture and precipitate was filtered and washed with hexane. Crude product was purified by column chromatography using 5% ethyl

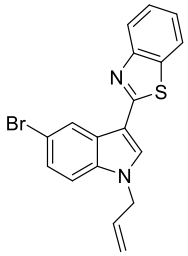

acetate in hexane as eluents. 850 mg; Redish solid; 61 % yield; R_f 0.3 (10% ethyl acetate in hexane); mp 111-114 ^oC; ^1H NMR ($CDCl_3$, 400 MHz): δ 8.62 (d, *J* = 1.84 Hz, 1H, ArH), 8.05 (d, *J* = 8.20 Hz, 1H, ArH), 7.88 (d, *J* = 8.64 Hz, 1H, ArH), 7.85 (s, 1H, ArH), 7.49-7.45 (m, 1H, ArH), 7.42 (dd, ^2J = 8.72 Hz, ^3J = 1.92 Hz, 1H, ArH), 7.36-7.32 (m, 1H, ArH), 7.26-7.24 (m, 1H, ArH), 6.07-5.97 (m, 1H, allyl-CH), 5.32 (d, *J* = 10.08 Hz, 1H, allyl-CH_2), 5.20 (d, *J* = 16.96 Hz, 1H, allyl-CH_2), 4.79-4.77 (m, 2H, allyl-CH_2); ^{13}C NMR ($CDCl_3$, 100 MHz): δ 162.0, 153.9, 135.6, 133.7, 132.0, 130.5, 127.3, 126.2, 124.4, 124.2, 122.3, 121.3, 118.8, 115.3, 111.7, 111.1 (Ar*C*), 49.5 (allyl-*C*H_2).

2-(1-Allyl-5-(4,4,5,5-tetramethyl-1,3,2-dioxaborolan-2-yl)-1*H*-indol-3-yl)benzo[*d*]thiazole (5): 2-(1-Allyl-5-bromo-1*H*-indol-3-yl)benzo[*d*]thiazole (**4**) (1 g, 2.71 mmol), bis(pinacolato)diboron (1.03 g, 4.06 mmol), $Pd(PPh_3)_2Cl_2$ (1.0 mol%) and KOAc (265 mg, 2.71 mmol) were taken in a dry RBF and 20 ml of dioxane was added. Reaction was allowed to reflux for 3 h. Reaction progression was observed by TLC. The solvent was evaporated under reduced pressure followed by 100 ml of water was added to it. Extraction was done with chloroform (3 × 50 ml) and dried the extract over anhydrous sodium sulphate. Chloroform was distilled off to get the crude product. Crude product was further used without purification.

6-(1-Allyl-3-(benzo[*d*]thiazol-2-yl)-1*H*-indol-5-yl)-1*H*,3*H*-benzo[*de*]isochromene-1,3-dione

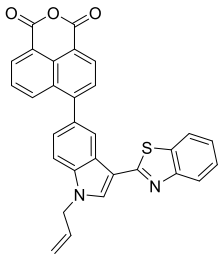

(7): 2-(1-Allyl-5-(4,4,5,5-tetramethyl-1,3,2-dioxaborolan-2-yl)-1*H*-indol-3-yl)benzo[*d*]thiazole (**5**) (500 mg, 1.20 mmol), 6-bromo-1*H*,3*H*-benzo[*de*]isochromene-1,3-dione (**6**) (330 mg, 1.20 mmol), $Pd(PPh_3)_4$ (1.0 mol%) and K_2CO_3 (165 mg, 1.20 mmol) were added to the RBF followed by addition of CH_3CN : water (9:1). Reaction was refluxed for 5 h and monitored through TLC. Solvent was evaporated under reduced pressure and 100 ml of water was added. Chloroform (3 × 30 ml) was used for extraction and dried over anhydrous sodium sulphate followed by evaporation of solvent to get the crude product. Column chromatography was used for purification using 30% ethyl acetate in chloroform as eluents. 486 mg; Yellow solid; 55 % yield; R_f 0.3 (30% ethyl acetate in chloroform); mp 255-258 ^oC; ^1H NMR ($CDCl_3$, 400 MHz): δ 8.72-8.63 (m, 2H, ArH), 8.52-8.46 (m, 1H, ArH), 8.01-7.94 (m, 2H, ArH), 7.92-7.83 (m, 2H, ArH), 7.78-7.64 (m, 2H, ArH), 7.61-7.56 (m, 1H, ArH), 7.49-7.43 (m, 2H, ArH), 7.36-7.32 (m, 1H, ArH), 6.20-6.08 (m, 1H, allyl-CH), 5.43-5.28 (m, 2H, allyl-CH_2), 4.94 (d, *J*

= 4.92 Hz, 2H, allyl-CH_2); ^{13}C NMR ($CDCl_3$, 100 MHz): 162.0, 161.0, 160.8, 153.8, 149.6, 136.8, 134.7, 133.3, 133.0, 132.1, 132.0, 131.6, 130.9, 130.8, 130.7, 128.8, 127.1, 126.1, 126.0, 124.9, 124.4, 123.1, 122.2, 121.2, 118.9, 117.1, 111.8, 110.5 (Ar*C*), 49.5 (allyl-*C*H_2); MS (ESI): m/z 487.1 (M^++1); Anal Calcd for $C_{30}H_{18}N_2O_3S$: C, 74.06; H, 3.73; N, 5.76; S, 6.59; found C, 74.11; H, 3.71; N, 5.70; S, 6.68.

6-(1-Allyl-3-(benzo[*d*]thiazol-2-yl)-1*H*-indol-5-yl)-2-substituted-1*H*-benzo[*de*]isoquinoline-1,3(2*H*)-dione (8-22): For the synthesis of 6-(1-allyl-3-(benzo[*d*]thiazol-2-yl)-1*H*-indol-5-yl)-2-substituted-1*H*-benzo[*de*]isoquinoline-1,3(2*H*)-dione (**8-22**), respective amine was treated with 6-(1-allyl-3-(benzo[*d*]thiazol-2-yl)-1*H*-indol-5-yl)-1*H*,3*H*-benzo[*de*]isochromene-1,3-dione (**7**) in refluxing ethanol. Thin layer chromatography was used to check the progress of reaction. Solvent was evaporated under reduced pressure and 50 ml of water was added to it. Filtered the precipitate and washed with water. Purification was done by column chromatography using ethyl acetate and chloroform as eluents.

6-(1-Allyl-3-(benzo[*d*]thiazol-2-yl)-1*H*-indol-5-yl)-2-butyl-1*H*-benzo[*de*]isoquinoline-1,3 (2*H*)-dione (8): Light yellow solid; 76% yield; mp 277-280 ^{o}C; ^{1}H NMR ($CDCl_3$, 400 MHz): δ (ppm) 8.68-8.62 (m, 3H, ArH), 8.38 (d, *J* = 8.36 Hz, 1H, ArH), 7.97 (s, 1H, ArH), 7.96 (d, *J* = 8.08 Hz, 1H, ArH), 7.85 (t, *J* = 6.00 Hz, 2H, ArH), 7.69 (t, *J* = 7.64 Hz, 1H, ArH), 7.56 (d, *J* = 8.44 Hz, 1H, ArH), 7.46-7.40 (m, 2H, ArH), 7.32 (t, *J* = 7.40 Hz, 1H, ArH), 6.16-6.07 (m, 1H, allyl-CH), 5.39 (d, *J* = 10.16 Hz, 1H, allyl-CH_2), 5.32 (d, *J* = 17.16 Hz, 1H, allyl-CH_2), 4.91 (d, *J* = 5.32 Hz, 2H, allyl-CH_2), 4.26 (t, *J* = 7.48 Hz, 2H, butyl-CH_2), 1.80-1.73 (m, 2H, butyl-CH_2), 1.53-1.44 (m, 2H, butyl-CH_2), 1.02 (t, 3H, *J* = 7.32 Hz, butyl-CH_3); ^{13}C NMR ($CDCl_3$, 100 MHz): δ (ppm) 164.5, 164.3, 162.1, 153.8, 147.8, 136.7, 133.6, 133.1, 132.4, 132.1, 131.1, 130.8, 130.6, 130.5, 128.3, 126.7, 126.0, 125.9, 125.1, 124.3, 122.9, 122.8, 122.2, 121.3, 121.2, 119.1, 118.8, 110.3 (Ar*C*), 49.5 (allyl-*C*H_2), 40.2 (butyl-*C*H_2), 30.2 (butyl-*C*H_2), 20.4 (butyl-*C*H_2), 13.9 (butyl-*C*H_3); MS (ESI): m/z 542.2 (M^++1); Anal Calcd for $C_{34}H_{27}N_3O_2S$: C, 75.39; H, 5.02; N, 7.76; S, 5.92; found C, 75.44; H, 5.09; N, 7.61; S, 5.98.

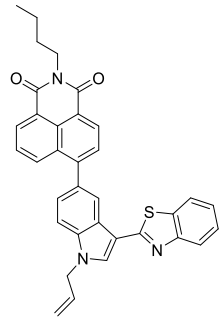

6-(1-Allyl-3-(benzo[*d*]thiazol-2-yl)-1*H*-indol-5-yl)-2-(2-aminoethyl)-1*H*-benzo[*de*] isoquinoline-1,3(2*H*)-dione (9): Yellow solid; 67% yield; mp 271-274 ^{o}C; ^{1}H NMR ($CDCl_3$, 400 MHz): δ (ppm) 8.68-8.61 (m, 3H, ArH), 8.38 (d, *J* = 8.44 Hz, 1H, ArH), 7.98 (s, 1H, ArH), 7.96 (d, *J* = 7.96 Hz, 1H, ArH), 7.85 (t, *J* = 8.44 Hz , 2H, ArH), 7.69 (t, *J* = 8.00 Hz, 1H, ArH), 7.56 (d,

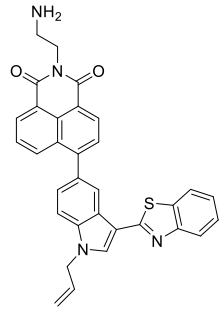

J = 8.52 Hz, 1H, ArH), 7.46-7.41 (m, 2H, ArH), 7.33 (t, *J* = 7.76 Hz, 1H, ArH), 6.17-6.07 (m, 1H, allyl-CH), 5.39 (d, *J* = 10.16 Hz, 1H, allyl-CH_2), 5.32 (d, *J* = 17.04 Hz, 1H, allyl-CH_2), 4.92 (d, *J* = 5.44 Hz, 2H, allyl-CH_2), 4.41 (t, *J* = 6.96 Hz, 2H, ethyl-CH_2), 2.72 (t, *J* = 7.20 Hz, 2H, ethyl-CH_2); ^{13}C NMR ($CDCl_3$, 100 MHz): δ (ppm) 164.5, 164.3, 162.1, 153.8, 148.0, 136.7, 133.6, 133.2, 132.4, 132.1, 131.1, 130.9, 130.6, 130.5, 128.7, 128.3, 126.6, 126.0, 125.9, 125.1, 124.3, 123.0, 122.7, 122.2, 121.2, 118.8, 111.7, 110.3 (Ar*C*), 56.9 (ethyl-*C*H_2), 49.5 (allyl-*C*H_2), 38.1 (ethyl-*C*H_2); MS (ESI): m/z 529.2 (M^++1); Anal Calcd for $C_{34}H_{27}N_3O_2S$: C, 72.71; H, 4.58; N, 10.60; S, 6.06; found C, 72.67; H, 4.51; N, 10.71; S, 6.12.

6-(1-Allyl-3-(benzo[*d*]thiazol-2-yl)-1*H*-indol-5-yl)-2-(2-(dimethylamino)ethyl)-1*H*- benzo[*de*] isoquinoline-1,3(2*H*)-dione (10): Yellow solid; 73% yield; mp 274-277 °C; ^{1}H NMR ($CDCl_3$, 400

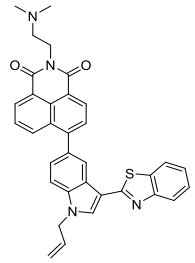

MHz): δ (ppm) 8.67-8.61 (m, 3H, ArH), 8.37 (d, *J* = 8.36 Hz, 1H, ArH), 7.98 (s, 1H, ArH), 7.96 (d, *J* = 8.04 Hz, 1H, ArH), 7.85-7.80 (m, 2H, ArH), 7.68 (t, *J* = 7.80 Hz, 1H, ArH), 7.55 (d, *J* = 8.44 Hz, 1H, ArH), 7.45-7.40 (m, 2H, ArH), 7.32 (t, *J* = 7.40 Hz, 1H, ArH),6.17-6.07 (m, 1H, allyl-CH), 5.39 (d, *J* = 10.28 Hz, 1H, allyl-CH_2), 5.31 (d, *J* = 17.00 Hz, 1H, allyl-CH_2), 4.91 (d, *J* = 5.36 Hz, 2H, allyl-CH_2), 4.40 (t, *J* = 7.00 Hz, 2H, ethyl-CH_2), 2.72 (t, *J* = 7.20 Hz, 2H, ethyl-CH_2), 2.39 (s, 6H, N-CH_3); ^{13}C NMR ($CDCl_3$, 100 MHz): δ (ppm) 164.5, 164.3, 162.1, 153.8, 148.0, 136.7, 133.6, 133.2, 132.4, 132.1, 131.1, 130.9, 130.6, 130.5, 128.7, 128.3, 126.6, 126.0, 125.9, 125.1, 124.3, 123.0, 122.7, 122.2, 121.2, 118.8, 111.7, 110.3 (Ar*C*), 56.9 (ethyl-*C*H_2), 49.5 (allyl-*C*H_2), 45.7 (N-*C*H_3), 38.1 (ethyl-*C*H_2); MS (ESI): m/z 557.2 (M^++1); Anal Calcd for $C_{34}H_{28}N_4O_2S$: C, 73.36; H, 5.07; N, 10.06; S, 5.76; found C, 73.31; H, 5.01; N, 10.01; S, 5.81.

6-(1-Allyl-3-(benzo[*d*]thiazol-2-yl)-1*H*-indol-5-yl)-2-(2-(diethylamino)ethyl)-1*H*-benzo[*de*] isoquinoline-1,3(2*H*)-dione (11): Light Yellow solid; 67% yield; mp 281-284 °C; ^{1}H NMR

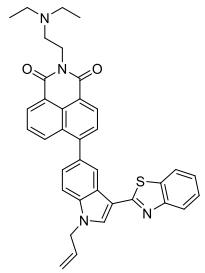

($CDCl_3$, 400 MHz): δ (ppm) 8.68-8.61 (m, 3H, ArH), 8.38 (d, *J* = 8.40 Hz, 1H, ArH), 7.97 (s, 1H, ArH), 7.96 (d, *J* = 8.20 Hz, 1H, ArH), 7.85-7.81 (m, 2H, ArH), 7.69 (t, *J* = 7.68 Hz, 1H, ArH), 7.55 (d, *J* = 8.48 Hz, 1H, ArH), 7.45-7.40 (m, 2H, ArH), 7.33-7.29 (m, 1H, ArH), 6.16-6.06 (m, 1H, allyl-CH), 5.39 (d, *J* = 10.28 Hz, 1H, allyl- CH_2), 5.31 (d, *J* = 17.16 Hz, 1H, allyl-CH_2), 4.91 (d, *J* = 5.16 Hz, 2H, allyl-CH_2), 4.37 (t, *J* = 7.48 Hz, 2H, ethyl-CH_2), 2.86 (t, *J* = 7.36 Hz, 2H, ethyl-CH_2), 2.73 (q, *J* = 7.04 Hz, 4H, ethyl-CH_2), 1.15 (t, *J* = 7.08 Hz, 6H, ethyl-CH_3);^{13}C

NMR ($CDCl_3$, 100 MHz): δ (ppm) 164.4, 164.2, 162.1, 153.8, 147.9, 136.7, 133.6, 133.2, 132.4, 132.1, 131.1, 130.8, 130.6, 130.5, 130.1, 128.7, 128.3, 126.7, 126.0, 125.9, 125.1, 124.3, 122.9, 122.2, 121.2, 118.8, 118.5, 111.7, 110.3 (Ar*C*), 49.8 (ethyl-*C*H_2), 49.5 (allyl-*C*H_2), 47.6 (ethyl-*C*H_2), 37.9 (ethyl-*C*H_2), 12.2 (ethyl-CH_3); MS (ESI): m/z 585.2 (M^++1); Anal Calcd for $C_{36}H_{32}N_4O_2S$: C, 73.95; H, 5.52; N, 9.58; S, 5.48; found C, 73.91; H, 5.48; N, 9.64; S, 5.42.

6-(1-Allyl-3-(benzo[*d*]thiazol-2-yl)-1*H*-indol-5-yl)-2-(2-hydroxyethyl)-1*H*-benzo[*de*] isoquinoline-1,3(2*H*)-dione (12): Light Yellow solid; 69% yield; mp 292-295 ^oC; ^1H NMR

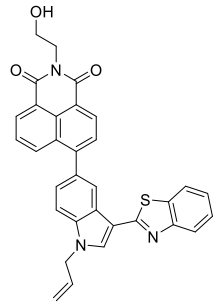

($CDCl_3$, 400 MHz): δ (ppm) 8.76 (d, *J* = 7.80 Hz, 1H, ArH), 8.72 (d, *J* = 7.28 Hz, 1H, ArH), 8.64 (s, 1H, ArH), 8.47 (d, *J* = 8.60 Hz, 1H, ArH), 7.99 (s, 1H, ArH), 7.96 (d, *J* = 8.08 Hz, 1H, ArH), 7.89 (d, *J* = 7.40 Hz, 1H, ArH), 7.85 (d, *J* = 7.76 Hz, 1H, ArH), 7.75 (t, *J* = 8.08 Hz, 1H, ArH), 7.58 (d, *J* = 8.40 Hz, 1H, ArH), 7.47-7.41 (m, 2H, ArH), 7.33 (t, *J* = 7.56 Hz, 1H, ArH), 7.00 (t, *J* = 8.28 Hz, 4H, 2 × ethyl-CH_2), ethyl-CH_2), 6.17-6.08 (m, 1H, allyl-CH), 5.40 (d, *J* = 10.24 Hz, 1H, allyl-CH_2), 5.32 (d, *J* = 17.08 Hz, 1H, allyl-CH_2), 4.92 (d, *J* = 5.36 Hz, 2H, allyl-CH_2); ^{13}C NMR ($CDCl_3$, 100 MHz): δ (ppm) 165.3, 165.2, 162.1, 153.7, 148.3, 136.7, 133.5, 133.5, 132.2, 132.1, 131.3, 131.0, 130.7, 130.4, 128.7, 128.3, 126.6, 126.1, 125.8, 125.0, 124.3, 122.9, 122.3, 122.2, 121.2, 120.9, 118.8, 111.6, 110.4 (Ar*C*), 61.9 (ethyl-*C*H_2), 49.5 (allyl-*C*H_2), 42.8 (ethyl-*C*H_2); MS (ESI): m/z 530.1 (M^++1); Anal Calcd for $C_{32}H_{23}N_3O_3S$: C, 72.57; H, 4.38; N, 7.93; S, 6.05; found C, 72.62; H, 4.42; N, 7.89; S, 6.09.

6-(1-Allyl-3-(benzo[*d*]thiazol-2-yl)-1*H*-indol-5-yl)-2-(prop-2-yn-1-yl)-1*H*-benzo[*de*] isoquinoline-1,3(2*H*)-dione (13): Light Yellow solid; 76% yield; mp 282-285 ^oC; ^1H NMR

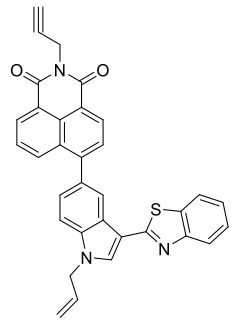

($CDCl_3$, 400 MHz): δ (ppm) 8.69 (d, *J* = 7.56 Hz, 1H, ArH), 8.65 (d, *J* = 7.20 Hz, 1H, ArH), 8.61 (s, 1H, ArH), 8.39 (d, *J* = 8.08 Hz, 1H, ArH), 7.97 (s, 1H, ArH), 7.95 (d, *J* = 8.08 Hz, 1H, ArH), 7.84 (d, *J* = 7.88 Hz, 1H, ArH), 7.82 (d, *J* = 7.56 Hz, 1H, ArH), 7.68 (t, *J* = 8.20 Hz, 1H, ArH), 7.55 (d, *J* = 8.48 Hz, 1H, ArH), 7.45-7.39 (m, 2H, ArH), 7.32 (t, *J* = 7.20 Hz, 1H, ArH), 6.17-6.07 (m, 1H, allyl- CH), 5.39 (d, *J* = 10.32 Hz, 1H, allyl-CH_2), 5.32 (d, *J* = 17.08 Hz, 1H, allyl-CH_2), 5.02 (d, *J* = 2.36 Hz, 2H, propagyl-CH_2), 4.92 (d, *J* = 5.44 Hz, 2H, allyl-CH_2), 2.24 (t, *J* = 2.40 Hz, 1H, propagyl-CH); ^{13}C NMR ($CDCl_3$, 100 MHz): δ (ppm) 163.7, 163.5, 162.0, 153.8, 148.4, 136.7, 133.6, 132.2, 132.1, 131.4, 131.2, 130.7, 130.6, 128.7, 128.3, 126.7, 126.0, 125.9, 125.1, 124.3, 123.0, 122.3, 122.2, 121.2, 120.9, 118.8, 111.7,

110.3 (Ar*C*), 78.7(propargyl-*C*), 70.4 (propargyl-*C*H), 49.5 (allyl-*C*H_2), 29.4 (propargyl-*C*H_2); MS (ESI): m/z 524.1 (M^++1); Anal Calcd for $C_{33}H_{21}N_3O_2S$: C, 75.70; H, 4.04; N, 8.03; S, 6.12; found C, 75.68; H, 4.09; N, 8.07; S, 6.10.

6-(1-Allyl-3-(benzo[*d*]thiazol-2-yl)-1*H*-indol-5-yl)-2-(2-morpholinoethyl)-1*H*-benzo[*de*]isoquinoline-1,3(2*H*)-dione (14): Yellow solid; 72% yield; mp 285-288 °C; ^{1}H NMR ($CDCl_3$, 400 MHz): δ (ppm) 8.68-8.62 (m, 3H, ArH), 8.39 (d, *J* = 8.36 Hz, 1H, ArH), 7.98 (s, 1H, ArH), 7.96 (d, *J* = 8.00 Hz, 1H, ArH), 7.84 (d, *J* = 7.44 Hz, 2H, ArH), 7.71 (t, *J* = 7.88 Hz, 1H, ArH), 7.56 (d, *J* = 8.48 Hz, 1H, ArH), 7.49-7.40 (m, 2H, ArH), 7.32 (t, *J* = 7.40 Hz, 1H, ArH), 6.15-6.07 (m, 1H, allyl-CH), 5.39 (d, *J* = 10.40 Hz, 1H, allyl-CH_2), 5.32 (d, *J* = 17.12 Hz, 1H, allyl-CH_2), 4.91 (d, *J* = 5.08 Hz, 2H, allyl- CH_2), 4.42 (t, *J* = 6.80 Hz, 2H, ethyl-CH_2), 3.72 (t, *J* = 3.92 Hz, 4H, morph-CH_2), 2.77 (t, *J* = 6.84 Hz, 2H, ethyl-CH_2), 2.63 (bs, 4H, morph-CH_2); ^{13}C NMR ($CDCl_3$, 100 MHz): δ (ppm) 164.5, 164.3, 162.1, 153.8, 148.0, 136.7, 133.6, 133.2, 132.4, 132.1, 131.1, 130.9, 130.6, 130.5, 128.7, 128.4, 126.7, 126.0, 125.9, 125.1, 124.3, 123.0, 122.7, 122.2, 121.2, 118.8, 111.7, 110.3 (Ar*C*), 67.0 (morph-*C*H_2), 56.1 (ethyl-*C*H_2), 53.8 (morph-*C*H_2), 49.5 (allyl-*C*H_2), 37.1 (ethyl-*C*H_2); MS (ESI): m/z 599.2 (M^++1); Anal Calcd for $C_{36}H_{30}N_4O_3S$: C, 72.22; H, 5.05; N, 9.36; S, 5.35; found C, 72.20; H, 5.11; N, 9.31; S, 5.30.

2-Allyl-6-(1-allyl-3-(benzo[*d*]thiazol-2-yl)-1*H*-indol-5-yl)-1*H*-benzo[*de*]isoquinoline-1,3(2*H*)-dione (15): Yellow solid; 79% yield; mp 288-291 °C; ^{1}H NMR ($CDCl_3$, 400 MHz): δ (ppm) 8.69-8.60 (m, 3H, ArH), 8.39 (t, *J* = 7.48 Hz, 1H, ArH), 8.15 (s, 1H, ArH), 7.97-7.94 (m, 1H, ArH), 7.86 (t, *J* = 8.12 Hz, 1H, ArH), 7.70 (d, *J* = 8.36 Hz, 1H, ArH), 7.66 (d, *J* = 8.52 Hz, 1H, ArH), 7.56-7.41 (m, 3H, ArH), 7.34 (t, *J* = 7.44 Hz, 1H, ArH), 6.14-6.00 (m, 2H, allyl-CH), 5.38 (d, *J* = 17.12 Hz, 2H, allyl-CH_2), 5.25 (d, *J* = 10.36 Hz, 2H, allyl- CH_2), 4.87 (d, *J* = 5.60 Hz, 4H, allyl-CH_2); ^{13}C NMR ($CDCl_3$, 100 MHz): δ (ppm) 164.2, 164.0, 153.8, 147.9, 135.9, 133.7, 133.2, 132.9, 132.2, 131.3, 131.0, 128.4, 127.0, 126.7, 126.1, 125.9, 125.6, 124.5, 123.8, 123.7, 123.1, 122.6, 122.4, 121.2, 117.4, 115.6, 113.2, 110.2 (Ar*C*), 42.4 (allyl-*C*H_2); MS (ESI): m/z 526.1 (M^++1); Anal Calcd for $C_{33}H_{23}N_3O_2S$: C, 75.41; H, 4.41; N, 7.99; S, 6.10; found C, 75.35; H, 4.40; N, 7.90; S, 6.16.

6-(1-Allyl-3-(benzo[*d*]thiazol-2-yl)-1*H*-indol-5-yl)-1*H*-benzo[*de*]isoquinoline-1,3(2*H*)-dione (16): Yellow solid; 66% yield; mp 277-280 °C; ^{1}H NMR ($CDCl_3$, 400 MHz): δ (ppm) 8.70-8.62

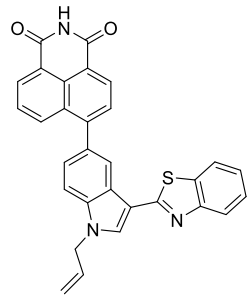

(m, 3H, ArH), 8.58 (s, 1H, NH), 8.50-8.41 (m, 1H, ArH), 7.99 (d, *J* = 2.80 Hz, 1H, ArH), 7.96 (d, *J* = 8.04 Hz, 1H, ArH), 7.89 (t, *J* = 7.56 Hz, 1H, ArH), 7.85 (t, *J* = 4.76 Hz, 1H, ArH), 7.75-7.68 (m, 1H, ArH), 7.58-7.55 (m, 1H, ArH), 7.46-7.41 (m, 2H, ArH), 7.33 (t, *J* = 7.76 Hz, 1H, ArH), 6.17-6.07 (m, 1H, allyl-CH), 5.40 (d, *J* = 10.36 Hz, 1H, allyl-CH_2), 5.32 (d, *J* = 17.20 Hz, 1H, allyl-CH_2), 4.92 (d, *J* = 5.40 Hz, 2H, allyl-CH_2); ^{13}C NMR ($CDCl_3$, 100 MHz): δ (ppm) 162.0, 161.1, 160.9, 153.9, 149.7, 136.9, 134.8, 133.3, 133.1, 132.1, 131.7, 131.0, 130.9, 130.8, 128.8, 128.6, 128.5, 127.2, 126.2, 126.1, 125.0, 124.5, 123.2, 122.3, 121.3, 119.0, 117.2, 111.9, 110.6 (Ar*C*), 49.6 (allyl-*C*H_2); MS (ESI): m/z 486.1 (M^++1); Anal Calcd for $C_{30}H_{19}N_3O_2S$: C, 74.21; H, 3.94; N, 8.65; S, 6.60; found C, 74.15; H, 3.99; N, 8.60; S, 6.66.

6-(1-Allyl-3-(benzo[*d*]thiazol-2-yl)-1*H*-indol-5-yl)-2-benzyl-1*H*-benzo[*de*]isoquinoline-1,3(2*H*)-dione (17): Yellow solid; 74% yield; mp 281-284 °C; ^{1}H NMR ($CDCl_3$, 400 MHz): δ

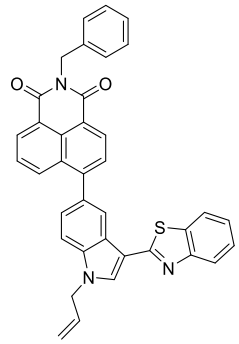

(ppm) 8.70-8.61 (m, 3H, ArH), 8.38 (d, *J* = 8.12 Hz, 1H, ArH), 7.97-7.93 (m, 2H, ArH), 7.85-7.81 (m, 2H, ArH), 7.69-7.64 (m, 2H, ArH), 7.59 (d, *J* = 7.40 Hz, 2H, ArH), 7.55 (t, *J* = 8.52 Hz, 1H, ArH), 7.47-7.40 (m, 2H, ArH), 7.35 (t, *J* = 7.20 Hz, 3H, ArH), 6.16-6.06 (m, 1H, allyl-CH), 5.44 (s, 2H, benzyl-CH_2), 5.39 (d, *J* = 10.32 Hz, 1H, allyl-CH_2), 5.31 (d, *J* = 17.12 Hz, 1H, allyl-CH_2), 4.90 (d, *J* = 5.40 Hz, 2H, allyl-CH_2); MS (ESI): m/z 576.1 (M^++1); Anal Calcd for $C_{37}H_{25}N_3O_2S$: C, 77.20; H, 4.38; N, 7.30; S, 5.57; found C, 77.25; H, 4.30; N, 7.38; S, 5.62.

6-(1-Allyl-3-(benzo[*d*]thiazol-2-yl)-1*H*-indol-5-yl)-2-(phenylamino)-1*H*-benzo[*de*] isoquinoline-1,3(2*H*)-dione (18): Yellow solid; 65% yield; mp 273-276 °C; ^{1}H NMR ($CDCl_3$, 400

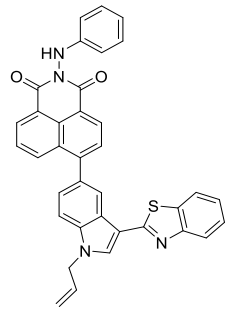

MHz): δ (ppm) 8.76 (d, *J* = 7.48 Hz, 1H, ArH), 8.72 (d, *J* = 7.20 Hz, 1H, ArH), 8.64 (s, 1H, ArH), 8.47 (d, *J* = 8.48 Hz, 1H, ArH), 7.99 (s, 1H, ArH), 7.97 (d, *J* = 8.16 Hz, 1H, ArH), 7.89 (d, *J* = 7.52 Hz, 1H, ArH), 7.86 (d, *J* = 7.92 Hz, 1H, ArH), 7.75 (t, *J* = 7.92 Hz, 1H, ArH), 7.58 (d, *J* = 8.44 Hz, 1H, ArH), 7.48-7.41 (m, 2H, ArH), 7.33 (t, *J* = 7.64 Hz, 1H, ArH), 7.29-7.25 (m, 1H, ArH), 7.00-6.96 (m, 4H, ArH), 6.17-6.08 (m, 1H, allyl-CH), 5.40 (d, *J* = 10.20 Hz, 1H, allyl-CH_2), 5.32 (d, *J* = 17.04 Hz, 1H, allyl-CH_2), 4.93 (d, *J* = 5.44 Hz, 2H, allyl-CH_2); ^{13}C NMR ($CDCl_3$, 100 MHz): δ (ppm) 163.5, 163.3, 162.1, 161.5, 153.8, 148.9,

146.3, 136.8, 134.1, 132.8, 132.6, 132.2, 132.1, 131.8, 130.8, 130.7, 129.2, 128.6, 126.9, 127.0, 126.1, 125.1, 124.3, 123.1, 122.3, 122.2, 121.2, 120.8, 118.8, 114.9, 110.4 (Ar*C*), 49.5 (allyl-*C*H_2); MS (ESI): m/z 598.2 (M^++1); Anal Calcd for $C_{36}H_{24}N_4O_2S$: C, 74.98; H, 4.20; N, 9.72; S, 5.56; found C, 74.90; H, 4.15; N, 9.78; S, 5.50.

6-(1-Allyl-3-(benzo[*d*]thiazol-2-yl)-1*H*-indol-5-yl)-2-cyclohexyl-1*H*-benzo[*de*]isoquinoline-1,3(2*H*)-dione (19): Yellow solid; 69% yield; mp 285-288 ^oC; ^1H NMR ($CDCl_3$, 400 MHz): δ

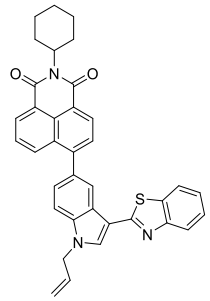

(ppm) 8.64-8.58 (m, 3H, ArH), 8.35 (t, *J* = 7.68 Hz, 1H, ArH), 7.97 (t, *J* = 8.40 Hz, 1H, ArH), 7.86-7.79 (m, 2H, ArH), 7.68 (t, *J* = 8.28 Hz, 2H, ArH), 7.57-7.40 (m, 3H, ArH), 7.34 (t, *J* = 7.44 Hz, 1H, ArH), 6.16-6.05 (m, 1H, allyl-CH), 5.39 (d, *J* = 10.20 Hz, 1H, allyl-CH_2), 5.32 (d, *J* = 17.12 Hz, 1H, allyl-CH_2), 5.11-5.04 (m, 1H, cyclohex-CH), 4.91 (d, *J* = 5.36 Hz, 2H, allyl-CH_2), 2.65-2.56 (m, 2H, cyclohex-CH_2), 1.94-1.90 (m, 2H, cyclohex-CH_2), 1.80-1.72 (m, 2H, cyclohex-CH_2), 1.53-1.33 (m, 3H, cyclohex-CH_2); ^{13}C NMR ($CDCl_3$, 100 MHz): δ (ppm) 164.9, 164.7, 154.1, 147.5, 130.9, 130.7, 128.3, 126.8, 126.7, 126.1, 126.0, 125.9, 125.6, 124.5, 123.9, 123.4, 123.1, 123.0, 122.9, 122.4, 122.0, 121.2, 118.8, 115.5, 113.2, 110.3, 110.2 (Ar*C*), 53.7 (cyclohex-*C*H), 49.5 (allyl-*C*H_2), 29.1 (cyclohex-*C*H_2), 26.5 (cyclohex-*C*H_2), 25.5 (cyclohex-*C*H_2); MS (ESI): m/z 568.2 (M^++1); Anal Calcd for $C_{36}H_{29}N_3O_2S$: C, 76.17; H, 5.15; N, 7.40; S, 5.65; found C, 76.25; H, 5.11; N, 7.45; S, 5.60.

6-(1-Allyl-3-(benzo[*d*]thiazol-2-yl)-1*H*-indol-5-yl)-2-(2-(piperazin-1-yl)ethyl)-1*H*- benzo[*de*] isoquinoline-1,3(2*H*)-dione (20): Yellow solid; 76% yield; mp 294-297 ^oC; ^1H NMR ($CDCl_3$, 400

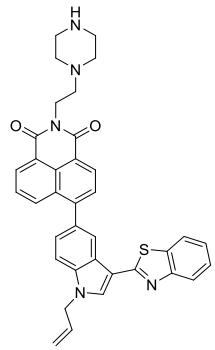

MHz): δ (ppm) 8.66-8.59 (m, 3H, ArH), 8.37 (t, *J* = 8.20 Hz, 1H, ArH), 7.96-7.92 (m, 1H, ArH), 7.84-7.79 (m, 2H, ArH), 7.68-7.62 (m, 2H, ArH), 7.54-7.38 (m, 3H, ArH), 7.32 (t, *J* = 7.56 Hz, 1H, ArH), 6.14-6.03 (m, 1H, allyl-CH), 5.37 (d, *J* = 10.20 Hz, 1H, allyl-CH_2), 5.29 (d, *J* = 17.08 Hz, 1H, allyl-CH_2), 4.89 (d, *J* = 5.36 Hz, 2H, allyl-CH_2), 4.40 (t, *J* = 6.92 Hz, 2H, ethyl-CH_2), 2.90 (t, *J* = 4.72 Hz, 4H, pip- CH_2), 2.74 (t, *J* = 7.24 Hz, 2H, ethyl-CH_2), 2.60 (bs, 4H, pip-CH_2); ^{13}C NMR ($CDCl_3$, 100 MHz): δ (ppm) 164.4, 164.2, 153.8, 147.8, 136.6, 135.9, 133.7, 133.1, 132.1, 131.1, 130.8, 128.7, 128.3, 127.0, 126.7, 126.1, 125.9, 124.5, 123.8, 123.1, 122.7, 121.2, 118.8, 115.6, 113.2, 111.7, 110.2 (Ar*C*), 56.3 (ethyl-*C*H_2), 54.5 (pip-*C*H_2), 49.5 (allyl-*C*H_2), 46.0 (pip-*C*H_2), 37.3 (ethyl-*C*H_2); MS (ESI): m/z

568.2 (M^++1); Anal Calcd for $C_{36}H_{31}N_5O_2S$: C, 72.34; H, 5.23; N, 11.72; S, 5.36; found C, 72.39; H, 5.28; N, 11.70; S, 5.32.

6-(3-(Benzo[*d*]thiazol-2-yl)-1-propyl-1*H*-indol-5-yl)-2-(4-fluorophenyl)-1*H*-benzo[*de*] isoquinoline-1,3(2*H*)-dione (21): Light brown solid; 61% yield; mp 288-291 °C; ^{1}H NMR ($CDCl_3$, 400 MHz): δ (ppm) 8.62 (t, *J* = 3.72 Hz, 2H, ArH), 8.58 (d, *J* = 7.28 Hz, 1H, ArH), 8.42 (d, *J* = 8.44 Hz, 1H, ArH), 8.36 (s, 1H, ArH), 7.97 (d, *J* = 7.64 Hz, 1H, ArH), 7.93 (t, *J* = 7.32 Hz, 1H, ArH), 7.86 (t, *J* = 8.16 Hz, 2H, ArH), 7.77 (d, *J* = 8.40 Hz, 1H, ArH), 7.49-7.39 (m, 4H, ArH), 7.36-7.31 (m, 3H, ArH), 6.21-6.11 (m, 1H, allyl-CH), 5.33 (d, *J* = 11.20 Hz, 1H, allyl-CH_2), 5.29 (d, *J* = 18.40 Hz, 1H, allyl-CH_2), 5.07 (d, *J* = 4.60 Hz, 2H, allyl-CH_2); MS (ESI): m/z 580.1 (M^++1); Anal Calcd for $C_{36}H_{22}FN_3O_2S$: C, 74.60; H, 3.83; F, 3.28; N, 7.25; S, 5.53; found C, 74.69; H, 3.78; F, 3.35; N, 7.38; S, 5.73.

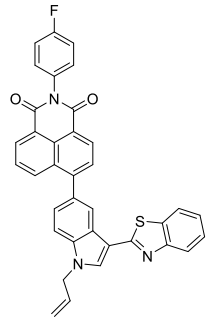

2-Amino-6-(3-(benzo[*d*]thiazol-2-yl)-1-propyl-1*H*-indol-5-yl)-1*H*-benzo[*de*]isoquinoline-1,3(2*H*)-dione (22): Light brown solid; 62% yield; mp 289-292 °C; ^{1}H NMR ($CDCl_3$, 400 MHz): 8.73 (*J* = 7.16 Hz, 1H, ArH), 8.60 (s, 1H, ArH), 8.44 (d, *J* = 8.60 Hz, 1H, ArH), 7.99 (s, 1H, ArH), 7.96 (d, *J* = 8.12 Hz, 1H, ArH), 7.87 (t, *J* = 7.76 Hz, 2H, ArH), 7.73 (t, *J* = 8.08 Hz, 1H, ArH), 7.59 (d, *J* = 8.36 Hz, 1H, ArH), 7.46-δ (ppm) 8.73 (d, *J* = 7.40 Hz, 1H, ArH), 8.68 (d, 7.41 (m, 2H, ArH), 7.32 (t, *J* = 7.40 Hz, 1H, ArH), 5.60 (s, 2H, NH_2), 4.28 (t, *J* = 7.16 Hz, 2H, propyl-CH_2), 2.09-1.99 (m, 2H, propyl-CH_2), 1.08 (t, *J* = 7.28 Hz, 3H, propyl-CH_3); ^{13}C NMR ($CDCl_3$, 100 MHz): δ (ppm) 161.0, 153.8, 148.8, 136.9, 136.8, 133.9, 133.6, 132.6, 132.1, 131.4, 131.2, 130.7, 130.6, 128.5, 127.4, 126.8, 126.0, 125.9, 125.0, 124.2, 123.0, 122.1, 121.2, 111.6, 110.3 (Ar*C*), 48.7 (propyl-*C*H_2), 23.4 (propyl-*C*H_2), 11.5 (propyl-*C*H_3); MS (ESI): m/z 503.1 (M^++1); Anal Calcd for $C_{30}H_{22}N_4O_2S$: C, 71.69; H, 4.41; N, 11.15; S, 6.38; found C, 71.62; H, 4.39; N, 11.10; S, 6.31.

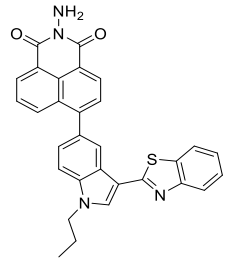

(i) *In vitro* anticancer screening protocol

The human tumor cell lines of the cancer screening panel were grown in RPMI 1640 medium containing 5% fetal bovine serum and 2 mM L-glutamine. Cells were inoculated into 96 well microtiter plates in 100 ml at plating densities ranging from 5,000 to 40,000 cells/well depending on the doubling time of individual cell lines. The microtiter plates were then incubated at 37 °C, 5% CO_2, 95% air and 100% relative humidity for 24 h.

After 24 h, two plates of each cell line were fixed in situ with TCA, to represent a measurement of the cell population for each cell line. Experimental drugs were solubilized in DMSO at 400-fold the desired final maximum test concentration and stored frozen prior to use. At the time of drug addition, an aliquot of frozen concentrate was thawed and diluted to twice the desired final maximum test concentration with complete medium containing 50 μg/ml gentamicin. Additional four, 10-fold or ½ log serial dilutions were made to provide a total of five drug concentrations plus control. Aliquots of 100 μL of these different drug dilutions were added to the appropriate microtiter wells, resulting in the required final drug concentrations. Following drug addition, the plates were incubated for an additional 48 h at 37 °C, 5% CO_2, 95% air, and 100% relative humidity. For adherent cells, the assay was terminated by the addition of cold TCA. Cells were fixed in situ by the gentle addition of 50 μL of cold 50% (w/v) TCA and incubated for 60 min at 4 °C. The supernatant was discarded, and the plates were washed five times with tap water and air dried. Sulforhodamine B (SRB) solution (100 μL) at 0.4% (w/v) in 1% acetic acid was added to each well, and plates were incubated for 10 min at room temperature. After staining, unbound dye was removed by washing five times with 1% acetic acid and the plates were air dried and then subsequently solubilized with 10 mM trizma base, and the absorbance was read on an automated plate reader at a wavelength of 515 nm. Using the seven absorbance measurements [time zero (T_z), control growth (C), and test growth in the presence of drug at the five concentration levels (T_i)], the percentage growth was calculated at each of the drug concentration levels. Percentage growth inhibition was calculated as:

$[(Ti - Tz)/(C - Tz)] \times 100$ for concentrations for which $T_i \geq Tz$; $[(Ti - Tz)/Tz] \times 100$ for concentrations for which $Ti < Tz$.

Three dose response parameters were calculated for each experimental agent. Growth inhibition of 50% (GI_{50}) was calculated from [(Ti -Tz)/(C - Tz)] × 100 = 50. The drug concentration resulting in total growth inhibition (TGI) was calculated from T_i = Tz. The LC_{50} was calculated from [(Ti-Tz)/Tz]×100 = 50.

Anticancer activities were evaluated at 9 panels of cancer cells including 60 different cancer cell lines at NCI, USA. These cancer cell lines are: panel (cell lines); Leukemia (CCRF-CEM, HL-60(TB), K-562, MOLT-4, RPMI-8226, SR), Non-Small Cell Lung Cancer (A549/ATCC, EXVX, HOP-62, HOP-92, NCI-H226, NCI-H23, NCI-H322M, NCI-H460, NCI-522), Colon Cancer (COLO 205, HCC-2998, HCT-116, HCT-15, HT29, KM12, SW-620), CNS Cancer (SF-268, SF-295, SF-539, SNB-19, SNB-75, U251), Melanoma (LOX IMVI, MALME-3M, M14, MDA-MB-435, SK-MEL-2, SK-MEL-28, SK-MEL-5, UACC-257, UACC-62), Ovarian Cancer (IGROV1, OVCAR-3, OVCAR-4, OVCAR-5, OVCAR-8, NCI/ADR-RES, SK-OV-3), Renal Cancer (786-0, A498, ACHN, CAKI-1, RXF 393, SN12C, TK-10, UO-31), Prostate Cancer (PC-3, DU-145), Breast Cancer (MCF7, MDA-MB-231/ATCC, HS 578T, BT-549, T-47D, MDA-MB-468).

(ii) MTT assay protocol

A549 (Lung), MCF7 (Breast) and HeLa (cervix) human cancer cells as well as Hek293 (kidney) human normal cells were cultured in Ham's media or DMEM with 50 mM glutamine, 10% FBS, 100 U/ml pencillin and 100 mg/ml streptomycin. Cells were seeded in two different 96 well plates at the density of $1x10^{-5}$ cells/well in DMEM media supplemented with 10% FBS cells. Cells were incubated at 37 °C in 5% CO_2 incubator. Cells were treated with compound**s** at five concentrations (10^{-4}, 10^{-5}, 10^{-6}, 10^{-7}, 10^{-8} M) at 37 °C for 48 h. 10 μl of MTT (prepared in 1* PBS buffer) from 5 mg/ml stock was added in each well and incubated at 37 °C for 4 h in dark. The formazan crystals were dissolved using 100 μl of DMSO. Further, the amount of formazan crystal formation was measured as difference in absorbance by Bio-Tek ELISA plate reader at 570 nm reference wavelength. All experiments were independently performed at least three times. The relative cell toxicity (%) related to control wells containing culture medium without test material was calculated by using formula (eq. 1):

$$\%\ \text{Cell Toxicity} = 100 - \frac{\text{OD (Compound treated wells)}}{\text{OD (Untreated Wells)}}\ X\ 100 \ldots\ldots\ldots (1)$$

(iii) Cell cycle analysis protocol

Cell cycle analysis was performed using flow cytometer. Cells (MDA-MB-468) were seeded in 6 well plates at a density of 10^5 cells/well in RPMI1640 medium. Cells were incubated for 24 h at

37 °C with 5% CO_2. Then medium was removed and added culture medium containing 1 μM concentration of compounds along with control (without any compound) and incubated for 24 h. Propidium iodide (PI) was used for cell staining. For staining process, approx 10^6 cells were suspended in 0.5 mL of PBS and gently aspirated several times with a Pasteur pipet to obtain a mono-dispersed cell suspension, with minimal cell aggregation. Cells were fixed by transferring this suspension, with a Pasteur pipet, into centrifuge tubes containing 1 mL of 70% ethanol, on ice. Cells were kept in ethanol for at least 2 h at 4°C. The ethanol-suspended cells were centrifuged for 5 min at 300g and then ethanol was poured thoroughly. Suspended the cell pellet in 0.5 mL of PBS, for approx 30 s and centrifuged at 300g for 5 min. Suspended the cell pellet in 0.5 mL of PI staining solution. Kept in the dark at room temperature for 30 min. and then transferred the sample to the flow cytometer and cell fluorescence was measured.

(iv) Sample preparation for DNA and BSA/HSA

The stock solution of calf thymus (ct)-DNA was prepared by dissolving the DNA in 10 mM Tris with 1 mM EDTA (*p*H 7.4) at room temperature. Ratio of absorbance at 260 nm to 280 nm was used to calculate the purity of DNA solution. Concentration of stock solution of DNA was measured taking average extinction coefficient 6600 M^{-1} cm^{-1} of a single nucleotide at 260 nm. The stock solutions (10^{-3} M) of compounds and BSA/HSA were prepared in DMSO and distilled water, respectively.

(v) UV-visible spectroscopic study protocol

The fixed concentration of compounds was titrated with incremental addition of ct-DNA in phosphate buffer (*p*H 7.4) at 298 K. The experiment for BSA/HSA interaction with compounds was performed by taking fixed concentration of BSA/HSA in phosphate buffer (*p*H 7.4) and incremental addition of compounds in phosphate buffer (*p*H 7.4) at 298 K. In both ct-DNA and BSA/HSA interactions studies, base line corrections were carried out using blank solution containing phosphate buffer and UV-visible spectra were noted in the range of 200-800 nm. Binding constants (K_b) were determined from Benesi-Hildebrand equation (eq. 2).

$$\frac{A_0}{(A-A_0)} = \frac{\varepsilon_f}{(\varepsilon_b - \varepsilon_f)} + \frac{\varepsilon_f}{(\varepsilon_b - \varepsilon_f)\, K_b\, [Analyte]} \quad \text{.....(2)}$$

Where A_o is the initial absorbance of the free compound/BSA/HSA, A is the absorbance of compound/BSA/HSA in the presence of analyte (ct-DNA or compound), ε_f and ε_b are molar extinction coefficients of the compound or BSA/HSA in its free and fully bound forms, respectively. The plot of $A_o/(A-A_o)$ versus 1/[analyte] was constructed using the titration data and

linear fitting, and the value of K_b is determined by taking ratio of the intercept to the slope.The free energy of interaction has been calculated using the following relation (eq. 3) with binding constant:

$$\Delta G_{obs} = -RT \ln K_b \text{ …….. (3)}$$

Where $\Delta G_{obs,}$ K_b, T and R are observed binding free energy, binding constant, absolute temperature and gas constant (1.987 cal/K mol), respectively.

(vi) Fluorescence study protocol

For ct-DNA studies, fluorescence emission spectra of compounds were recorded using excitation wavelength of respective compound. The emission intensity of fixed concentration of compounds was recorded with varying concentration of ct-DNA in phosphate buffer (*p*H 7.4) at 298 K, 308 K and 318 K. For BSA/HSA studies, fluorescence spectral measurements were carried out for fixed concentration of BSA/HSA with varying concentration of compounds in phosphate buffer (*p*H 7.4) at 298 K, 308 K and 318 K.

All emission spectra for DNA and BSA/HSA studies were noted in the range of 200 to 800 nm. The excitation and emission slit widths have been maintained constant throughout the experiment. Stern-Volmer equation (eq. 4) was used to find quenching process and to calculate the quenching constants.

$$\frac{F_0}{F} = 1 + K_{sv}\,[\text{Analyte}] = 1 + K_q \tau_o [\text{Analyte}] \text{ …….. (4)}$$

Where F_o and F are the intensities of emission spectra of compounds/BSA/HSA in the absence (free form) and presence of anlyte (ct-DNA or compound), respectively. The Stern-Volmer quenching constant (K_{SV}), which is considered to be a measure of efficiency of fluorescence quenching by analyte and bimolecular quenching constants (K_q), were calculated from plot of F_o/F versus [analyte].

Modified Stern-Volmer equation (eq. 5) was used to get the values of binding constant (K_b) and the average number of binding sites (n).

$$\log \frac{F_o - F}{F} = log K_b + n log[analyte] \text{ …….. (5)}$$

The parameters are same as those of the Stern-Volmer equation. The binding constants (K_b) and the average number of binding sites (n) were calculated from antilog of intercept and slope of the straight regression line respectively, from the plot of log {(F_o-F)/F versus log [analyte]}.

To calculate the thermodynamic parameters i.e. the enthalpy change (ΔH) and entropy change (ΔS), the van't Hoff equation (eq. 6) was used.

$$logK_b = -\frac{\Delta H}{2.303RT} + \frac{\Delta S}{2.303R} \ldots\ldots\ldots\ldots\ldots\ldots (6)$$

Where K_b, T and R are the binding constant, absolute temperature and gas constant, respectively. In addition, the free energy change (ΔG) for the binding of analyte at different temperatures was calculated using the following equation (eq. 7):

$$\Delta G = \Delta H - T\Delta S \ldots\ldots\ldots\ldots\ldots\ldots (7)$$

(vii) DNA melting study protocol

DNA melting experiments were performed by recording the absorption of ct-DNA and complex of ct-DNA with compounds at the wavelength of 260 nm at different temperatures with the spectrophotometer attached with peltier. Melting temperature of the DNA (T_m) was calculated to be the transition midpoint.

(viii) Competitive displacement assay protocol

Ethidium bromide (EB) displacement assay was carried out by adding ligand to EB-DNA complex solution. The ethidium bromide and DNA were titrated with varying concentration of ligand. The EB-DNA complex was excited at 520 nm and emission spectra were recorded between 200 nm and 800 nm. Hoechst dye displacement assay was performed by taking fixed concentration of Hoechst dye and ct-DNA and incremental additions of compounds. Emission spectra were noted between 200-800 nm using 345 nm as an excitation wavelength.

(ix) Circular dichroism (CD) study protocol

CD spectra of ct-DNA and complex of ct-DNA and ligand were recorded using an applied photophysics CD spectrophotometer. All the CD spectra were recorded in a range from 220 nm to 400 nm. The average of four scans was taken in all the experiments. The background spectrum of buffer solution was subtracted from the spectra of DNA and the ligand-DNA complex.

(x) Viscosity measurements protocol

The fixed concentration of ct-DNA was used while varying in compound concentration in viscosity measurement experiment. The digital stopwatch was used to note the flow time. The values of relative viscosity was taken as $(\eta/\eta_o)^{1/3}$ versus ([compound]/[ct-DNA]), where η_o and η are the viscosity contributions of ct-DNA in free form and bound with compound, respectively. The average value of three readings of a sample was recorded for the viscosity determination.

(xi) Iodide quenching study protocol

Iodide quenching studies were completed with incremental addition of potassium iodide solution in compounds and complex of compound-ct-DNA. Emission spectra were recorded in the range of 200-800 nm.

(xii) Synchronous fluorescence spectroscopic study protocol

Synchronous fluorescence study of HSA was completed by taking fixed concentration of BSA/HSA with incremental addition of compounds. Emission spectra were recorded in the range of 200-800 nm and the difference among the excitation and emission wavelengths ($\Delta\lambda = \lambda_{emi} - \lambda_{exc}$) was maintained at 15 nm and 60 nm.

(xiii) FRET between compounds and BSA/HSA protocol

Energy transfer experiment was performed by recording the absorption spectrum of compounds and emission spectrum of BSA/HSA while excited at 280 nm. The energy transfer from donor to acceptor (E), the critical distance on 50% transfer efficiency (R_o), overlap integral of absorption spectrum of the acceptor (compound) with emission spectrum of the donor (BSA/HSA) (*J*) could be calculated using the following equations (eq. 8, 9 and 10):

$$E = 1 - \frac{F}{F_o} = \frac{R_0^6}{R_0^6 + r^6} \quad \text{..... (8)}$$

F_o and F are the intensities of the fluorescence of HSA in the absence and presence of compound. R_o and r are the critical distance on 50% transfer efficiency and distance between donor and acceptor, respectively.

$$R_o^6 = 8.8 \times 10^{-25} k^2 \eta^{-4} \phi J \quad \text{..... (9)}$$

k^2 is orientation factor of dipoles, η is refracted index of medium, *J* is overlap integral of electronic absorption spectrum of the acceptor (compound) with emission spectrum of the donor (BSA/HSA) and Φ is fluorescence quantum yield of donor (HSA).

$$J = \frac{\sum F(\lambda)\varepsilon(\lambda)\lambda^4 \Delta\lambda}{\sum F(\lambda)\Delta\lambda} \quad \text{..... (10)}$$

Where $F(\lambda)$ is the intensity of emission of the donor (HSA) in absence of the acceptor (compound) at the wavelength λ, and $\varepsilon(\lambda)$ is molar absorption coefficient of acceptor (compound) at the same wavelength.

(xiv) Shake-flask method

Partition coefficient of derivatives was measured with *n*-octanol-phosphate buffer (0.15 M, *p*H = 7.4) at volumes of 10:1. Stock solutions of derivatives were made in dimethylsulfoxide (HPLC grade) at 10^{-3} M concentration. All solutions throughout the experimentation were prepared in glass vials; stock solution and phosphate buffer (250 μL, 125 μL) were added to the glass vial using micropipette. The wavelength was chosen according to the λ_{max} of derivative. Initial absorbance (A_i) of each derivative was recorded using stock solution in the buffer phase. Then, *n*-octanol was added to the each glass vial and shaken together on a mechanical shaker (METREX, Cat No. MRS-50H) for 50 minutes. All glass vials were centrifuged (REMI R-24) at 2500 rpm for 35 minutes to get thoroughly separation of both phases. Octanol layer was removed from the vial and final absorbance (A_f) of the buffer layer was recorded. P values for all derivatives were calculated using following equation (eq. 11):

$$P = \frac{A_i - A_f}{A_f} \times \frac{V_w}{V_o} \quad \text{..... (11)}$$

Where V_w and V_o denote the volume of the aqueous phase and organic phase, respectively.

(xv) Docking Simulation protocol

Molecular docking of the complexes into 3-D X-ray structure of DNA (PdB: 1BNA) was carried out using the AutoDock software package (vina). The ligand structures in docking protocol were used as a crystal structure. The graphical user interface AutoDockTools (1.5.6rc3) was performed to setup every ligand DNA interaction, where all hydrogen atoms were added, gasteiger charges were calculated and nonpolar hydrogen atoms were merged to carbon atoms. The 3D structures of the ligands were optimized using Gaussian 09W program and saved in pdb format. The partial charges of pdb file were further modified by using the ADT package (version 1.5.6rc3), so that the charges of the nonpolar hydrogen atoms would be assigned to the atom to which the hydrogen is attached. The resulting file was saved as Pdbqt file. The AutoDockTools program was used to generate the docking put files. In all docking, a grid pointing in x, y and z directions were built. A grid spacing of 0.375 Å was used. Default settings were used with an initial population.

References

1. Cancer Research UK; https://www.cancerresearchuk.org/health-professional/cancer-statistics/worldwide-cancer#heading-Two [Accessed on July/2019]
2. M. Ferlay, I. Colombet, C. Soerjomataram, D. M. Mathers, M. Parkin, A. Piñeros, F. Znaor, Bray, Estimating the global cancer incidence and mortality in 2018: GLOBOCAN sources and methods, *Int. J. Cancer*, **2019**, *144*, 1941-1953.
3. P. Singh, R. Raj, V. Kumar, M. P. Mahajan, P. Bedi, T. Kaur, A. Saxena, 1, 2, 3-Triazole tethered β-lactam-chalcone bifunctional hybrids: synthesis and anticancer evaluation, *Eur. J. Med. Chem.*, **2012**, *47*, 594-600.
4. Z. Chen, X. Liang, H. Zhang, H. Xie, J. Liu, Y. Xu, W. Zhu, Y. Wang, X. Wang, S. Tan, A new class of naphthalimide-based antitumor agents that inhibit topoisomerase II and induce lysosomal membrane permeabilization and apoptosis, *J. Med. Chem.*, **2010**, *53*, 2589-2600.
5. H. Prinz, A. K. Ridder, K. Vogel, K. J. Böhm, I. Ivanov, J. B. Ghasemi, E. Aghaee, K. J. Müller, *N*-heterocyclic (4-phenylpiperazin-1-yl) methanones derived from phenoxazine and phenothiazine as highly potent inhibitors of tubulin polymerization, *Med. Chem.*, **2017**, *60*, 749-755.
6. R. Morphy, Z. Rankovic, Designed multiple ligands. An emerging drug discovery paradigm, *J. Med. Chem.*, **2005**, *48*, 6523-6543.
7. A. L. Hopkins, Network pharmacology: the next paradigm in drug discovery, *Nat. Chem. Biol.*, **2008**, *4*, 682-690.
8. S. Fortin, G. Bérubé, Advances in the development of hybrid anticancer drugs, *Expert Opin. Drug Discov.*, **2013**, *8*, 1029-1047.
9. R. Morphy, C. Kay, Z. Rankovic, From magic bullets to designed multiple ligands, *Drug Discov. Today*, **2004**, *9*, 641-651.
10. J. Walsh, A. Bell, Hybrid drugs for malaria, *Curr. Pharm. Des.*, **2009**, *15*, 2970-2985.
11. L. K. Gediya, V. C. O. Njar, Promise and challenges in drug discovery and development of hybrid anticancer drugs, *Expert Opin. Drug Discov.*, **2009,** *4*, 1099-1111.
12. C. Viegas-Junior, A. Danuello, B. V. da Silva, E. J. Barreiro, C. A. Fraga, Molecular hybridization: a useful tool in the design of new drug prototypes, *Curr. Med. Chem.*, **2007**, *14*, 1829-1852.

13. H. H. Gong, D. Addla, J. S. Lv, C. H. Zhou, Heterocyclic naphthalimides as new skeleton structure of compounds with increasingly expanding relational medicinal applications, *Curr. Top. Med. Chem.*, **2016**, *16*, 3303-3364.

14. S. Banerjee, E. B. Veale, C. M. Phelan, S. A. Murphy, G. M. Tocci, L. J. Gillespie, D. O. Frimannsson, J. M. Kelly, T. Gunnlaugsson, Recent advances in the development of 1,8-naphthalimide based DNA targeting binders, anticancer and fluorescent cellular imaging agents, *Chem. Soc. Rev.*, **2013**, *42*, 1601-1618.

15. J. S. Lv, X. M. Peng, B. Kishore, C. H. Zhou, 1,2,3-Triazole derived naphthalimides as a novel type of potential antimicrobial agents: Synthesis, antimicrobial activity, interaction with calf thymus DNA and human serum albumin, *Bioorg. Med. Chem. Lett.*, **2014**, *24*, 308-313.

16. F. J. Dai, Q. Li, Y. X. Wang, C. C. Ge, C. Y. Feng, S. Q. Xie, H. Y. He, X. J. Xu, C. J. Wang, Design, synthesis, and biological evaluation of mitochondria-targeted flavone-naphthalimide polyamine conjugates with antimetastatic activity, *J. Med. Chem.*, **2017**, *60*, 2071-2083.

17. K. Xu, P. M. Schwarz, R. F. Ludueña, Interaction of nocodazole with tubulin isotypes, *Drug Dev. Res.*, **2002**, *55*, 91-96.

18. (a) L. A. Hammond, K. Davidson, R. Lawrence, J. B. Camden, D. D. Von Hoff, S. Weitman, E. Izbicka, Exploring the mechanisms of action of FB642 at the cellular level, *J. Cancer Res. Clin. Oncol.*, **2001**, *127*, 301-313; (b) D. Hao, J. D. Rizzo, S. Stringer, R. V. Moore, J. Marty, D. L. Dexter, G. L. Mangold, J. B. Camden, D. D. Von Hoff, S. D. Weitman, Preclinical antitumor activity and pharmacokinetics of methyl-2-benzimidazolecarbamate (FB642), *Invest. New. Drugs*, **2000**, *20*, 261-270.

19. C. K. Donawho, Y. Luo, Y. Luo, T. D. Penning, J. L. Bauch, J. J. Bouska, V. D. Bontcheva-Diaz, B. F. Cox, T. L. DeWeese, L. E. Dillehay, D. C. Ferguson, N. S. Ghoreishi-Haack, D. R. Grimm, R. Guan, E. K. Han, R. R. Holley-Shanks, B. Hristov, K. B. Idler, K. Jarvis, E. F. Johnson, L. R. Kleinberg, V. Klinghofer, L. M. Lasko, X. Liu, K. C. Marsh, T. P. McGonigal, J. A. Meulbroek, A. M. Olson, J. P. Palma, L. E. Rodriguez, Y. Shi, J. A. Stavropoulos, A. C. Tsurutani, G. D. Zhu, S. H. Rosenberg, V. L. Giranda, D. J. Frost, ABT-888, an orally active poly(ADP-Ribose) polymerase inhibitor that potentiates DNA-damaging agents in preclinical tumor models, *Clin. Cancer Res.*, **2007**, *13*, 2728-2737.

20. A. E. Guerini, L. Triggiani, M. Maddalo, M. L. Bonù, F. Frassine, A. Baiguini, A. Alghisi, D. Tomasini, P. Borghetti, N. Pasinetti, R. Bresciani, S. M. Magrini, M. Buglione, Mebendazole as a candidate for drug repurposing in oncology: An extensive review of current literature, *Cancers,* **2019**, *11*, 1284-1296.

21. M. Hegde, K. S. S. Kumar, E. Thomas, E. Ananda, S. C. Raghavan, K. S. Rangappa, A novel benzimidazole derivative binds to the DNA minor groove and induces apoptosis in leukemic cells, *RSC Adv.,* **2015,** *5*, 93194-93208.

22. A. S. Alpan, S. Zencir, I. Zupkó, G. Coban, B. Réthy, H. S. Gunes, Z. Topcu, Biological activity of bis-benzimidazole derivatives on DNA topoisomerase I and HeLa, MCF7 and A431 cells, *J. Enzyme Inhib. Med. Chem.,* **2009**, *24*, 844-849.

23. B. Maji, K. Kumar, M. Kaulage, K. Muniyappa, S. Bhattacharya, Design and synthesis of new benzimidazole-carbazole conjugates for the stabilization of human telomeric DNA, telomerase inhibition, and their selective action on cancer cells, *J. Med. Chem.,* **2014**, *57*, 6973-6988.

24. N. Bouloc, J. M. Large, M. Kosmopoulou, C. Sun, A. Faisal, M. Matteucci, J. Reynisson, N. Brown, B. Atrash, J. Blagg, E. McDonald, S. Linardopoulos, R. Bayliss, V. Bavetsias, Structure-based design of imidazo[1,2-*a*]pyrazine derivatives as selective inhibitors of Aurora-A kinase in cells, *Bioorg. Med. Chem. Lett.,* **2010**, *20*, 5988-5993.

25. S. M. Gonzalez, A. I. Hernandez, C. Varela, S. Rodriguez-Aristegui, R. M. Alvarez, A. B. Garcia, M. Lorenzo, V. Rivero, J. Oyarzabal, O. Rabal, J. R. Bischoff, M. Albarran, A. Cebria, P. Alfonso, W. Link, J. Fominaya, J. Pastor, Imidazo[1,2-*a*]pyrazines as novel PI3K inhibitors, *Bioorg. Med. Chem. Lett.,* **2012**, *22*, 1874-1878.

26. H. Zeng, D. B. Belanger, P. J. Curran, Jr. G. W. Shipps, H. Miao, J. B. Bracken, M. A. Siddiqui, M. Malkowski, Y. Wang, Discovery of novel imidazo[1,2-*a*]pyrazin-8-amines as Brk/PTK6 inhibitors, *Bioorg. Med. Chem. Lett.*, **2011**, *21*, 5870-5875.

27. T. P. Matthews, T. McHardy, S. Klair, K. Boxall, M. Fisher, M. Cherry, C. E. Allen, G. J. Addison, G. Ellard, G. W. Aherne, I. M. Westwood, R. V. Montfort, M. D. Garrett, J. C. Reader I. Collins, Design and evaluation of 3,6-di(hetero)aryl imidazo[1,2-*a*]pyrazines as inhibitors of checkpoint and other kinases, *Bioorg. Med. Chem. Lett.* **2010**, *20,* 4045-4049.

28. K. S. Currie, J. E. Kropf, T. Lee, P. Blomgren, J. Xu, Z. Zhao, S. Gallion, J. A. Whitney, D. Maclin, E. B. Lansdon, P. Maciejewski, A. M. Rossi, H. Rong, J. Macaluso, J. Barbosa,

J. A. D. Paolo, S. A. Mitchell, Discovery of GS-9973, a selective and orally efficacious inhibitor of spleen tyrosine kinase *J. Med. Chem*., **2014**, *57*, 3856-3873.

29. A. T. Baviskar, C. Madaan, R. Preet, P. Mohapatra, V. Jain, A. Agarwal, S. K. Guchhait, C. N. Kundu, U. C. Banerjee, P. V. Bharatam, *N*-fused imidazoles as novel anticancer agents that inhibit catalytic activity of topoisomerase IIα and induce apoptosis in G1/S phase, *J. Med. Chem*., **2011**, *54*, 5013-5030.

30. M. P. Dwyer, K. Paruch, C. Alvarez, R. J. Doll, K. Keertikar, J. Duca, T. O. Fischmann, A. Hruza, V. Madison, E. Lees, D. Parry, W. Seghezzi, N. Sgambellone, F. Shanahan, D. Wiswell T. J. Guzi, Versatile templates for the development of novel kinase inhibitors: Discovery of novel CDK inhibitors, *Bioorg. Med. Chem. Lett.,* **2007**, *17*, 6216-6224.

31. E. A. Steck, A. R. Day, Reactions of phenanthraquinone and retenequinone with aldehydes and ammonium acetate in acetic acid solution, *J. Am. Chem. Soc.,* **1943**, *65*, 452-456.

32. A. Sharma, V. Luxami, K. Paul, Purine-benzimidazole hybrids: Synthesis, single crystal determination and *in vitro* evaluation of antitumor activities, *Eur. J. Med. Chem.,* **2015**, *93,* 414-422.

33. P. Singla, V. Luxami, K. Paul, Synthesis and *in vitro* evaluation of novel triazine analogues as anticancer agents and their interaction studies with bovine serum albumin, *Eur. J. Med. Chem.*, **2016**, *117*, 59-69.

34. P. Q. Espinoza, P. M. Acosta, A. Amesty, P. M. Rodríguez, I. L. Castrillejo, L. F. Pérez, F. Machín, A. E. Braun, 5-Ethynylarylnaphthalimides as antitumor agents: Synthesis and biological evaluation, *Bioorg. Med. Chem.,* **2017**, *25*, 1976-1983.

35. R. S. Keri, M. R. Patil, S. A. Patil, S. Budagumpi, A comprehensive review in current developments of benzothiazole-based molecules in medicinal chemistry, *Eur. J. Med. Chem.*, **2015**, *89*, 207-251.

36. S. A. Patil, R. Patil, D. D. Miller, Indole molecules as inhibitors of tubulin polymerization: potential new anticancer agents, *Future Med. Chem.,* **2012**, *4*, 2085-2115.

37. X. Lin, D. Kang, X. Li, P. Zhan, X. Liu, Q. Zhang, Discovery and characterization of novel imidazopyridine derivative CHEQ-2 as a potent CDC25 inhibitor and promising anticancer drug candidate, *Eur. J. Med. Chem.*, **2014**, *82*, 293-307.

38. P. Ramanathan, Synthesis, spectral characterization and biological studies of 2-(4-methoxynaphthalen-1-Yl)-1-(4-methoxyphenyl)-1*H*-phenanthro[9,10-*d*]imidazole, *Mod. Chem. Appl.*, **2017**, *205*, 4-9.

39. (a) P. C. Shyma, B. Kalluraya, S. K. Peethambar, S. Telkar, T. Arulmoli, Synthesis, characterization and molecular docking studies of some new 1, 3, 4-oxadiazolines bearing 6-methylpyridine moiety for antimicrobial property, *Eur. J. Med. Chem.*, **2013**, *68*, 394-404; (b) A. M. Vijesh, A. M. Isloor, S. K. Peethambar, Hantzsch reaction: synthesis and characterization of some new 1, 4-dihydropyridine derivatives as potent antimicrobial and antioxidant agents, *Eur. J. Med. Chem.*, **2011**, *46*, 5591-5597.

40. S. Tan, H. Yin, Z. Chen, X. Qian, Y. Xu, Oxo-heterocyclic fused naphthalimides as antitumor agents: Synthesis and biological evaluation, *Eur. J. Med. Chem*., **2013**, *62*, 130-138.

41. X. Wang, Z. Chen, L. Tong, S. Tan, W. Zhou, T. Peng, K. Han, J. Ding, H. Xie, Y. Xu, Naphthalimides exhibit *in vitro* antiproliferative and antiangiogenic activities by inhibiting both topoisomerase II (topo II) and receptor tyrosine kinases (RTKs), *Eur. J. Med. Chem*., **2013**, *65*, 477-486.

42. K. R. Wang, F. Qian, Q. Sun, C. L. Ma, R. X. Rong, Z. R. Cao, X. M. Wang, X. L. Li, Substituent effects on cytotoxic activity, spectroscopic property, and DNA binding property of naphthalimide derivatives, *Chem. Biol. Drug Des.*, **2016**, *87*, 664-672.

43. R. X. Rong, Q. Sun, C. L. Ma, B. Chen, W. Y. Wang, Z. A. Wang, K. R. Wang, Z. R. Cao, X. L. Li, Development of novel bis-naphthalimide derivatives and their anticancer properties, *Med. Chem. Comm.*, **2013**, *7*, 679-685.

44. Y. Huang, C. X. Wu, Y. Song, M. Huang, D. N. Tian, X. B. Yang, Y. R. Fan, Synthesis, DNA binding, and anticancer properties of bis-naphthalimide derivatives with lysine-modified polyamine linkers, *Molecules*, **2018**, *23*, 266-77.

45. L. Yurttas, Ş. Demirayak, G. A. Çiftçi, Ş. U. Yıldırım, Z. A. Kaplancıklı, Synthesis and biological evaluation of some 1,2-disubstituted benzimidazole derivatives as new potential anticancer agents, *Arch. Pharm. Chem. Life Sci.*, **2013**, *346*, 403-414.

46. K. P. Shao, X. Y. Zhang, P. J. Chen, D. Q. Xue, P. He, L. Y. Ma, J. X. Zheng, Q. R. Zhang, H. M. Liu, Synthesis and biological evaluation of novel pyrimidine-benzimidazole hybrids as potential anticancer agents, *Bioorg. Med. Chem. Lett.*, **2014**, *24*, 3877-3881.

47. A. S. A. Rahim, S. M. Salhimi, N. Arumugam, L. C. Pin, N. S. Yee, N. N. Muttiah, W. B. Keat, S. A. Hamid, H. Osman, I. b. Mat, Microwave-assisted synthesis of *sec/tert*-butyl 2-arylbenzimidazoles and their unexpected antiproliferative activity towards ER negative breast cancer cells, *J. Enzyme Inhib. Med. Chem.*, **2013**, *28*, 1255-1260.

48. C. G. Mortimer, G. Wells, J. P. Crochard, E. L. Stone, T. D. Bradshaw, M. F. G. Stevens, A. D. Westwell, Antitumor benzothiazoles. 26. 2-(3,4-Dimethoxyphenyl)-5-fluorobenzothiazole (GW 610, NSC 721648), a simple fluorinated 2-arylbenzothiazole, shows potent and selective inhibitory activity against lung, colon, and breast cancer cell lines, *J. Med. Chem.*, **2006**, *49*, 179-185.

49. D. Osmaniye, S. Levent, A. B. Karaduman, S. Ilgın, Y. Özkay, Z. A. Kaplancıklı, Synthesis of new benzothiazole acylhydrazones as anticancer agents, *Molecules*, **2018**, *23*, 1054-1068.

50. S. Myadaraboina, M. Alla, V. Saddanapu, V. R. Bommenaa, A. Addlagatta, Structure activity relationship studies of imidazo[1,2-*a*]pyrazine derivatives against cancer cell lines, *Eur. J. Med. Chem.*, **2010**, *45*, 5208-5216.

51. S. Xu, C. Sun, C. Chen, P. Zheng, Y. Zhou, H. Zhou, W. Zhu, Synthesis and biological evaluation of novel 8-morpholinoimidazo[1,2-*a*]pyrazine derivatives bearing phenylpyridine/phenylpyrimidine-carboxamides, *Molecules*, **2017**, *22*, 310-323.

52. S. Demirayak, I. Kayagil, Synthesis of some 6,8-diarylimidazo[1,2-*a*]pyrazine derivatives by using either reflux or microwave irradiation method and investigation of their anticancer activities, *J. Heterocyclic Chem*., **2005**, *42*, 319-325.

53. A. Patel, S. Y. Sharp, K. Hall, W. Lewis, M. F. G. Stevens, P. Workman, C. J. Moody, Fused imidazoles as potential chemical scaffolds for inhibition of heat shock protein 70 and induction of apoptosis. Synthesis and biological evaluation of phenanthro[9,10-*d*]imidazoles and imidazo[4,5-*f*][1,10]phenanthrolines, *Org. Biomol. Chem*., **2016**, *14*, 3889-3905.

54. S. Wanga, H. Li, C. Chen, J. Zhang, S. Li, X. Qin, X. Li, K. Wang, Cytotoxicity and DNA binding property of phenanthrene imidazole with polyglycol side chains, *Bioorg. Med. Chem. Lett.*, **2012**, *22*, 6347-6351.

55. S. Liao, Z. Zhang, Q. Wub, X. Wangc, W. Mei, Microwave-assisted synthesis of phenanthroimidazole derivatives as stabilizer of c-myc G-quadruplex DNA, *Bioorg. Med. Chem.*, **2014**, *22*, 6503-6508.

56. K. Liu, W. Rao, H. Parikh, Q. Li, T. L. Guo, S. Grant, G. E. Kellogg, S. Zhang, 3,5-Disubstituted-thiazolidine-2,4-dione analogs as anticancer agents: Design, synthesis and biological characterization, *Eur. J. Med. Chem.*, **2012**, *47*, 125-137.

57. V. Patil, K. Tilekar, S. Mehendale-Munj, R. Mohan, C. S. Ramaa, Synthesis and primary cytotoxicity evaluation of new 5-benzylidene-2, 4-thiazolidinedione derivatives, *Eur. J. Med. Chem.*, **2010**, *45*, 4539-4544.

58. G. L. Regina, R. Bai, A. Coluccia, V. Naccarato, V. Famiglini, M. Nalli, D. Masci, A. Verrico, P. Rovella, C. Mazzoccoli, E. D. Pozzo, C. Cavallini, C. Martini, S. Vultaggio, G. Dondio, M. Varasi, C. Mercurio, E. Hamel, P. Lavia, R. Silvestri, New 6- and 7-heterocyclyl-1*H*-indole derivatives as potent tubulin assembly and cancer cell growth inhibitors. *Eur. J. Med. Chem.*, **2018**, *152*, 283-297.

59. G. Regina, R. Bai, A. Coluccia, V. Famiglini, S. Pelliccia, S. Passacantilli, C. Mazzoccoli, V. Ruggieri, A. Verrico, A. Miele, L. Monti, M. Nalli, R. Alfonsi, L. D. Marcotullio, A. Gulino, B. Ricci, A. Soriani, A. Santoni, M. Caraglia, S. Porto, E. D. Pozzo, C. Martini, A. Brancale, L. Marinelli, E. Novellino, S. Vultaggio, M. Varasi, C. Mercurio, C. Bigogno, G. Dondio, E. Hamel, P. Lavia, R. Silvestri, New indole tubulin assembly inhibitors cause stable arrest of mitotic progression, enhanced stimulation of natural killer cell cytotoxic activity, and repression of hedgehog-dependent cancer, *J. Med. Chem.*, **2015**, *58*, 5789-5807.

60. R. Gaikwad, Y. Bobde, R. Ganesh, T. Patel, A. Rathore, B. Ghosh, K. Das, S. Gayen, 2-Phenylindole derivatives as anticancer agents: Synthesis and screening against murine melanoma, human lung and breast cancer cell lines, *Synth. Commun.*, **2019**, *49*, 2258-2269.

61. J. Chena, J. Yana, J. Hua, Y. Panga, L. Huanga, X. Lia, Synthesis, biological evaluation and mechanism study of chalcone analogues as novel anti-cancer agents, *RSC Adv.*, **2015**, *5*, 68128-76835.

62. Z. Wanga, X. Denga, S. Xionga, R. Xionga, J. Liua, L. Zoua, X. Leia, X. Caoa, Z. Xiea, Y. Chenb, Y. Liua, X. Zhenga, G. Tanga, Design, synthesis and biological evaluation of

chrysin benzimidazole derivatives as potential anticancer agents, *Nat. Prod. Res.,* **2018**, *32*, 2900-2909.

63. S. Li, S. Xu, Y. Tang, S. Ding, J. Zhang, S. Wanga, G. Zhou, C. Zhou, X. Li, Synthesis, anticancer activity and DNA-binding properties of novel 4-pyrazolyl-1,8-naphthalimide derivatives, *Bioorg. Med. Chem. Lett*., **2014**, *24*, 586-590.

64. P. Singla, V. Luxami, K. Paul, Synthesis, *in vitro* antitumor activity, dihydrofolate reductase inhibition, DNA intercalation and structure-activity relationship studies of 1,3,5-triazine analogues, *Bioorg. Med. Chem. Lett.*, **2016**, *26*, 518-523.

65. W. O. Foye, Cancer chemotherapeutic agents, American chemical society, Washington, DC, **1995**, ISBN: 0-8412-2920-1.

66. A. Mukherjee, W. D. Sasikala, Chapter one-Drug-DNA intercalation: From discovery to the molecular mechanism, *Adv. Protein Chem. Struct., Biol.,* **2013**, *92*, 1-62.

67. K. Paul, A. Sharma, V. Luxami, Synthesis and *in vitro* antitumor evaluation of primary amine substituted quinazoline linked benzimidazole, *Bioorg. Med. Chem. Lett.* **2014**, *24*, 624-629.

68. M. Verma, V. Luxami, K. Paul, Synthesis, *in vitro* evaluation and molecular modelling of naphthalimide analogue as anticancer agents, *Eur. J. Med. Chem.,* **2013**, *68*, 352-360.

69. V. A. Sontakke, A. N. Kate, S. Ghosh, P. More, R. Gonnade, N. M. Kumbhar, A. A. Kumbhar, B. A. Chopade, V. S. Shinde, Synthesis, DNA interaction and anticancer activity of 2-anthryl substituted benzimidazole derivatives, *New J. Chem.,* **2015**, *39*, 4882-4890.

70. R. Goel, V. Luxami, K. Paul, Palladium catalyzed novel monoarylation and symmetrical/unsymmetrical diarylation of imidazo[1,2-*a*]pyrazines and their *in vitro* anticancer activities, *RSC Adv.,* **2014**, *19*, 9885-9892.

71. (a) M. R. Grever, S. A. Sehepartz, B. A. Chabners, The national cancer institute: Cancer drug discovery and development program, *Semin. Oncol.* **1992**, *19*, 622-638; (b) A. Monks, D. Schudiero, P. Skehan, R. Shoemaker, K. Paull, D. Vistica, C. Hose, J. Langley, P. Cronise, A. Vaigro-Wolff, M. Gray-Goodrich, H. Campbell, J. Mayo, M. J. Boyd, Feasibility of a high-flux anticancer drug screen using a diverse panel of cultured human tumor cell lines, *J. Natl. Cancer Inst.* **1991**, *83*, 757-766; (c) M. R. Boyd, K. D. Paull, Some practical considerations and applications of the National Cancer Institute *in vitro* anticancer drug discovery screen, *Drug Dev. Res.* **1995**, *34*, 91-109.

72. F. Arjmand, M. Aziz, Synthesis and characterization of dinuclear macrocyclic cobalt (II), copper(II) and zinc(II) complexes derived from 2,2,20,20-S,S[bis(bis-*N*,*N*-2-thiobenzimidazolyloxalato-1,2-ethane)]: DNA binding and cleavage studies, *Eur. J. Med. Chem.,* **2009**, *44*, 834-844.

73. H. A. Benesi, J. H. Hildebrand, A spectrophotometric investigation of the interaction of iodine with aromatic hydrocarbons, *J. Am. Chem. Soc.*, **1949**, *71*, 2703-2707.

74. R. Palchaudhuri, P. J. Hergenrother, DNA as a target for anticancer compounds: Methods to determine the mode of binding and the mechanism of action, *Curr. Opin. Biotechnol.*, **2007**, *18*, 497-503.

75. M. R. Eftink, C. A. Ghiron, Fluorescence quenching studies with proteins, *Anal. Biochem.*, **1981**, *114*, 199-227.

76. J. R. Lakowicz, G. Weber, Quenching of protein fluorescence by oxygen. Detection of structural fluctuations in proteins on the nanosecond time scale, *Biochemistry*, **1973**, *12*, 4171-4179.

77. J. R. Lakowicz, G. Webber, Quenching of fluorescence by oxygen. Probe for structural fluctuations in macromolecules, *Biochemistry,* **1973**, *12*, 4161-4170.

78. (a) I. Parveen, P. Khan, S. Ali, I. Md. Hassan, N. Ahmed, Synthesis, molecular docking and inhibition studies of novel 3-*N*-aryl substituted-2-heteroarylchromones targeting microtubule affinity regulating kinase 4 inhibitors, *Eur. J. Med. Chem.*, **2018**, *159*, 166-177; (b) P. Bourassa, S. Dubeau, G. M. Maharvi, A. H. Fauq, T. J. Thomas, H. A. Tajmir-Riahi, Locating the binding sites of anticancer tamoxifen and its metabolites 4-hydroxytamoxifen and endoxifen on bovine serum albumin, *Eur. J. Med. Chem.*, **2011**, *46*, 4344-4353.

79. I. Haq, Thermodynamics of drug-DNA interactions, *Arch. Biochem. Biophys.*, **2002**, *403*, 1-15.

80. J. B. Lepecq, C. Paoletti, A fluorescent complex between ethidium bromide and nucleic acids physical-chemical characterization, *J. Mol. Biol*., **1967**, *27*, 87-106.

81. M. Eriksson, B. Nordén, Linear and circular dichroism of drug-nucleic acid complexes, *Methods Enzymol.,* **2001**, *340*, 68-98

82. A. Rodger, B. Norden, In circular dichroism and linear dichroism, Oxford university press, New York, **1997**, Chapter 2.

83. C. A. Lipinski, F. Lombardo, B. W. Dominy, P. J. Feeney, Experimental and computational approaches to estimate solubility and permeability in drug discovery and development settings, *Adv. Drug Deliv. Rev.*, **1997**, *23*, 3-25.

84. P. Ertl, B. Rodhe, P. Selzer, Fast calculation of molecular polar surface areas as a sum of fragment based contribution and its application to the prediction of drug transport properties, *J. Med. Chem.*, **2000**, *43*, 3714-3717.

85. S. Prasanna, R. J. Doerksen, Topological polar surface area: a useful descriptor in 2D-QSAR, *Curr. Med. Chem.*, **2009**, *16*, 21-41.

86. N. Berova, K. Nakanishi, R. W. Woody, Circular dichroism principles and applications, 2nd ed., Wiley-VCH, New York, **2000**.

87. M. Mohamadi, S. Y. Ebrahimipour, M. Torkzadeh-Mahani, S. Foro, A. Akbari, A mononuclear diketone-based oxido-vanadium(IV) complex: structure, DNA and BSA binding, molecular docking and anticancer activities against MCF-7, HPG-2, and HT-29 cell lines, *RSC Adv.*, **2015**, *5*, 101063-101075.

88. S. Fortli, R. Huey, M. E. Pique, M. Sanner, D. S. Goodsele, A. J. Olson, Computational protein-ligand docking and virtual drug screening with the AutoDock suite, *Nat. Protoc.*, **2016**, *11*, 905-919.

89. T. Sarwar, M. A. Husain, S. Ur Rehman, H. M. Ishqi, M. Tabish, Multi-spectroscopic and molecular modelling studies on the interaction of esculetin with calf thymus DNA, *Mol. Biosyst.*, **2015**, *11*, 522-531.

90. F. Maya, J. M. Tour, Synthesis of terphenyl oligomers as molecular electronic device candidates, *Tetrahedron*, **2004**, *60*, 81-92.

91. L. H. Hurley, DNA and its associated processes as targets for cancer therapy, *Nat. Rev. Cancer*, **2002**, *2*, 188-200.

92. Z. F. Tao, L. Wang, K. D. Stewart, Z. H. Chen, W. Gu, M. H. Bui, P. Merta, H. Y. Zhang, P. Kovar, E. Johnson, C. Park, R. Judge, S. Rosenberg, T. Sowin, N. H. Lin, Structure-based design, synthesis, and biological evaluation of potent and selective macrocyclic checkpoint kinase 1 inhibitors, *J. Med. Chem.*, **2007**, *50*, 1514-1527.

93. M. F. Brana, A. Ramos, Naphthalimides as anti-cancer agents: Synthesis and biological activity, *Curr. Med. Chem. Anti-Cancer Agents*, **2001**, *1*, 237-255.

94. M. J. Ratain, R. Mick, F. Berezin, L. Janisch, R. L. Schilsky, N. J. Vogelzang, L. B. Lane, Phase I study of amonafide dosing based on acetylator phenotype, *Cancer Res.*, **1993**, *53*, 2304-2308.

95. M. F. Brana, M. Cacho, M. A. Garcia, B. de Pascual-Teresa, A. Ramos, M. T. Dominguez, J. M. Pozuelo, C. Abradelo, M. F. Rey-Stolle, M. Yuste, M. Banez-Coronel, J. C. Lacal, New analogues of amonafide and elinafide, containing aromatic heterocycles: Synthesis, antitumor activity, molecular modeling, and DNA binding properties, *J. Med. Chem.*, **2004**, *47*, 1391-1399.

96. I. Antonini, G. Santoni, R. Lucciarini, C. Amantini, S. Sparapani, A. Magnano, Synthesis and biological evaluation of new asymmetrical bisintercalators as potential antitumor drugs, *J. Med. Chem.*, **2006**, *49*, 7198-7207.

97. E. Van Quaquebeke, T. Mahieu, P. Dumont, J. Dewelle, F. Ribaucour, G. Simon, S. Sauvage, J. F. Gaussin, J. Tuti, M. El Yazidi, F. Van Vynckt, T. Mijatovic, F. Lefranc, F. Darro, R. Kiss, 2,2,2-Trichloro-*N*-({2-[2-(dimethylamino)ethyl]-1,3-dioxo-2,3-dihydro-1*H*-benzo[*de*]isoquinolin5-yl}carbamoyl)acetamide (UNBS3157), a novel nonhematotoxic naphthalimide derivative with potent antitumor activity, *J. Med. Chem.***,** **2007**, *50*, 4122-4134.

98. V. Tumiatti, A. Milelli, A. Minarini, M. Rosini, M. L. Bolognesi, M. Micco, V. Andrisano, M. Bartolini, F. Mancini, M. Recanatini, A. Cavalli, C. Melchiorre, Structure-activity relationships of acetylcholinesterase noncovalent inhibitors based on a polyamine backbone. Further investigation on the inner spacer, *J. Med. Chem.*, **2008**, *51*, 7308-7312.

99. Z. G. Li, Q. Yang, X. H. Qian, Novel thiazonaphthalimides as efficient antitumor and DNA photocleaving agents: Effects of intercalation, side chains, and substituent groups, *Bioorg. Med. Chem.*, **2005**, *13*, 4864–4870.

100. (a) Y. Bansal, O. Silakari, The therapeutic journey of benzimidazoles: A review, *Bioorg Med. Chem.*, **2012**, *20*, 6208-6236; (b) A. A. El Rashedy, H. Y. Aboul-Enein, Benzimidazole derivatives as potential anticancer agents, *Mini Rev. Med. Chem.*, **2013**, *13*, 399-407.

101. (a) A. Paul, S. Anbu, G. Sharma, M. L. Kuznetsov, B. Koch, M. F. C. G. da Silva, A. J. L. Pombeiro, Synthesis, DNA binding, cellular DNA lesion and cytotoxicity of a series of new benzimidazole-based Schiff base copper(II) complexes, *Dalton Trans*., **2015**, *44*,

19983-19996; (b) Y. Miao, M. P. H. Lee, G. N. Parkinson, A. Batista-Parra, M. A. Ismail, S. Neidle, D. W. Boykin, W. D. Wilson, Out-of-Shape DNA minor groove binders: Induced fit interactions of heterocyclic dications with the DNA minor groove, *Biochemistry*, **2005**, *44*, 14701-14708; (c) A. Paul, Y. Chai, D. W. Boykin, W. D. Wilson, Understanding mixed sequence DNA recognition by novel designed compounds: The kinetic and thermodynamic behavior of azabenzimidazole diamidines, *Biochemistry*, **2015**, *54*, 577-587; (d) L. Y. Sun, L. W. Zhu, Y. J. Tang, Increasing the distance between two monomers of topoisomerase IIβ under the action of antitumor agent 4β-sulfur-(benzimidazole) 4′-demethylepipodophyllotoxin, *Sci. Rep.*, **2018**, *8*, 14949-14958.

102. P. Pantziarka, G. Bouche, L. Meheus, V. Sukhatme, V. P. Sukhatme, Repurposing drugs in oncology (ReDO)-mebendazole as an anti-cancer agent, *Ecancermedicalscience*, **2014**, *8*, 443-459.

103. A. Kamal, A. V. S. Rao, M. V. P. S. Vishnuvardhan, T. S. Reddy, K. Swapna, C. Bagul, N. V. S. Reddy, V. Srinivasulu, Synthesis of 2-anilinopyridyl–triazole conjugates as antimitotic agents, *Org. Biomol. Chem.*, **2015**, *13*, 4879-4895.

104. J. C. Pessoa, I. Tomaz, Transport of therapeutic vanadium and ruthenium complexes by blood plasma components, *Curr. Med. Chem.*, **2010**, *17*, 3701-3738.

105. D.-S. Yim, Potency and plasma protein binding of drugs *in vitro*-a potentially misleading pair for predicting *in vivo* efficacious concentrations in humans, *Korean J. Physiol. Pha.*, **2019**, *23*, 231-236.

106. P. Mitra, U. Pal, N. C. Maiti, A. Ghosh, A. Anirban Bhunia, S. Basu, Identification of modes of interactions between 9-aminoacridine hydrochloride hydrate and serum proteins by low and high resolution spectroscopy and molecular modelling, *RSC Adv.*, **2016**, *6*, 53454-53468.

107. V. Rajendiran, R. Karthik, M. Palaniandavar, V. S. Periasamy, M. A. Akbarsha, B. S. Srinag, H. Krishnamurthy, Mixed-ligand copper(II)-phenolate complexes: Effect of coligand on enhanced DNA and protein binding, DNA cleavage, and anticancer activity, *Inorg. Chem.*, **2007**, *46*, 8208-8221.

108. M. D. Tomczyk, K. Z. Walczak, l,8-Naphthalimide based DNA intercalators and anticancer agents. A systematic review from 2007 to 2017, *Eur. J. Med. Chem.*, **2018**, *159*, 393-422.

109. I. Singh, V. Luxami, K. Paul, Synthesis and *in vitro* evaluation of naphthalimide-benzimidazole conjugates as potential antitumor agents, *Org. Biomol. Chem.*, **2019**, *17*, 5349-5366.

110. I. Singh, R. Rani, V. Luxami, K. Paul, Synthesis of 5-(4-(1*H*-phenanthro[9,10-*d*]imidazol-2-yl)benzylidene)thiazolidine-2,4-dione as promising DNA and serum albumin-binding agents and evaluation of antitumor activity, *Eur. J. Med. Chem*., **2019**, *166*, 267-280.

111. M. M. Vaidergorn, Z. A. Carneiro, C. D. Lopes, S. de Albuquerque, F. C. C. Reis, S. Nikolaou, J. F. R. Mello, G. L. Genesi, G. H. G. Trossini, A. Ganesan, F. S. Emery, β-amino alcohols and their respective 2-phenyl-*N*-alkyl aziridines as potential DNA minor groove binders, *Eur. J. Med. Chem*., **2018**, 157, 657-664.

112. L. Ma, J. Wang, Y. Zhang, Probing the characterization of the interaction of aflatoxins B1 and G1 with calf thymus DNA *in vitro*, *Toxins*, **2017**, *9*, 209-228.

113. (a) M. Sathish, B. Kavitha, V. L. Nayak, Y. Tangella, A. Ajitha, S. Nekkanti, A. Alarifi, N. Shankaraiah, N. Nagesh, A. Kamal, Synthesis of podophyllotoxin linked β-carboline congeners as potential anticancer agents and DNA topoisomerase II inhibitors, *Eur. J. Med. Chem*., **2018**, 144, 557-571; (b) N. Shahabadi, S. Hadidi, Spectroscopic studies on the interaction of calf thymus DNA with the drug levetiracetam, *Spectrochim. Acta A*, **2012**, *96*, 278-283.

114. G. Zhang, L. Wang, X. Zhou, Y. Li, D. Gong, Binding characteristics of sodium saccharin with calf thymus DNA *in vitro*, *J. Agric. Food Chem.*, **2014**, *62*, 991-1000.

115. F. G. Loontiens, P. Regenfuss, A. Zechel, L. Dumortier, R. M. Clegg, Binding characteristics of hoechst-33258 with calf thymus DNA, poly d(AT), and d(CCGGAATTCCGG)-multiple stoichiometries and determination of tight-binding with a wide spectrum of site affinities, *Biochemistry*, **1990**, *29*, 9029-9039.

116. J. G. Liu, Q. L. Zhang, X. F. Shi, L. N. Ji, Interaction of $[Ru(dmp)_2(dppz)]^{2+}$ and $[Ru(dmb)_2(dppz)]^{2+}$ with DNA: Effects of the ancillary ligands on the DNA-binding behaviors, *Inorg. Chem.*, **2001**, 40, 5045-5050.

117. H. Yang, P. Tang, B. Tang, Y. Huang, J. He, S. Li, H. Li, Studies of DNA-binding properties of lafutidine as adjuvant anticancer agent to calf thymus DNA using multi-spectroscopic approaches, NMR relaxation data, molecular docking and dynamical simulation, *Int J Biol Macromol.*, **2017**, *99*, 79-87.

118. D. Wu, D. Liu, Y. Zhang, Z. Zhang, H. Li, Unravelling the binding mechanism of benproperine with human serum albumin: A docking, fluorometric, and thermodynamic approach, *Eur. J. Med. Chem.*, **2018**, *146*, 245-250.

119. J. Yan, D. Wu, X. Ma, L. Wang, K. Xu, H. Li, Spectral and molecular modeling studies on the influence of *b*-cyclodextrin and its derivatives on aripiprazolehuman serum albumin binding, *Carbohydr. Polym.*, **2015**, *131*, 65-74.

120. H. Hadadzadeh, H. Farrokhpour, Z. Jannesari, Z. Amirghofran, Experimental and ONIOM computational evaluation of DNA- and BSA binding and cytotoxic activity of a mononuclear Pd(II) complex with piroxicam, *Inorg. Chim. Acta*, **2016**, *453*, 415-429.

121. N. Ibrahim, H. Ibrahim, S. Kim, J.-P. Nallet, F. Nepveu, Interactions between antimalarial indolone-*N*-oxide derivatives and human serum albumin, *Biomacromolecules*, **2010**, *11*, 3341-3351.

122. G.-F. Shena, T.-T. Liua, Q. Wanga, M. Jianga, J.-H. Shi, Spectroscopic and molecular docking studies of binding interaction of gefitinib, lapatinib and sunitinib with bovine serum albumin (BSA), *J. Photochem. Photobiol. B*, **2015**, *153*, 380-390.

123. Y.-Q. Wang, H.-M. Zhang, G.-C. Zhang, W.-H. Tao, Z.-H. Fei, Z.-T. Liu, Spectroscopic studies on the interaction between silicotungstic acid and bovine serum albumin, *J. Pharm. Biomed. Anal.*, **2007**, *43*, 1869-1875.

124. T. Sen, K. K. Haldar, A. Patra, Au nanoparticle-based surface energy transfer probe for conformational changes of BSA protein, *J. Phys. Chem. C*, **2008**, *112*, 17945-17951.

125. A. Satheshkumar, K. P. Elango, Spectroscopic and molecular docking studies on the charge transfer complex of bovine serum albumin with quinone in aqueous medium and its influence on the ligand binding property of the protein, *Spectrochim. Acta, Part A*, **2014**, *130*, 337-343.

126. M. Sarkar, S. S. Paul, K. K. Mukherjea, Interaction of bovine serum albumin with a psychotropic drug alprazolam: Physicochemical, photophysical and molecular docking studies, *J. Lumin.*, **2013**, *142*, 220-230.

127. R. Rohs, I. Bloch, H. Sklenar, Z. Shakked, Molecular flexibility in *ab initio* drug docking to DNA: Binding-site and binding-mode transitions in all-atom Monte Carlo simulations, *Nucleic Acids Res.*, **2005**, *33*, 7048-7057.

128. S. Ross, M. Finkelstein, R. Petersen, Solvent effects in the reactions of *N*-bromosuccinimide with toluene, fluorene and acenaphthene, *J. Am. Chem. Soc.*, **1958**, *80*, 4327-4330.

129. P. Grayshan, A. Kadhim, A. Peters, Heterocyclic derivatives of naphthalene-1,8-dicarboxylic anhydride, *J. Heterocycl. Chem.*, **1974**, *11*, 33-38.

130. L. F. Tietze, A. Modi, Multicomponent domino reactions for the synthesis of biologically active natural products and drugs, *Med. Res. Rev.*, **2000**, *20*, 304-322.

131. B. Ganem, Strategies for innovation in multicomponent reaction design, *Acc. Chem. Res.*, **2009**, *42*, 463-472.

132. L. A. Marcaurelle, C. W. Johannes, Application of natural product-inspired diversity oriented synthesis to drug discovery, *Prog. Drug Res.*, **2008**, *66*, 187-216.

133. A. Ulaczyk-Lesanko, D. G. Hall, Wanted: New multicomponent reactions for generating libraries of polycyclic natural products, *Curr. Opin. Chem. Biol.*, **2005**, *9*, 266-276.

134. A. Ahmed, M. Daneshtalab, Polycyclic quinolones (part 1)-thieno[2,3-*b*]benzo[*h*]-quinoline derivatives: design, synthesis, preliminary *in vitro* and *in silico* studies, *Heterocycles*, **2012**, *58*, 103-122.

135. I. Kock, D. Heber, M. Weide, U. Wolschendorf, B. Clement, Synthesis and biological evaluation of 11-substituted-6-aminobenzo[*c*]phenanthridine derivatives, a new class of antitumor agents, *J. Med. Chem.*, **2005**, *48*, 2772-2777.

136. I. A. Khan, M. V. Kulkarni, M. Gopal, M. S. Shahabuddin, C. M. Sun, Synthesis and biological evaluation of novel angularly fused polycyclic coumarins, *Bioorg. Med. Chem. Lett.*, **2005**, *15*, 3584-3587.

137. B. K. Banik, F. F. Becker, Polycyclic aromatic compounds as anticancer agents: Structure-activity relationships of chrysene and pyrene derivatives, *Bioorg. Med. Chem.*, **2001**, *9*, 593-605.

138. A. Rescifina, C. Zagni, G. Romeo, S. Sortino, Synthesis and biological activity of novel bifunctional isoxazolidinyl polycyclic aromatic hydrocarbons, *Bioorg. Med. Chem.*, **2012**, *20*, 4978-4984.

139. C. H. Lee, M. Jiang, M. Cowart, G. Gfesser, R. Perner, K. H. Kim, Y. G. Gu, M. Williams, M. F. Jarvis, E. A. Kowaluk, Discovery of 4-amino-5-(3-bromophenyl)-7-(6-morpholino-

pyridin-3-yl) pyrido [2, 3-*d*] pyrimidine, an orally active, non-nucleoside adenosine kinase inhibitor, *J. Med. Chem.*, **2001**, *44*, 2133-2138.

140. S. Kothavale, S. Bhalekar, N. Sekar, Highly fluorescent blue-green emitting phenanthroimidazole derivatives: Detail experimental and DFT study of structural and donating group effects on fluorescence properties, *Dyes Pigm.*, **2018**, *159*, 209-221.

141. P. Krawczyk, B. Jędrzejewska, M. Pietrzak, T. Janek, Synthesis, spectroscopic, physicochemical properties and binding site analysis of 4-(1*H*-phenanthro[9,10-*d*]-imidazol-2-yl)-benzaldehyde fluorescent probe for imaging in cell biology: Experimental and theoretical study, *J. Photochem. Photobiol. B*, **2016**, *164*, 112-122.

142. Z. Gao, Z. Wang, T. Shan, Y. Liu, F. Shen, Y. Pan, H. Zhang, X. He, P. Lu, B. Yang, Y. Ma, High-efficiency deep blue fluorescent emitters based on phenanthro[9,10-*d*]imidazole substituted carbazole and their applications in organic light emitting diodes, *Org. Electron.*, **2014**, *15*, 2667-2676.

143. Y. Suzuki, K. Yokoyama, Design and synthesis of intramolecular charge transfer-based fluorescent reagents for the highly-sensitive detection of proteins, *J. Am. Chem. Soc.*, **2005**, *127*, 17799-17802.

144. A. Mallick, B. Haldar, N. Chattopadhyay, Spectroscopic investigation on the interaction of ict probe 3-acetyl-4-oxo-6,7-dihydro-12*h* indolo-[2,3-*a*] quinolizine with serum albumins, *J. Phys. Chem. B*, **2005**, *109*, 14683-14690.

145. B. Côte, L. Boulet, C. Brideau, D. Claveau, D. Ethier, R.´Frenette, M. Gagnon, A. Giroux, J. Guay, S. Guiral, J. Mancini, E. Martins, F. Masse, N. Me´ thot, D. Riendeau, J. Rubin, D. Xu, H. Yu, Y. Ducharme, R.W. Friesen, Substituted phenanthrene imidazoles as potent, selective, and orally active mPGES-1 inhibitors, *Bioorg. Med. Chem. Lett.*, **2007**, *17*, 6816-6820.

146. Y. Ni, S. Su, S. Kokot, Spectrometric studies on the interaction of fluoroquinolones and bovine serum albumin, *Spectrochim. Acta A*, **2010**, *75*, 547-552.

147. J. R. Lakowicz, Principles of Fluorescence Spectroscopy, third ed., Springer Science, New York, 2006.

148. Y. Yue, X. Chen, J. Qin, X. Yao, Characterization of the mangiferin-human serum albumin complex by spectroscopic and molecular modeling approaches, *J. Pharm. Biomed. Anal.*, **2009**, *49*, 753-759.

149. F. Ding, J. Huang, J. Lin, Z. Li, F. Liu, Z. Jiang, Y. Sun, A study of the binding of C.I. Mordant Red 3 with bovine serum albumin using fluorescence spectroscopy, *Dyes Pigm.*, **2009**, *82*, 65-70.

150. N. Kishikawa, M. Wada, Y. Ohba, K. Nakashima, N. Kuroda, Highly sensitive and selective determination of 9,10-phenanthrenequinone in airborne particulates using high-performance liquid chromatography with pre-column derivatization and fluorescence detection, *J. Chromatogr. A*, **2004**, *1057*, 83-88.

151. M. K. Nayak, Synthesis, characterization and optical properties of aryl and diaryl substituted phenanthroimidazoles, *J. Photochem. Photobiol. A*, **2012**, *241*, 26-37.

152. B. E. Cohen, T. B. McAnaney, E. S. Park, Y. N. Jan, S. G. Boxer, L. Y. Jan, Probing protein electrostatics with a synthetic fluorescent amino acid, *Science*, **2002**, *296*, 1700-1703.

153. N. Bagi, R. Stefanovszky, J. Kaizer, G. Speier, The preparation of annulated 1,3-oxazoles from 1,3,2- oxazaphospholes and aldehydes, *Monatsh. Chem.*, **2016**, *147*, 425-428.

154. R. Rani, G. Kumar, K. Paul, V. Luxami, Donor-π-Acceptor (D-π-A) Dyad for ratiometric detection of Hg^{2+} and PPi, *New J. Chem.*, **2018**, *42*, 12729-12736 .

155. Y. Zhang, J.-H. Wang, G. Han, F. Lu, Q.-X. Tong, Phenanthroimidazole derivatives as emitters for non-doped deep-blue organic light emitting devices, *RSC Adv.*, **2016**, *6*, 70800-70809.

156. J. Akhtar, A. A. Khan, Z. Ali, R. Haider, M. S. Yar, Structure- activity relationship (SAR) study and design strategies of nitrogen containing heterocyclic moieties for their anticancer activities, *Eur. J. Med. Chem.*, **2017**, *125*, 143-189.

157. S. B. Marganakop, R. R, Kamble, J. Hoskeri, D. J. Prasad, G. Y. Meti, Facile synthesis of novel quinoline derivatives as anticancer agents, *Med. Chem. Res.*, **2014**, *23*, 2727-2735.

158. K. Saleem, W. A. Wani, A. Haque, A. Malhotra, I. Ali, Nanodrugs: Magic bullets in cancer chemotherapy, *Top. Anti-Cancer Res.*, **2013**, *58*, 437-494.

159. M. Pulkkinen, J. Pikkarainen, T. Wirth, T. Tarvainen, V. Haapa-aho, H. Korhonen, K. Järvinen, Three-step tumor targeting of paclitaxel using biotinylated PLA-PEG nanoparticles and avidin-biotin technology: formulation development and *in vitro* anticancer activity, *Eur. J. Pharm. Biopharm.*, **2008**, *70*, 66-74.

160. M. Kidwai, R. Venktaramanan, R. Mohan, P. Sapra, Cancer chemotherapy and heterocyclic compounds, *Curr. Med. Chem.*, **2002**, *9*, 1209-1228.

161. I. Ali, K. Kumerer, H. Y. Aboul-Enein, Mechanistic principles in chiral separations using liquid chromatography and capillary electrophoresis, *Chromatographia*, **2006**, *63*, 295-307.

162. I. Ali, M. N. Lone, Z. A. Al-Othman, A. Al-Warthan, M. M. Sanagi, Heterocyclic scaffolds: centrality in anticancer drug development, *Curr. Drug Targets*, **2015**, *16*, 711-734.

163. H. Y. Aboul-Enein, I. Ali, Comparative study of the enantiomeric resolution of chiral antifungal drugs econazole, miconazole and sulconazole by HPLC on various cellulose chiral columns in normal phase mode, *J. Pharm. Biomed. Anal.*, **2002**, *27*, 441-446.

164. W. W. Paudler, R. M. Sheets, Recent developments in naphthyridine chemistry, *Adv. Heterocycl. Chem.*, **1983**, *33*, 147-184.

165. D. Mahadevan, D. W. Northfelt, P. Chalasani, D. Rensvold, S. Kurtin, D. D. Von Hoff, M. J. Borad, R. Tibes, Phase I trial of UNBS5162, a novel naphthalimide in patients with advanced solid tumors or lymphoma, *Int. J. Clin. Oncol.*, **2013**, *18*, 934-941.

166. M. Lv, H. Xu, Overview of naphthalimide analogs as anticancer agents, *Curr. Med. Chem.* **2009**, *16*, 4797-4813.

167. L. Ingrassia, F. Lefranc, R. Kiss, T. Mijatovic, Naphthalimides and azonafides as promising anti-cancer agents, *Curr. Med. Chem.* **2009**, *16*, 1192-1213.

168. K. Pudhom, K. Kasai, H. Terauchi, H. Inoue, M. Kaiser, R. Brun, M. Ihara, K. Takasu, Synthesis of three classes of rhodacyanine dyes and evaluation of their *in vitro* and *in vivo* antimalarial activity, *Bioorg. Med. Chem.*, **2006**, *14*, 8550-8563.

169. M. Bhat, S. L. Belagali, Guanidinyl benzothiazole derivatives: Synthesis and structure activity relationship studies of a novel series of potential antimicrobial and antioxidants, *Res. Chem. Intermed.*, **2016**, *42*, 6195-6208.

170. R. M. Kumbhare, T. L. Dadmal, R. Pamanji, U. B. Kosurkar, L. R. Velatooru, K. Appalanaidu, Y. K. Rao, J. V. Rao, Synthesis of novel fluoro 1, 2, 3-triazole tagged amino bis (benzothiazole) derivatives, their antimicrobial and anticancer activity, *Med. Chem. Res.*, **2014**, *23*, 4404-4413.

171. S. Saeed, N. Rashid, P. G. Jones, M. Ali, R. Hussain, Synthesis, characterization and biological evaluation of some thiourea derivatives bearing benzothiazole moiety as potential antimicrobial and anticancer agents, *Eur. J. Med. Chem.*, **2010**, *45*, 1323-1331.

172. F. M. Shaikh, N. B. Patel, G. Sanna, B. Busonera, P. L. Colla, D. P. Rajani, Synthesis of some new 2-amino-6-thiocyanato benzothiazole derivatives bearing 2, 4-thiazolidinediones and screening of their *in vitro* antimicrobial, antitubercular and antiviral activities, *Med. Chem. Res.*, **2015**, *24*, 3129-3142.

173. F. Delmas, A. Avellaneda, C. D. Giorgio, M. Robin, E. D. Clercq, P. Timon-David, J.-P. Galy, Synthesis and antileishmanial activity of (1,3-benzothiazol-2-yl) amino-9-(10*H*)-acridinone derivatives, *Eur. J. Med. Chem.*, **2004**, *39*, 685-690.

174. C. Kharbanda, M. S. Alam, H. Hamid, K. Javed, S. Bano, A. Dhulap, Y. Ali, S. Nazreen, S. Haider, Synthesis and evaluation of pyrazolines bearing benzothiazole as anti-inflammatory agents, *Bioorg. Med. Chem.*, **2014**, *22*, 5804-5812.

175. M. Amir, S. Asif, I. Ali, M. Z. Hassan, Synthesis of benzothiazole derivatives having acetamido and carbothioamido pharmacophore as anticonvulsant agents, *Med. Chem. Res.*, **2012**, *21*, 2661-2670.

176. S. Ke, Y. Wei, Z. Yang, K. Wang, Y. Liang, L. Shi, Novel cycloalkylthiophene-imine derivatives bearing benzothiazole scaffold: Synthesis, characterization and antiviral activity evaluation, *Bioorg. Med. Chem. Lett.*, **2013**, *23*, 5131-5134.

177. A. Kamal, A. P. Kumar, P. Suresh, N. Shankaraiah, M. S. Kumar, An efficient one-pot synthesis of benzothiazolo-4β-anilino-podophyllotoxin congeners: DNA topoisomerase-II inhibition and anticancer activity, *Bioorg. Med. Chem. Lett.*, **2011**, *21*, 350-353.

178. R. M. Kumbhare, T. L. Dadmal, M. J. Ramaiah, K. S. V. Kishore, S. N. C. V. L. P. Valli, S. K. Tiwar, K. Appalanaidu, Y. K. Rao, M. P. Bhadra, Synthesis and anticancer evaluation of novel triazole linked N-(pyrimidin-2-yl) benzo [*d*] thiazol-2-amine derivatives as inhibitors of cell survival proteins and inducers of apoptosis in MCF-7 breast cancer cells, *Bioorg. Med. Chem. Lett.* **2015**, *25*, 654-658.

179. M. T. Gabr, N. S. El-Gohary, E. R. El-Bendary, M. El-Kerdawy, New series of benzothiazole and pyrimido[2,1-*b*]benzothiazole derivatives: Synthesis, antitumor activity, EGFR tyrosine kinase inhibitory activity and molecular modeling studies, *Med. Chem. Res.*, **2015**, *24*, 860-878.

180. A. Kamal, M. D. Ashraf, M. V. P. S. V. Vadhan, S. Faazil, V. L. Nayak, Synthesis and anticancer potential of benzothiazole linked phenylpyridopyrimidinones and their diones as mitochondrial apoptotic inducers, *Bioorg. Med. Chem. Lett.*, **2014**, *24*, 147-151.

181. D. F. Shi, T. D. Bradshaw, S. Wrigley, C. J. McCall, P. Lelieveld, I. Fichtner, M. F. G. Stevens, Antitumor benzothiazoles. Synthesis of 2-(4-aminophenyl)benzothiazoles and evaluation of their activities against breast cancer cell lines *in vitro* and *in vivo, J. Med. Chem.,* **1996**, *39*, 3375-3384.

182. T. D. Bradshaw, D. F. Shi, R. J. Schultz, K. D. Paull, L. Kelland, A. Wilson, H. H. Fiebig, S. Wrigley, M. F. G. Stevens, Influence of 2-(4-aminophenyl)benzothiazoles on the growth of human ovarian carcinoma cell lines *in vitro* and *in vivo*, *Br. J. Cancer*, **1998**, *78*, 421-429.

183. D. Kumar, N. M. Kumar, M. P. Tantak, M. Ogura, E. Kusaka, T. Ito, Synthesis and identification of α-cyano bis(indolyl)chalcones as novel anticancer agents, *Bioorg. Med. Chem. Lett.*, **2015**, *24*, 5170-5174.

184. G. Nesi, S. Sestito, V. Mey, S. Ricciardi, M. Falasca, R. Danesi, A. Lapucci, M. C. Breschi, S. Fogli, S. Rapposelli, Synthesis of novel 3,5-disubstituted-2-oxindole derivatives as antitumor agents against human nonsmall cell lung cancer, *ACS Med. Chem. Lett.*, **2013**, *4*, 1137-1141.

185. M. P. Fortes, P. B. N. da Silva, T. G. da Silva, T. S. Kaufman, G. C. G. Militão, C. C. Silveira, Synthesis and preliminary evaluation of 3-thiocyanato-1*H*-indoles as potential anticancer agents, *Eur. J. Med. Chem.*, **2016**, *118*, 21-26.

186. Y. Zhou, K. Duan, L. Zhu, Z. Liu, C. Zhang, L. Yang, M. Li, H. Zhang, X. Yang, Synthesis and cytotoxic activity of novel hexahydropyrrolo(2,3-*b*)indole imidazolium salts, *Bioorg. Med. Chem. Lett.*, **2016**, *26*, 460-465.

187. D. C. Schuck, A. K. Jordão, M. Nakabashi, A. C. Cunha, V. F. Ferreira, C. R. S. Garcia, Synthetic indole and melatonin derivatives exhibit antimalarial activity on the cell cycle of the human malaria parasite Plasmodium falciparum, *Eur. J. Med. Chem.*, **2014**, *78*, 375-382.

188. Y. J. Xu, K. Foubert, L. Dhooghe, F. Lemière, K. Cimanga, K. Mesia, S. Apers, L. Pieters, Chromatographic profiling and identification of two new iridoid-indole alkaloids by UPLC-MS and HPLC-SPE-NMR analysis of an antimalarial extract from Nauclea pobeguinii, *Phytochem. Lett.*, **2012**, *5*, 316-319.

189. L. F. Rocha de Silva, A. Montoiaa, R. C. N. Amorim, M. R. Melo, M. C. Henrique, S. M. Nunomura, M. R. F. Costa, V. F. A. Neto, D. S. Costa, G. Dantas, J. Lavrado, R. Moreira,

A. Paulo, A. C. Pinto, W. P. Tadei, R. S. Zacardi, M. N. Eberlin, A. M. Pohlit, Comparative *in vitro* and *in vivo* antimalarial activity of the indole alkaloids ellipticine, olivacine, cryptolepine and a synthetic cryptolepine analog, *Phytomedicine,* **2012**, *20*, 71-76.

190. G. A. Khan, J. A. War, G. A. Naikoo, U. J. Pandit, R. Das, Porous CuO catalyzed green synthesis of some novel 3-alkylated indoles as potent antitubercular agents. *J. Saudi Chem. Soc.*, **2018**, *22*, 6-15.

191. K. M. Naidu, S. Srinivasarao, N. Agnieszka, A. K. Ewa, M. M. K. Kumar, K. V. G. Chandra Sekhar, Seeking potent anti-tubercular agents: Design, synthesis, anti-tubercular activity and docking study of various ((triazoles/indole)-piperazin-1-yl/1,4-diazepan-1-yl)benzo(*d*)isoxazole derivatives, *Bioorg. Med. Chem. Lett.*, **2016**, *26*, 2245-2250.

192. (a) D. Rajaraman, G. Sundararajan, N. K. Loganath, K. Krishnasamy, Synthesis, molecular structure, DFT studies and antimicrobial activities of some novel 3-(1-(3,4-dimethoxyphenethyl)-4,5-diphenyl-1*H*-imidazol-2-yl)-1*H*-indole derivatives and its molecular docking studies, *J. Mol. Struct.*, **2017**, *1127*, 597-610; (b) N. Gokhale, U. Dalimba, M. Kumsi M, Facile synthesis of indolepyrimidine hybrids and evaluation of their anticancer and antimicrobial activity, *J. Saudi Chem. Soc.*, **2017**, *21*, 761-775.

193. P. Singh, J. Kaur, G. Singh, R. Bhatti, Tri-block conjugates: identification of a highly potent anti-inflammatory agent, *J. Med. Chem.*, **2015**, *58*, 5989-6001.

194. S. Mehndiratta, Y. L. Hsieh, Y. M. Liu, A. W. Wang, H. Y. Lee, L. Y. Liang, S. Kumar, C. M. Teng, C. R. Yang, J. P. Liou, Indole-3-ethyl sulfamoyl phenyl acrylamides: Potent histone deacetylase inhibitors with anti-inflammatory activity, *Eur. J. Med. Chem.*, **2014**, *85*, 468-479.

195. V. Sharath, H. V. Kumar, N. Naik, Synthesis of novel indole based scaffolds holding pyrazole ring as anti-inflammatory and antioxidant agents, *J. Pharm. Res.*, **2013**, *6*, 785-790.

196. (a) R. Patil, S. A. Patil, K. D. Beaman, S. A. Patil, Indole molecules as inhibitors of tubulin polymerization: Potential new anticancer agents, an update (2013-2015), *Future Med. Chem.*, **2016**, *8*, 1291-1316; (b) P. Martins, J. Jesus, S. Santos, L. Raposo, C. Roma-Rodrigues, P. Baptista, A. Fernandes, Heterocyclic anticancer compounds: Recent advances and the paradigm shift towards the use of nanomedicine's tool box, *Molecules,* **2015**, *20*, 16852-16891.

SUMMARY

Cancer is the most challenging disease globally and can be described as a cell cycle disorder with fast and uncontrolled production of abnormal cells. Nearby 17 million patients were diagnosed with cancer and about 9.6 million deaths from cancer were reported in 2018 globally. According to the cancer research reports, about 27.5 million new cancer cases will be occurred every year by 2040. Breast, lung, prostate and bowel cancers are the most common type of cancers diagnosed globally. There are many cancer inducing factors like age, obesity, overweight, genetics, smoking, alcohol, diet, physical inactivity etc. Cancer is one of the increasing worldwide burden, therefore prevention and treatment of cancer is one of the major challenging health problem of the 21st century.[1,2] The major techniques to cure cancer are surgery, chemotherapy, immunotherapy and radiotherapy. At present, cancer therapy includes medication that mainly target the some biological pathway.[3] With lots of progress in the area of cancer therapy, there are still many problems persist with the existing antitumor medicines. Most of the available anticancer drugs are unable to beat the resistance mechanism of cancer cells and are also incapable to distinguish cancer cells and normal cells of the body.[4] Large research efforts have been committed for the discovery and development of an efficient anticancer candidate. Immense research has been focused for the identification of tumor specific therapies, which can enhance the sensitivity of cancer cells toward anticancer drugs.[5] One of the best method for the development of new and efficient drug is to chemical modification in natural occurring or existing molecules with significant biological activity. Recently the interest is focused on the discovery of cytotoxic agent that simultaneously affect multiple targets for cancer therapy.[6,7] Currently, hybrid drugs are used to stimulate the multiple targets with a single drug for better therapeutic potential as well as to beat the side effects. Molecular hybridization (MH) is an efficient approach for the development of a more potent compound, which can simultaneously target two or more pathogenic pathways.[8] Molecular hybridization approach can be used to increase the efficacy and selectivity as well as to decrease the adverse effects of the drug.[9,10] This approach considered to be similar to the combination therapy, besides, two or more drugs are present in a single entity attached with covalent linkage.[11,12] Naphthalimides, benzimidazole, benzothiazole, imidazo[1,2-*a*]pyrazine, phenanthrene-imida-/oxa-zole etc. are well-known heterocyclic moieties, reported with their

potential anticancer activity. On account of these heterocyclic moieties, a potent antitumor candidate could be designed by molecular hybridization methodology.

Keeping in the view the above points, the following objectives have been designed

1. To synthesize and characterize the hybrids of two biologically significant moieties *viz.* imidazo[1,2-*a*]pyrazine and benzimidazole/naphthalimide.
2. To synthesize and characterize the hybrids of three biologically significant moieties *viz*. naphthalimide and indole/benzothiazole/phenanthroimidazole.
3. *In vitro* evaluation of synthesized compounds for anticancer activity and to investigate their structure activity relationship.

In the present investigation, we have synthesized the hybrids of imidazo[1,2-*a*]pyrazine and benzimidazole; benzimidazole and naphthalimides; naphthalimide and phenanthro[9,10-*d*]imidazole; naphthalimide, benzothiazole and indole; phenanthro[9,10-*d*]imidazole and others heterocyclic moieties. Synthesized hybrids were well characterized by NMR and mass spectrometry. These hybrids were further investigated for their cytotoxicity against 60 human cancer cell lines. These hybrids were also investigated for their binding interactions with DNA and serum albumins (HSA/BSA). To check the molecular interaction of synthesized hybrids with DNA, molecular docking studies were also performed.

Chapter 2: Synthesis, characterization, *in vitro* evaluation, interaction with DNA/BSA, and molecular docking studies of imidazo[1,2-*a*]pyrazine and benzimidazole conjugates

2.1. Synthesis

All compounds (**9-23**, **31-49** and **53-57**) were prepared according to the **Schemes 1-3** starting from 1,3- and 1,4-dibromobenzene. 1,4-Dibromobenzene (**1**) was first nitrated with 1:4 ratio of HNO_3:H_2SO_4 to yield 1,4-dibromo-2-nitrobenzene **2** in 93% yield. Compound **2** was subjected to regioselective nucleophilic substitution reaction with cyclohexylamine in the presence K_2CO_3 to afforded **3** in 75% yield. Boronation of **3** was then carried out using bis(pinacolato)diboron in the presence of $Pd(PPh_3)_2Cl_2$ and KOAc, afforded **4** in 82% yield. Suzuki-Miyaura cross coupling reaction of **4** with dibromo imidazo[1,2-*a*]pyrazine **5** has been proceeded using $Pd(PPh_3)_4$ and K_2CO_3 to yield **6** in 73% yield with traces of disubstituted product. Reduction of **6** was carried out using sodium dithionite to afford **7** which was subsequently cyclized with triethylorthoformate in acetic acid to afford the requisite 6-bromo-8-(1-cyclohexyl-1*H*-benzo[*d*]imidazol-5-

yl)imidazo[1,2-*a*]pyrazine **8** in 75% yield (**Scheme 1**). Compound **8** was further used for Suzuki reaction with substituted phenyl, thienyl and naphthyl boronates to give **9-23** in 75-86% yields.

Scheme 1. Synthesis of 6-substituted-8-(1-cyclohexyl-1*H*-benzo[*d*]imidazol-5-yl)imidazo[1,2-*a*]pyrazine [a]

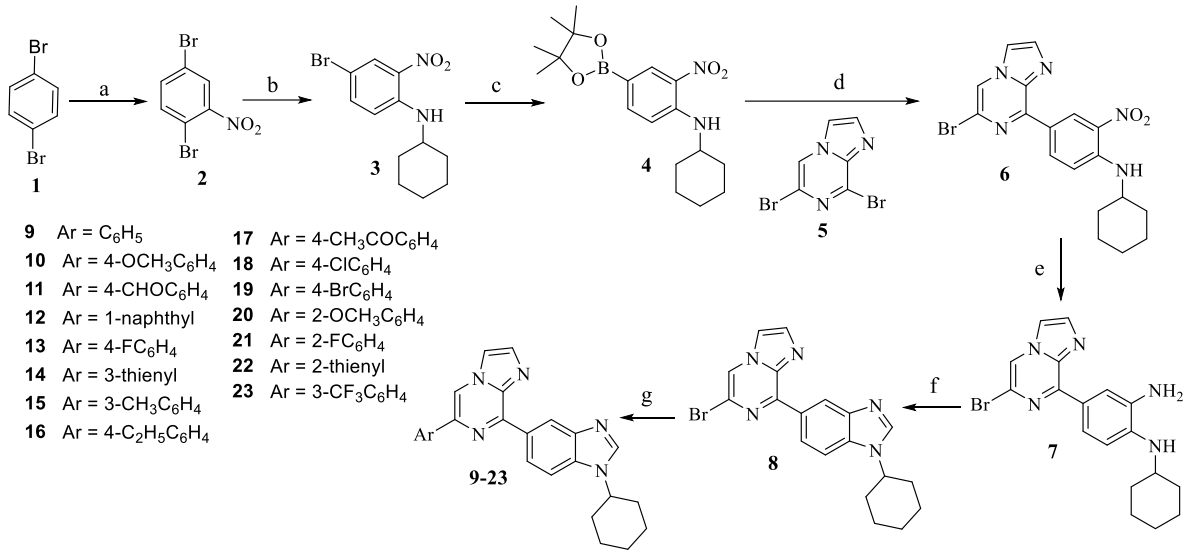

[a]Reagents and conditions: (a) H_2SO_4, HNO_3, DCM, 0 °C, 30 min., 93%; (b) Cyclohexyl amine, K_2CO_3, DMF, 100 °C, 18 h, 75%; (c) Bis(pinacolato)diboron, $Pd(PPh_3)_2Cl_2$, KOAc, 1,4-dioxane, reflux, 10 h, 82%; (d) $Pd(PPh_3)_4$, K_2CO_3, CH_3CN : water (9:1), N_2, reflux, 10-12 h, 73%; (e) $Na_2S_2O_4$, aq. NH_3, THF : water, rt, 1 h; (f) Triethylorthoformate, AcOH, rt, 10 min., 75%; (g) $ArB(OH)_2$, $Pd(PPh_3)_4$, K_2CO_3, CH_3CN : water (9:1), N_2, reflux, 12-15 h, 75-86%

The synthesis of intermediate **30a-b** of imidazo[1,2-*a*]pyrazine and benzimidazole conjugates followed the similar procedure using 1,3-dibromobenzene as starting material (**Scheme 2**). The commercial available 1,3-dibromobenzene **24** was nitrated to yield **25** in 95% yield which was regioselectively substituted with cyclohexylamine and benzylamine in DMF, afforded **26a** and **26b** respectively. Boronation of **26a** and **26b**, using bis(pinacolato)diboron in the presence of $Pd(PPh_3)_2Cl_2$ and KOAc provided **27a** and **27b**, respectively. Suzuki cross-coupling of **27a-b** with dibromo-imidazo[1,2-*a*]pyrazine **5** and $Pd(PPh_3)_4$, afforded compound **28a-b** alongwith traces of disubstituted products. Reduction of derivatives with sodium dithionite in ammonia provided amines **29a-b** followed by cyclization with triethylorthoformate in acetic acid to obtain intermediates **30a** and **30b** in 90% and 80% yields, respectively. Suzuki reactions of intermediates with phenyl, thienyl and naphthyl boronates were carried out in CH_3CN:H_2O using $Pd(PPh_3)_4$ and K_2CO_3 afforded **31-49** in 75-85% yields.

Scheme 2. Synthesis of 6-substituted-8-(1-cyclohexyl-1*H*-benzo[*d*]imidazol-6-yl)imidazo[1,2-*a*]pyrazine [b]

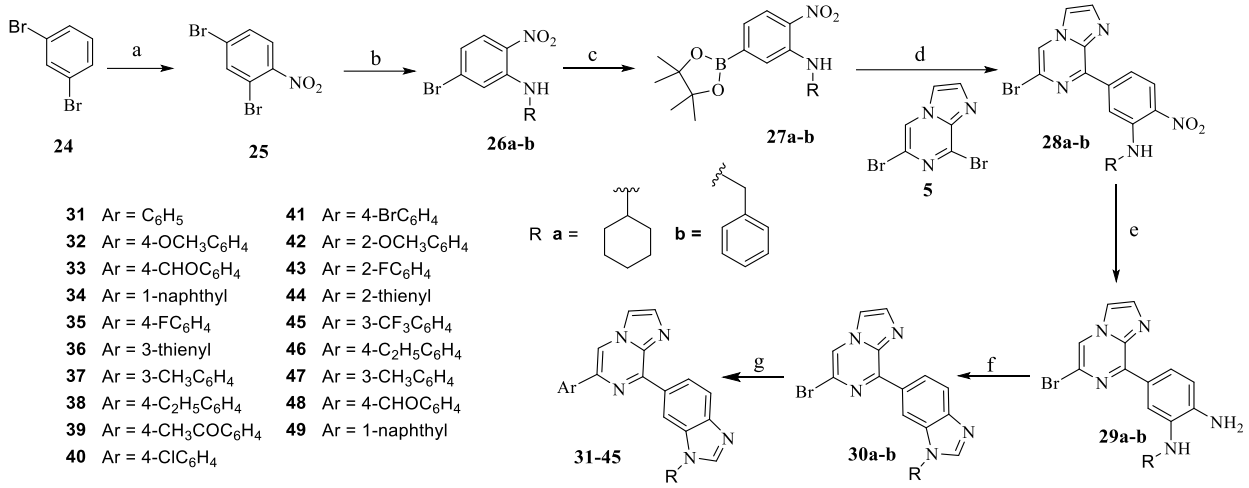

[b]Reagents and conditions: (a) H_2SO_4, HNO_3, DCM, 0 °C, 30 min., 95%; (b) Cyclohexyl amine/benzyl amine, K_2CO_3, DMF, 100 °C, 18 h; (c) Bis(pinacolato)diboron, $Pd(PPh_3)_2Cl_2$, KOAc, 1,4-dioxane, reflux, 10 h; (d) $Pd(PPh_3)_4$, K_2CO_3, CH_3CN : water (9:1), N_2, reflux, 10-12 h; (e) $Na_2S_2O_4$, aq. NH_3, THF : water, rt, 1 h; (f) Triethylorthoformate, AcOH, rt, 10 min., 80-90%; (g) $ArB(OH)_2$, $Pd(PPh_3)_4$, K_2CO_3, CH_3CN : water (9:1), N_2, reflux, 12-15 h, 75-85%

Interestingly, the scope of another benzimidazole at C-6 position of imidazo[1,2-*a*]pyrazine for Suzuki reaction was also explored with different synthetic route (**Scheme 3**). Reductions of **3**

Scheme 3. Synthesis of 6,8-bis(1-cyclohexyl-1*H*-benzo[*d*]imidazol-5/6-yl)imidazo[1,2-*a*]pyrazine [c]

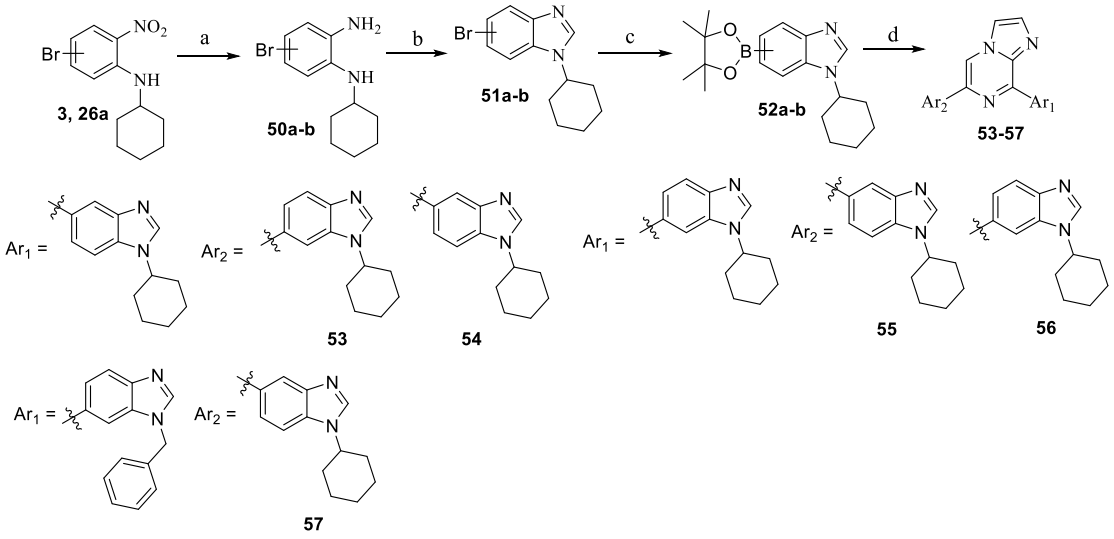

[c]Reagents and conditions: (a) $Na_2S_2O_4$, aq. NH_3, THF : water (3:2), rt, 1 h; (b) Triethylorthoformate, AcOH, rt, 10 min.,; (c) Bis(pinacolato)diboron, $Pd(PPh_3)_2Cl_2$, KOAc, 1,4-dioxane, reflux, 12 h; (d) **8, 30a-b**, $Pd(PPh_3)_4$, K_2CO_3, CH_3CN : Twater (9:1), N_2, reflux, 10-12 h, 75-81%

and **26a** were carried out with sodium dithionite in the presence of ammonia to afford **50a** and **50b**, respectively, followed by cyclization with triethylorthoformate in acetic acid, produced respective benzimidazoles **51a** and **51b**. Boronation of derivatives using bis(pinacolato)diboron in the presence of $Pd(PPh_3)_2Cl_2$ and KOAc afforded **52a** and **52b**. Suzuki-Miyaura cross-couplings of benzimidazole boronates **52a-b** with **8** and **30a-b** have been performed using $Pd(PPh_3)_4$ and K_2CO_3 to afford **53-57** in 75-81% yields.

2.2. Characterization

All ^1H and ^{13}C NMR characterization were performed on Jeol ECS 400 NMR spectrometer, which was operated at 400 MHz for ^1H nuclei and 100 MHz for ^{13}C nuclei, taking $CDCl_3$ as solvent. The synthesized compounds have also been characterized by mass spectrometry using Water Micromass-Q-T of Micro and purity was checked with CHN analysis. The molecular structure and the assignment of **31** were unambiguously confirmed by single-crystal X-ray diffraction study.

2.3. Biology

2.3.1. Cytotoxicity: In a preliminary test, compounds were assayed at single dose concentration (10^{-6} M) in the full panel of NCI 60 cancer cell lines. The tested compounds showed diverse but strong cytotoxicity on the evaluated panel of cell lines and most of the compounds exhibited more than 50% inhibition of tumor growth at micromolar concentration. As revealed from results of 29 tested compounds, seven compounds with wide range of growth percentage displayed strong growth inhibitory activity (-98.48 to 99.61) at 10 μM concentration. The bisbenzimidazole derivatives **53** and **57** demonstrated superior activity than mono benzimidazoles with cytotoxic effects towards 51 and 43 cell lines, respectively and among the monobenzimidazoles, 4-methoxyphenyl at C6 position of imidazo[1,2-*a*]pyrazine **32** indicated better cytostatic activity than phenyl **31**, 4-ethylphenyl **46** and 4-formylphenyl **48** derivatives in the same isomeric series of compounds. Such findings denote that bisbenzimidazole moiety is more favorable for cytotoxic and mono benzimidazole for cytostatic activity. Compounds **32**, **53** and **57** attributed pronounced cytotoxic activity over the majority of tested cancer cell lines with mean GP values of 20.32, -44.92 and -26.50, respectively. Compounds **32**, **53** and **57** have been explored for five dose assay, the mono- and bis-benzimidazole derivatives seemed to contribute equally toward the tumor growth inhibitory activities which is evident from the similar average GI_{50} of compounds **32** (2.10 μM), **53** (2.12 μM) and **57** (2.23 μM) as these values disguise significant cell selectivity. The mean GI_{50} graph of 4-methoxyphenyl (**32**) showed potent (compared to **53** and **57**) activity in the leukemia,

non-small cell lung, colon, CNS, ovarian, prostate and breast cancer subpanels. Higher LC_{50} values of compounds (usually > 100 μM) to most of the cell panels indicated their low toxicity profile. Cytotoxicity effect of compounds **32** and **53** was determined against human normal cell lines (Hek293). It has been observed that derivative **32** showed only 19.05%, 16.51%, 15.07%, 14.79% and 13.96% cytotoxicity to Hek293 cells whereas compound **53** exhibited 18.05%, 14.53%, 14.11%, 13.60% and 12.08% cytotoxicity to Hek293 cells at 10^{-4}, 10^{-5}, 10^{-6}, 10^{-7} and 10^{-8} M concentrations, respectively.

2.3.2. DNA interaction studies: Three most potent compounds **32**, **53** and **57** were studied with ct-DNA to investigate the interactions of these compounds with DNA using UV-visible, fluorescence and circular dichroism. DNA studies suggested that compounds were interacted with DNA through intercalation binding mode. The binding constants (K_b) determined using UV-visible spectroscopy for compound-DNA complexes have been determined from the Benesi-Hildebrand equation which were found to be 3.34×10^4 M^{-1} for **32**, 1.25×10^4 M^{-1} for **53** and 3.18×10^4 M^{-1} for **57**. These binding constants conclude that compound **32** has more affinity to bind with ct-DNA followed by compound **57** and **53**.

2.3.3. Bovine serum albumin (BSA) interactions: The possible binding interactions of compounds **32**, **53** and **57** with BSA have been investigated by UV-visible and fluorescence spectroscopy. The binding constants (K_b) were calculated using Benesi-Hildebrand equation and found to be 1.95×10^5 M^{-1} for **32**, 3.79×10^4 M^{-1} for **53** and 2.65×10^4 M^{-1} for **57**. Thus BSA binding affinities follow the order of **32** > **53** > **57**, indicating that monobenzimidazole derivatives have more ability to penetrate into the cell than bisbenzimidazole moieties.

2.4. Molecular properties and drug-likeness

The results from the calculations revealed that all the derivatives fulfilled the Lipinski's rule of five except compounds **53-57**, in which violation was due to high molecular mass.

2.5. Docking studies

Docking studies of compounds **32**, **53** and **57** with DNA have been performed to find the interactions between compounds and DNA.

Chapter 3: Synthesis, characterization, *in vitro* evaluation and interaction with DNA/BSA of hybrids of benzimidazole and naphthalimide conjugates

3.1. Synthesis

Nitration of 1,4- and 1,3-dibromobenzene **1a-b** with nitric acid and sulphuric acid, yielded 1,4-dibromo-2-nitro-benzene **2a** and 2,4-dibromo-1-nitro-benzene **2b**, both of which were subjected to regioselective nucleophilic substitution with cyclohexylamine to afford **3a-b**. Boronation of **3a-b** with bis(pinacolato)diboran in the presence of $Pd(PPh_3)_2Cl_2$ and KOAc, generated **4a-b**. Suzuki-Miyaura cross coupling of **4a-b** was carried out with 6-bromo-1*H*,3*H*-benzo[*de*]isochromene-1,3-dione **5** to obtain **6a-b**. Compound **6a-b** was further reduced with sodium dithionite in the presence of ammonia to afford mixture of **7a-b** and **8a-b** which were subsequently cyclized with triethylorthoformate in acetic acid at room temperature to afford the requisite **9a-b** and **10a-b**, respectively. On refluxing of **9a-b** with alkyl and aryl amines in ethanol, compounds **11-26** were achieved in the yields of 71-86% (**Scheme 4**).

Scheme 4. Synthesis of 6-(1-cyclohexyl-1*H*-benzo[*d*]imidazol-5/6-yl)-2-substituted-1*H*-benzo[*de*]isoquinoline-1,3(2*H*)-dione

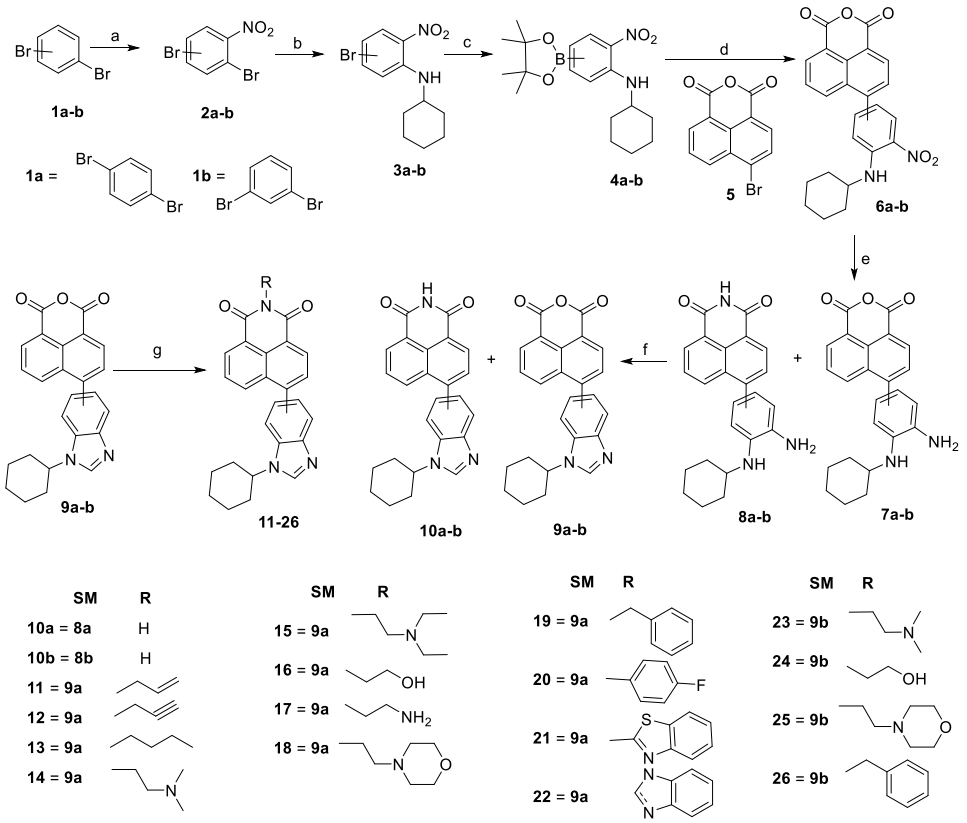

Reagents and conditions: (a) HNO_3, H_2SO_4, DCM, 0 °C, 30 min., 90-95%; (b) Cyclohexyl amine, K_2CO_3, DMF, 100 °C, 18 h, 70-75%; (c) Bis(pinacolato)diboron, $Pd(PPh_3)_2Cl_2$, KOAc, dioxane, reflux, 10 h, 78-82%; (d) $Pd(PPh_3)_4$, K_2CO_3, CH_3CN : water (9:1), N_2, reflux, 10-12 h, 70-73%; (e) $Na_2S_2O_4$, aq. NH_3, THF : water, 1 h, rt; (f) Triethylorthoformate, AcOH, 30 min., rt; (g) RNH_2, ethanol, reflux, 12-15 h, 71-86%

3.2. Characterization

All ^{1}H and ^{13}C NMR characterization were performed on Jeol ECS 400 NMR spectrometer, which was operated at 400 MHz for ^{1}H nuclei and 100 MHz for ^{13}C nuclei, taking $CDCl_3$ as solvent. The synthesized compounds were characterized by mass spectra using Water Micromass-Q-T of Micro.

3.3. Biological Activities

3.3.1. Cytotoxicity: National Cancer Institute (NCI) has selected eighteen naphthalimide-benzimidazoles (**9a-b**, **10b, 11-23, 25** and **26**) for one-dose screening in the panel of 60 human cancer cell lines. The results indicated that many of these naphthalimides exhibited equal or better cytotoxicity than amonafide or mitonafide. Five compounds showed cytotoxic effects in a broad range of cell lines at 10^{-5} M level and two of them showed cytotoxic activity with cytostatic and cytotoxic effects against all the 58 tested cell lines. Compounds **15** and **23** fulfilled the selection criteria set by NCI for cytotoxicity in this assay and thus, selected for further evaluation at the full panel of cancer cell lines at five dose concentrations (10^{-4}-10^{-8} M). *In vitro* evaluation of these compounds indicated that derivatives **15** and **23** exhibited cytotoxic activity towards most of the human cell lines, showing MG-MID GI_{50} values of 1.43 and 1.83 μM, respectively. Both the derivatives showed particular efficacy against colon and leukemia subpanels having GI_{50} values in the range of 0.42-1.03 μM. Overall, the naphthalimide substituted with 5-benzimidazole (**15**) led to more potency than the 6-benzimidazole analogue (**23**).

3.3.2. Cell cycle analysis

Cell cycle analysis was performed using flow cytometer on the compounds **15** and **23** on MDA-MB-468 breast cancer cells. The results indicated that compound **15** had no significant effect at cell cycle whereas compound **23** arrested the cell cycle at G_2/M phase. About 25.23% of cells were found in G2/M phase when treated with 1 μM of compound **23** for 24 h.

3.3.3. DNA interaction studies

The binding properties of DNA with compounds **15** and **23** as a model of naphthalimide-benzimidazole conjugates have been studied with calf thymus (ct)-DNA using UV-visible and fluorescence spectroscopy as well as circular dichroism experiment. Studies showed that compounds intercalated into adjacent base pairs of DNA. To access the stability of an adduct formed between DNA and substrate in absorption spectroscopy, Benesi-Hildebrand equation has been used to calculate the intrinsic binding constant (K_b) for compounds **15** and **23** and were found

to be 3.62×10^5 M^{-1} and 2.23×10^5 M^{-1}, respectively. The results indicated that compound **15** showed strong interaction with ct-DNA than compound **23**. The thermal denaturation experiment revealed a T_m value of 75.6 ± 0.2 ˚C under our experimental conditions, whereas the melting temperature of DNA in the presence of compounds **15** and **23** were successively increased to 89.8 ± 0.2 ˚C and 81.5 ± 0.3 ˚C, respectively. Fluorescence studies of compounds **15** and **23**, indicated that the mechanism of quenching might be a static process. Moreover, the observed negative values of ΔG for compounds revealed that the binding process is spontaneous and favourable. The negative values of ΔH and ΔS for **15** and **23** indicated that the interaction with DNA is mainly enthalpy driven by which hydrogen bonding and van der Waals contacts contributed towards the stability of complexes. Intercalation of compounds was further confirmed by ethidium bromide competitive displacement assay and circular dichroism study.

3.3.4. BSA binding studies

UV-visible spectroscopic studies revealed good interactions between BSA and compounds **15** and **23**. Binding constant (K_b) for the interaction of compounds with BSA have been calculated using Benesi-Hildebrand equation and were found to be 6.96×10^4 M^{-1} for **15** and 5.64×10^4 M^{-1} for **23**, signifying better binding affinity of compound **15** with serum albumin than **23**. Fluorescence study suggested that, the binding of compounds to BSA probably involves the stating quenching with formation of complex at ground state.

Chapter 4: Synthesis, characterization, *in vitro* evaluation, interaction with DNA/HSA, and molecular docking studies of naphthalimide and phenanthro[9,10-*d*]imidazole hybrids

4.1. Synthesis

Commercial available acenaphthene (**1**) was treated with *N*-bromosuccinimide in DMF at room temperature to afford 5-bromo acenaphthene (**2**) in 94% yield. Oxidation of **2** was accomplished with sodium dichromate in acetic acid to obtain compound **3** in 72% yield. Condensation of 4-formylphenylboronic acid (**4**) with 9,10-phenanthrenequinone (**5**) in the presence of ammonium acetate in acetic acid gave **6** in 58% yield. Suzuki-Miyaura cross-coupling reaction of compound **6** with **3** in the presence of $Pd(PPh_3)_4$ and K_2CO_3 in CH_3CN and water (9:1) gave compound **7** in 72% yield. Intermediate **7** was refluxed with various aliphatic and aromatic amines in ethanol for 7-9 h to afford compounds **8-21** in 78-91% yields (**Scheme 5**).

Scheme 5. Synthesis of 6-(4-(1*H*-phenanthro[9,10-*d*]imidazol-2-yl)phenyl)-2-substituted-1*H*-benzo[*de*]isoquinoline-1,3(2*H*)-dione

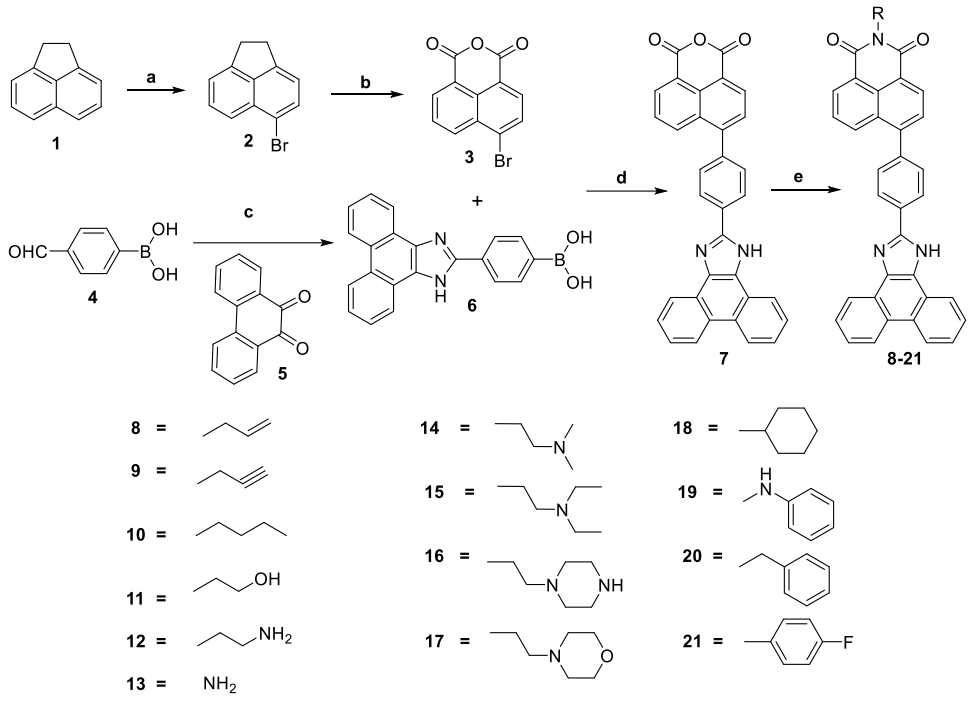

Reagents and conditions: (a) NBS, DMF, rt, 3 h, 94%; (b) Sodium dichromate, AcOH, reflux, 2.5 h, 72%; (c) Ammonium acetate, AcOH, reflux, 10 h, 58%; (d) $Pd(PPh_3)_4$, K_2CO_3, CH_3CN : water (9:1), N_2, reflux, 12 h, 72%; (g) RNH_2, ethanol, reflux, 7-9 h, 78-91%

4.2. Characterization

All ^1H and ^{13}C NMR characterization were performed on Jeol ECS 400 NMR spectrometer, which was operated at 400 MHz for ^1H nuclei and 100 MHz for ^{13}C nuclei, taking $CDCl_3$ as solvent. The synthesized compounds were characterized by mass spectra using Water Micromass-Q-T of Micro.

4.3. Biology

4.3.1. Cytotoxicity: Among all the tested compounds, 1-ethylpiperazine substituted, compound **16**, found to be most active compound of the series with the range of growth inhibition -55.78-94.53. Compound **16** has been found sensitive against 14 cancer cell lines out of 56 tested cell lines and found most susceptible against LOXIMVI of melanoma panel of cancer cell lines. Compound **16** found to be least active against full panel of CNS and renal cancer cell lines. Compound **14** substituted with *N*,*N*-dimethylethylamine showed cytostatic activity towards K-562 (leukemia), SR (leukemia), 786-0 (renal cancer) and MCF7 (breast cancer) cell lines.

4.3.2. DNA interaction studies: For a qualitative determination of the interaction between compound **16** and ct-DNA, the binding constant (K_b) was calculated using the Benesi-Hildebrand equation and found to be 7.81×10^4 M^{-1}. Fluorescence emission spectroscopy confirmed the quenching mechanism in compound **16** and ct-DNA interactions and was found to be static quenching. A strong (1.55×10^5 M^{-1}) and weak (1.36×10^4 M^{-1}) binding constant for competitive displacement assay for the Hoechst dye and the ethidium bromide, respectively, suggested that compound **16** interacted through strong groove binding and partial intercalation. Groove binding was further supported by viscosity measurements and iodide quenching studies.

4.3.3. HSA binding studies: UV-Vis absorption spectroscopy gave strong interaction and the binding constant (K_b) was calculated to be 0.51×10^5 M^{-1} using Benesi-Hildebrand plot. Results of fluorescence emission spectroscopy revealed that the binding process was static, spontaneous and exothermic in nature. Synchronous fluorescence spectroscopic studies had revealed that both Tyr and Trp residues contribute equally to the quenching of the HSA emission and the HSA molecule undergoes conformational changes around both Tyr and Trp residues upon binding to compound **16**.

4.4. Molecular docking

Docking studies of compounds **16** with DNA have been performed to find the interactions between compound and DNA.

Chapter 5: Synthesis, characterization, *in vitro* evaluation, interaction with DNA/BSA, and molecular docking studies of phenanthro[9,10-*d*]imidazole and other heterocyclic moieties conjugates

5.1. Synthesis

Compounds **3** and **4** were synthesized by heating the phenanthrene-9,10-dione (**1**) and substituted aromatic aldehydes (**2a-h**) at 100 ^oC for 2-5 h in the presence of ammonium acetate and acetic acid (**Scheme 6**). Compound **3h** was further used for the reaction with 2-amino-benzo[*de*]isoquinoline-1,3-dione (**5**) and thiazolidine-2,4-dione (**7**) in ethanol for 3-4 h to obtain **6** and **8**. The series of benzimidazoles were formed by the condensation of **3h** with (3,4-diamino-phenyl)-(phenyl)-methanone (**9**) and 1,2-diamino-anthracene-9,10-dione (**11**) at 60 ^oC in nitrobenzene for 2 h to obtain compound **10** and **12** (**Scheme 7**). 2,3-Diaryl 1*H*-phenanthro[9,10-*d*]imidazole was obtained with phenanthrene-9,10-dione (**1**), employing aniline and benzaldehyde in the presence of ammonium acetate and acetic acid and the corresponding product, compound **14** (**Scheme 8**).

For SAR studies involving variation of the imidazole moiety, compounds **16** and compound **17** were prepared by condensation of acenaphthylene-1,2-dione with respective salicylaldehyde, and terephthaldehyde, in the presence of ammonium acetate and acetic acid as shown in **Scheme 9**.

Scheme 6. Synthesis of 2-(subsitituted aryl)-1*H*-phenanthro[9,10-*d*]imidazole/oxazole (**3a-h** and **4a-c**).

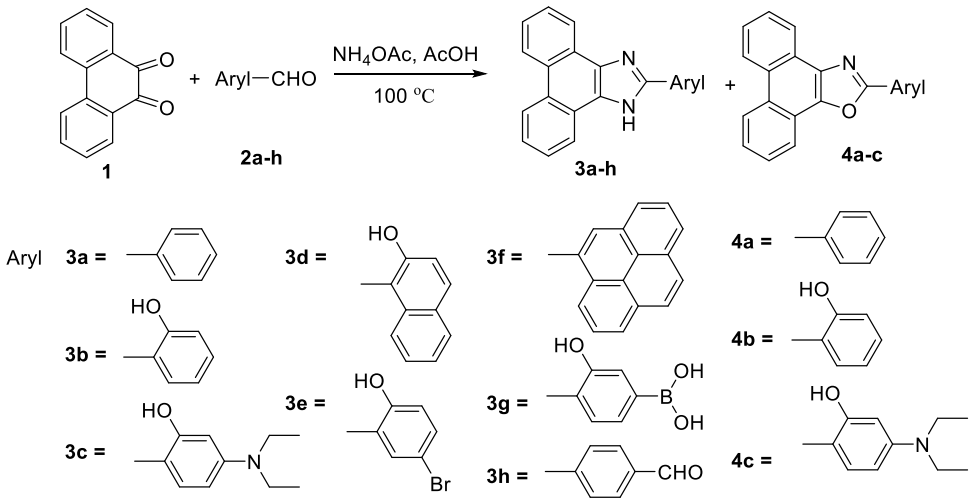

Scheme 7. Synthesis of naphthalimide (**6**), thiazolidine (**8**) and benzimidazoles (**10** and **12**) of 4-(1*H*-phenanthro[9,10-*d*]imidazol-2-yl)benzaldehyde

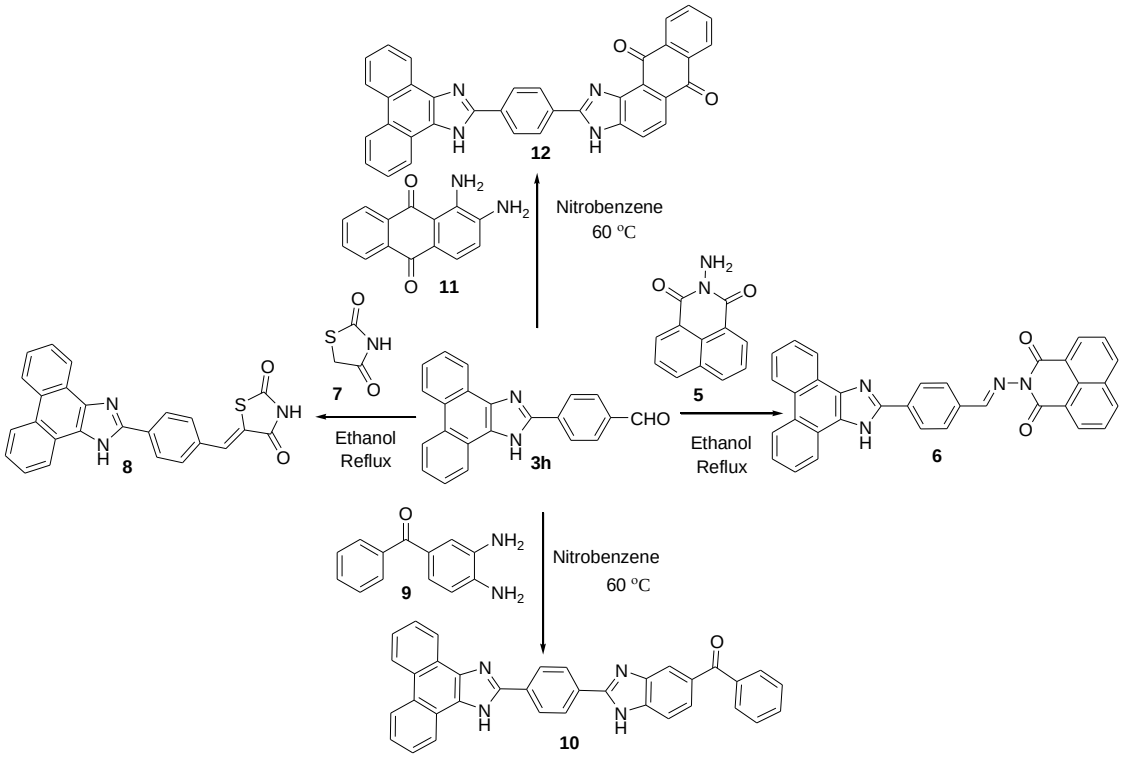

Scheme 8. Synthesis of 1,2-diphenyl-1*H*-phenanthro[9,10-*d*]imidazole (**14**)

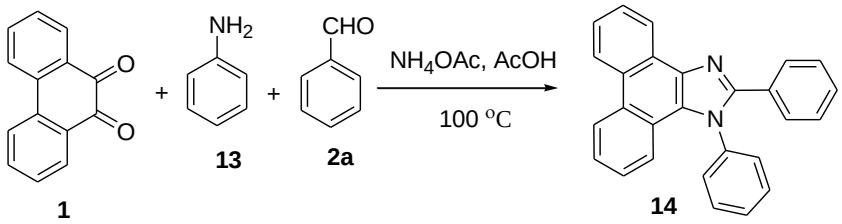

Scheme 9. Synthesis of 2-(7-phenyl-7*H*-acenaphtho[1,2-*d*]imidazol-8-yl)phenol (**16**) and 4-(7*H*-acenaphtho[1,2-*d*]imidazol-8-yl)benzaldehyde (**17**)

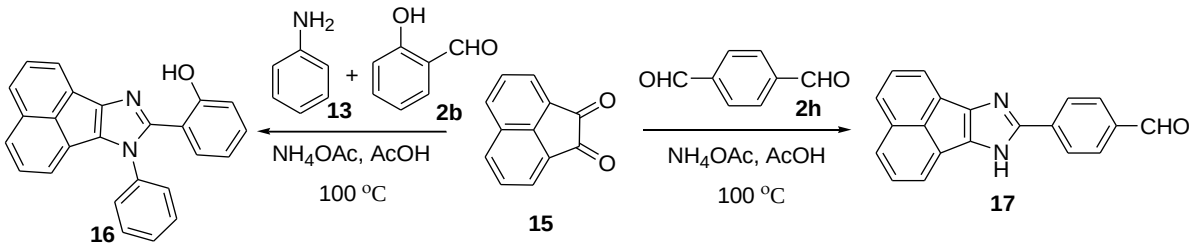

5.2. Characterization

All ^{1}H and ^{13}C NMR characterization were performed on Jeol ECS 400 NMR spectrometer, which was operated at 400 MHz for ^{1}H nuclei and 100 MHz for ^{13}C nuclei, taking $CDCl_3$ as solvent. The synthesized compounds were characterized by mass spectra using Water Micromass-Q-T of Micro.

5.3. Biology

5.3.1. Cytotoxicity: Preliminary *in vitro* cytotoxicity screening revealed that derivatives **3f**, **4c** and **17** showed moderate inhibition, while compound **8** indicated more than 50% growth inhibition for most of the cancer cell lines and in some cases, exhibited better growth inhibition than 5-fluorouracil (5-FU). 1*H*-Phenanthro[9,10-*d*]imidazole/oxazole derivatives **3b, 3c, 4b** and **12** showed lower activity for cancer cell lines and were considered to be the least effective. 1*H*-Phenanthro[9,10-*d*]imidazole **3f** showed selectivity towards non-small cell lung cancer cell lines NCI-H226 and breast cancer cell lines MDA-MB-468 with growth inhibition (GI) values of 76.22% and 78.07%, respectively. Similarly, 2-phenanthro[9,10-*d*]oxazole having 5-diethylamino-2-hydroxyphenyl group **4c** at 2-position showed selectivity towards leukemia cancer cell lines, colon cancer cell lines and melanoma cancer cell lines. Derivative **17** displayed selective potency towards breast cancer cell lines MCF7 and T-47D with GI values of 51.61% and 57.05%, respectively. Compound **8** showed excellent inhibition against leukemia cancer cell lines CCRF-

CEM (65.23%), HL-60(TB) (57.70%), K-562 (68.08%), RPMI-8226 (66.09%) and SR (79.21%), colon cancer cell lines HCT-116 (65.54%) and HCT-15 (50.01%), melanoma cancer cell lines MDA-MB-435 (67.42%), renal cancer cell lines A498 (92.98%), prostate cancer cell lines PC-3 (51.87%) and breast cancer cell lines BT-549 (63.72%) and MDA-MB-468 (51.74%). To evaluate the safety, the cytotoxic effect of active derivative **8** on human normal cell lines (Hek293) was also carried out. It has been observed that derivative **8** showed only 15%, 9%, 6%, 5% and 4% cytotoxicity to Hek293 cells at the higher level of concentration.

5.3.2. DNA binding studies: In order to determine the interaction of compound with calf thymus and human DNA, binding property of most active compound **8** has been assessed using UV-visible and fluorescence spectrophotometer. UV-vis studies suggested that compound intercalated strongly into human DNA ($K_b = 5.24 \times 10^6\ M^{-1}$) than ct-DNA ($K_b = 2.95 \times 10^6\ M^{-1}$).

5.3.3. Serum albumin binding studies: The absorption experiment confirmed that compound **8** showed worthy interaction with BSA and HSA. UV-visible absorption spectroscopy revealed that binding constant of compound **8** and HSA has been found to be $9.35 \times 10^4\ M^{-1}$ which is more than that with BSA ($6.57 \times 10^4\ M^{-1}$). Fluorescence emission study showed that the process of quenching was static in nature and mainly enthalpy driven and involved the hydrogen bonding interaction. FRET studies with BSA indicated that energy transfer occurred from BSA to compound **8** with high probability.

5.4. Molecular docking

Docking studies of compounds **8** with DNA have been performed to find the interactions between compound and DNA.

Chapter 6: Synthesis, characterization, *in vitro* evaluation of naphthalimide, benzothiazole and indole conjugates

6.1. Synthesis

Commercially available 5-bromo indole **1** was subjected to react with the Vilsmeier-Haack reagent to get 5-bromo-1*H*-indole-3-carbaldehyde **2**. Compound **2** was treated with allyl bromide in acetone-aqueous NaOH at room temperature to give brown color solid of compound **3**. Further, compound **3** was reacted with 2-aminothiophenol in the presence of nitrobenzene at 80 °C for 8 h gave the reddish color solid of compound **4**. Boronate of compound **4** was synthesized using bis(pinacolato)diboron in the presence of bis(triphenylphosphine)palladium chloride, potassium acetate in refluxing dioxane for 3 h. Suzuki coupling of compound **5** with **6** gave the light yellow

colored solid of compound **7** in the presence of tetrakis(triphenylphosphine) palladium (0), potassium carbonate in acetonitrile-water condition. Compound **8-22** were synthesized by the condensation between various amines i. e. allyl, butyl, propagyl, cyclohexyl, ethanol amine and compound **7** in the presence of ethanol (**Scheme 10**).

Scheme 10. Synthesis of 6-(1-allyl-3-(benzo[*d*]thiazol-2-yl)-1*H*-indol-5-yl)-2-substituted-1*H*-benzo[*de*]isoquinoline-1,3(2*H*)-dione

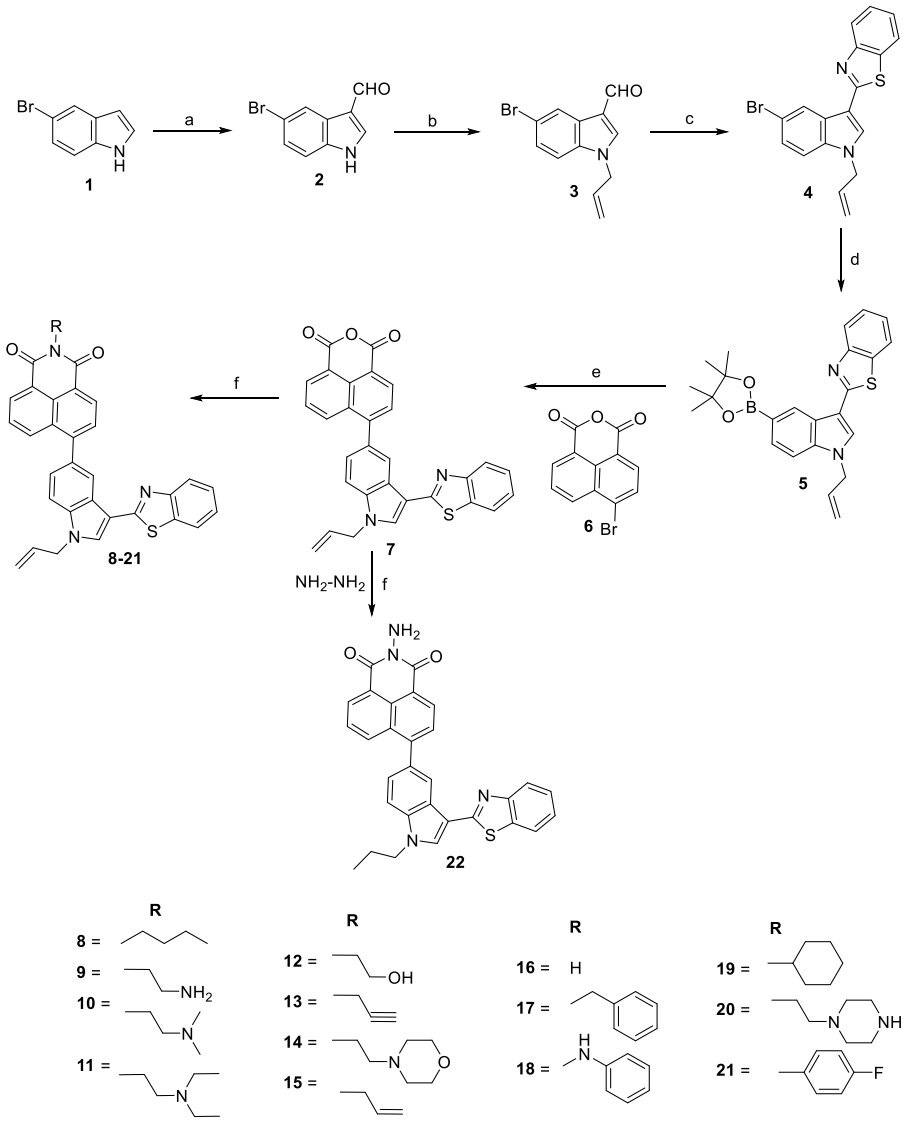

Reagents and conditions: (a) $POCl_3$, DMF, 0 °C, 1 h., 93%; (b) Allyl bromide, acetone-aq. NaOH, RT, 2 h, 86%; (c) 2-Aminothiophenol, nitrobenzene, 80 °C, 8 h, 62%; (d) Bis(pinacolato)diboron, $Pd(PPh_3)_2Cl_2$, KOAc, dioxane, reflux, 3 h, 61%; (e) $Pd(PPh_3)_4$, K_2CO_3, CH_3CN : water (9:1), N_2, reflux, 5 h, 55%; (f) RNH_2, ethanol, reflux, 4-6 h, 68-75%

6.2. Characterization

All ^{1}H and ^{13}C NMR characterization were performed on Jeol ECS 400 NMR spectrometer, which was operated at 400 MHz for ^{1}H nuclei and 100 MHz for ^{13}C nuclei, taking $CDCl_3$ as solvent. The synthesized compounds were characterized by mass spectra using Water Micromass-Q-T of Micro.

6.3. Biology

Cytotoxicity: Compounds **7-22** were tested for their cytotoxicity against A549 (Lung), MCF7 (Breast) and HeLa (cervix) human cancer cells at 1.0, 10 and 100 μM concentrations. Compounds exhibited more sensitivity towards A549 than MCF7 and HeLa cancer cells at all said concentrations. Compound **12** revealed potent cytotoxicity against A549 cancer cells with the IC_{50} value of 140 nM. Compound **13** showed excellent cytotoxicity for A549 with IC_{50} value of 314 nM. Compound **15** substituted with allyl showed IC_{50} value of 1.89 μM for A549, 0.38 μM for MCF7 and 2.71 μM for HeLa cancer cells, found effective against all tested cancer cells. To find out the safety profile, compounds **7-22** were evaluated against Hek293 (Kidney) human noncancerous cell line at 100 μM concentration. Results showed that compound **11** exhibited maximum growth inhibition by 18% followed by compound **8**, which displayed growth inhibition by 16%.

References

1. Cancer Research UK; https://www.cancerresearchuk.org/health-professional/cancer-statistics/worldwide-cancer#heading-Two [Accessed on July/2019]
2. M. Ferlay, I. Colombet, C. Soerjomataram, D. M. Mathers, M. Parkin, A. Piñeros, F. Znaor, Bray, Estimating the global cancer incidence and mortality in 2018: GLOBOCAN sources and methods, *Int. J. Cancer*, **2019**, *144*, 1941-1953.
3. P. Singh, R. Raj, V. Kumar, M. P. Mahajan, P. Bedi, T. Kaur, A. Saxena, 1, 2, 3-Triazole tethered β-lactam-chalcone bifunctional hybrids: synthesis and anticancer evaluation, *Eur. J. Med. Chem.*, **2012**, *47*, 594-600.
4. Z. Chen, X. Liang, H. Zhang, H. Xie, J. Liu, Y. Xu, W. Zhu, Y. Wang, X. Wang, S. Tan, A new class of naphthalimide-based antitumor agents that inhibit topoisomerase II and induce lysosomal membrane permeabilization and apoptosis, *J. Med. Chem.*, **2010**, *53*, 2589-2600.
5. H. Prinz, A. K. Ridder, K. Vogel, K. J. Böhm, I. Ivanov, J. B. Ghasemi, E. Aghaee, K. J. Müller, *N*-heterocyclic (4-phenylpiperazin-1-yl) methanones derived from phenoxazine and

phenothiazine as highly potent inhibitors of tubulin polymerization, *Med. Chem.*, **2017**, *60*, 749-755.

6. R. Morphy, Z. Rankovic, Designed multiple ligands. An emerging drug discovery paradigm, *J. Med. Chem.*, **2005**, *48*, 6523-6543.

7. A. L. Hopkins, Network pharmacology: the next paradigm in drug discovery, *Nat. Chem. Biol.*, **2008**, *4*, 682-690.

8. S. Fortin, G. Bérubé, Advances in the development of hybrid anticancer drugs, *Expert Opin. Drug Discov.*, **2013**, *8*, 1029-1047.

9. R. Morphy, C. Kay, Z. Rankovic, From magic bullets to designed multiple ligands, *Drug Discov. Today*, **2004**, *9*, 641-651.

10. J. Walsh, A. Bell, Hybrid drugs for malaria, *Curr. Pharm. Des*., **2009**, *15*, 2970-2985.

11. L. K. Gediya, V. C. O. Njar, Promise and challenges in drug discovery and development of hybrid anticancer drugs, *Expert Opin. Drug Discov*., **2009,** *4*, 1099-1111.

12. C. Viegas-Junior, A. Danuello, B. V. da Silva, E. J. Barreiro, C. A. Fraga, Molecular hybridization: a useful tool in the design of new drug prototypes, *Curr. Med. Chem.*, **2007**, *14*, 1829-1852.

LIST OF PUBLICATIONS

1. I. Singh, V. Luxami, K. Paul, Singh, Synthesis of naphthalimide-phenanthro [9, 10-*d*] imidazole derivatives: *In vitro* evaluation, binding interaction with DNA and topoisomerase inhibition, *Bioorg. Chem.,* **2020**, *96*, 103631-103642.
2. I. Singh, V. Luxami, K. Paul, Synthesis, cytotoxicity, pharmacokinetic profile, binding with DNA and BSA of new imidazo [1, 2-*a*] pyrazine-benzo [*d*] imidazol-5-yl hybrids, *Sci. Rep.,* **2020**, *10*, 1-14.
3. I. Singh, V. Luxami, K. Paul, Synthesis and *in vitro* evaluation of naphthalimide-benzimidazole conjugates as potential antitumor agents, *Org. Biomol. Chem.*, **2019**, *17*, 5349-5366.
4. I. Singh, R. Rani, V. Luxami, K. Paul, Synthesis of 5-(4-(1*H*-phenanthro [9, 10-*d*] imidazol-2-yl) benzylidene) thiazolidine-2, 4-dione as promising DNA and serum albumin-binding agents and evaluation of antitumor activity, *Eur. J. Med. Chem.,* **2019**, *166*, 267-280.
5. I. Singh, V. Luxami, K. Paul, Effective synthesis of benzimidazoles-imidazo [1, 2-*a*] pyrazine conjugates: A comparative study of mono-and bis-benzimidazoles for antitumor activity, *Eur. J. Med. Chem.,* **2019**, *180*, 546-561.
6. I. Singh, R. Tandon, V. Luxami, N. Tandon, K. Paul, Recent advances and developments of *in vitro* evaluation of heterocyclic moieties on cancer cell lines, *Chem. Rec.*, **2018**, *19*, 362-393.
7. I. Singh, V. Luxami, K. Paul, Synthesis, cytotoxicity, topoisomerase inhibition, and HSA binding of novel conjugates of indole, benzothiazole, and naphthalimide. (manuscript prepared)

Publications other than thesis work

1. I. Singh, V. Luxami, K. Paul, Spectroscopy and molecular docking approach for investigation on the binding of nocodazole to human serum albumin, *Spectrochim. Acta A*, **2020**, *235*, 118289-118298.
2. G. Kumar, I. Singh, K. Paul, V. Luxami, Triple signalling (CHEF-ESICT-ESIPT) mechanism for a chromo-fluorescent ratiometric sensing of Al^{3+} and F^{-} ions, (communicated).

3. I. Singh, K. Paul, V. Luxami, Naphthalimide-benzimidazole conjugate for selective fluorescent chemosensor for Hg^{2+} as an "on-off" switch and logic gate (manuscript prepared)
4. I. Singh, V. Luxami, K. Paul, A review on the importance of C-H functionalization on biologically active moieties. (manuscript prepared)
5. G. Kumar, I. Singh, V. Luxami, K. Paul, Naphthalimide based "*turn-on*" responsive detection of SO_4^{2-} in 100% water. (manuscript under preparation)

POSTERS IN CONFERENCES

1. Iqubal Singh and Kamaldeep Paul, "Synthesis of 6-(1-cyclohexyl-1*H*-benzo[*d*]imidazol-5/6-yl)-2-substituted-1*H*-benzo[*de*]isoquinoline-1,3(2*H*)-dione and study their effects upon human cancer cell lines, DNA and BSA interactions" 8th National Symposium on Advances in Chemical Sciences held at Guru Nanak Dev University, Amritsar on 15-16 Feb, **2019**.
2. Iqubal Singh and Kamaldeep Paul, "Synthesis of 1*H*-phenanthro[9,10-*d*]imidazole/oxazole and 7*H*-acenaphtho[1,2-*d*]imidazole derivatives for human cancer cell lines, DNA intercalation and BSA binding studies" 11th National Conference on "Recent Trends in Chemical and Environmental Sciences - 2019 (RTCES-2019)" held at the Department of Chemistry Punjabi University, Patiala on 07-08 Feb, **2019**.
3. Iqubal Singh and Kamaldeep Paul, "Design, synthesis and *in vitro* anticancer activities of imidazo[1,2-*a*]pyarzine and benzimidazole hybrids via molecular hybridization technique" International Conference on Drug Discovery: Biotech and Pharma at Cross Roads held at Thapar Institute of Engineering and Technology, Patiala on 15-17 Feb, **2018**.
4. Iqubal Singh and Kamaldeep Paul, "Design, synthesis and *in vitro* anticancer activities of imidazo[1,2-*a*]pyarzine and benzimidazole hybrids via molecular hybridization technique" National Conference on Impact of pharmaceutical Biotechnology on Future of Medicine held at Geetanjali University, Udaipur on 24-25 March, **2017**.
5. Iqubal Singh and Kamaldeep Paul, "Design, synthesis and *in vitro* anticancer activities of imidazo[1,2-*a*]pyarzine and benzimidazole hybrids via molecular hybridization technique" National Conference on Recent Advancement in Drug Discovery and Development held at Geetanjali University, Udaipur on 4-5 Feb, **2017**.

Workshops

1. Iqubal Singh, DST-SERB Sponsored Workshop on "Computational Drug Design using Molecular Docking and Virtual Screening" held at Thapar Institute of Engineering and Technology, Patiala on 27-29 April, **2018**.
2. Iqubal Singh, Punjab State Council for Science and Technology (PSCST), Chandigarh Sponsored Workshop on "Intellectual Property Rights and Patenting" held at Thapar Institute of Engineering and Technology, Patiala on 17 Feb, **2018**.